An Automated Methodology for Flight Simulation Model Calibration to Manufacturer and Flight Test Validation Data

by

Madison Harper

A thesis submitted to the Graduate Faculty of
Auburn University
in partial fulfillment of the
requirements for the Degree of
Master of Science

Auburn, Alabama
May 2, 2026

Keywords: flight simulation, calibration, general aviation

Approved by

Imon Chakraborty, Chair, Associate Professor of Aerospace Engineering
Nicoletta Fala, Assistant Professor of Aerospace Engineering
Anwar Ahmed, Professor of Aerospace Engineering

Abstract

Flight simulation models require calibration to available aircraft data to accurately reproduce real aircraft performance and handling characteristics. In practice, this calibration is typically carried out using high-effort system identification methods or iterative, manual tuning, both of which demand significant time and engineering resources. This work presents an automated two-stage calibration approach for physics-based general aviation aircraft models developed within the PEACE/MADCASP framework. The first stage calibrates aerodynamic, propulsion, and propeller characteristics to steady-state climb and cruise performance data from the aircraft's Pilot's Operating Handbook. The second stage extends calibration to flight test data, addressing aircraft attitude, control surface deflections, and dynamic response characteristics. The methodology is demonstrated on a Cessna 172 Skyhawk model using data provided by Frasca International, with results showing agreement within prescribed performance tolerances derived from FAA Part 60 Level 5 FTD requirements. A supplemental steady-state calibration of a Cirrus SR20 model provides an initial demonstration of the methodology's generality.

Artificial Intelligence (AI) Use Disclosure Statement

In the preparation of the thesis, the following Artificial Intelligence (AI) tools were used: Claude (Anthropic). These tools were used primarily to support editing, clarity, and organization during the technical writing process. The author acknowledges full responsibility for the intellectual content of this work and has ensured that all AI-assisted sections have been reviewed and revised for accuracy and appropriate academic style. All AI-generated content was reviewed and validated for relevance, appropriateness, and accuracy before incorporation into the final document to maintain scholarly integrity of this research.

Digital Accessibility Disclosure

In the preparation of this thesis, the following digital accessibility tools were used to ensure this document complies with federal requirements: Claude (Anthropic). The author acknowledges full responsibility for the intellectual content of this work and has made a good faith effort to comply with digital accessibility requirements in publishing, wherein the nature of the content does not significantly change in order to do so. Furthermore, all content has been reviewed and revised to meet these requirements prior to final publication.

Acknowledgments

First, I would like to thank my advisor, Dr. Chakraborty, for giving me the opportunity to pursue this rigorous goal of completing a thesis alongside my master's degree, all remotely from over 650 miles away, while working my full-time "day job". The past three years have been the most rewarding (and tiring) period of my life and I am beyond thankful that I was given this opportunity. Additionally, I would like to thank Dr. Chakraborty for his time as a professor during my undergraduate studies which shaped my interests in the aerospace field and equipped me with the knowledge, work ethic, and interests that led to the career that I have today.

I would also like to thank my management and colleagues at Frasca International. Without the support of the company and people, this endeavor would have never been possible. Particularly, I would like to thank my manager, Jonathan Wisdom, who has always been willing to accommodate my school schedule, scan through my manuscripts on short notice, and work with me for months to obtain permission to use the company's flight test data in support of this research. Additionally, I would like to thank my peers that were willing to brain storm with me at times that I felt stuck.

Thank you to the members of VSDDL that helped me along the way, particularly, Bikash Kunwar and Dr. Aashutosh Mishra. Without their support, there would be no flight simulation models to calibrate. Thank you to my committee members, Dr. Fala and Dr. Ahmed, for your support and willingness to join in on this last step of completing my degree requirements.

Finally, thank you to my family and friends that have stuck by my side through this crazy period.

To my research buddy, Savannah Lynn, thank you for the countless hours of "parallel play" phone calls. Doing this work would have been a lot lonelier without a friend like you.

To my babies, Finn, Koda, Grey, and Wilson, thank you for always sticking right by my side no matter how late I was working into the night. You keep me sane and always know how to make me smile when I need it most.

To my family, thank you for your understanding the last three years of constant work. I also want to thank my grandmother. Meme, you are the reason I love learning. I miss you every single day.

Most importantly, to my love, Bekka, thank you for your unconditional support and love. I would not be where I am today if you were not by my side. I love you most!

I will forever be grateful for my time at Auburn University. *I believe in Auburn and love it. War Eagle!*

Table of Contents

List of Tables

List of Figures

List of Abbreviations

6-DOF six-degree-of-freedom

CT&M correct trend and magnitude

FAA Federal Aviation Administration

FPM feet per minute

FTD Flight Training Device

MADCASP Modular Aircraft Dynamics and Control Algorithm Simulation Platform

MAP manifold pressure

PEACE Parametric Energy-based Aircraft Configuration Evaluator

PID proportional-integral-derivative

POH Pilot Operating Handbook

Chapter 1

Introduction

1.1 Motivation

Flight simulation models serve a broad role in aviation, supporting applications ranging from pilot training to aircraft design and safety analysis. Across these applications, the underlying flight dynamics and propulsion models are at the core of the simulation's function, providing the forces and moments acting on the aircraft that govern simulated aircraft motion [1, 2]. Typically, these models are initially developed using a combination of theoretical methods, semi-empirical approximations, manufacturer-provided data, and databases derived from computational fluid dynamics simulations or wind tunnel testing [3, 4, 5]. These methods provide a reasonable initial estimate of the aircraft's flight model, but frequently display discrepancies when objectively compared to real-world flight test data. These discrepancies necessitate a calibration routine against available reference data to satisfy objective accuracy standards.

One particularly well-established application of flight simulation models is pilot training, where Flight Simulation Training Devices (FSTDs) provide a cost-effective, low-risk environment for trainees to practice procedures, avionics usage, and aircraft handling. Previous studies have quantitatively characterized the positive impact of such devices, showing that FSTDs, or more specifically, Flight Training Device (FTD) level simulators for general aviation training, typically reduce the number of trials required for pilots to achieve proficiency in aviation classwork tasks [6] and demonstrate a significant degree of effective transfer for many studied in-flight tasks [7]. To ensure simulation fidelity, regulatory bodies establish objective accuracy standards for these devices. In the United States, the Federal Aviation

Administration's (FAA) Title 14 Code of Federal Regulations Part 60 [8] defines these requirements, with similar frameworks established internationally by the European Aviation Safety Agency Certification Specification CS-FSTD(A) [9] and Transport Canada Aeroplane and Rotorcraft Simulator Manual [10]. For a model to meet these requirements, it must be capable of reproducing aircraft performance and handling characteristics accurately across a wide range of operating conditions.

Several approaches exist for improving initial aircraft models, with system identification methods and manual tuning being the two most common within the research and industry sectors. While system identification techniques produce high-fidelity aerodynamic models, the method is resource-intensive, requiring extensive instrumentation and post-processing analysis [11, 12, 13]. Alternatively, many models are calibrated in an iterative, "guess and check" manner by a simulation engineer. Although the manual method is widely used in practice, it is not well documented in academic literature, and multiple works by Morelli highlight limitations. In one paper, Morelli mentions that updates to simulation databases are often time-consuming and iterative and executed "in an ad hoc way" [14]. In another work, they advocate for an automatic, systematic update of model databases by highlighting two crucial drawbacks of the system identification and manual tuning methods: both approaches (1) require a large time commitment from a human analyst with good judgment and (2) may work well for the targeted maneuver but translate poorly to the wider flight envelope [15].

These limitations motivate the development of a systematic, automated approach to calibration that is able to satisfy prescribed accuracy metrics. This research outlines an efficient approach for calibration of general aviation flight simulation models to available validation data, adjusting model parameters to satisfy prescribed accuracy requirements, with application demonstrated in the context of FAA Part 60 Level 5 FTD qualification standards.

1.2 Literature Review

1.2.1 Related Work in Aircraft Simulation Model Development and Calibration

Several works have explored the development of automated approaches for improving the accuracy of flight simulation models. Although many studies address the same fundamental gap in model development and calibration, they differ in their intended applications and validation standards. An important distinction exists between methods that construct aerodynamic models directly from flight test data and methods that calibrate an existing baseline model to available validation data. The former is an example of system identification technique application, known as parameter identification, and treats flight data as the source from which the model itself is built. Classical aircraft system identification foundations – such as output-error, equation-error, and maximum likelihood parameter estimation methods – are presented in detail in texts by Jategaonkar [12] and Morelli and Klein [13]. Specific applications of these foundations are spread widely throughout literature. Morelli and Grauer provide a comprehensive survey of recent advances in system identification techniques used at NASA Langley Research Center including frequency-domain modeling techniques, real-time autonomous global aerodynamic modeling, and rapid simulation development and updates using flight test data [11]. These methods produce high-fidelity aerodynamic databases for simulation models applied across a wide range of aircraft, but require extensively instrumented flight tests with carefully designed excitation inputs even for adoption for simpler, smaller aircraft classes like general aviation [16]. These resources are rarely available to an engineer developing general aviation models, where Pilot Operating Handbook (POH) performance charts and limited flight test data packages are the typical sources of information and validation. Therefore, this work falls within the calibration methodology category where manufacturer or flight test data is treated as a validation target against which an existing model is refined.

Several publications present approaches to calibration methodology of existing flight simulation models. Morelli and Ward present an automated method that aims to modify wind-tunnel-derived aerodynamic databases based on real-world flight test data [15]; while Brian and Morelli extend this work to automatic application to models during real-time simulations [17]. Their approach blends the baseline aerodynamic data with flight measurement data through statistical weighting and utilizes a blending model ensuring the updates are applied only for regions of the flight envelope directly supported by the flight test data. Three conceptual similarities exist between their work and the proposed methodology: both approaches acknowledge that (1) there should exist a reasonable baseline model, (2) real-world validation data should update that reasonable baseline model, not replace it, and (3) the process should be automated and not manual.

Differences arise in the application and verification of the methods. Their approach is designed for application to updating high-fidelity aerodynamic databases derived from wind-tunnel testing, typically for aircraft with extensive flight test datasets. The method presented in this work targets general aviation models created with a combination of semi-empirical estimations for aerodynamic lifting surfaces, basic load coefficient lookup tables for non-lifting surfaces, manufacturer operating handbook data for propulsion models, and blade element analysis for propeller models, with a more limited set of available validation data. Additionally, the verification spaces of both approaches differ fundamentally. Their method updates aerodynamic coefficients and validates against coefficients derived directly from the available flight test data, while the method presented in this work targets matching performance metrics available in the aircraft's POH and flight test data. Finally, the methods differ in their handling of propulsion modeling. Morelli and Ward's method treats propulsion forces, or thrust, as a known input and applies the calibration routine to the aerodynamics database exclusively. The presented work treats the propulsion, propeller, and aerodynamic models as a coupled problem where parameters must be adjusted within each to meet validation metrics.

Two additional works, focused on complex aircraft types, independently reinforce the shared motivation against manual calibration of coupled aero-propulsion models. Deiler presents a physics-based process for updating aerodynamic and engine thrust models of an Airbus A320neo using a large database of routine operational flight recordings for the purpose of optimizing autopilot descent guidance [18]. Rather than a dedicated flight test campaign package, the method utilizes a database of 844 commercial flights (recorded at 50 Hz producing roughly 55.5 million data points) to adjust lift and drag coefficients and engine thrust predictions using a least-squares algorithm. Notably, dynamic damping behavior is explicitly excluded from the calibration and is noted as irrelevant to their need of flight performance prediction where only steady-state force balances are essential. In a similar application case, Thacker and Blaesser present a multidisciplinary optimization framework for simultaneous calibration of airframe and engine models of a Boeing 737 MAX 8 to publicly available payload-range and fuel flow data using a particle swarm optimization algorithm within the OpenMDAO [19] framework [20]. Their work is explicitly motivated by the inefficiencies of manual calibration processes for which they described their process as highly iterative, requiring the model to be passed between propulsion and aerodynamic calibration teams until model convergence to an acceptable fidelity. Both Deiler and Thacker and Blaesser's works demonstrate that an automated coupled aero-propulsion calibration is desired across several flight simulation disciplines, spanning fidelity levels and aircraft types. However their work differs from the approach presented in this thesis at the point of accuracy standards and validation approaches. These methods only require steady-state performance matches and do not address the desire for the calibrated model to reproduce dynamic behavior with a real or simulated pilot or control system in the loop.

Despite the success of these automated calibration methods for their intended applications, a gap remains for an automated coupled aerodynamic-propulsion-propeller calibration method specifically applicable to general aviation flight simulation models built from physics-based methods and limited available validation data.

Puranik et al. introduced an automated calibration framework that begins to address this gap by presenting an automated framework for calibrating general aviation performance models against the aircraft's POH performance charts and available flight test data, obtained from the data logs of Garmin G1000-equipped aircraft for use in safety analysis [21, 22]. The authors present a two-level framework, similar to the method in the proposed calibration framework, with the first level focusing on performance metrics from the aircraft's POH and the second level incorporating flight test data. The second stage is calibrated to match the specific total energy rate (STER), derived from accelerations and velocities from the flight test data, with the thrust–drag balance and velocity predicted by the simulation model. Their framework is demonstrated with two general aviation aircraft models, the Cessna 172 and Piper Archer, and shows good predictive capabilities for retrospective safety analysis applications such as flap position inference using scalar energy metric values. The approach shares similarities with the presented study for which both approaches (1) use a two-level calibration structure, (2) calibrate a coupled aerodynamic-propulsion-propeller model, (3) focus on general aviation aircraft, (4) use optimization algorithms to modify model characteristics, and (5) treat the baseline model as a valid model that validation data should refine and not overwrite. The two methods also share similarities in their aerodynamic, propulsion, and propeller model parameterization strategies.

Though the studies show several similarities, important differences arise in intended execution, application, and validation of the methods. Puranik's work targets retrospective and predictive safety analysis for general aviation aircraft, defining model accuracy using the STER derived from low-sampled flight recorder data. The methodology presented here targets a different accuracy standard, matching instrumented flight test data within objective performance and dynamic behavior tolerances, including pitch attitudes, control surface deflections, and dynamic response characteristics. The data sources also differ, where Puranik's framework calibrates against low-sampled Garmin G1000 flight data recordings, while the approach proposed in this work drives a six-degree-of-freedom (6-DOF) simulation through

time-domain trajectories flown during instrumented test flights, enabling direct comparison of dynamic rates, control surface deflections, aircraft attitudes, and other time-history response characteristics. Finally, Puranik's first-level calibration to flight test data outputs a Pareto-optimal set of candidate models using a genetic algorithm, while the proposed calibration framework produces a single calibrated model using a gradient-based, least squares optimizer.

Puranik's method is validated in their publications to be a viable option for retrospective safety analysis of general aviation flights, showing successful flap position inference for Cessna 172 and Piper Archer flights. Although promising results are presented, a gap remains for methods specifically designed to calibrate general aviation flight simulation models to meet objective performance and dynamic behavior tolerances derived from available validation data.

Despite differences in intended application and validation strategies of previous work, many conceptual foundations are shared with the presented research. The studies share the assumptions that a reasonable initial model exists, the available validation data should refine that initial model and not replace, and an automated approach is desired. These assumptions form a common philosophy that is foundational to the method presented in this thesis. The key distinction between the presented approach and all prior work is the definition of accuracy that motivates the calibration. Each prior study defines their output model as "good enough" in terms of its targeted application such as aerodynamic coefficient recovery for simulation database updates, steady-state performance prediction for operational big data calibration and emissions assessment, and scalar energy metric matching for safety inference. The present work targets a different standard of "good enough": the flight simulation model must reproduce aircraft performance – in conditions such as climb and cruise – while also matching aircraft attitudes, control surface deflections, and dynamic response characteristics within defined objective tolerances. This is necessary to ensure the pilot or control system in the loop experiences accurate aircraft behavior in real-time.

1.2.2 Development of the Proposed Calibration Framework

In addition to the external work relating to automated calibration methodologies, intermediate stages in the development of the proposed calibration approach have been presented in conference publications throughout the course of the thesis. The first published iteration of the method included only the first stage of the approach, in which Cessna 172 Skyhawk and Cirrus SR20 flight simulation models were calibrated to their respective POH performance charts [23]. Additionally, this version of the method was exercised in an additional conference proceeding in which Diamond DA40 and DA42 aircraft models were calibrated for use in a hybrid-electric aircraft study [24]. The iteration utilized a basic parameterization of aerodynamic, propulsion, and propeller characteristics, optimized using a MATLAB-native constrained non-linear multi-variable optimization algorithm, `fmincon` [25].

These works demonstrated that the basic foundation of the methodology was viable, showing good steady-state performance agreement with POH climb and cruise charts. Despite these promising results, the first iteration highlighted aspects of the approach requiring further refinement, such as slow optimization times and flight-condition-dependent optimized parameters, such as output power factor dependencies on velocity.

The second published iteration of the method addressed these refinement points, introducing a more-flexible parameterization of aerodynamic, propulsion, and propeller models, reducing optimization times, and eliminating flight-condition-dependent optimized parameters [26]. This work focuses on calibration of the Cessna 172 model with a more robust calibration to POH performance charts and an initial implementation of the calibration to flight test data, primarily focusing on steady-state conditions of climb and cruise. However, while the second iteration incorporated an initial implementation of calibration to flight test data, the approach was still primarily focused on steady-state performance metrics and did not yet address calibration to dynamic response characteristics required for simulator qualification.

The work presented in this thesis builds upon these earlier iterations of the calibration framework by extending the methodology to include full calibration to flight test data, including aircraft attitude, control surface deflections, and dynamic response characteristics. With these additions, the proposed methodology enables a complete automated calibration of general aviation flight simulation models, demonstrated in the context of FTD-level simulation devices.

1.3 Contributions

This work outlines an automated calibration methodology for general aviation flight simulation models capable of matching available validation data, including POH performance charts and flight test data, within regulated accuracy tolerances through optimization-based parameter adjustment. The approach treats the aerodynamic, propulsion, and propeller models as a coupled system, adjusting parameters across all three domains to produce acceptable simulated aircraft performance.

The first stage of the calibration matches steady-state climb and cruise performance to POH performance charts. This stage is computationally efficient, producing a single set of optimized parameters in a matter of minutes. Multiple MATLAB-native nonlinear optimization algorithms were evaluated, with the final selection based on a balance of speed and calibration accuracy as described in Section 3.1.2. This stage enables the development of a reasonable simulation model using manufacturer performance data alone when flight test data is not available.

The second stage of the calibration treats the results of the first stage as a starting point and extends the process to calibration against flight test data. This stage enables calibration of aircraft attitudes, control surface deflections, and dynamic response characteristics. The calibration is performed using a time-domain 6-DOF aircraft model driven by flight test trajectories within the Modular Aircraft Dynamics and Control Algorithm Simulation Platform (MADCASP) [27], executed in Simulink. Nonlinear optimization algorithms are

again applied to the time-domain model, targeting agreement with flight test data within prescribed performance tolerances.

The method is demonstrated on a Cessna 172 Skyhawk flight simulation model initially created using the Parametric Energy-based Aircraft Configuration Evaluator (PEACE) aircraft sizing framework [28, 29]. The Cessna 172 model is calibrated to performance charts from the POH [30] and a proprietary flight test dataset provided by Frasca International, Inc. The final calibrated model produces simulated aircraft performance within the tolerances prescribed for an FAA Level 5 FTD simulation, defined as a device with aerodynamic programming sufficient to represent an aircraft [8], with selected supplemental tests derived from Level 6 and 7 qualification objective tests. The results are summarized within the paper's body, and a full report of objective test results is included in Appendix C as a complete presentation of the validation results. To provide an initial demonstration of the methodology's generality, the steady-state calibration stage is additionally applied to a Cirrus SR20 flight simulation model and results are presented alongside the Cessna 172 validation.

Overall, the proposed method provides a systematic and automated methodology for refining existing general aviation flight simulation models using both steady-state performance data from the aircraft's manufacturer data and attitude, control surface, and dynamics data from flight test campaigns. With the combination of an efficient baseline calibration routine to POH performance charts and subsequent calibration to time-domain flight test data, the framework provides means for calibration of models to meet objective requirements. The remainder of this thesis describes the formulation of the proposed calibration framework, its implementation, and the results obtained from its application.

1.4 Thesis Organization

The remainder of this thesis is organized into the following chapters. Chapter 2 describes the foundation of the baseline model, introducing the flight simulation modeling framework

and underlying physics model. Chapter 3 outlines the two-stage calibration approach, including parameterization, cost function formulations, and optimization strategies. Chapter 4 presents validation of the method, using a Cessna 172 Skyhawk general aviation aircraft as the platform, including a supplemental steady-state validation case performed on a Cirrus SR20 model. Finally, Chapter 5 presents conclusions, limitations, and suggestions for future work.

Chapter 2

Flight Simulation Model

This chapter outlines the modeling approach for the Cessna 172 flight simulation model on which the proposed method is applied. The model is integrated into MADCASP, a MATLAB/Simulink-based framework developed with funding from National Aeronautics and Space Administration (NASA) Langley Research Center under the Transformational Tools and Technologies (TTT) project [27]. The framework provides a modular environment for modeling aircraft aerodynamics, propulsion, controls, and vehicle dynamics while allowing for integration with control algorithms or external simulation tools, such as visualization engines and hardware controls. Supporting both steady-state trim analysis and time-domain simulation, the framework allows for evaluation of aircraft performance, stability characteristics, and control response.

The MADCASP trim solver treats control surfaces and propulsors as control effectors, identifying optimal trim solutions for given conditions via constrained optimization. The trimming functionality of the framework is used within this project for trimming the aircraft to POH-prescribed steady-state performance conditions and for setting initial trimmed conditions for time-domain trajectories.

The time-domain simulations are executed using the Simulink component of the MADCASP framework. A top-level view of the MADCASP Simulink architecture is included in Figure 2.1. The Controllers block contains proportional-integral-derivative (PID) control logic, emulating pilot or autopilot control action and allocating the commanded control deflections and propulsion levers as appropriate. The Flight Mechanics and Systems Models (FM&S) computes aerodynamic, propulsion, control surface, and propeller dynamics to determine the net forces and moments. The forces and moments are then fed into the Vehicle

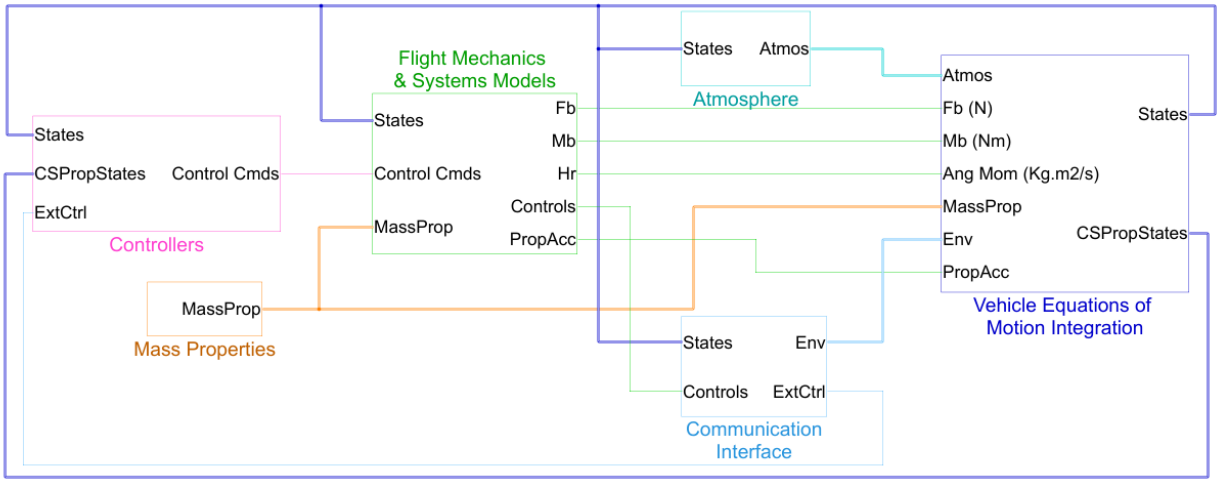

Figure 2.1: Top-level of MADCASP Simulink model

Equations of Motion Integration block, which determines the vehicle states using 6-DOF, rigid body equation of motion. It also outputs crucial information about the vehicle such as body axis velocities (u,v,w), angular velocities (p, q, r), position, and orientation (ϕ, θ, ψ).

The remaining subsystems set up the simulation's environment. The Mass Properties block provides the weight, center of gravity location, and moments of inertia of the aircraft which feed into the equations of motion. The Atmosphere block contains wind models and provides key atmospheric parameters such as density, pressure, and temperature. The Communications Interface allows for interfacing with hardware, external controls, and external visual rendering software, such as X-Plane [31] or FlightGear [32], which can also provide terrain elevation data to the model. The simulation is integrated using a fourth-order Runge-Kutta numerical scheme with a timestep of 1/60 seconds.

The following sections provide an overview of the Cessna 172 Skyhawk aircraft, the application platform, and describe the formulation of the major model components within the simulation, including the geometry, aerodynamic, propulsion, propeller, and controls models.

2.1 Aircraft Overview

The Cessna 172 Skyhawk was selected as the representative platform for this thesis due to its widespread use in flight training. Since its introduction in 1956, more than 44,000 aircraft have been produced [33], making it one of the most widely used general aviation aircraft worldwide.

Table 2.1: Key parameters of the Cessna 172 Skyhawk [30]

Parameter	**Value**
Length	27 ft 2 in
Height	8 ft 11 in
Wing Span	36 ft 1 in
Wing Area	174 ft^2
Maximum Takeoff Gross Weight	2,550 lb
Maximum Landing Weight	2,550 lb
Standard Empty Weight	1,663 lb
Wing Loading	14.7 lb/ft^2
Power Loading	14.2 lb/hp
Engine Rating	180 HP @ 2700 RPM

The Skyhawk is a single-engine general aviation aircraft used primarily for flight training and personal transportation. The aircraft is equipped by a fuel-injected Lycoming IO-360-L2A internal combustion engine rated at 180 HP at 2700 RPM and a two-bladed, constant-pitch 76 inch McCauley propeller. A summary of key aircraft parameters from the POH is provided in Table 2.1 [30]. The flight test data used for the time-domain calibration stage was gathered by Frasca International on a Cessna 172SP aircraft [1].

2.2 Aircraft Geometry and Mass Properties Model

The geometry and mass properties of the Cessna 172 Skyhawk model were generated using the PEACE [28, 29] framework. PEACE was developed as an energy-based vehicle

[1] Frasca International's *Flight Test Report for the Cessna 172SP* is proprietary and not made accessible to the public.

sizing framework applicable to evaluating novel vehicle configurations and propulsion architectures. In the case of a known aircraft configuration, information from the manufacturer's documentation can treated as input into the framework, allowing generation of a parametric geometry model and component weight estimates, based on historical data. The framework also creates of a MADCASP-compatible MATLAB data structure with vehicle information required for simulation. The converged model's geometry is included in Figure 2.2. The large blue dot within the fuselage displays the converged center of gravity location.

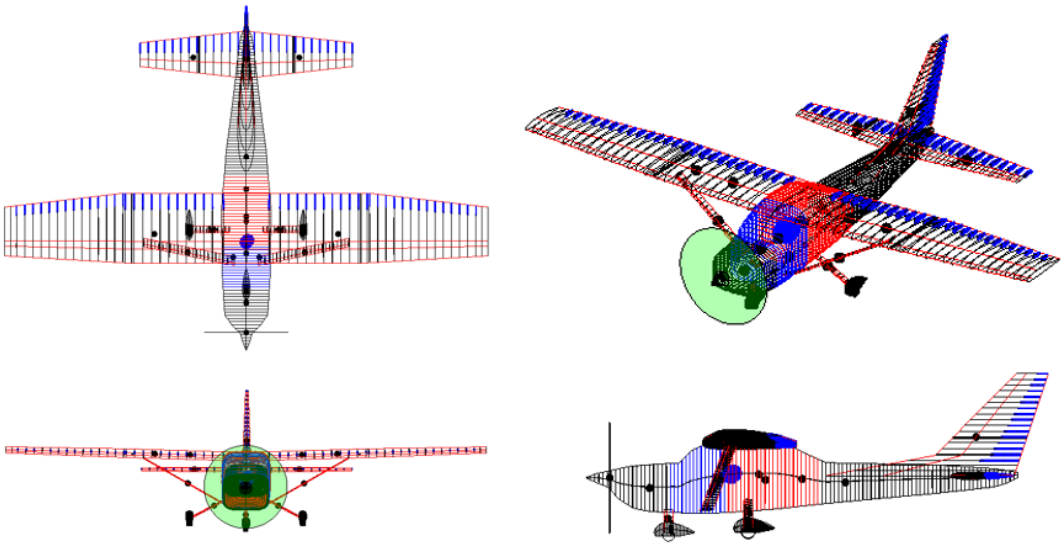

Figure 2.2: Cessna 172 Skyhawk PEACE geometry model [23, 26]

PEACE also offers estimates for mass properties of the vehicle including center of gravity and moments of inertia from the historical weight build up methods. In this project, those values are overwritten during the entirety of the calibration routine. During the calibration to POH data, the weight is taken from the performance chart conditions and a center of gravity is chosen from the aircraft's allowable envelope. During the time-domain stage, center of gravity location is available in flight test data and is set in the model.

Moments of inertia do not influence steady-state trim solutions because trim corresponds to an equilibrium condition with zero angular acceleration. Therefore, the moments of inertia

are irrelevant for trimmed, steady-state performance points. For time-domain simulation, the moments of inertia of the aircraft are estimated from historical data using Equations 2.1-2.3.

$$I_{xx} = \frac{b^2 W \bar{R}_x^2}{4g} \tag{2.1}$$

$$I_{yy} = \frac{L^2 W \bar{R}_y^2}{4g} \tag{2.2}$$

$$I_{zz} = \left(\frac{b+L}{2}\right) \frac{W \bar{R}_z^2}{4g} \tag{2.3}$$

where I_{xx}, I_{yy}, and I_{zz} are the moments of inertia about the principal axes, W is the weight of the aircraft, b is the wingspan, L is the overall length of the aircraft, g is the gravitational constant, and $\bar{R}_x, \bar{R}_y$, and $\bar{R}_z$ are the non-dimensional radii of gyration about the principal axes. Values for the non-dimensional radii of gyration are taken as $\bar{R}_x = 0.25$, $\bar{R}_y = 0.38$, and $\bar{R}_z = 0.39$ as adopted from historical data of single-engine prop-driven aircraft [34].

2.3 Aerodynamics Model

2.3.1 Modeling of Lifting Surfaces

A strip theory-based aerodynamic modeling approach is adopted for lifting surfaces, wings, horizontal tail, and vertical tail, on the aircraft as described by Kunwar [35]. In strip theory, the lifting surfaces are discretized into spanwise strips as shown in Figure 2.3. For each strip, sectional aerodynamic characteristics, coefficients of lift (c_l), drag (c_d), and pitching moment (c_m), are queried as a function of the effective angle of attack, α_{eff}, at each strip. These lookup tables are generated for each lifting surface using XFOIL [36].

The effective angle of attack experienced by each lifting surface strip is determined using simplified lifting-surface theory assuming symmetrical loading, which provides the spanwise loading (dimensionless circulation) distribution, G, used to generate a simplified model for

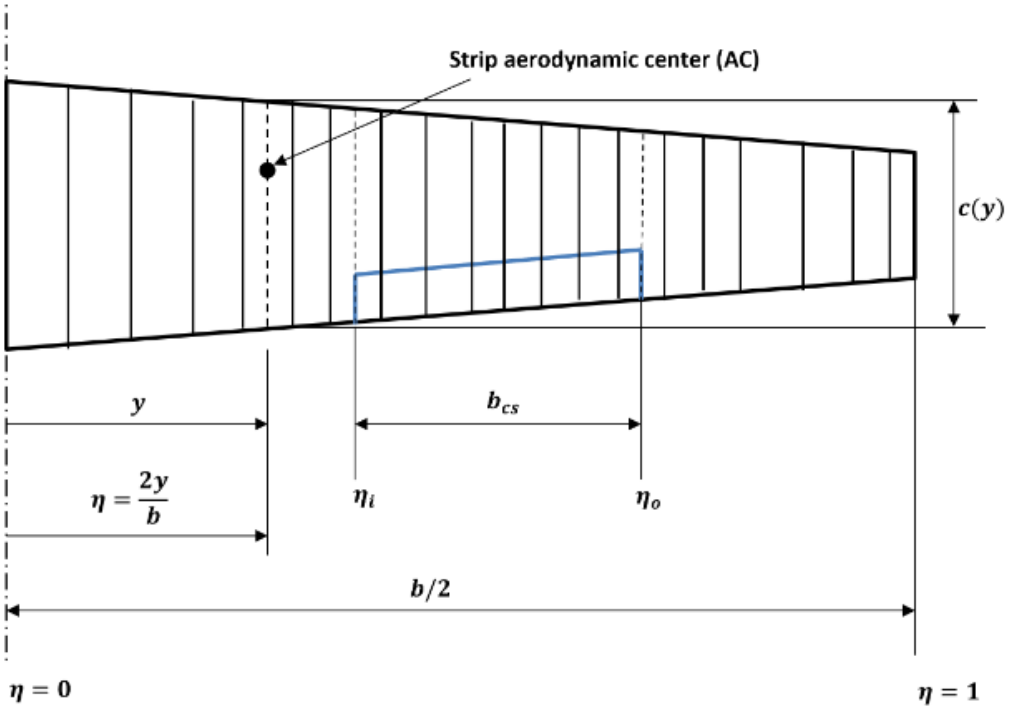

Figure 2.3: Strip theory representation of a lifting surface with a control surface [35]

the downwash distribution over the finite-span wing lifting surface [37]. Using this method, a lifting surface may be treated as a full-chord, full-span flap for which charts of spanwise loading coefficient, G/δ, as a function of lifting surface geometry, airfoil, and operating conditions are available and implemented as gridded interpolants. For a lifting surface, the control surface, δ, is replaced with the geometric angle of attack, α, relative to the zero-lift angle of attack, $\alpha_{C_L=0}$. The loading coefficient of the lifting surface lookup function can be defined as written in Equation 2.4 which is queried at the aerodynamic center at the mid-section of each strip.

$$\frac{G}{\alpha} = f\left(\eta, \frac{\beta A}{k}, \Lambda_\beta, \lambda\right) \tag{2.4}$$

where η is the dimensionless lateral coordinate of the strip's mid-section, β is a compressibility parameter, k is the ratio of the sectional lift-curve slope to $\frac{2\pi}{\beta}$ at the operating Mach

number, A is the wing aspect ratio, Λ_β is a surface sweep parameter which accounts for compressibility, and λ is the wing taper ratio.

After querying the loading coefficient, the geometric angle of attack is used to determine the spanwise loading as in Equation 2.5.

$$G = \frac{G}{\alpha}\alpha \tag{2.5}$$

The spanwise loading, along with lifting surface span and free-stream velocity, V_∞, is then used to calculate the circulation distribution, Γ, via Equation 2.6.

$$\Gamma = \frac{G}{bV_\infty} \tag{2.6}$$

Prandtl's lifting-line theory is used to obtain the induced angle of attack, α_i, for each strip with lateral coordinate y_0 and free-stream velocity V_∞ by summing the effect of circulation gradient due to all other strips as shown in Equation 2.7 [38].

$$\alpha_i(y_0) = \frac{1}{4\pi}\int_{-b/2}^{b/2} \frac{1}{V_\infty(y_0)} \frac{d\Gamma/dy}{y_0 - y} dy \tag{2.7}$$

After obtaining the induced angle of attack, the effective angle of attack for each lifting surface strip can be taken as

$$\alpha_{eff} = \alpha - \alpha_i \tag{2.8}$$

and used to query the sectional aerodynamic tables for coefficients of lift (c_l), drag (c_d), and pitching moment (c_m). Figure 2.4 geometrically defines the different angle of attacks for a lifting surface strip and shows the aerodynamic coefficient decomposition as an effect of downwash where $c_{l,w}$ is the coefficient of lift in the wind axes, $c_{d,0}$ is the parasitic drag component, $c_{d,i}$ is the induced drag component, and w is the downwash velocity.

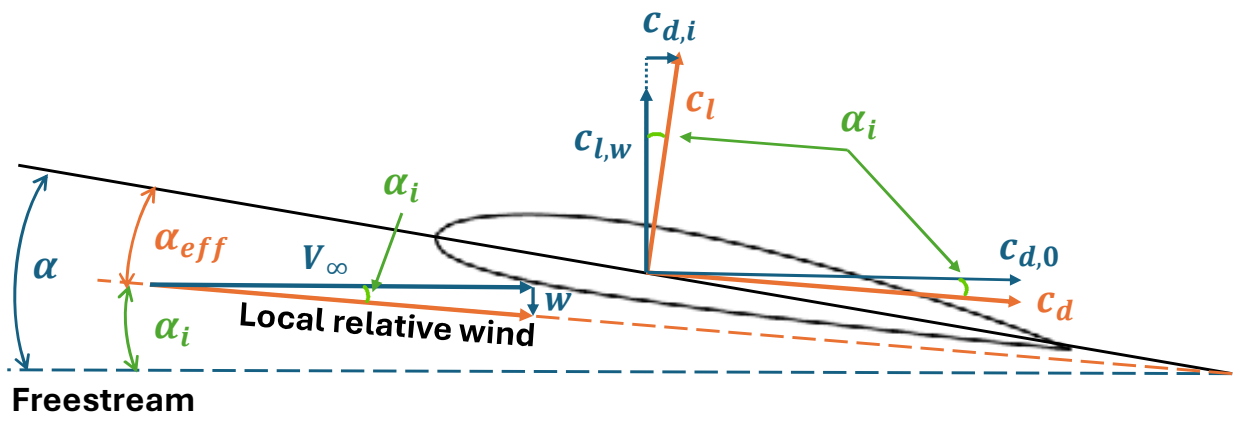

Figure 2.4: Downwash and decomposition of lift and drag coefficients on a lifting surface strip (adapted from [23, 26])

2.3.2 Modeling of Wing Downwash on the Horizontal Tail

To account for the downwash experienced by the horizontal tail due to the wings, the downwash angle, ϵ, is queried from estimation tables [34] adapted from USAF (United States Air Force) Stability and Control DATCOM (Data Compendium) [3], originally presented by Decker [39], as a function of the wing's angle of attack. Equations 2.4 - 2.8 are used for the horizontal tail sectional aerodynamic calculations, with modification of the geometric angle of attack by the downwash angle, $\alpha_{HT} = \alpha - \epsilon$. The modified horizontal tail angle of attack is substituted for α in Equations 2.5 and 2.8.

2.3.3 Modeling of Control Surfaces

Aerodynamic effects of control surfaces are modeled based on the change in spanwise loading, G, due to deflection, δ, assuming anti-symmetrical span loading [41]. All control surfaces – flaps, ailerons, elevators, and rudder – are treated identically. Similarly to Equation 2.4, the span-loading coefficient due to control surface deflection, G/δ, is taken as

$$\frac{G}{\delta} = f\left(\eta, \frac{\beta A}{k}, \Lambda_\beta, \lambda, \eta_{CS}\right) \tag{2.9}$$

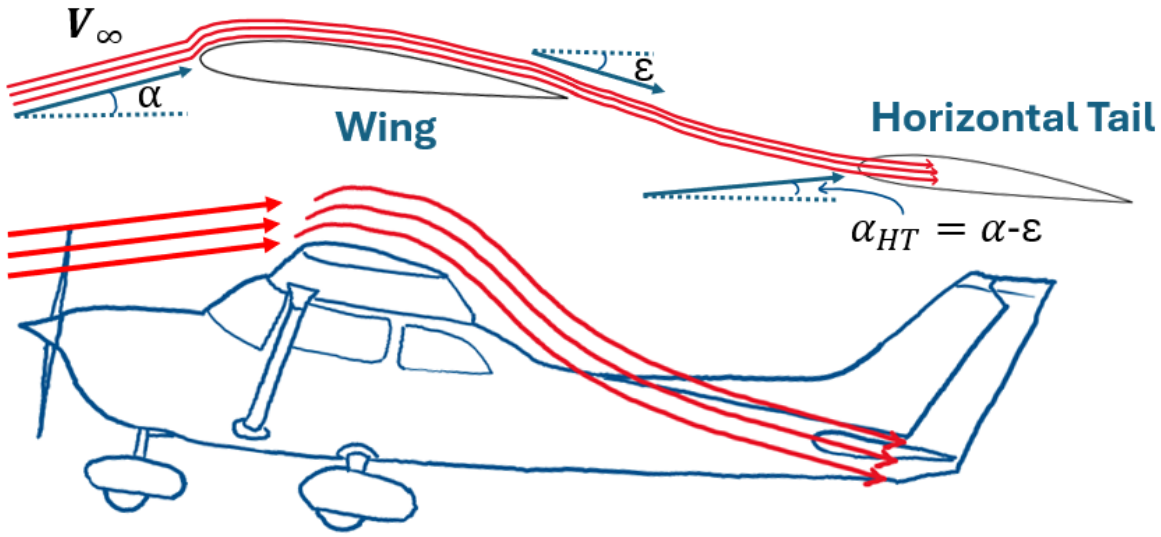

Figure 2.5: Effect of wing downwash on the horizontal tail (adapted from [40])

where η_{CS} is a term introduced to capture the effect of control surface position between the inboard and outboard stations of the parent lifting surface.

The span-loading coefficient is then used to calculate the additional lift coefficient due to the control surface deflection as

$$\Delta c_l = \frac{2b}{c}\frac{G}{\delta}\alpha_\delta \delta \tag{2.10}$$

where b is the span of the parent lifting surface, c is the control surface's chord distribution over its span, and α_δ is an empirical correction of lift effectiveness as a function of deflection and chord ratio, $\alpha_\delta = f(\delta, c_{CS}/c_{PLS})$, where c_{CS} is the control surface's chord and c_{PLS} is the chord of the parent lifting surface [3]. Spanwise loading is additive therefore Δc_l due to the control surface deflection is added to the lift distribution of the parent surface.

The additional drag due to control surface deflection is also considered. The component of Δc_l along the freestream produces the additional induced drag. The additional profile drag coefficient, $\Delta c_{d,0}$, is calculated as

$$\Delta c_{d,0} = f(\delta, c_{CS}/c_{PLS}) K_{\Delta c_{d,0}} \tag{2.11}$$

where $f(\delta, c_{CS}/c_{PLS})$ is a lookup table queried as a function of control surface chord fraction and deflection and $K_{\Delta c_{d,0}}$ is an empirical correction factor [3].

2.3.4 Modeling Non-lifting Surfaces

Aerodynamic coefficients of the non-lifting surfaces of the aircraft, such as landing gear and fuselage, are queried from gridded interpolants as a function of angle of attack, α, and sideslip angle, β. These gridded interpolants are created by evaluating the full geometry in FlightStream® [42] over a range of angle of attack and sideslip angles. The gridded interpolants output coefficients of axial (C_X), lateral (C_Y), and normal (C_Z) force along with rolling ($C_{M,x}$), pitching ($C_{M,y}$), and yawing ($C_{M,z}$) moment coefficients. After dimensionalization, these forces and moments are added to the lifting surface force and moments to produce the total aerodynamic forces and moments acting on the aircraft.

2.4 Propeller Model

Propeller design and analysis tools QMIL [43] and QPROP [44] are utilized for creating a propeller model. First, QMIL designs propeller blades by computing blade chord and twist distributions along the blade's span, optimizing for minimum induced loss conditions, or MIL. The tool requires inputs of blade airfoil sectional data (obtained using XFOIL [36]), number of blades, propeller diameter, design lift coefficient, operating altitude, propeller speed (RPM), and either thrust or power requirements. When creating a model for the Cessna 172, the propeller is designed to be most efficient in cruise conditions while maintaining climb capabilities.

QPROP then tests the QMIL-designed propeller geometry over a range of off-design cases at combinations of freestream velocities, RPMs, and blade pitches. The program outputs thrust and torque coefficient, C_T and C_Q, curves as a function of advance ratio, J, and blade pitch at 75% radial station, β_P, which are implemented in the flight simulation

model as gridded interpolants. These coefficients may then be dimensionalized and added to the overall forces and moments acting on the aircraft.

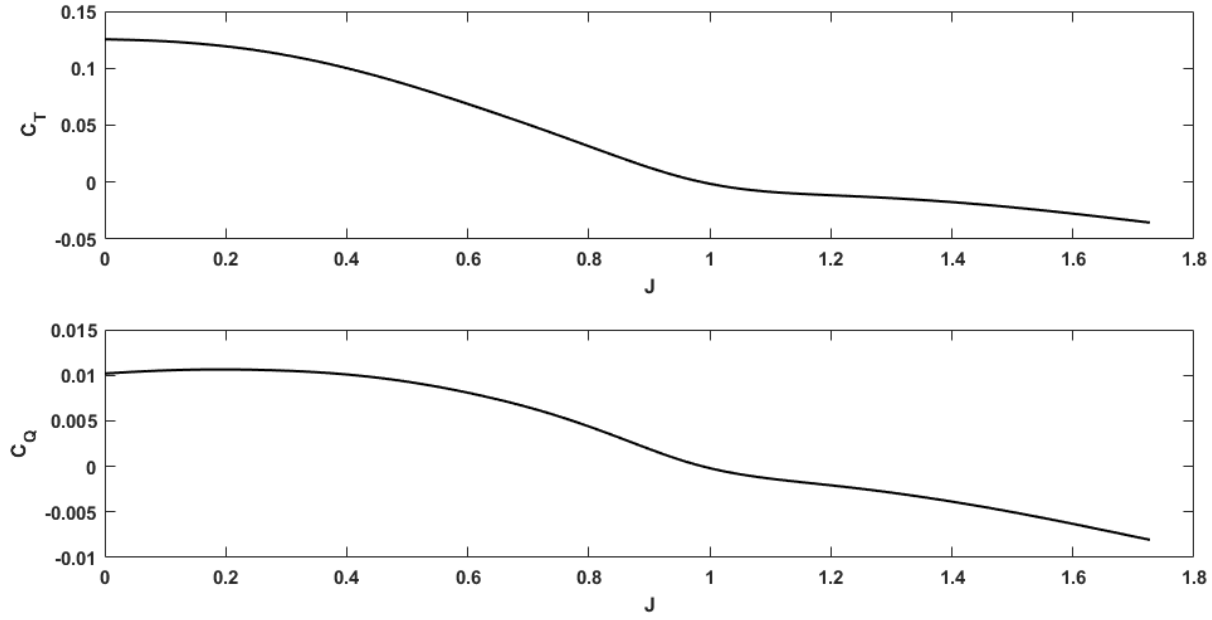

Figure 2.6: Coefficient of thrust and torque curves generated by QPROP for the Cessna 172 Skyhawk's propeller

For the Cessna 172, which is equipped with a fixed-pitch propeller, the coefficient queries become only a function of advance ratio with a set blade pitch. Using information obtained from the McCauley propeller operator's manual, the blade pitch of the 1A170E/JHA7660 model propeller (as equipped per the Cessna 172 Skyhawk POH [30]) at 75% radius is determined as approximately $\beta_P = 18.5°$. This was calculated using the McCauley propeller naming convention [45] where the final four numbers of the model identifier represent the propeller diameter (in inches) and the inches of geometric pitch at 75% radius. Therefore, it is gathered that the installed propeller is 76 inches in diameter with 60 inches of geometric pitch at the 75% radial position. The blade pitch at the 75% radial position can then be found as

$$\beta_P = tan^{-1}\left(\frac{P_{75\%}}{C_{75\%}}\right) \tag{2.12}$$

where $P_{75\%}$ is the geometric pitch at 75% radial position in inches and $C_{75\%}$ is the circumference of the propeller at 75% radial position in inches. Figure 2.6 shows the smoothed thrust and torque coefficient curves generated by QPROP as a function of advance ratio at a set $\beta_P = 18.5°$.

2.5 Propulsion Model

The piston engine performance model is implemented using data available in the engine operator's manual, specifically for the Lycoming IO-360-L2A [46], rated for 180 horsepower at 2,700 RPM, for the Cessna 172 model. All information required for the output power modeling can be obtained from the standard sea level and altitude performance charts regularly included in piston engine manuals. These charts are digitized and implemented in the model as gridded interpolants. The output power is modeled using the following interpolation steps.

First, the maximum manifold pressure (MAP) , MAP_{max}, is queried as a function of pressure altitude and RPM, $MAP_{max} = f(ALT, RPM)$, which corresponds to a fully open throttle setting. The minimum MAP, MAP_{min}, is estimated within the model and corresponds to the manifold pressure with a fully closed throttle. The actual MAP at the given conditions and normalized throttle setting, δ_t, is then taken as

$$MAP = MAP_{min} + (MAP_{max} - MAP_{min})\delta_t \tag{2.13}$$

The throttle position can be mapped to model non-linear throttle valves, for example, a butterfly valve could be simply modeled as, $\delta_t = \sin(90° \times \delta_{t_{act}})$, where $\delta_{t_{act}}$ is the actual normalized throttle position based on physical position of the throttle lever.

Next, the normalized sea-level power output at best power mixture, HP_{SL}, is queried as a function of MAP and RPM from the sea-level performance chart. Additionally, the intersection point of MAP and RPM is identified on the altitude performance chart and its corresponding normalized power, HP_A, and corresponding pressure altitude, ALT_A, at best

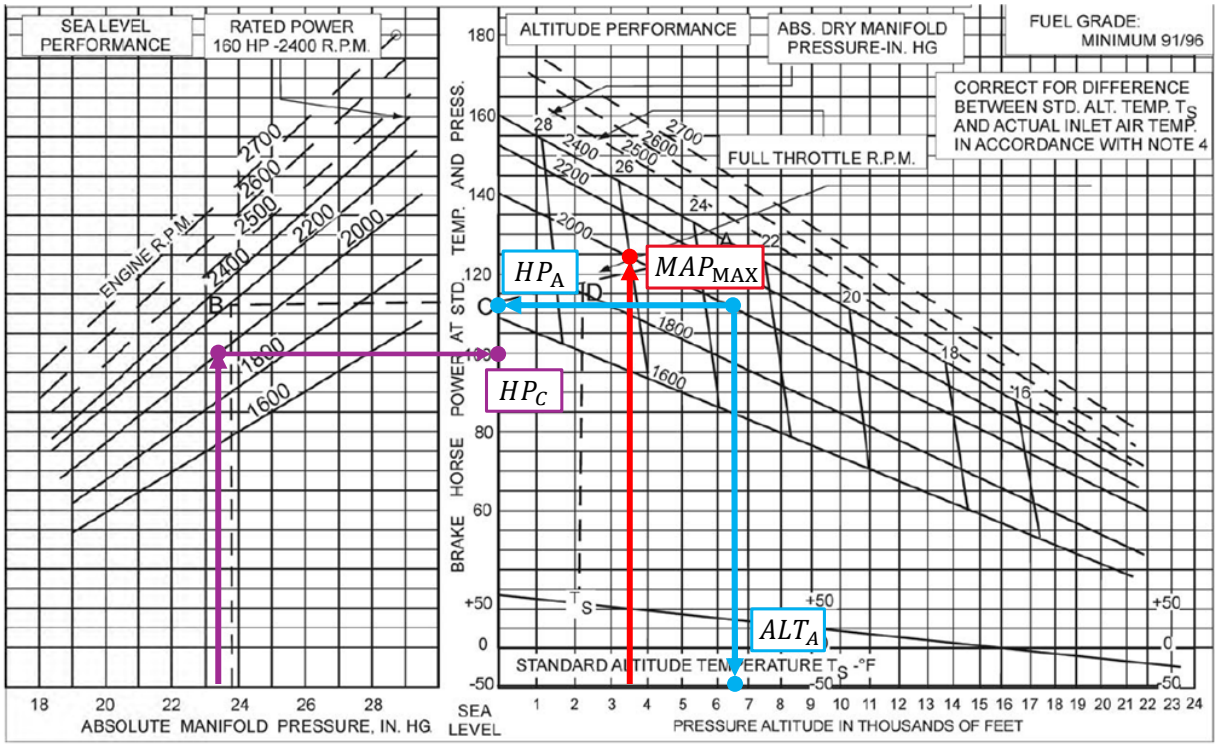

Figure 2.7: Engine performance parameter identification from IO-360-L2A performance charts [46]

power mixture is queried. The values are interpolated to find the normalized power at best power mixture, $HP_{ALT_{BPM}}$ at actual pressure altitude, ALT_{act} using Equation 2.14.

$$HP_{ALT_{BPM}} = HP_{SL} + ALT_{act}\left(\frac{HP_A - HP_{SL}}{ALT_A - 0}\right) \tag{2.14}$$

Figure 2.7 shows how the required values are identified on the engine's performance chart for a given operating point (3,500 ft, 2,000 RPM and $\delta_t = 0.9$). This value is then corrected by a provided factor as a function of actual temperature by $\sqrt{T_S/T}$, where T_S is the standard temperature at the pressure altitude and T is the actual temperature at the operating condition, where the temperatures are represented in Rankine.

Finally, the output power is corrected by mixture lever position and scaled by the engine's power rating, HP_{rated}. The fuel to air mixture, F/A, is found as a simple function of the normalized mixture lever position, δ_m, $F/A = 0.1\delta_m$. The mixture correction factor

or power factor, PF, is queried as a function of fuel to air ratio from a digitized lookup table [1]. The final output power is then expressed as

$$HP = HP_{ALT_{BPM}} \sqrt{\frac{T_S}{T}} (PF)(HP_{rated}) \tag{2.15}$$

Specific fuel consumption (SFC) is determined in a similar manner. The best power SFC is queried from digitized engine manual plots as a function of percent power output and RPM and corrected by a ratio of actual SFC, SFC, to best power SFC, SFC_0, as a function of fuel to air mixture. The actual fuel flow, FF, at the flight condition can be found by multiplying SFC by the output power.

$$FF = HP \times SFC \tag{2.16}$$

2.6 Controls Model

Primary pilot controls — control yoke and pedals — are linearly mapped to control surface deflections — elevator, ailerons, and rudder, respectively, using travel ranges derived from flight test data, the aircraft POH, or maintenance manuals. For example, within the model, $u_{lat} = [-1, +1]$ is mapped to maximum and minimum aileron deflection. Similarly, $u_{long} = [-1, +1]$ is mapped to elevator limits and $u_{dir} = [-1, +1]$ is mapped to rudder limits. These linear mappings are updated within the Cessna 172 model to reflect the real-world control yoke to surface deflection relationships. The modified mappings are shown in Figure 2.8. Table 2.2 lists the maximum and minimum pilot control stick positions for the primary controls and surface deflection limits of the control surfaces derived from flight test control sweeps.

For steady-state trimming in MADCASP, the trimmed control positions are determined via constrained optimization. For time-domain simulations, the control inputs are driven via PID controllers which follow specific parameters, for example, a controller may be activated

Table 2.2: Primary control travels of the Cessna 172 derived from flight test data

Axis Name	**Cockpit Control**	**Cockpit Control Endstops [min, max]**	**Control Surface**	**Control Surface Endstops [min, max]**
Longitudinal	Column	[0", 7"]	Elevator	[-22.15°, 35°]
Lateral	Wheel	[-73°, 80°]	Aileron	[-22.2°, 19.5°]
Directional	Pedals	[19.5", 23.6"]	Rudder	[-17°, 21.4°]

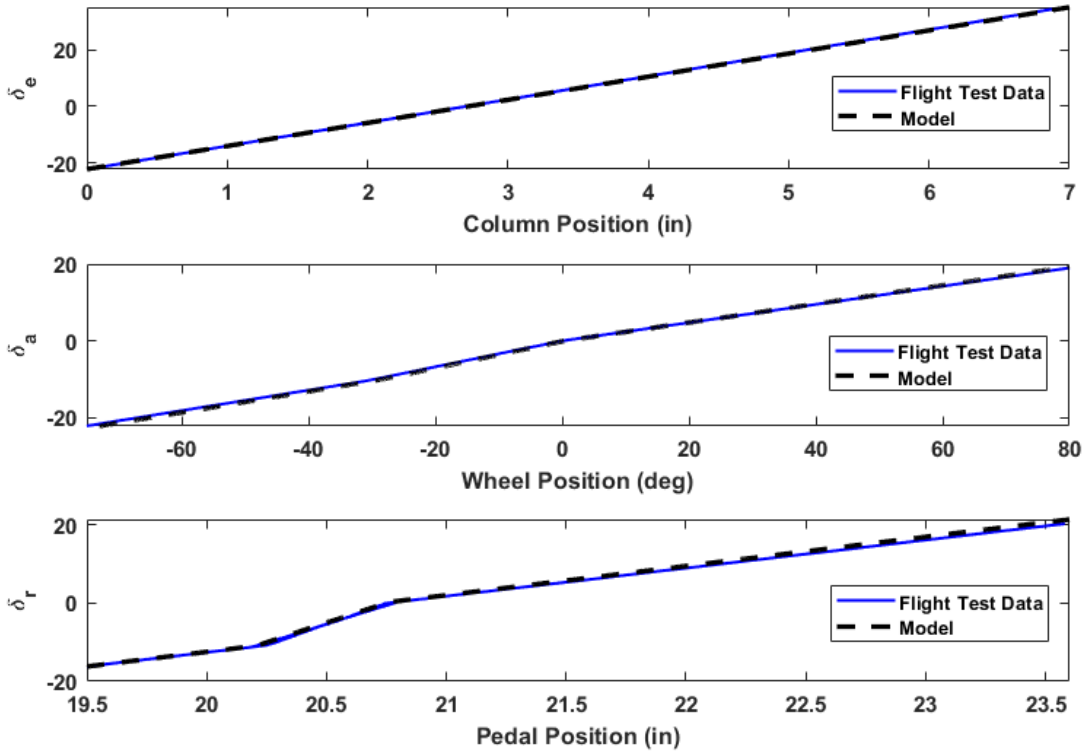

Figure 2.8: Cessna 172 cockpit control position to control surface deflection mapping

that moves the column to match a time history of altitude or the wheel may be driven to meet bank time histories from flight test data. Alternatively, the cockpit controls may be driven to match time histories of the actual pilot control. This mode of control of the time-domain simulation is referred to as "open loop" control mode throughout this study.

Within this control modeling framework, cockpit control and surface deflections are defined via the sign conventions shown in Figure 2.9. Pulling the column aft is defined as a positive control position change which results in a positive elevator deflection, δ_e, with

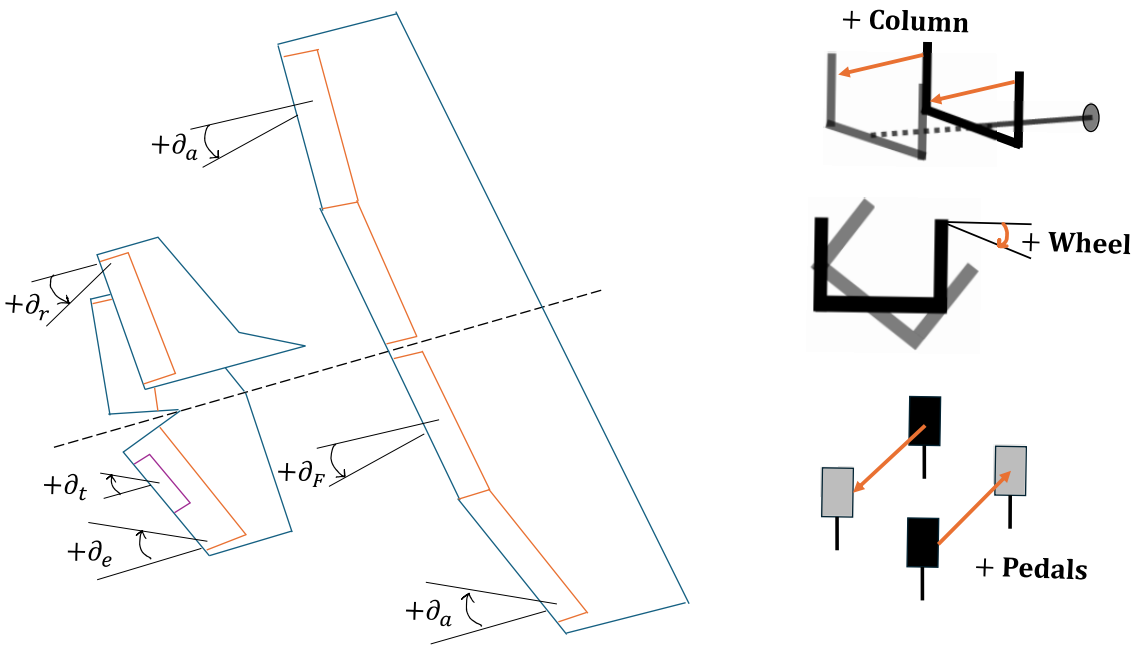

Figure 2.9: Cockpit control and surface deflection sign conventions [26]

trailing edge up and creates a nose-up pitching moment. Deflecting the wheel to the right is defined as a positive control position change which results in a positive aileron deflection, δ_a, with right aileron trailing edge up and creates a rolling moment to the right. Pushing the right pedal forward is defined as a positive control change which results in a positive rudder deflection, δ_r, with the rudder trailing edge to the right resulting in a positive yawing moment to the right.

Secondary controls, including flaps, parking brake, toe brakes, and nosewheel steering are set explicitly. Within the steady-state MADCASP trim routine, only the flaps are accounted for and are set for each trim point. Within time-domain simulations, these secondary controls are driven directly from flight test data time histories.

Together, the aerodynamic, propeller, propulsion, and control models described in this chapter form the physics-based Cessna 172 Skyhawk flight simulation framework implemented within MADCASP. This framework serves as the foundation on which the calibration methodology described in the following chapter is applied.

Chapter 3

Calibration Methodology

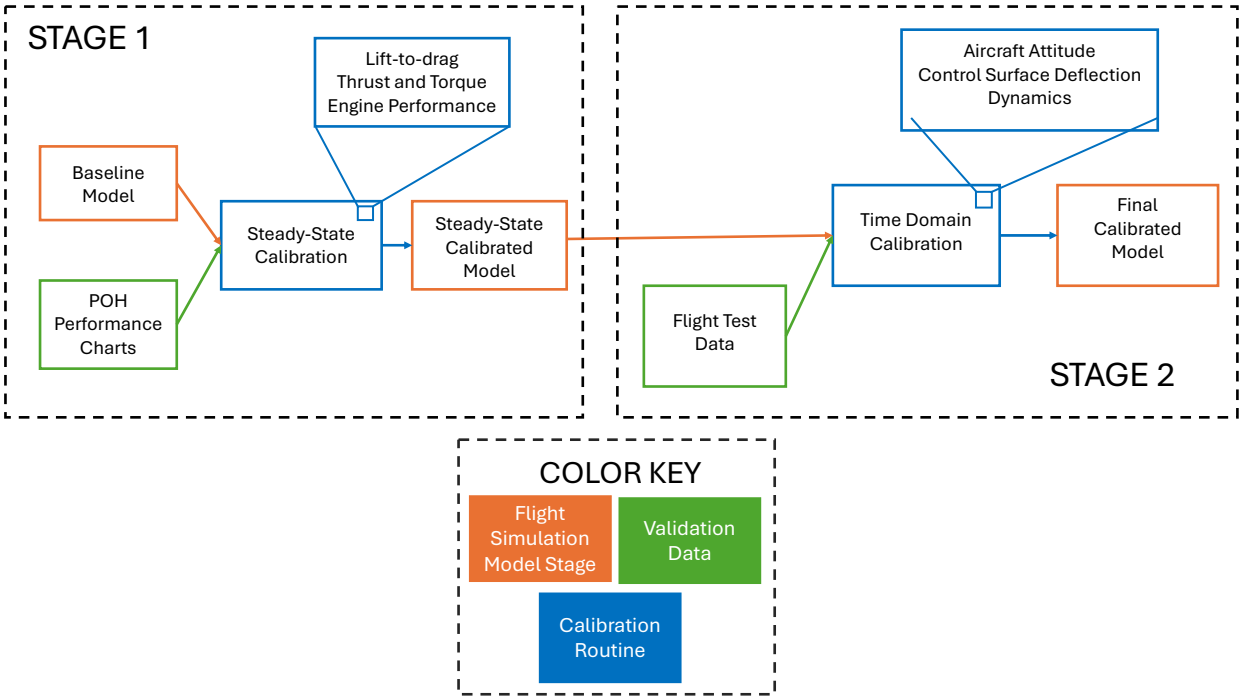

Figure 3.1: Top-level calibration methodology flowchart

The proposed calibration routine consists of two sequential stages. In the first, the "steady-state calibration," aerodynamic, propeller, and propulsion model parameters are adjusted to match steady-state climb and cruise performance data from the aircraft POH. In the second, the "time-domain calibration," the model is further refined to match real-world flight test metrics within prescribed accuracy tolerances, demonstrated here against FAA Part 60 Level 5 FTD requirements [8]. The sequential structure ensures steady-state accuracy is established before dynamic behavior is addressed. The driving tool of both stages

is the non-linear MATLAB least-squares optimization algorithm `lsqnonlin` [47]. The following sections describe the parameterization, cost function formulations, and optimization implementation for each stage.

3.1 Steady-State Calibration

The steady-state calibration targets lift-to-drag ratio, propeller thrust and torque characteristics, and engine performance parameters using climb and cruise performance charts readily available in any general aviation aircraft's operating handbook. The stage is computationally efficient, completing in under eleven minutes for the Cessna 172 validation case and approximately 20 minutes for the Cirrus SR20. The following subsections describe the calibration parameterization, cost function, and a comparison of two candidate optimization algorithms.

3.1.1 Model Parameterization

The aerodynamic and propeller models incorporate fifteen calibration factors allowing flexibility during the optimization routine. Two additional scaling factors are introduced into the propulsion model to match output power and fuel flow values from POH steady-state cruise performance charts. Table 3.1 outlines optimization parameters that are present during the steady-state calibration stage along with their allowable bounds. Parameter bounds are selected to constrain the optimized solution to physically meaningful values. The mathematical representations of the parameters follow.

Aerodynamic Parameterization

Aerodynamic calibration factors are applied at the strip-level lift and drag coefficient level. First, when the sectional lift and drag coefficients, c_l and c_d, are queried from lookup tables as a function of effective angle of attack, α_{eff}, an additive correction, α_{shift}, is applied

Table 3.1: Steady-state calibration optimization parameters and bounds (adapted from [26])

Factor	Model Component	Minimum	Maximum
α_{shift}	Aerodynamics	-4°	4°
$K_{c_{l_{slope}}}$	Aerodynamics	0.7	1.3
$K_{c_{l,0_{offset}}}$	Aerodynamics	-0.3	0.3
$K_{c_{d,0_{slope}}}$	Aerodynamics	0.7	1.3
$K_{c_{d,0_{offset}}}$	Aerodynamics	-0.05	0.05
$K_{c_{d,i}}$	Aerodynamics	0.7	1.3
J_{anchor}	Propeller	0.45	0.75
$K_{C_{T_{shift}}}$	Propeller	-0.1	0.1
$K_{C_{T_{scale}}}$	Propeller	0.8	1.2
$K_{C_{T_{tilt}}}$	Propeller	-0.1	0.1
$K_{C_{T_{quad}}}$	Propeller	-0.2	0.2
$K_{C_{Q_{shift}}}$	Propeller	-0.1	0.1
$K_{C_{Q_{scale}}}$	Propeller	0.8	1.2
$K_{C_{Q_{tilt}}}$	Propeller	-0.1	0.1
$K_{C_{Q_{quad}}}$	Propeller	-0.2	0.2
K_{HP}	Propulsion	0.8	1.2
K_{FF}	Propulsion	0.8	1.2

prior to the table query. This is expressed in Equations 3.1 and 3.2, where $\mathcal{L}_{c_l}$ and $\mathcal{L}_{c_d}$ denote the lift and drag coefficient lookup tables, respectively, and illustrated in Figure 3.2.

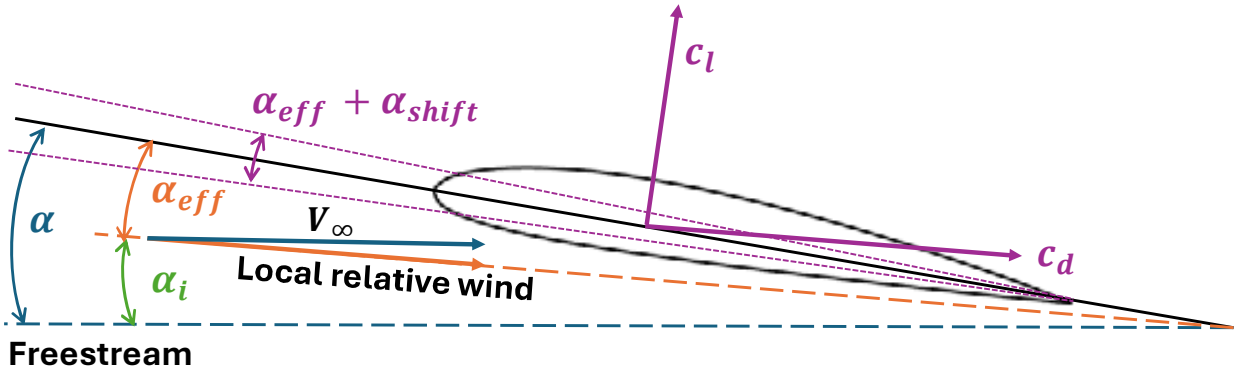

Figure 3.2: Queried wing c_l and c_d as a function of $\alpha_{eff} + \alpha_{shift}$ in local strip wind axes [26]

$$c_l = \mathcal{L}_{c_l}(\alpha_{eff} + \alpha_{shift}) \tag{3.1}$$

$$c_d = \mathcal{L}_{c_d}(\alpha_{eff} + \alpha_{shift}) \tag{3.2}$$

The queried coefficients are defined in the local strip wind axes and must be transformed to the global wind axes using the induced angle of attack, α_i. This transformation allows the separation of induced and parasitic drag components, $c_{d,i}$ and $c_{d,0}$, for independent calibration. The transformations are outlined in Equations 3.3 - 3.5, including the representation of the global wind axes lift coefficient, $c_{l,w}$. Additionally, a visual representation is included in Figure 3.3.

$$c_{d,i} = c_l \sin \alpha_i \tag{3.3}$$

$$c_{d,0} = c_d \cos \alpha_i \tag{3.4}$$

$$c_{l,w} = c_l \cos \alpha_i - c_d \sin \alpha_i \tag{3.5}$$

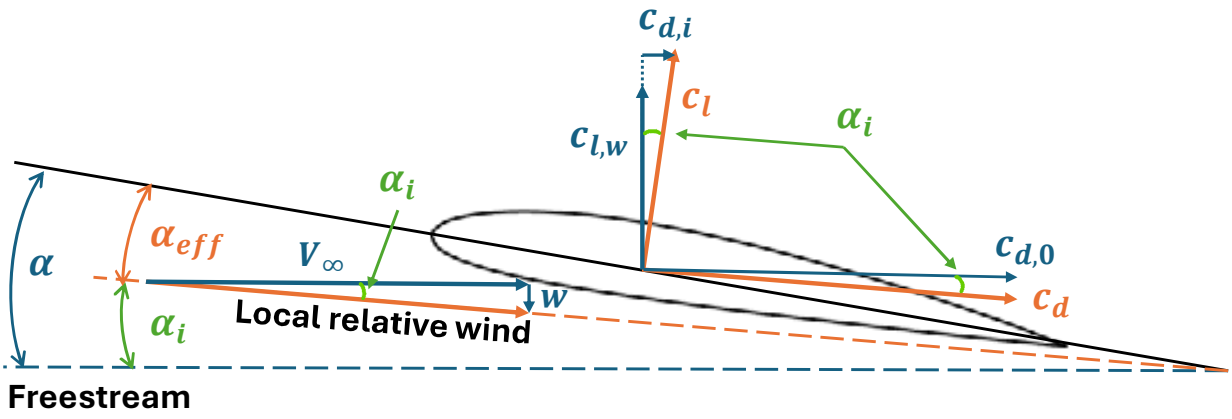

Figure 3.3: Reproduced from Figure 2.4 for reference: Decomposed lift and drag coefficients in local strip axes (orange) and global wind axes (blue) (adapted from [23, 26])

The remaining aerodynamic calibration factors are applied to these transformed coefficients, $c_{d,i}$, $c_{d,0}$ and c_{l_w}. Two factors are applied to the lift coefficient of the wing, a

slope-scaling factor, $K_{c_{l_{slope}}}$, and an additive offset, $K_{c_{l,0_{offset}}}$. The calibrated sectional lift coefficient, $c_{l,w}^{cal}$, is given in Equation 3.6, where the slope factor effectively adjusts the lift-curve slope and the offset accounts for deviations in the zero-lift angle of attack. This calibration is only applied to the wing sectional strips as the wing is the primary contributor to the overall lift of the aircraft.

$$c_{l,w}^{cal} = K_{c_{l_{slope}}} c_{l,w} + K_{c_{l,0_{offset}}} \tag{3.6}$$

The parasitic drag component is handled in a similar manner. Two factors are applied to all lifting surfaces' parasitic drag coefficient, a slope-scaling factor, $K_{c_{d,0_{slope}}}$ and a zero-lift drag coefficient correction, $K_{c_{d,0_{offset}}}$. Additionally, the same parasitic drag factors are applied to the fuselage's x-direction force coefficient, $C_{X_{fuse}}$, as the fuselage is a large component of the overall parasitic drag on the vehicle (approximately 30% [48]). Equation 3.7 shows the calibration of the parasitic drag coefficient, $c_{d,0}^{cal}$, while Equation 3.8 outlines the calibration applied to the fuselage's x-force coefficient, $C_{X_{fuse}}^{cal}$ where $\mathcal{L}_{C_{X_{fuse}}}$ is the FlightStream® [42] generated force coefficient lookup table.

$$c_{d,0}^{cal} = K_{c_{d,0_{slope}}} c_{d,0} + K_{c_{d,0_{offset}}} \tag{3.7}$$

$$C_{X_{fuse}}^{cal} = K_{c_{d,0_{slope}}} \mathcal{L}_{C_{X_{fuse}}}(\alpha, \beta) + K_{c_{d,0_{offset}}} \tag{3.8}$$

The final aerodynamic calibration factor, $K_{c_{d,i}}$, scales the induced drag contribution using Equation 3.9, producing the calibrated induced drag coefficient, $c_{d,i}^{cal}$. Induced drag is defined as $c_{d,i} = kc_l^2$ with $k = \frac{1}{\pi A e}$, where A is the aspect surface ratio, a value set by geometry, and e is the Oswald efficiency factor. The induced drag calibration factor is equivalent to adjustment of the Oswald efficiency factor.

$$c_{d,i}^{cal} = K_{c_{d,i}} c_{d,i} \tag{3.9}$$

These calibrated coefficients are then transformed back into the local strip wind axes. First, the total section drag in the global wind axes, $c_{d,w}^{cal}$, is obtained by summing the calibrated parasitic and induced drag components.

$$c_{d,w}^{cal} = c_{d,0}^{cal} + c_{d,i}^{cal} \tag{3.10}$$

The transformation by the induced angle of attack can then be performed to obtain the calibrated coefficients of lift and drag, c_l^{cal} and c_d^{cal}, in the local strip axes as given in Equations 3.11 and 3.12.

$$c_l^{cal} = c_{l,w}^{cal} \cos \alpha_i + c_{d,w}^{cal} \sin \alpha_i \tag{3.11}$$

$$c_d^{cal} = -c_{l,w}^{cal} \sin \alpha_i + c_{d,w}^{cal} \cos \alpha_i \tag{3.12}$$

The effects of each aerodynamic calibration factor on the overall aircraft's lift and drag coefficient curves are illustrated in Figures 3.4 and 3.5.

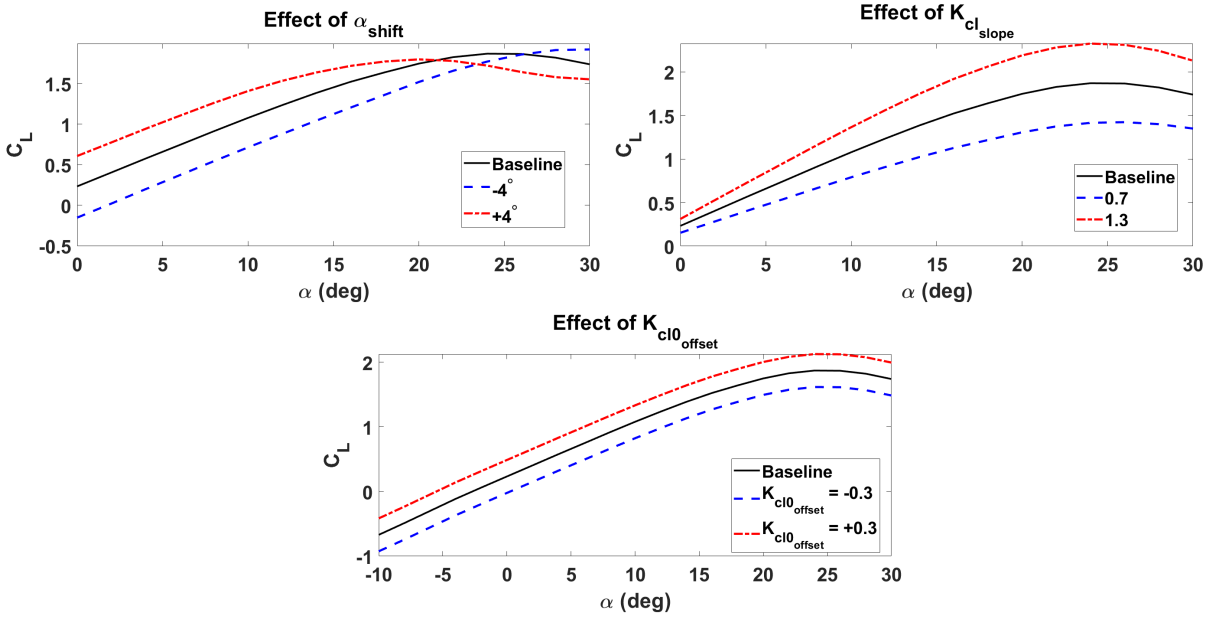

Figure 3.4: Effect of aerodynamic calibration factors on the aircraft's C_L curve

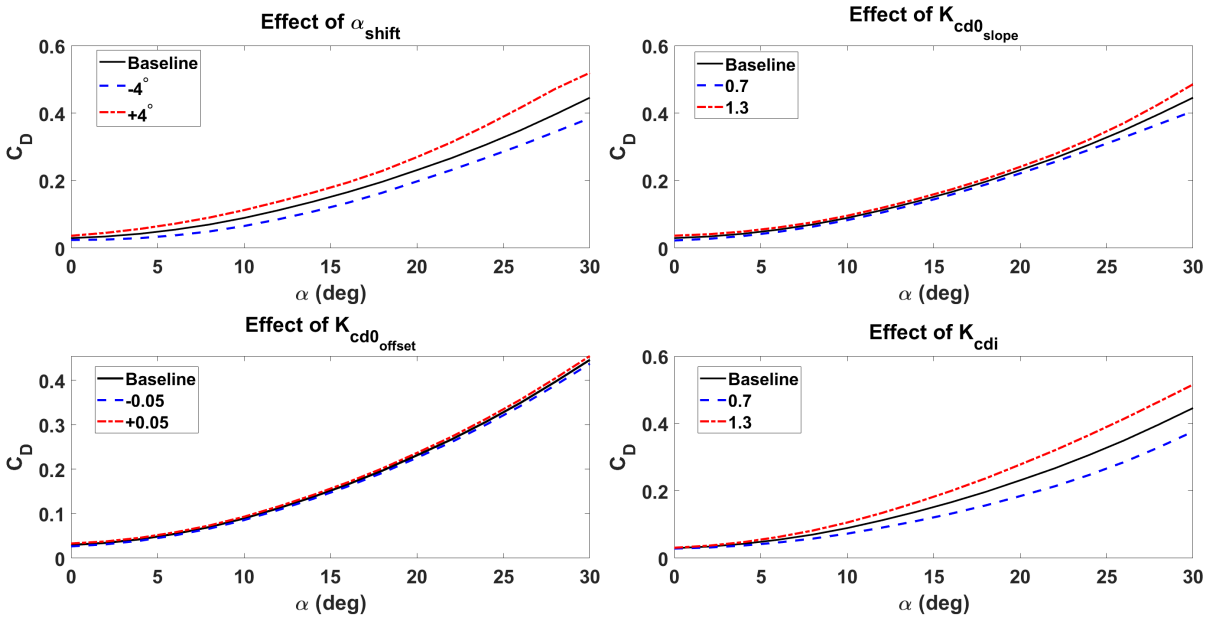

Figure 3.5: Effect of aerodynamic calibration factors on the aircraft's C_D curve

Propeller Parameterization

As described in Section 2.4, the propeller model provides thrust and torque forces and moments acting on the aircraft using QPROP-generated [44] non-dimensional thrust and torque coefficients as functions of advance ratio, J, and propeller pitch, β_P. In the case of the fixed-pitch propeller equipped on the Cessna 172, the coefficients are queried as a function of advance ratio only. The advance ratio is defined as $J = \frac{V_\infty}{nD}$, where V_∞ is the freestream velocity, n is the propeller speed, and D is the diameter of the propeller.

The parameterization scheme must be flexible enough to address both low-speed climb thrust and high-speed cruise power absorption requirements simultaneously. This flexibility is achieved with a set of nine calibration factors, four applied to the thrust coefficient curve, four applied to the torque coefficient curve, and one advance ratio query value modification. The factors are applied as follows. First, the thrust and torque coefficients, C_T and C_Q, are queried from their respective lookup tables, $\mathcal{L}_{C_T}$ and $\mathcal{L}_{C_Q}$, as a function of a modified advance ratio and the propeller blade pitch. These shifting factors, $K_{C_{T_{shift}}}$ and $K_{C_{Q_{shift}}}$,

allow flexibility to shift the operating point horizontally along the coefficient curves as defined in Equation 3.13.

$$J' = J + K_{shift} \tag{3.13}$$

where K_{shift} represents $K_{C_{T_{shift}}}$ and $K_{C_{Q_{shift}}}$ for the thrust and torque curves respectively. In the case of the Cessna 172, the blade pitch is a constant value, $\beta_P = 18.5°$.

$$C_T = \mathcal{L}_{C_T}(J', \beta_P) \tag{3.14}$$

$$C_Q = \mathcal{L}_{C_Q}(J', \beta_P) \tag{3.15}$$

Next, the coefficients are scaled and reshaped by the remaining factors, a scaling term and linear and quadratic shape terms relative to an advance ratio anchor, J_{anchor}, an optimization parameter. These terms allow for flexibility across the operating range without requiring additional flight condition dependencies, such as scheduled thrust factors as a function of airspeed. Equations 3.16 and 3.17 detail the application of the remaining factors to obtain the calibrated thrust and torque coefficients, C_T^{cal} and C_Q^{cal}.

$$C_T^{cal} = K_{C_{T_{scale}}} C_T \left[1 + K_{C_{T_{tilt}}}(J' - J_{anchor}) + K_{C_{T_{quad}}}(J' - J_{anchor})^2\right] \tag{3.16}$$

$$C_Q^{cal} = K_{C_{Q_{scale}}} C_Q \left[1 + K_{C_{Q_{tilt}}}(J' - J_{anchor}) + K_{C_{Q_{quad}}}(J' - J_{anchor})^2\right] \tag{3.17}$$

The implementation preserves the general shape of the original lookup tables while providing sufficient flexibility to match performance across the aircraft's operating envelope. Effects of each factor on the Cessna 172 model's thrust curve are illustrated in Figure 3.6, with the torque coefficient curve parameterized identically.

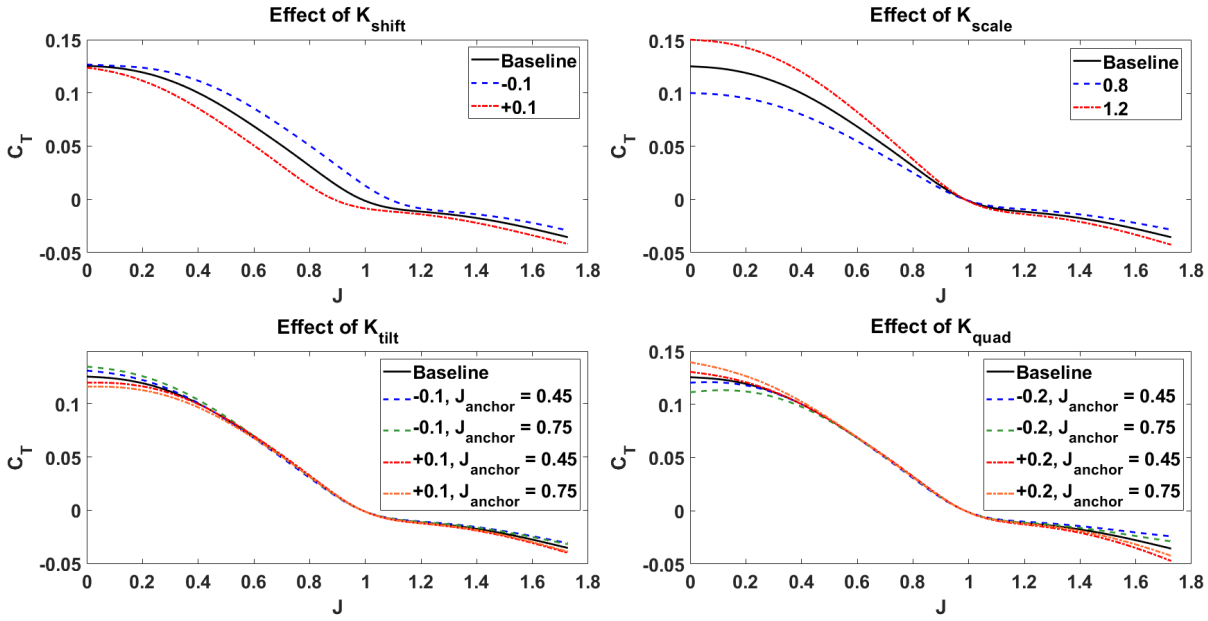

Figure 3.6: Effect of propeller calibration factors on C_T curve

Propulsion Parameterization

The two final steady-state calibration parameters, K_{HP} and K_{FF}, are applied within the propulsion model. These factors are implemented as simple, multiplication factors applied directly to the model-predicted output power, Equation 2.15, and fuel flow, Equation 2.16, from the digitized engine lookup table propulsion model described in Section 2.5.

$$HP^{cal} = K_{HP} \times HP \tag{3.18}$$

$$FF^{cal} = K_{FF} \times FF \tag{3.19}$$

3.1.2 Optimization Framework

Cost Function Formulation

The steady-state calibration cost function quantifies the error between the trimmed simulation model and POH reference data across a set of prescribed operating conditions. A set of performance points for en-route best-rate-of-climb and steady-state cruise are taken

directly from POH performance charts or tables representing a range of atmospheric conditions, airspeeds, and power settings. During the optimization routine, the calibration parameters are normalized to the range [-1,1] based on their allowable bounds (noted in Table 3.1) to improve optimizer conditioning and forcing similar scaling across parameters of differing units and magnitudes.

At a subset of the performance points, MADCASP trims the aircraft model to equilibrium at the prescribed condition using the current parameter set described in Section 3.1.1. The trim routine produces steady-state performance outputs which are compared against the corresponding POH reference values. The metrics of interest are driven by commonly available POH performance chart metrics and their associated tolerances are derived from FAA Part 60 FTD objective test criteria [8]. For climb performance points, rate of climb is selected as the metric of interest with a tolerance of ± 100 feet per minute (FPM), taken from the normal climb objective test requirements. For cruise points, percent power and propeller speed serve as the metrics on interest with tolerances of $\pm 5\%$ power and ± 50 RPM respectively. No objective test explicitly lists these tolerances, but the adopted tolerances are comparable to given cruise performance objective test requirements. Each error is normalized by its corresponding tolerance to ensure that all residual components contribute comparably to the cost function regardless of difference in units or magnitude.

$$r_{FPM,i} = \frac{\Delta FPM_i}{\tau_{FPM}} \tag{3.20}$$

$$r_{PP,j} = \frac{\Delta PP_j}{\tau_{PP}} \tag{3.21}$$

$$r_{RPM,j} = \frac{\Delta RPM_j}{\tau_{RPM}} \tag{3.22}$$

where $\Delta(\cdot)$ is the error between model output and POH reference value at each point, $\tau(\cdot)$ is the corresponding tolerance, i is an individual climb point, j is an individual cruise point, and PP is percent power.

Along with the defined set of reasonable ranges for each optimization parameter, as an additional safeguard against convergence to a physically infeasible solution, penalty multipliers are applied to the climb and cruise residuals when constraint violations are present. A gain is applied to all cruise residuals if any trim point converges to a throttle position exceeding the physical maximum. An equivalent penalty is applied if any climb or cruise trim point fails to converge which may happen when the equilibrium condition requires control surface deflections outside of their allowable ranges. These applied penalties steer the optimizer away from parameter combinations that produce unrealistic operating conditions without requiring more complex range constraints on the optimization parameters.

The full residual vector supplied to the optimization algorithm is assemlbed as

$$\boldsymbol{r} = \begin{bmatrix} r_{FPM,i} & r_{PP,j} & r_{RPM,j} \end{bmatrix}^T \tag{3.23}$$

This definition of the residual vector allows for use across multiple types of non-linear optimization schemes. Non-linear least-square optimizers, such as `lsqnonlin` [47], work to minimize the Euclidean norm of the residual vector, while general constrained optimizers, like `fmincon` [25], minimize a scalar cost found as the mean-square error of the residuals.

Fuel flow calibration is conducted independently from the primary steady-state optimization, as the fuel flow scaling factor K_{FF} has no influence on the trim solution or any quantity in the primary residual vector, $\boldsymbol{r}$. Following convergence of the primary scheme, the fuel flow scaling parameter is adjusted in a separate routine to align the model's fuel flow with POH cruise data at the same prescribed conditions. It is also possible to calibrate the K_{HP} parameter in this separate step if the POH cruise performance tables contain the appropriate information, such as output power, manifold pressure, and RPM. This would allow the propulsion model to be calibrated independently from the larger flight simulation

model. Manifold pressure validation data does not exist within the Cessna 172's POH [30]. Therefore, the output power scaling factor, K_{HP} is grouped into the larger, primary steady-state scheme. The selection of the optimization algorithm used to minimize the residual vector, $\boldsymbol{r}$, is discussed in the following section.

Optimization Algorithm Selection Study

A study was performed using two MATLAB-native optimization algorithms, `fmincon` [25] and `lsqnonlin` [47], applied to the Cessna 172 Skyhawk baseline model to evaluate their accuracy and computational speed during the steady-state calibration routine. The cost function is smooth and continuous, the parameter space is relatively low-dimensional with prescribed bounds, and fast convergence is critical given that each function evaluation requires running MADCASP trim solutions across all test points. These characteristics make gradient-based methods a reasonable fit. While the coupled nature of the aerodynamic, propulsion, and propeller parameters means multiple local minima may exist, the efficiency gains over population-based approaches like genetic algorithms or particle swarm make gradient-based methods the practical choice for a methodology where speed is a core goal. Additionally, as mentioned in discussions of Puranik's contributions [21, 22] (Section **??**), this work aims to construct a fully automated routine requiring no post-optimization human selection judgment. This motivates the choice of gradient-based methods which produce a single optimized parameter set over Pareto algorithms which output a set of candidate solutions. Both candidate optimization algorithms, `fmincon` and `lsqnonlin` require no MATLAB toolboxes beyond the Optimization Toolbox [49] and integrate easily with the existing MATLAB simulation framework, making them straightforward to implement and test.

Both optimization algorithms were executed using the same initial parameter set and an identical subset of nine climb and seven cruise steady-state performance points followed by the separate fuel flow optimizer. The converged sets of parameters are applied to the model and tested against the full set of Cessna 172 POH performance points (approximately

110 cruise points and 30 climb points) to allow for equivalent comparison. This evaluation on the full POH dataset, which is significantly larger than the subset used during optimization, serves as an initial check on the generalization of the calibrated parameters beyond the specific conditions used to train the optimizer. A set of quantitative accuracy metrics were applied to each set of results: root-mean-square error (RMSE), mean absolute percentage error (MAPE), normalized mean bias error (nMBE), and percentage of total points within the prescribed tolerances for the target metrics. As described in the cost function formulation, steady-state climb points are assessed for climb rate accuracy (±100 FPM) and cruise points are compared to percent power (±5%), propeller speed (±50 RPM), and fuel flow (±5%) POH validation data. The RMSE, MAPE, and nMBE are computed using all POH performance points for the target metrics using the standard definitions in Equations 3.24 - 3.26.

$$RMSE = \sqrt{\frac{1}{N}\sum_{k=1}^{N}(\Delta x_k)^2} \tag{3.24}$$

where N is the total number of points and Δx_k is the error in the metric of interest at trim point k. RMSE captures overall error magnitude and heavily penalizes points with large deviations from validation data. The value is expressed in the units of the target metric.

$$MAPE = \frac{100}{N}\sum_{k=1}^{N}\left|\frac{\Delta x_k}{x_{k,POH}}\right| \tag{3.25}$$

where $x_{k,POH}$ is the published POH metric at point k. MAPE captures relative accuracy. The value is expressed as an absolute value percentage of the published value.

$$nMBE = \frac{100}{N}\sum_{k=1}^{N}\frac{\Delta x_k}{x_{k,POH}} \tag{3.26}$$

The nMBE expresses an average signed percentage error representing the systematic bias of the model compared to validation data. The "percentage within tolerance" metric is computed by evaluating whether each point trimmed by the model falls within the prescribed

tolerance metrics. The count of in-tolerance points are then expressed as a percentage of the total points. Convergence time is also recorded for each optimizer as a practical measure of computational efficiency[1]. A consolidated summary of the accuracy metrics and runtime for the baseline, `fmincon`-calibrated, and `lsqnonlin`-calibrated models' trim points is provided in Table 3.2.

Table 3.2: Summary of accuracy metrics and runtime for baseline and converged optimizers (adapted from [26])

Metric	**Baseline**	**`fmincon`**	**`lsqnonlin`**	**Units**
Climb Rate (FPM)				
RMSE	104.4	28.3	29.8	FPM
MAPE	27.5	6.0	6.1	%
nMBE	27.5	0.2	1.6	%
% Within Tol	51.9	100	100	%
Percent Power (%)				
RMSE	14.3	1.2	1.2	% Power
MAPE	21.5	1.2	1.2	%
nMBE	-21.5	-0.1	-0.01	%
% Within Tol	0.9	100	100	%
Propeller Speed (RPM)				
RMSE	16.4	14.7	14.7	RPM
MAPE	0.6	0.5	0.5	%
nMBE	-0.6	0.2	0.2	%
% Within Tol	100	100	100	%
Fuel Flow (GPH)				
RMSE	0.7	0.2	0.2	GPH
MAPE	7.4	1.8	1.8	%
nMBE	-7.3	0.3	0.3	%
% Within Tol	26.1	97.3	98.2	%
Runtime	N/A	34.4	10.5	min

As an additional check, the best rate of climb speed, V_y, and the best angle of climb speed, V_x are evaluated against the Cessna 172 POH reference values with the converged parameter sets applied. These airspeeds are not included in the optimization objective, so

[1]All optimization times reported were obtained on an Intel®Core™ Ultra 7 255H, 20-core, 32 GB RAM machine running MATLAB R2024b. Both optimization algorithms were executed with the `UseParallel` option enabled.

agreement with POH data provides an independent indication of whether the calibrated coupled aerodynamic-propeller-propulsive balance generalizes beyond the directly optimized metrics. A summary of the key airspeeds in the baseline and calibrated models are provided in Table 3.3.

Table 3.3: Comparison of best angle and best rate of climb indicated airspeeds (KIAS) with converged parameters (adapted from [26])

Key Airspeed	**Altitude (ft)**	**POH Value (KIAS)**	**Baseline (KIAS)**	**`fmincon` (KIAS)**	**`lsqnonlin` (KIAS)**
V_x	0	62	72	66	64
V_x	10,000	67	78	69	68
V_y	0	74	100+	77	76
V_y	10,000	72	93	74	71

As shown in Table 3.2, both optimizers produce dramatic improvements over the uncalibrated baseline across all metrics. The baseline model shows particularly large errors in percent power and fuel flow, with fewer than 1% and 27% of points within tolerance respectively, while both calibrated models bring these to approximately 98% and 100% within tolerance. Climb rate accuracy improves from 51.9% to 100% of points within tolerance for both optimizers. The key airspeeds in Table 3.3 show similar improvement — the baseline V_y error of over 26 knots at sea level is reduced to within 3 knots by both calibrated models, and V_x errors are similarly reduced to within the ± 3 kt tolerance at most conditions. Across all metrics, the two optimizers are essentially equivalent in accuracy.

Although the two optimization algorithms produced nearly identical accuracy metrics, the key difference arises in the computational efficiency with `lsqnonlin` converging in approximately 30% of the time of `fmincon`. The difference in convergence time, with no meaningful sacrifice in accuracy, provides sufficient justification to adopt `lsqnonlin` for the steady-state calibration routine. Additionally, its proven performance in the steady-state stage justifies its continued use as the optimization algorithm throughout the remainder of the calibration methodology.

3.1.3 Summary

The steady-state stage parameterization, cost function formulation, and optimization strategy allows for efficient modification of a flight simulation model to meet POH performance points within a prescribed tolerance. The framework of this stage equips the calibration routine to produce a model with substantially improved steady-state performance over the uncalibrated baseline. Despite its strengths, the calibration stage is limited by the information available in the flight manual. Important parameters such as aircraft attitude, control surface deflections, and dynamic response characteristics are not captured in these steady-state performance points and therefore cannot be addressed without additional validation data. This gap motivates the development of a second stage of the calibration routine, in which flight test data is used to refine the model further, targeting dynamic and attitude-based metrics required to meet objective regulatory requirements.

3.2 Time-Domain Calibration

The time-domain calibration stage refines the steady-state calibrated model using instrumented flight test data. This stage targets aircraft attitude, control surface deflections, and dynamic response characteristics that are not addressed in manufacturer performance data. While the stage is referred to as "time-domain calibration," several steps within it employ steady-state trim solutions derived from flight test data which is within the time-domain in nature. The stage employs a sequential, multi-step optimization approach for which each step calibrates a specific set of model characteristics while treating all prior stage's results as fixed, illustrated in Figure 3.7.

All calibration factors established during the steady-state stage are frozen at their converged values and carried forward as fixed inputs to the time-domain stage, ensuring that steady-state performance accuracy is preserved while time-domain parameters are independently modified. The sequential approach limits parameter coupling between steps and is designed to be adaptable, with steps that may be added, removed, or modified based on

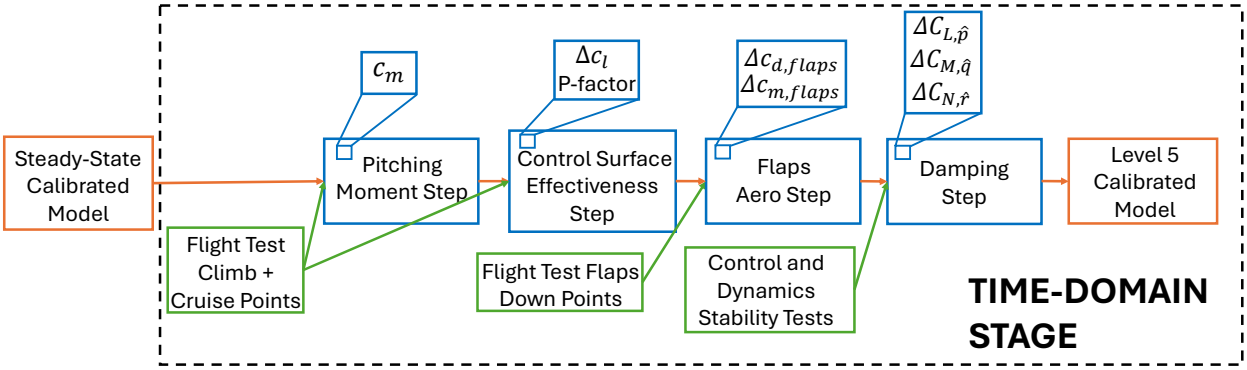

Figure 3.7: Time-domain calibration stage flowchart as implemented during calibration of the Cessna 172 Skyhawk flight simulation model

the validation data available for a given aircraft and application. For the Cessna 172 validation case, the time-domain calibration targets aerodynamic model parameters exclusively with fifteen parameters, as the available flight test dataset does not provide sufficient information to independently identify propulsion or propeller model corrections beyond those established in the steady-state stage. The following sections describe the parameterization and cost function formulation at each step as applied to the Cessna 172 model, followed by a description of the flight test data used for validation.

3.2.1 Pitching Moment Step

The steady-state calibration stage accounts for aerodynamic and propulsive performance characteristics in cruise and vertical speed in climb, but contains no information about the pitch attitude of the aircraft. This step aims to ensure that the calibrated lift and drag curves produce the correct coefficients at the correct angles of attack, using pitch attitude from flight test data as an indirect indicator of aerodynamic balance.

Parameterization

Three aerodynamic calibration factors are optimized during the pitching moment step of the time-domain calibration stage. Again, these parameters are bounded to avoid non-physical solutions. The parameter bounds for the time-domain calibration stage are wider

than those of the steady-state stage because the steady-state calibrated model already produces a trimmed, physically consistent solution. The parameters adjusted in this step refine the aerodynamic characteristics without much risk of driving the model to a non-trimming condition, allowing for greater flexibility in the allowable correction range. These calibration factors are listed in Table 3.4 with their bounds.

Table 3.4: Pitching moment step calibration parameters and bounds

Factor	**Minimum**	**Maximum**
$\alpha_{shift_{addl}}$	-2°	2°
$K_{c_{m_{slope}}}$	0.2	3
$K_{c_{m,0_{offset}}}$	-0.5	0.5

The first parameter, $\alpha_{shift_{addl}}$, is an additional additive shift applied to the effective angle of attack, α_{eff}, that are used to query the wings' sectional aerodynamic coefficients. This is similar to the α_{shift} term introduced in the steady-state calibration routine and is treated as additive to the previously calibrated term. The wings' sectional aerodynamic coefficients are then queried as

$$c_l = \mathcal{L}_{c_l}(\alpha_{eff} + \alpha_{shift} + \alpha_{shift_{addl}}) \tag{3.27}$$

$$c_d = \mathcal{L}_{c_d}(\alpha_{eff} + \alpha_{shift} + \alpha_{shift_{addl}}) \tag{3.28}$$

$$c_m = \mathcal{L}_{c_m}(\alpha_{eff} + \alpha_{shift} + \alpha_{shift_{addl}}) \tag{3.29}$$

where c_m is the wing's sectional pitching moment coefficient and $\mathcal{L}_{c_m}$ denotes the pitching moment coefficient lookup table generated with XFOIL [36].

The next two optimization parameters, $K_{c_{m_{slope}}}$ and $K_{c_{m,0_{offset}}}$, are applied identically to the lift and parasitic drag factors during the steady-state calibration. $K_{c_{m_{slope}}}$ adjusts the

slope of the pitching moment coefficient and $K_{c_{m,0_{offset}}}$ adjusts the zero-lift pitching moment coefficient. The parameters are applied to obtain the calibrated sectional pitching moment coefficient, c_m^{cal}, as defined in Equation 3.30.

$$c_m^{cal} = K_{c_{m_{slope}}} c_m + K_{c_{m,0_{offset}}} \tag{3.30}$$

These three factors collectively allow the optimizer to adjust the wing strips' pitching moment coefficient characteristics to match the pitch attitudes observed in flight test data.

Cost Function and Optimization Routine

The pitching moment step cost function measures the agreement between the model's trimmed pitch attitude and pitch attitudes derived from flight test data at quasi-steady-state points. At each extracted point, MADCASP trims the model to the prescribed flight conditions and the pitch attitude error is normalized by a tolerance of $\pm 1^\circ$, as shown in Equation 3.31, derived from FAA Part 60 longitudinal trim objective test requirements [8].

$$r_{\theta,i} = \frac{\Delta\theta_i}{\tau_\theta} \tag{3.31}$$

where $\Delta\theta_i$ is the pitch attitude error at trim point i and τ_θ is the prescribed tolerance of $\pm 1^\circ$ pitch.

Similar to the steady-state calibration cost function implementation, penalty functions are implemented within the pitching moment step's cost function to steer the optimization away from non-physical, non-trimmable solutions. The criteria for the penalty application is identical to the steady-state calibration routine, but the implementation differs. Within this cost function, the penalties are applied as entries into the cost function's residual vector as r_{THR_i}, penalty for cruise points that require a throttle position greater than its physical range, and r_{fail}, a single penalty value directly related to the amount of points within the optimization routine that return an untrimmed solution. The penalties are defined as

$$r_{THR,i} = max\left(0, \frac{\delta_{t,i} - 1}{0.05}\right) \tag{3.32}$$

$$r_{fail} = 20 \times N_{fail} \tag{3.33}$$

where $\delta_{t,i}$ is the normalized throttle position at point i and N_{fail} is the number of points within the validation data set that fail to trim. The full residual vector supplied to the optimization algorithm is assembled as

$$\boldsymbol{r} = \begin{bmatrix} r_{\theta,i} & r_{THR,i} & r_{fail} \end{bmatrix}^T \tag{3.34}$$

The step was validated using eleven quasi-steady-state points from the Cessna 172 flight test data package, three climb, derived from normal climb data sets, and eight cruise points, derived from longitudinal trim tests and additional tests that contain points at which the aircraft is flown in a trimmed, cruise-like flight condition. This stage converged using `lsqnonlin` [47], proven to be accurate, efficient, and well-suited, in 114 seconds or 1.9 minutes.

The converged parameter set from the pitching moment step is fixed and carried forward as the starting point for the next time-domain calibration step, control surface effectiveness.

3.2.2 Control Surface Effectiveness Step

Having addressed pitch attitude in the previous step, and with bank angle and heading set as trim targets within the MADCASP trim routine, the control surface effectiveness step focuses on calibrating the control surface deflections required to achieve the trimmed attitudes observed in flight test data. This step addresses the control surface effectiveness by applying factors to the circulation, Γ_{CS}, created by deflection of the surface, δ. Flap deflections are excluded from this step and addressed separately in the dedicated flap calibration

step due to the unique aerodynamic characteristics and cost function metrics, for example, meeting vertical climb metrics in flaps-down climb.

Additionally, analysis of the results during the step revealed a systematic yaw bias at high power, low airspeed conditions consistent with propeller P-factor effects not captured by the baseline model due to its exclusion of an explicit propeller slipstream model. A P-factor correction term is included in this step to address the asymmetric loading caused by the shifting of the center of thrust on the propeller disc.

Parameterization

Seven aerodynamic factors are optimized during the control surface effectiveness step of the time-domain calibration stage. Six parameters are applied as slope modifications and offsets to the circulation generated by the three types of control surfaces, elevators, ailerons, and rudder. The final parameter is an additive factor, as a function of angle of attack and thrust, applied to the yawing moment of each lifting-surface strip at its aerodynamic center to account for the left-yawing moment as a result of P-factor. These calibration factors are listed in Table 3.5 with their bounds.

Table 3.5: Control surface effectiveness calibration parameters and bounds

Factor	**Minimum**	**Maximum**
$K_{\delta,e_{slope}}$	0.5	3
$K_{\delta,e_{offset}}$	-5 m^2/s	5 m^2/s
$K_{\delta,a_{slope}}$	0.5	3
$K_{\delta,a_{offset}}$	-5 m^2/s	5 m^2/s
$K_{\delta,r_{slope}}$	0.5	3
$K_{\delta,r_{offset}}$	-5 m^2/s	5 m^2/s
K_{PF}	0	0.5

The slope and offset factors are applied to the circulation created by the control surface, Γ_{CS}, to modify the lift coefficient increment due to the deflection, Δc_l. First, the Δc_l is computed from the spanwise loading coefficient, G/δ, using Equation 2.10. The intermediate

circulation distribution due to control surface deflection is related to the lift increment as shown in Equation 3.35.

$$\Gamma_{CS} = \frac{\Delta c_l \cdot c \cdot V_\infty}{2} \tag{3.35}$$

where c is the chord distribution over the span of the control surface and V_∞ is the freestream velocity at each control surface strip's location. Calibration factors are applied directly to Γ_{CS} for each control surface followed by the recovery of the calibrated lift increment, Δc_l^{cal}.

$$\Gamma_{CS}^{cal} = K_{\delta_{slope}} \Gamma_{CS} + K_{\delta_{offset}} \tag{3.36}$$

where $K_{\delta_{slope}}$ and $K_{\delta_{offset}}$ are the calibration factors relevant to the specific control surface. The calibrated lift increment is then taken as shown in Equation 3.37.

$$\Delta c_l^{cal} = \frac{2\Gamma_{CS}^{cal}}{V_\infty c} \tag{3.37}$$

Asymmetric propeller loading, or P-factor, is an aerodynamic effect that occurs when an aircraft is flying at a positive angle of attack. In this situation, the downward-moving propeller blade(s) are traveling through an area of higher resultant velocity than the upward-moving blade(s). Because of the blade's airfoil shape, the increased velocity environment of the downward-moving blade(s) generates more lift than the upward-moving blade(s), moving the center of thrust of the propeller disc towards the downward-moving blade(s). For clockwise turning propellers, typical in American single-engine general aviation aircraft, a resultant left yawing moment is generated [50]. The effect of P-factor is increased at high angles of attack and thrust, typical of takeoff and climb conditions. Analysis of control surface deflection residuals from the Cessna 172 flight simulation model after the application of the first six optimization factors showed discrepancies in the rudder deflections required in high-powered climb. These deflection errors are mitigated using the final calibration factor representing P-factor, K_{PF}. A yawing moment increment representing the P-factor effect

is given in Equation 3.38, expressed as a function of angle of attack, α_{ac}, thrust, T, and propeller diameter, D. This left-yawing moment increment is added directly to the total aerodynamic yawing moment in body axes.

$$N_{PF} = -K_{PF} T \frac{D}{2} \sin \alpha_{ac} \tag{3.38}$$

Cost Function and Optimization Routine

The cost function for the control effectiveness step quantifies the discrepancy between the model's trimmed control surface positions and control surface positions from flight test data at the same quasi-steady-state points used during the pitching moment step. At each point, MADCASP trims the model to satisfy prescribed flight conditions including bank and heading angles and the resulting elevator, aileron, and rudder deflections are compared to flight test data values. The error is normalized by a tolerance of $\pm 1^\circ$, as shown in Equation 3.39.

$$r_{CS,i} = \frac{\Delta \delta_{CS,i}}{\tau_{\delta_{CS}}} \tag{3.39}$$

where $r_{CS,i}$ is the control surface deflection residual for each surface $\Delta \delta_{CS,i}$ is the surface deflection error at point i, and $\tau_{\delta_{CS}}$ is the applied tolerance of $\pm 1^\circ$ deflection. The CS subscript is replaced for each control surface to be δ_e for elevator deflection, δ_a for aileron deflection, and δ_r for rudder deflection. The same penalty metrics given in Equations 3.32 and 3.33 are applied to the full residual vector. The full residual vector for the control surface effectiveness step is given as

$$\boldsymbol{r} = \begin{bmatrix} r_{\delta_e,i} & r_{\delta_a,i} & r_{\delta_r,i} & r_{THR,i} & r_{fail} \end{bmatrix}^T \tag{3.40}$$

The P-factor calibration parameter is optimized in a second routine where the full residual vector is defined as

$$\boldsymbol{r} = \begin{bmatrix} r_{\delta_r,i} & r_{THR,i} & r_{fail} \end{bmatrix}^T \tag{3.41}$$

The step was validated against the same data set of quasi-steady-state points from the Cessna 172 flight test data package used in the previous pitching moment calibration step. Both calibration routines are performed using `lsqnonlin` with the larger control surface effectiveness routine converging in 192 seconds, or 3.2 minutes, and the P-factor routine converging in 19 seconds, or 0.3 minutes, for a total time of 211 seconds, or 3.5 minutes.

The converged parameter set from the control surface effectiveness step is fixed and carried forward as the starting point for the next time-domain calibration step, flap aerodynamics.

3.2.3 Flap Aerodynamics Step

In the case of the Cessna 172 manufacturer data used when developing this methodology, no flap performance charts are available. This necessitates the flap aerodynamic calibration to occur during the time-domain calibration stage where flaps-down flight test data is available. The flap step is treated separately from the control surface effectiveness step because flap deflections drive large changes in drag and pitching moment that directly impact climb rate and trim attitude in a way that the conventional control surface parameterization does not address. This calibration step introduces factors that adjust the incremental parasitic drag and pitching moment due to flap deflection to match climb rate in flaps-down climb and pitch attitude in quasi-steady state flaps-down flight conditions.

Parameterization

Two aerodynamic factors are optimized during the flap aerodynamics step of the time-domain calibration stage. Both factors scale incremental aerodynamic coefficients, parasitic drag and pitching moment, for wing strips on which the flaps lie. These calibration factors are listed in Table 3.6 along with their bounds.

Table 3.6: Flap aerodynamics step calibration parameters and bounds

Factor	Minimum	Maximum
$K_{\Delta c_{d,0_{flaps}}}$	-2	2
$K_{\Delta c_{m_{flaps}}}$	-3	3

The first optimization parameter, $K_{\Delta c_{d,0_{flaps}}}$, addresses the incremental increase in parasitic drag due to flap deflection, δ_f, applied to the parent lifting surface's sectional parasitic drag coefficients of the strips spanning the flap region of the wing. The calibrated drag increment, $\Delta c^{cal}_{d,0_{flaps}}$, defined in Equation 3.42, is added to the profile drag coefficient computed in Equation 2.11.

$$\Delta c^{cal}_{d,0_{flaps}} = K_{\Delta c_{d,0_{flaps}}} \frac{\delta c_{d,0}}{\delta_f} \delta_f \tag{3.42}$$

where $\frac{\delta c_{d,0}}{\delta_f}$ is an initial per-degree parasitic drag scaling estimate used to give the calibration factor a physically meaningful magnitude, with $K_{\Delta c_{d,0_{flaps}}}$ applied as a correction to account for both discrepancies in the baseline profile drag calculation and three-dimensional installation and interference effects not captured by the strip theory model. The dependency on flap deflection ensures that the calibrated correction does not affect clean configuration performance. The parasitic drag coefficient on each wing strip containing the flap then becomes

$$c^{cal,total}_{d,0} = c^{cal}_{d,0} + \Delta c_{d,0} + \Delta c^{cal}_{d,0_{flaps}} \tag{3.43}$$

where $c^{cal}_{d,0}$ is the calibrated drag coefficient from the steady-state calibration stage, defined in Equation 3.7, and $\Delta c_{d,0}$ is the profile drag increment due to the control surface deflection from Equation 2.11.

The pitching moment increment due to flap deflection is applied similarly, where the calibration parameter, $K_{\Delta c_{m_{flaps}}}$, addresses the incremental change in pitching moment,

$\Delta c_{m,flaps}$, due to the flap deflection, δ_f, applied to the parent lifting surface's sectional pitching moment coefficient of the strips containing the flap surface. The calibrated pitching moment increment, $\Delta c^{cal}_{m,flaps}$, defined in Equation 3.44, is added to the flap strips' pitching moment coefficient queried as shown in Equation 3.30 to obtain the calibrated pitching moment coefficient, c^{cal}_m.

$$\Delta c^{cal}_{m,flaps} = K_{\Delta c_{m_{flaps}}} \frac{\delta c_m}{\delta_f} \delta_f \tag{3.44}$$

$$c^{cal}_m = c_m + \Delta c^{cal}_{m,flaps} \tag{3.45}$$

where $\frac{\delta c_m}{\delta_f}$ is an initial per-degree pitching moment scaling estimate used to give the calibration factor a meaningful magnitude, with $K_{\Delta c_{m_{flaps}}}$ applied as a correction to account for pitching moment coefficient errors not captured by the baseline pitching moment model.

Cost Function and Optimization Routine

The cost function for the flaps aerodynamics step measures the error between the model's trimmed pitch attitude and climb rate from flight test data at a set of quasi-steady-state points. At each point, MADCASP is trimmed with prescribed flap deflections and flight conditions. Climb rate is selected as it is most sensitive to the flap drag correction while pitch attitude captures the effect of the pitching moment correction, allowing the optimizer to independently identify each parameter. The error is normalized by a tolerance of ±100 FPM for climb rate and ±1° for pitch attitude, derived from FAA Part 60 objective test requirements [8]. The climb rate residual is defined as

$$r_{FPM_j} = \frac{\Delta FPM_j}{\tau_{FPM}} \tag{3.46}$$

where ΔFPM_j is the climb rate error at climb point j and τ_{FPM} is the ±100 FPM tolerance. The pitch residual is defined as in Equation 3.31 where point i, is all points, cruise and climb.

The full residual vector for the flaps aerodynamic step is assembled as

$$\boldsymbol{r} = \begin{bmatrix} r_{FPM_j} & r_{\theta,i} & r_{THR,i} & r_{fail} \end{bmatrix}^T \tag{3.47}$$

subject to the same trim protection penalties as defined in Equations 3.32 and 3.33. During the Cessna 172 validation case, three takeoff configuration (10° deflection) climb points and twelve cruise quasi-steady-state points with 10°, 20°, and 30° flap deflections are used as the data set. The `lsqnonlin` optimization algorithm converged in 232 seconds, or 3.9 minutes.

The converged parameter set from the flaps aerodynamics step is fixed and carried forward as the starting point for the next time-domain calibration step, damping.

3.2.4 Damping Step

The final step of the time-domain calibration stage addresses dynamic response discrepancies. Review of simulation results following the flaps aerodynamics step revealed significantly under-damped behavior on pitch, roll, and yaw axes when compared to flight test data. The axes are optimized separately by introducing an additional damping term for each axis applied as additive corrections to the roll, pitch, and yaw moment equations respectively. This calibration step aims to match parameters derived from dynamic aircraft flight test data.

Parameterization

Three optimization factors are introduced in this step, with separate optimization routines adjusting the parameters. The calibration factors implemented in this step are listed in Table 3.7 along with their bounds. It was found to be necessary to extend the bounds of the pitch damping optimization parameter due to the longitudinal reference length being much smaller than the lateral reference length used for dimensionalization of the rolling

and yawing moments, requiring wider bounds for the pitch damping parameter to achieve equivalent correction authority.

Table 3.7: Damping step calibration parameters and bounds

Factor	**Minimum**	**Maximum**
$K_{C_{L,p}}$	-0.02	0.02
$K_{C_{M,q}}$	-0.1	0.1
$K_{C_{N,r}}$	-0.02	0.02

These correction terms are applied as additive corrections to the assembled aerodynamic moments, supplementing the implicit damping contributions already present in the strip theory model through spanwise force integration.

The additional roll damping term, ΔL_p, is defined using the optimization parameter $K_{C_{L,p}}$ as

$$\Delta L_p = -K_{C_{L,p}} \hat{p} \bar{q} S b_{lat} \tag{3.48}$$

where the negative sign ensures a positive restoring moment opposing the roll rate. Here, $\bar{q}$ is the dynamic pressure, S is the reference area, b_{lat} is the lateral reference length, and $\hat{p}$ is the non-dimensional roll rate defined by Equation 3.49.

$$\hat{p} = \frac{p b_{lat}}{2V_\infty} \tag{3.49}$$

where p is the roll rate and V_∞ is the freestream velocity. The additional roll damping term is added onto the assembled rolling aerodynamic moment applied on the aircraft, L_{aero}, to define the calibrated rolling aerodynamic moment, L_{aero}^{cal} as

$$L_{aero}^{cal} = L_{aero} + \Delta L_p \tag{3.50}$$

The pitching and yawing axes are handled similarly. The additional pitch damping term, ΔM_q, is defined using optimization parameter $K_{C_{M,q}}$ as

$$\Delta M_q = -K_{C_{M,q}} \hat{q} \bar{q} S b_{long} \tag{3.51}$$

where b_{long} is the longitudinal reference length and $\hat{q}$ is the non-dimensional pitch rate as defined by Equation 3.52.

$$\hat{q} = \frac{q b_{long}}{2V_\infty} \tag{3.52}$$

where q is the pitch rate. The additional pitch damping term is added onto the assembled pitching aerodynamic moment, M_{aero}, defining the calibrated pitching aerodynamic moment, M_{aero}^{cal}, as

$$M_{aero}^{cal} = M_{aero} + \Delta M_q \tag{3.53}$$

Finally, the additional yaw damping term, ΔN_r, is defined using optimization parameter $K_{C_{N,r}}$ as

$$\Delta N_r = -K_{C_{N,r}} \hat{r} \bar{q} S b_{lat} \tag{3.54}$$

where $\hat{r}$ is the non-dimensional yaw rate as defined by Equation 3.55.

$$\hat{r} = \frac{r b_{lat}}{2V_\infty} \tag{3.55}$$

where r is the yaw rate. The additional yaw damping term is added to the assembled yawing aerodynamic moment, N_{aero}, producing the calibrated yawing aerodynamic moment, N_{aero}^{cal} using

$$N_{aero}^{cal} = N_{aero} + \Delta N_r \tag{3.56}$$

Cost Function and Optimization Routines

The damping step is the most flexible in terms of data requirement, heavily dependent on the data sets included in the available flight test package. Unlike the previous time-domain calibration steps which rely on quasi-steady-state trim solutions, this step executes full 6-DOF time-domain simulations driven by flight test control inputs, allowing dynamic response characteristics to be directly compared against flight test data. The cost function may be constructed from any combination of dynamic flight test maneuvers that sufficiently excite the axis of interest, with tolerances set to match available validation data or applicable regulatory requirements. It is ideal to choose data cases that decouple axis dynamics as much as possible. The cost functions used for the Cessna 172 calibration routine are presented. Each axis is optimized in separate routines using the `lsqnonlin` algorithm.

Roll Damping The roll damping cost function is composed of two types of tests: (1) dynamic control check tests where the roll controller, or wheel, is displaced in an approximately one second long pulse input and maximum roll rate response is compared and (2) roll rate response test where the roll controller is subject to a step input and the resulting steady state roll rate is compared. The dynamic control test data available from the Cessna 172 flight test package does not fall cleanly within the test procedures for any FAA Part 60 objective tests [8], but resembles a combination of the roll control response and small roll control inputs tests. The test maneuver itself is executed closely to the dynamic control check tests, but "free response" control behavior, the objective for the dynamic controls check tests, is not feasible to execute in the available flight simulation model as it lacks a force-based control loading component necessary to model reversible control behavior. Because of this limitation, tolerances are derived from the small roll control inputs objective test, which measures a similar control profile to body rate comparison, but is intended for smaller control inputs. The $\pm 20\%$ of peak roll rate after control input is adopted for quantifying roll damping accuracy. A graphical example of how the tolerance is applied to the

flight test maneuver data is shown in Figure 3.8, where the shaded region is the tolerance band in which the model's maximum roll rate must fall.

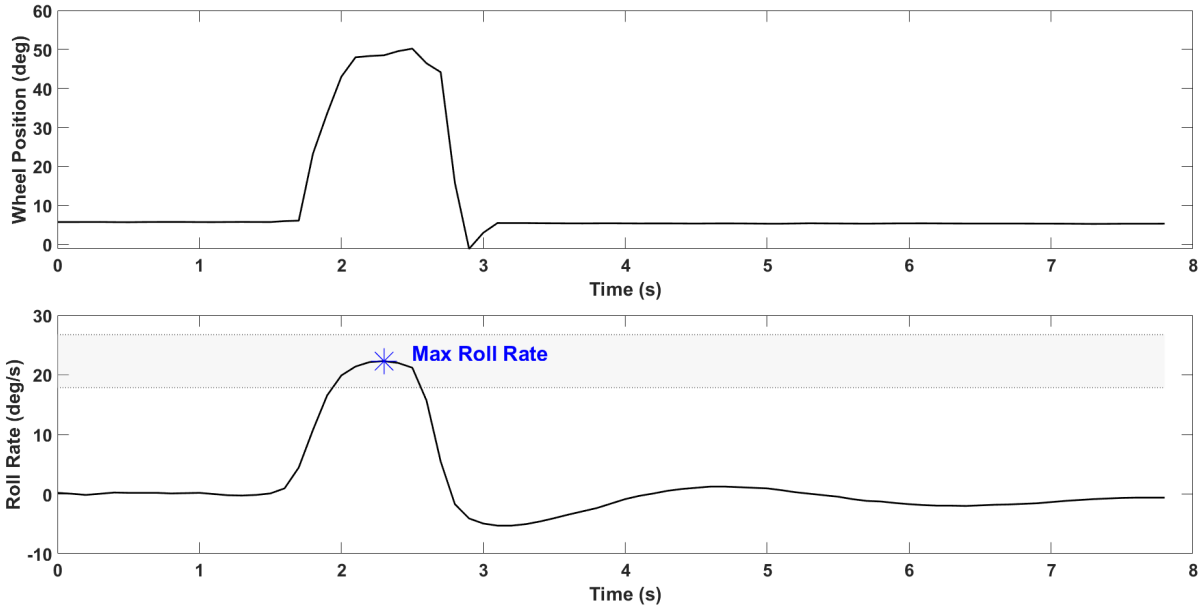

Figure 3.8: Example of dynamic control check tolerances applied to a roll axes flight test data time history trace

The residual term derived from this maneuver, $r_{DCC,\phi}$, is taken as

$$r_{DCC,\phi} = \frac{\Delta\dot{\phi}_{max}}{\tau_{\dot{\phi}_{max}}} \tag{3.57}$$

where $\Delta\dot{\phi}_{max}$ is the error in the maximum roll rate as a result of the pulse wheel input and $\tau_{\dot{\phi}_{max}}$ is the $\pm 20\%$ of peak roll rate tolerance applied to the flight test maneuver's maximum roll rate. Two cases of this test type are implemented into the roll damping optimization step, one with a clean aircraft configuration and one with a takeoff flap configuration to ensure the roll damping correction is valid across both clean and flaps-extended configurations, and the residuals are denoted as $r_{DCC,\phi,1}$ and $r_{DCC,\phi,2}$.

The second type of test used in the cost function formulation is a roll response test maneuver, an objective test required for Level 5 FTD simulations. This test is performed by a step input of the roll controller to approximately 30% of the maximum deflection in

one direction. The steady-state roll rate established as a result of the step input is averaged across the time period for which the control is held at its deflected position and used as the accuracy metric for the cost function formulation. FAA Part 60 roll response objective test requires the simulation replicate this roll rate within a tolerance of $\pm 2°/s$ or $\pm 10\%$ of the roll rate [8]. The $\pm 2°/s$ tolerance is adopted for cost function formulation. A graphical example of how the tolerance is applied to the roll response maneuver is shown in Figure 3.9, where the shaded region is the tolerance band in which the model's average steady-state roll rate must fall.

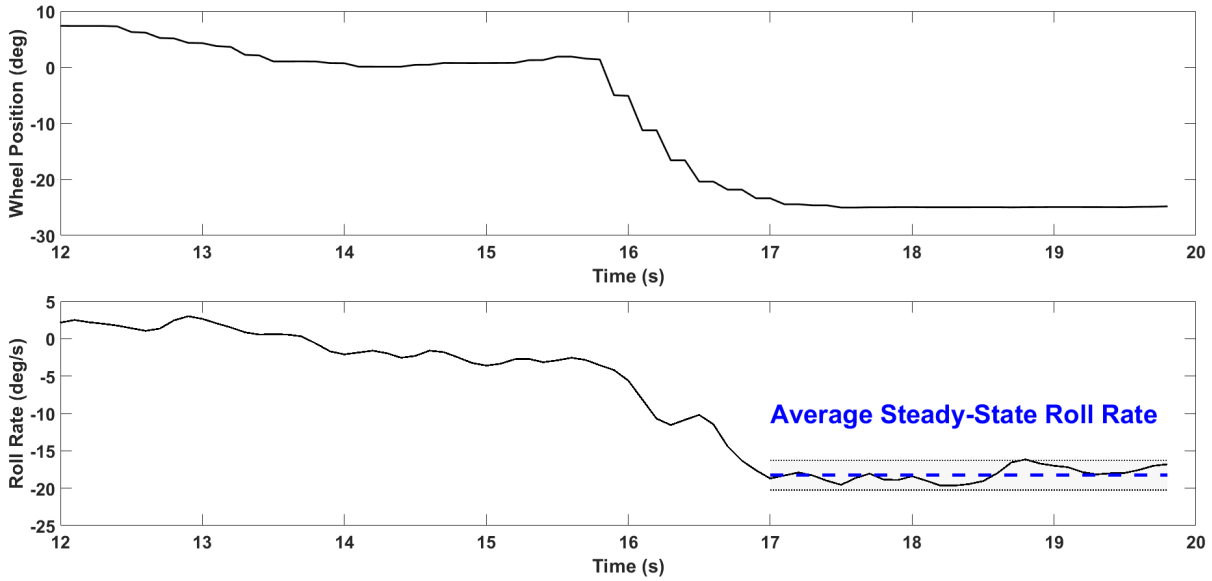

Figure 3.9: Example of roll response tolerances applied to a flight test data time history trace

The residual term derived from this maneuver, r_{RR}, is defined as

$$r_{RR} = \frac{\Delta\dot{\phi}_{SS}}{\tau_{\dot{\phi}}} \tag{3.58}$$

where $\Delta\dot{\phi}_{SS}$ is the error in the averaged steady-state roll rate as a result of the wheel step input and $\tau_{\dot{\phi}}$ is the $\pm 2°/s$ roll rate tolerance. Two cases of roll response tests, cruise and approach aircraft configurations, are implemented into the roll damping cost function and the residuals are denoted as $r_{RR,1}$ and $r_{RR,2}$.

The full residual for the roll damping optimization during the time-domain damping step is assembled as

$$\boldsymbol{r} = \begin{bmatrix} r_{DCC,\phi,1} & r_{DCC,\phi,2} & r_{RR,1} & r_{RR,2} \end{bmatrix}^T \tag{3.59}$$

The trim failure protection factors, Equations 3.32 and 3.33, are not implemented within the damping step as the calibration parameters, which are a function of attitude rates, has no effect on trimming as attitude rates are zero when the aircraft is trimmed. The optimization routine using two dynamic control check tests and two roll response tests converged in 582 seconds or 9.7 minutes using `lsqnonlin`.

Pitch Damping The pitch damping cost function is implemented similarly with two types of tests: (1) dynamic control check tests with a pulse input of column, as described for the wheel on the roll axis and (2) phugoid tests where a quick pulse is input with the controller, exciting the dynamic phugoid mode. The same ±20% of peak rate tolerance is adopted for the dynamic control check maneuvers. The residual term from the maneuver, $r_{DCC,\theta}$, is defined as

$$r_{DCC,\theta} = \frac{\Delta\dot{\theta}_{max}}{\tau_{\dot{\theta}_{max}}} \tag{3.60}$$

where $\Delta\dot{\theta}_{max}$ is the error in the maximum pitch rate as a result of the pulse column input and $\tau_{\dot{\theta}_{max}}$ is the ±20% of peak pitch rate tolerance applied to the flight test maneuver's maximum pitch rate. Two cases of this test type are implemented into the pitch damping optimization step, one with a clean aircraft configuration and one with a takeoff flap configuration. The residuals are denoted as $r_{DCC,\theta,1}$ and $r_{DCC,\theta,2}$.

The second maneuver used for calibration of pitch damping characteristics is phugoid excitation. The metric of interest for calibration purposes is the period of the phugoid response. The period, T, is taken as the time difference between the first and second airspeed

peaks during the response, as shown in Figure 3.10. FTD Level 5 regulations state a ±10% tolerance on the period [8].

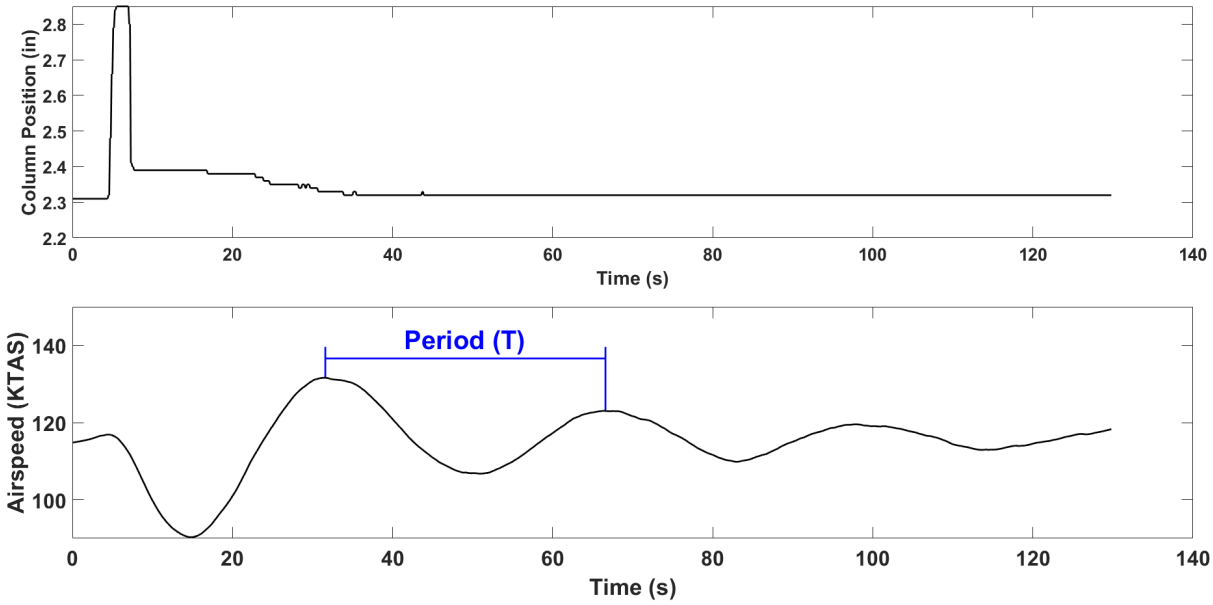

Figure 3.10: Example of phugoid period derived from flight test data

The phugoid response residual term, r_{ph}, is defined as

$$r_{ph} = \frac{\Delta T}{\tau_T} \tag{3.61}$$

where ΔT is the error in measured period and τ_T is the ±10% period tolerance applied to the phugoid flight test data's period. Phugoid damping ratio is not included as a cost function metric as the period is the primary regulated quantity for Level 5 devices. The phugoid damping ratio, while not explicitly calibrated, showed adequate agreement with flight test data as a result of the pitch damping calibration.

The full residual for the pitch damping optimization during the time-domain damping step is assembled as

$$\boldsymbol{r} = \begin{bmatrix} r_{DCC,\theta,1} & r_{DCC,\theta,2} & r_{ph} \end{bmatrix}^T \tag{3.62}$$

The optimization routine which incorporates two dynamic control check and one phugoid tests converged in approximately 44 minutes using `lsqnonlin`. The larger convergence time of this routine is due to the length of the phugoid test which represents over two minutes of flight time.

Yaw Damping The yaw damping calibration relies on dynamic control check tests, which provide sufficient excitation of the yaw mode for damping characterization. The same ±20% of peak rate tolerance is adopted for the dynamic control check maneuvers. The residual term from the maneuver, $r_{DCC,\psi}$, is defined as

$$r_{DCC,\psi} = \frac{\Delta\dot{\psi}_{max}}{\tau_{\dot{\psi}_{max}}} \tag{3.63}$$

where $\Delta\dot{\psi}_{max}$ is the error in the maximum yaw rate as a result of the pulse pedal input and $\tau_{\dot{\psi}_{max}}$ is the ±20% of peak yaw rate tolerance applied to the flight test maneuver's maximum yaw rate. Two dynamic control check data sets are used, one flown with a clean configuration and one with 30° flaps, and are denoted as $r_{DCC,\psi,1}$ and $r_{DCC,\psi,2}$.

The full residual vector is assembled as

$$\boldsymbol{r} = \begin{bmatrix} r_{DCC,\psi,1} & r_{DCC,\psi,2} \end{bmatrix}^T \tag{3.64}$$

The optimization routine performed with `lsqnonlin` converges in 246 seconds or 4.1 minutes. After the damping step, the model is considered calibrated and may then be employed for a final comparison to flight test data. The total time-domain calibration time for the Cessna 172 model is approximately 67 minutes, demonstrating its efficiency.

3.3 Validation Data Overview

The calibration methodology presented in this chapter targets agreement with available reference data within tolerances derived from FAA Part 60 requirements for Level 5 FTD

objective tests [8]. These objective test tolerances serve as the regulatory benchmark and define the accuracy standard against which the final calibrated model is measured. For comparison against POH data points, applicable tolerances are derived from Level 5 objective test tolerances. A summary of the FAA Part 60 Level 5 objective tests and tolerances, along with basic maneuver descriptions [8, 51] and notes applicable to evaluation against the MADCASP 6-DOF flight simulation framework, is provided in Appendix A, Level 5 FTD Regulatory Objective Tests. The Cessna 172 model is validated against these regulatory requirements in addition to extension of validation results to select higher level requirements (Level 6/7 FTD objective tests).

3.4 Methodology Summary

The proposed two-stage calibration methodology provides a systematic, automated approach to refining a physics-based general aviation flight simulation model using available manufacturer and flight test data. The steady-state calibration stage efficiently adjusts aerodynamic, propeller, and propulsion model parameters to match POH performance table metrics using a gradient-based least-squares optimizer.

The time-domain calibration stage extends this foundation through a sequential, multi-step process that fills gaps left when only validating against POH data, addressing aircraft pitch attitude, control surface effectiveness, flap aerodynamics, and dynamic damping characteristics using instrumented flight test data. Each step targets a specific set of model parameters, with prior results treated as fixed to limit parameter coupling. The final calibrated model is assessed against FAA Part 60 Level 5 FSTD objective test tolerances, providing a regulatory benchmark for evaluating the methodology's effectiveness.

Though presented to ultimately meet Level 5 FTD objective requirements with the Cessna 172 model, this two-stage calibration methodology may be adapted for the fidelity of the available data. In most cases, general aviation aircraft POHs will contain similar climb and cruise performance charts, making the steady-state stage application reasonably constant

across aircraft platforms. The time-domain stage is created to be adaptable based on real-world validation data availability, allowing for easy addition and removal of steps within the stage. This is particularly useful in cases where only partial data sets are available.

Results for validation of the Cessna 172 steady-state and final time-domain calibrated models are presented in the following chapter. Steady-state calibration results for the Cirrus SR20 are additionally presented to provide an initial indication of the methodology's generalization to other general aviation aircraft.

Chapter 4

Results

This chapter presents the validation results for the calibrated Cessna 172 Skyhawk model after both calibration stages: (1) the steady-state calibration stage and (2) the time-domain calibration stage. Additionally, steady-state calibration results for the Cirrus SR20 are presented as an initial demonstration of the methodology's generality to other general aviation aircraft.

4.1 Steady-State Calibration Results

The steady-state calibration routine was applied to two general aviation aircraft models: the primary validation model, Cessna 172 Skyhawk, and an additional Cirrus SR20 model to demonstrate generality of the methodology. The calibration stage, executed using `lsqnonlin` [47], converged in approximately eleven minutes for the Cessna 172 and twenty minutes for the Cirrus SR20. The following sections present the calibrated model validation results for each aircraft against the respective POH performance datasets using the post-steady-state calibration stage models.

4.1.1 Primary Cessna 172 Model Validation

The steady-state calibration routine was applied to the Cessna 172 Skyhawk baseline model, converging to the seventeen optimization parameters presented in Table 4.1, reflecting the results for factors presented in Table 3.1. The converged parameters reflect small but coupled corrections across the aerodynamic, propulsion, and propeller model components. While no single parameter requires major adjustment from its initial value, identifying the correct combination across seventeen coupled parameters manually demands significant engineering time and effort, a key motivation of the development of the automated method.

Table 4.1: Converged steady-state stage optimization parameters for the Cessna 172 Skyhawk flight simulation model

Factor	**Converged Value**
α_{shift}	0.3044°
$K_{c_{l_{slope}}}$	1.1002
$K_{c_{l,0_{offset}}}$	-0.0552
$K_{c_{d,0_{slope}}}$	0.9878
$K_{c_{d,0_{offset}}}$	0.0271
$K_{c_{d,i}}$	1.0632
J_{anchor}	0.5901
$K_{C_{T_{shift}}}$	0.0074
$K_{C_{T_{scale}}}$	1.0264
$K_{C_{T_{tilt}}}$	-0.0713
$K_{C_{T_{quad}}}$	-0.0204
$K_{C_{Q_{shift}}}$	-0.0660
$K_{C_{Q_{scale}}}$	1.0195
$K_{C_{Q_{tilt}}}$	0.0792
$K_{C_{Q_{quad}}}$	0.0500
K_{HP}	0.9829
K_{FF}	0.9000

The effects of the calibrated parameter application on the aerodynamic coefficient curves is included in Figure 4.1. The calibrated lift coefficient curve reflects an increased lift-curve slope and higher maximum lift coefficient than the baseline model along with an increase of drag across the range, with the most notable deviation from the baseline occurring at mid-to-high angles of attack. Although the drag polar shows the calibrated model producing more lift than the baseline at a given drag value, the lift-to-drag ratio, L/D, across the range of operating angles of attack is nearly identical to the baseline model. This shows that the optimizer adjusted lift and drag as necessary to meet performance requirements but preserved the overall aerodynamic efficiency of the baseline model.

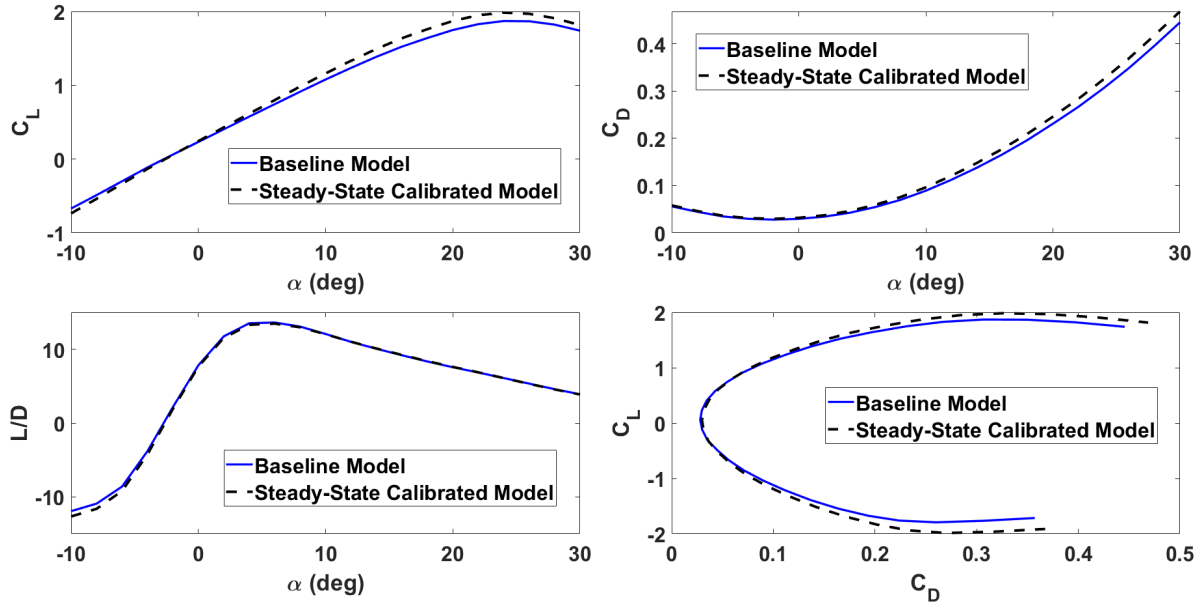

Figure 4.1: Steady-state calibrated aerodynamic coefficient curves for the Cessna 172 Skyhawk model, compared to baseline model

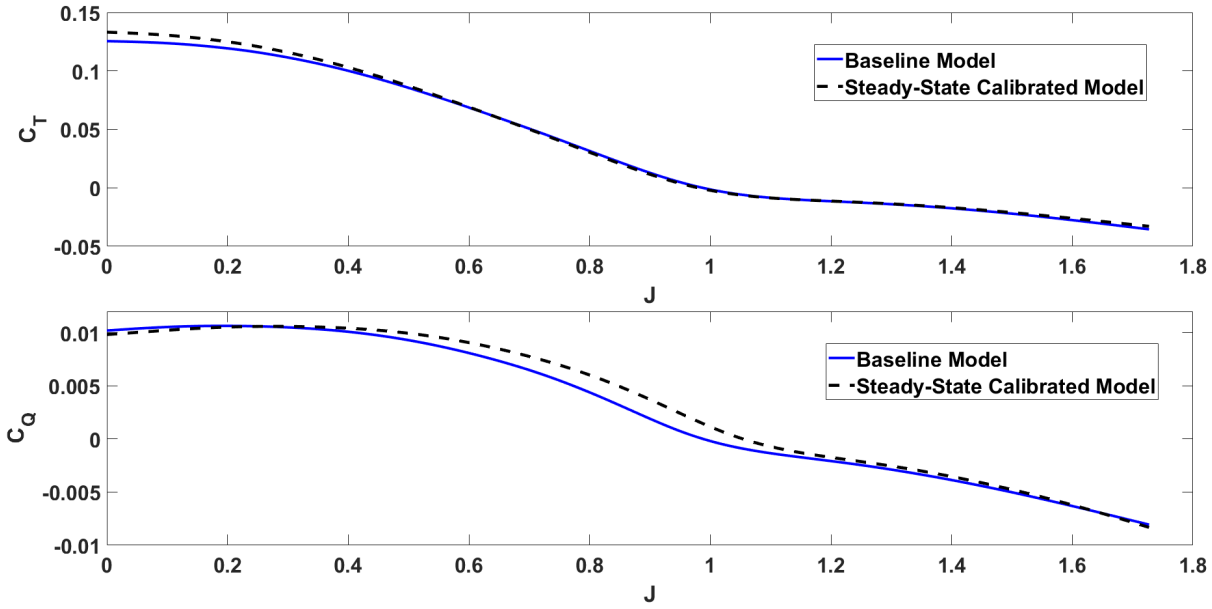

Figure 4.2: Steady-state calibrated propeller coefficient curves for the Cessna 172 Skyhawk model, compared to baseline model

The propeller coefficient comparison curves are presented in Figure 4.2 as a function of the advance ratio, J, defined as

$$J = \frac{V}{nD} \tag{4.1}$$

where V is the axial inflow velocity, n is the propeller speed, and D is the propeller's diameter. Climb conditions lie in the low advance ratio regime due to lower airspeeds and higher RPM settings, while cruise typically lies in the mid-to-high advance ratio range due to the higher airspeed and lower RPM conditions. The calibrated thrust coefficient shows a small increase at low advance ratios, boosting thrust in climb conditions, while converging back to baseline coefficient values at higher advance ratios. The calibrated torque coefficient shows the most deviation at mid-to-high advance ratios, increasing the propeller's torque absorption in cruising conditions.

The effects of the converged propulsion optimization parameters on the engine's sea level output power and fuel flow predictions are shown in Figure 4.3. The output power scaling factor, K_{HP}, produces a small uniform reduction, approximately 2%, in the output power across the manifold pressure and RPM operating range. The fuel flow scaling factor, K_{FF}, applies an uniform reduction in the predicted fuel flow across all power settings, indicating that the baseline model over-predicts fuel flow by 10% when compared to POH cruise table data.

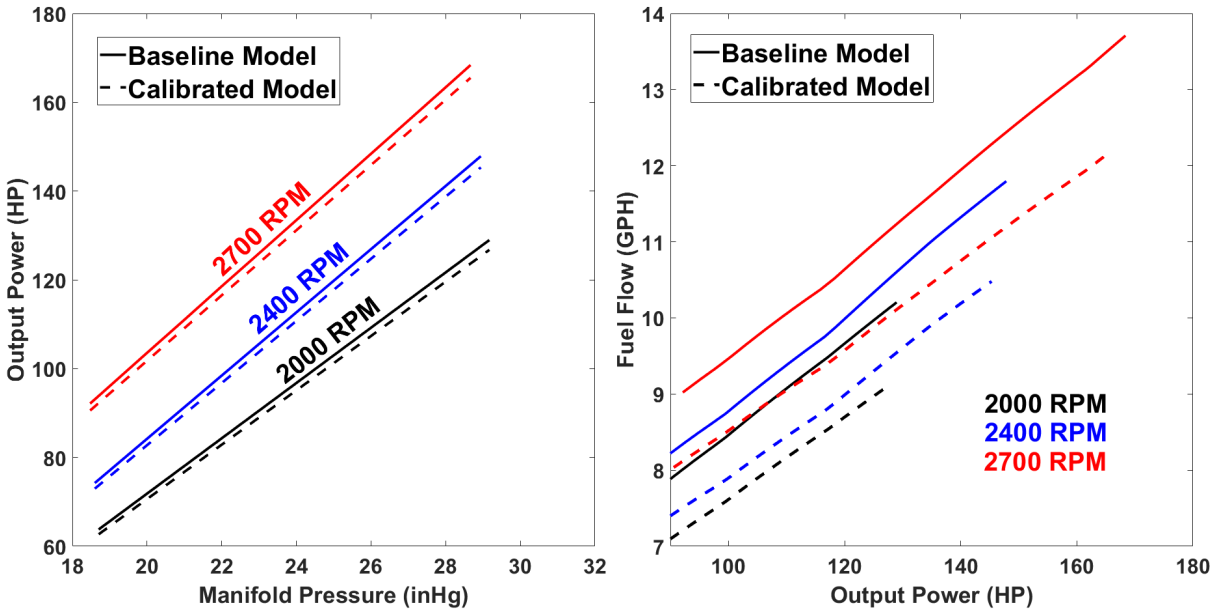

Figure 4.3: Steady-state calibrated propulsion model sea level output power and fuel flow curves for the Cessna 172 Skyhawk model, compared to baseline model

The steady-state calibrated model is evaluated against the full set of Cessna 172 POH climb and cruise performance tables [30]. An overall quantitative summary of the calibrated model's accuracy across the full POH dataset, using the metrics defined in Section 3.1.2, is provided in Table 4.2.

Table 4.2: Quantitative accuracy metrics for the steady-state calibrated Cessna 172 Skyhawk model (adapted from Table 3.2)

Metric	**Test Type**	**RMSE**	**MAPE**	**nMBE**	**Points Within Tolerance**
Climb Rate	Climb	29.8 FPM	6.2%	1.6%	100%
Percent Power	Cruise	1.2%	1.2%	-0.01%	100%
Propeller Speed	Cruise	14.7 RPM	0.5%	0.2%	100%
Fuel Flow	Cruise	0.2 GPH	0.8%	0.3%	98.2%

Climb results are presented in Table 4.3 subject to a ±100 FPM tolerance derived from the FAA Part 60 normal climb, all engines operating objective test [8]. All validated points fall within the prescribed tolerance.

A subset of the available cruise data points (standard atmospheric conditions) are presented in Table 4.4 with comparison to the full cruise performance table presented in Appendix B, Full Cessna 172 Skyhawk Steady-State Calibration Results. The metrics for validation along with tolerances include ±5% output power, ±50 RPM, and ±5% fuel flow. These tolerances are not directly taken from FAA Part 60 objective test requirements but are comparable to the cruise performance objective test criteria. All output powers, RPMs, and fuel flows at standard atmospheric conditions fall within the prescribed tolerances. For non-standard atmospheric conditions presented in Appendix B, all points fall within tolerance with the exception of two high-altitude, high-temperature points falling less than 1% outside of prescribed fuel flow tolerances, representing extreme operating conditions at the boundary of the published POH performance data. Error values are presented with green text indicating points within tolerance and red text indicating points outside of tolerance.

Table 4.3: Steady-state calibrated Cessna 172 Skyhawk model maximum rate of climb results at 2,550 lb, clean configuration, maximum throttle (POH data from [30])

Outside Air Temp (°C)	**Pressure Altitude (ft)**	**Climb Speed (KIAS)**	**Climb Rate (FPM)**			**Pass/Fail (±100 FPM)**
			POH	**Model**	**Error**	
-20	0	74	855	831	-24	**PASS**
	2000	73	760	704	-56	**PASS**
	4000	73	685	649	-36	**PASS**
	6000	73	575	548	-27	**PASS**
	8000	72	465	450	-15	**PASS**
	10000	72	360	346	-14	**PASS**
	12000	72	255	222	-33	**PASS**
0	0	74	785	784	-1	**PASS**
	2000	73	695	657	-38	**PASS**
	4000	73	620	602	-18	**PASS**
	6000	73	515	502	-13	**PASS**
	8000	72	405	405	0	**PASS**
	10000	72	300	301	1	**PASS**
	12000	72	195	178	-17	**PASS**
20	0	74	710	739	29	**PASS**
	2000	73	625	613	-12	**PASS**
	4000	73	555	558	3	**PASS**
	6000	73	450	459	9	**PASS**
	8000	72	345	363	18	**PASS**
	10000	72	240	262	22	**PASS**
	12000	72	135	138	3	**PASS**
40	0	74	645	697	52	**PASS**
	2000	73	560	571	11	**PASS**
	4000	73	495	521	26	**PASS**
	6000	73	390	433	43	**PASS**
	8000	72	285	343	58	**PASS**
	10000	72	180	242	62	**PASS**
	12000	72	–	–	–	–

Table 4.4: Steady-state calibrated Cessna 172 Skyhawk model standard atmospheric conditions cruise performance at 2,550 lb (POH data from [30])

Press Alt (ft)	KTAS	RPM			% Power			GPH		
		POH	Model	Error	POH	Model	Error	POH	Model	Error
2000	118	2550	2570	20	77	76	1	10.5	10.3	-1.9%
	115	2500	2510	10	73	71	-2	9.9	9.7	-2.0%
	110	2400	2420	20	64	64	0	9.0	8.8	-2.2%
	104	2300	2310	10	57	57	0	8.1	7.9	-2.5%
	97	2200	2190	-10	50	50	0	7.3	7.1	-2.7%
	90	2100	2080	-20	44	44	0	6.6	6.4	-3.0%
4000	120	2600	2620	20	77	75	-2	10.4	10.4	0.0%
	117	2550	2560	10	73	71	-2	9.9	9.8	-1.0%
	115	2500	2530	30	69	68	-1	9.5	9.4	-1.1%
	109	2400	2420	20	61	61	0	8.5	8.5	0.0%
	102	2300	2300	0	54	53	-1	7.7	7.6	-1.3%
	96	2200	2200	0	48	48	0	7.0	6.9	-1.4%
	89	2100	2090	-10	42	43	1	6.4	6.3	-1.6%
6000	122	2650	2670	20	77	75	2	10.4	10.4	0.0%
	119	2600	2610	10	73	71	2	9.9	9.9	0.0%
	114	2500	2520	20	65	65	0	9.0	9.0	0.0%
	108	2400	2420	20	57	58	-1	8.2	8.2	0.0%
	101	2300	2300	0	51	51	0	7.4	7.4	0.0%
	94	2200	2190	-10	45	46	1	6.7	6.7	0.0%
8000	124	2700	2720	20	77	75	-2	10.4	10.5	1.0%
	122	2650	2680	30	72	72	0	9.9	10.2	3.0%
	119	2600	2630	30	68	69	1	9.4	9.6	2.1%
	112	2500	2500	0	61	60	-1	8.6	8.6	0.0%
	106	2400	2400	0	54	54	0	7.8	7.8	0.0%
	99	2300	2290	-10	48	49	1	7.1	7.1	0.0%
	92	2200	2190	-10	43	44	1	6.5	6.4	-1.5%
10000	123	2700	2710	10	72	71	-1	9.8	10.1	3.1%
	120	2650	2660	10	68	67	-1	9.4	9.6	2.1%
	117	2600	2610	10	64	64	0	9.0	9.1	1.1%
	111	2500	2500	0	57	58	1	8.2	8.3	1.2%
	104	2400	2390	-10	51	52	1	7.5	7.5	0.0%
	97	2300	2280	-20	46	47	1	6.8	6.9	1.5%
12000	119	2650	2660	10	64	64	0	8.9	9.2	3.4%
	116	2600	2610	10	61	61	0	8.5	8.9	4.7%
	109	2500	2490	-10	54	55	1	7.8	8.0	2.6%
	102	2400	2380	-20	49	49	0	7.1	7.3	2.8%
	95	2300	2290	-10	44	45	1	6.6	6.8	3.0%

As an independent check on the aerodynamic-propulsive balance present in the steady-state calibrated model, key climb airspeeds – best rate of climb speed, V_y, and best angle of climb speed, V_x – are evaluated against POH reference values. These airspeeds were not included as an objective within the optimization cost function therefore agreement with POH data indicates that the calibrated parameter set generalizes beyond the directly optimized climb and cruise metrics. These airspeeds are evaluated against a ±3 kt tolerance, derived from FAA Part 60 normal climb objective test requirements [8]. Results for V_y and V_x at sea level and 10,000 ft altitudes are presented in Table 4.5. All key airspeeds presented fall within the prescribed airspeed tolerance.

Table 4.5: Steady-state calibrated Cessna 172 Skyhawk model key climb airspeed results (POH data from [30])

Key Airspeed	**Altitude (ft)**	**Airspeed (KIAS)**			**Pass/Fail (±3 KIAS)**
		POH	**Model**	**Error**	
V_x	0	62	64	2	**PASS**
V_x	10,000	67	68	1	**PASS**
V_y	0	74	76	2	**PASS**
V_y	10,000	72	71	-1	**PASS**

The steady-state calibration stage produces a Cessna 172 Skyhawk flight simulation model that meets prescribed performance tolerances across the full set of POH climb and cruise validation data, including key climb airspeeds not targeted by the optimization routine. The results demonstrate that the steady-state calibration stage alone produces significant improvement over the uncalibrated baseline model, providing a simulation model capable of aircraft performance prediction using only manufacturer performance data when flight test data is unavailable. The calibrated model serves as the starting point for the time-domain calibration stage.

4.1.2 Additional Cirrus SR20 Model Validation

To provide an initial demonstration of the steady-state calibration methodology's generality beyond the main validation case of the Cessna 172, the steady-state calibration stage was additionally applied to a Cirrus SR20 flight simulation model created using the methods described in Chapter 2. The SR20 calibration follows the same procedure described in Section 3.1 and is presented as a supplementary validation case with results compared against standard atmospheric condition climb and cruise performance data from the SR20 POH [52].

Like the Cessna 172, the Cirrus SR20 is a single engine, piston-propeller driven general aviation aircraft. The relevant key difference between the two aircraft models is the propeller type, where the Cirrus SR20 includes a constant-speed propeller in contrast to the Cessna 172's fixed-pitch propeller. The propeller is driven by a Teledyne Continental IO-360-ES powerplant with a rating of 200 horsepower at 2,700 RPM [52]. The PEACE-generated Cirrus SR20 geometry is included in Figure 4.4.

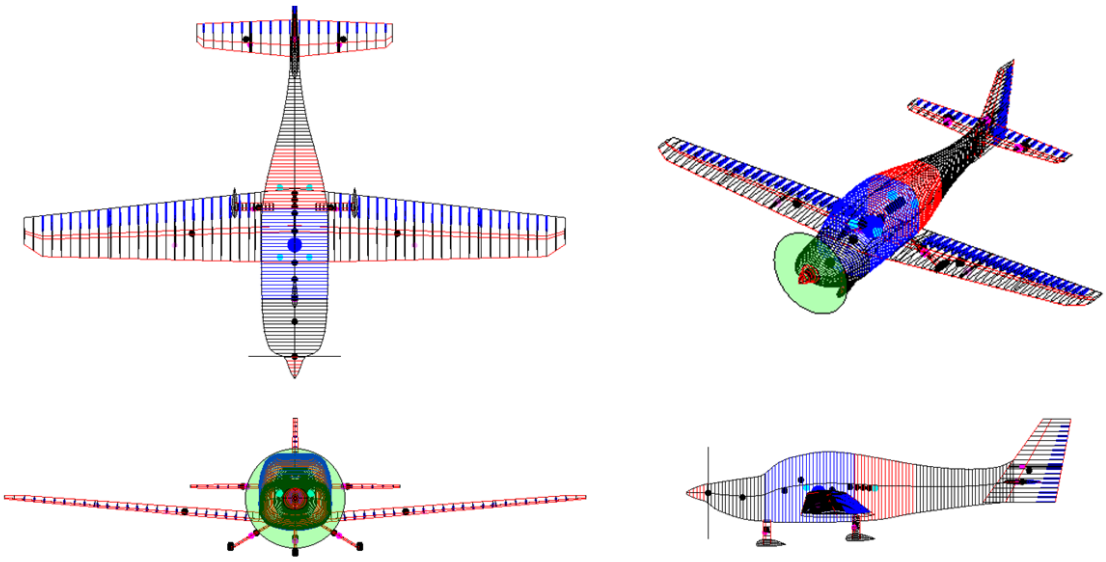

Figure 4.4: Cirrus SR20 PEACE geometry model [23]

The converged parameter set for the Cirrus SR20 model is presented in Table 4.6. The parameters reflect modest corrections across most model components, consistent with convergence behavior observed in the Cessna 172 steady-state calibration. The most notable deviations from baseline values occur in the angle of attack shift, α_{shift}, which is larger than the corresponding Cessna 172 corrections and suggests the baseline SR20 model required a more significant adjustment to align sectional lift and drag tables with the aircraft's actual operating range, and the fuel flow scaling factor, which indicates the SR20 baseline model under-predicts fuel flow relative to POH cruise data, in contrast to the over-prediction observed in the Cessna 172 baseline. Additionally, it is notable that the propeller torque coefficient corrections are small, consistent with the constant-speed propeller configuration for which the propeller governor adjusts blade pitch to maintain a commanded propeller speed, reducing the sensitivity of the trim solution to the shape of the torque coefficient curve.

Table 4.6: Converged steady-state stage optimization parameters for the Cirrus SR20 flight simulation model

Factor	**Converged Value**
α_{shift}	1.2048°
$K_{c_{l_{slope}}}$	1.0615
$K_{c_{l,0_{offset}}}$	0.0814
$K_{c_{d,0_{slope}}}$	0.9355
$K_{c_{d,0_{offset}}}$	-0.0088
$K_{c_{d,i}}$	0.9833
J_{anchor}	0.5673
$K_{C_{T_{shift}}}$	0.0602
$K_{C_{T_{scale}}}$	1.0802
$K_{C_{T_{tilt}}}$	-0.0045
$K_{C_{T_{quad}}}$	-0.1139
$K_{C_{Q_{shift}}}$	0.0059
$K_{C_{Q_{scale}}}$	1.0099
$K_{C_{Q_{tilt}}}$	-0.0063
$K_{C_{Q_{quad}}}$	0.0863
K_{HP}	0.9712
K_{FF}	1.0676

The steady-state calibrated model is evaluated against the set of Cirrus SR20 POH climb and cruise standard atmospheric conditions performance tables [52]. An overall quantitative summary of the calibrated model's accuracy across the full POH dataset, using the metrics defined in Section 3.1.2, is provided in Table 4.7.

Table 4.7: Quantitative accuracy metrics for the steady-state calibrated Cirrus SR20 model

Metric	**Test Type**	**RMSE**	**MAPE**	**nMBE**	**Points Within Tolerance**
Climb Rate	Climb	58.9 FPM	14.0%	11.2%	93.8%
Percent Power	Cruise	2.0%	2.6%	-1.0%	100%
Propeller Speed	Cruise	10.7 RPM	0.1%	0.1%	100%
Fuel Flow	Cruise	0.4 GPH	2.5%	-1.5%	87.2%

Climb results are presented in Table 4.8 subject to a ±100 FPM tolerance derived from the FAA Part 60 normal climb objective test requirements [8]. One performance point falls outside of the prescribed tolerance by 5 FPM, occurring at a high-altitude and maximum gross weight condition, representing the most constrained corner of the operating envelope where reduced air density limits engine and propeller performance while maximum weight increases the thrust required to maintain climb.

Table 4.8: Steady-state calibrated Cessna SR20 model standard atmospheric conditions enroute climb results with clean configuration and maximum throttle (POH data from [52])

Weight (lb)	**Pressure Altitude (ft)**	**Climb Speed (KIAS)**	**Climb Rate (FPM)**			**Pass/Fail (±100 FPM)**
			POH	**Model**	**Error**	
3000	0	96	880	819	-61	**PASS**
	2000	95	775	713	-62	**PASS**
	4000	94	671	639	-32	**PASS**
	6000	93	566	581	6	**PASS**
	8000	92	452	505	43	**PASS**
	10000	91	357	430	73	**PASS**
	12000	91	252	335	83	**PASS**
	14000	90	148	253	105	**FAIL**
2500	0	93	1132	1125	-7	**PASS**
	2000	92	1016	999	-17	**PASS**
	4000	92	900	900	0	**PASS**
	6000	91	785	808	23	**PASS**
	8000	90	670	721	51	**PASS**
	10000	89	555	627	72	**PASS**
	12000	88	440	517	77	**PASS**
	14000	88	325	410	85	**PASS**

Cruise performance results are presented in Table 4.9 for all POH data points at standard atmospheric conditions. The acceptable tolerances are given again as ±5% percent power, ±50 RPM, and ±5% fuel flow. Four performance points fall outside of the prescribed tolerances, all existing at cruise power setting above the POH's recommended cruise normal procedure values, 50% - 75% power [52]. At low-altitude, high-power cruise settings, the model indicates that the propeller struggles to absorb the engines power at 2,700 RPM settings, with the model's RPM being driven to a higher speed. These conditions are extrema for Cirrus SR20 cruise and are noted as not recommended flying conditions in the POH [52].

Table 4.9: Steady-state calibrated Cirrus SR20 model standard atmospheric conditions cruise performance at 2,600 lb (POH data from [52])

Press Alt (ft)	KTAS	RPM			% Power			GPH		
		POH	Model	Error	POH	Model	Error	POH	Model	Error
2000	160	2700	2750	50	95	92	-3	15.0	14.3	-4.7%
	154	2500	2500	0	85	81	-4	13.4	12.4	-7.5%
	151	2500	2500	0	80	78	-2	12.8	12.1	-5.5%
	147	2500	2500	0	75	73	-2	11.6	11.5	-0.9%
	143	2500	2500	0	70	69	-1	11.1	10.9	-1.8%
	139	2500	2500	0	65	65	0	10.6	10.5	-0.9%
	136	2500	2500	0	62	63	1	10.2	10.2	0.0%
	127	2500	2500	0	52	57	5	9.2	9.5	3.3%
4000	159	2700	2720	20	89	86	-3	14.4	13.5	-6.3%
	153	2500	2500	0	79	76	-3	12.7	11.8	-7.1%
	150	2500	2500	0	75	73	-2	11.6	11.5	-0.9%
	146	2500	2500	0	70	69	-1	11.1	10.9	-1.8%
	141	2500	2500	0	65	64	-1	10.5	10.3	-1.9%
	136	2500	2500	0	60	60	0	10.0	9.9	-1.0%
	131	2500	2500	0	55	57	2	9.4	9.6	2.1%
6000	159	2700	2737	37	83	82	-1	13.0	13.0	0.0%
	152	2500	2500	0	74	71	-3	11.5	11.3	-1.7%
	148	2500	2500	0	70	68	-2	11.1	10.8	-2.7%
	144	2500	2500	0	65	63	-2	10.6	10.3	-2.8%
	140	2500	2500	0	61	60	-1	10.0	9.9	-1.0%
	134	2500	2500	0	55	56	1	9.5	9.5	0.0%
8000	157	2700	2700	0	77	75	-2	11.6	11.2	-3.4%
	150	2500	2500	0	69	67	-2	11.0	10.6	-3.6%
	146	2500	2500	0	65	63	-2	10.5	10.2	-2.9%
	142	2500	2500	0	60	59	-1	10	9.8	-2.0%
	136	2500	2500	0	55	55	0	9.5	9.4	-1.0%
	131	2500	2500	0	50	52	2	8.9	9.1	2.2%
10000	155	2700	2700	0	72	70	-2	11.2	11.5	2.7%
	148	2500	2500	0	64	62	-2	10.5	10.1	-3.8%
	144	2500	2500	0	60	58	-2	10.0	9.7	-3.0%
	139	2500	2500	0	55	55	0	9.5	9.3	-2.1%
	134	2500	2500	0	50	52	2	9.0	9.0	0.0%
12000	153	2700	2700	0	66	65	-1	10.7	10.9	1.9%
	146	2500	2500	0	59	57	-2	9.9	9.6	-3.0%
	141	2500	2500	0	55	54	-1	9.5	9.2	-3.2%
	136	2500	2500	0	50	51	1	8.9	8.9	0.0%
14000	151	2700	2700	0	62	61	-1	10.2	10.4	2.0%
	144	2500	2500	0	55	53	-2	9.5	9.2	-3.2%
	142	2500	2500	0	50	52	2	9.0	9.0	0.0%

The steady-state calibration stage applied to the Cirrus SR20 demonstrates the methodology is applicable beyond its primary development case on the Cessna 172 model and is capable of handling multiple propeller configuration types. The SR20 steady-state calibrated model meets prescribed performances across the majority of the aircraft's standard atmospheric conditions operating envelope with discrepancies isolated to extreme operating conditions consistent with normal operation limitations outlined in the POH [52]. Together, the included steady-state calibration results demonstrate that the proposed steady-state calibration stage methodology is an efficient and generalized approach to flight simulation model calibration to POH performance chart data for general aviation aircraft.

4.2 Time-Domain Calibration Results

The following section presents the time-domain calibration stage results for the Cessna 172 Skyhawk model, modifying the steady-state calibrated model to match flight test data aircraft attitudes, control surface deflections, and dynamic response characteristics. The calibrated factors obtained at each step – pitching moment, control surface effectiveness, flap aerodynamics, and damping steps – are presented along with a summary of the final calibrated model's performance compared to available instrumented flight test data. Appendix C, Full Cessna 172 Skyhawk Calibrated Model Time-Domain Results, presents the complete set of objective test results for the final calibrated model, covering all FAA Part 60 Level 5 FTD requirements [8] as outlined in Appendix A, with additional cases drawn from Level 6 and 7 requirements for broader model characterization. Each test presents simulation and validation data alongside prescribed tolerance bands for direct comparison.

4.2.1 Pitching Moment Calibration Step

The converged parameter set obtained during the pitching moment step, outlined in Table 3.4, are listed in Table 4.10. The effects of the calibrated parameter application to aerodynamic coefficient curves is included in Figure 4.5 with comparisons to the baseline

and steady-state calibrated model's curves. The figure presents the modified lift and drag coefficient curves along with the pitching moment coefficient due to their dependence on the $\alpha_{shift_{addl}}$ optimization parameter considered in this calibration step.

Table 4.10: Converged pitching moment optimization step calibration parameters for the Cessna 172 Skyhawk flight simulation model

Factor	Converged Value
$\alpha_{shift_{addl}}$	1.3760°
$K_{c_{m_{slope}}}$	1.7991
$K_{c_{m,0_{offset}}}$	0.1822

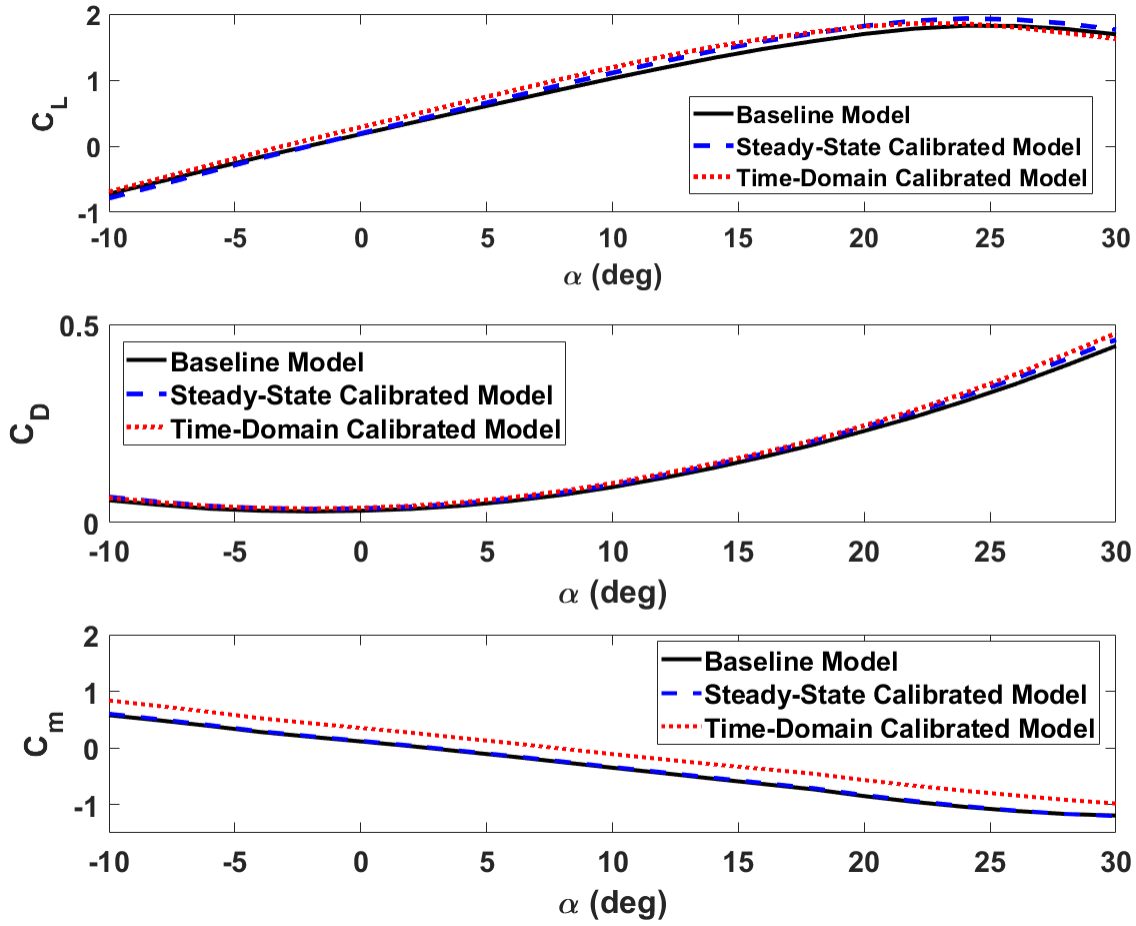

Figure 4.5: Pitching moment step calibrated Cessna 172 Skyhawk model aerodynamic coefficient curves compared to baseline and steady-state calibrated models

The converged pitching moment step parameters reflect larger corrections to the underlying aerodynamic model than those observed in the steady-state calibration stage, indicating that the baseline model required more significant adjustments to match the real-world aircraft's pitch attitude in trimmed conditions. The additional angle of attack shift factor adjusts the α at which the coefficients are queried at a given trim point, while the remaining two factors address the under-prediction of pitching moment coefficient slope and zero-lift pitching moment coefficient present in the steady-state calibrated model. The lift and drag coefficients show modest incremental shifts due to the further shifting of the effective angle of attack that sectional aerodynamic tables are queried at while the pitching moment curve shows the most dramatic adjustment, illustrating the notable pitching moment slope and zero-lift pitching moment offsets present in the converged parameter set.

The pitching moment calibration factors are applied exclusively to the wing sectional strips, absorbing any trimmed pitching attitude errors, such as wing and horizontal tail sectional pitching moment coefficient lookup table errors, horizontal tail lift coefficient errors, downwash model errors, and uncaptured fuselage interference effects, present in the model when calibrated to match available flight test data. The design decision to focus optimization efforts on a singular surface's aerodynamic characteristics is driven by the desire to avoid parameter identification issues that may arise when multiple surfaces are assigned independent pitching moment calibration factors. Trimmed pitch attitude alone does not provide sufficient information to distinguish the contributions of individual surfaces to the total pitching moment balance, leaving the optimizer without a physical basis for distributing corrections across components. Isolating pitching moment corrections to the wing aerodynamics allows for a well-posed optimization problem that meets the objective of this calibration step, to match trimmed pitch attitudes to real-world validation data, but may result in coefficient corrections that do not accurately represent pitching moment contribution distribution across the aircraft's surfaces.

Validation of the converged parameters is assessed using the trimmed pitch attitude compared to real-world flight test data. Figure 4.6 presents a parity plot for a subset of climb and cruise points including the optimizer targets and additional verification points, with only one falling out of tolerance. A comprehensive evaluation of the results is provided through the comparison of trimmed pitch initial conditions for the time-domain objective tests in Appendix C, Full Cessna 172 Skyhawk Calibrated Model Time-Domain Results.

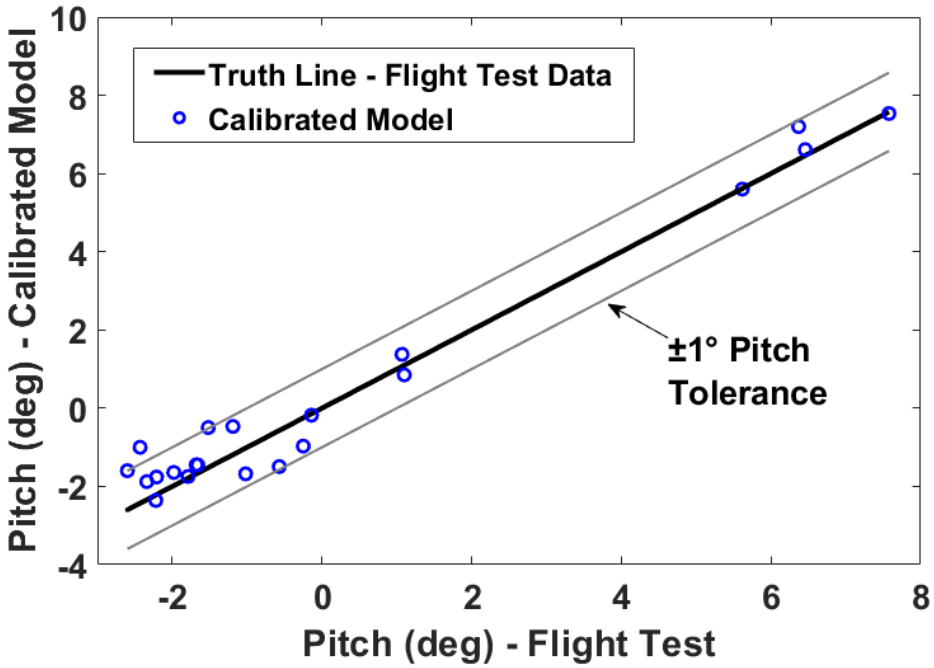

Figure 4.6: Parity plot of calibrated Cessna 172 Skyhawk pitch attitude versus flight test data for a subset of climb and cruise trim points following pitching moment calibration step

4.2.2 Control Surface Effectiveness Calibration Step

The converged parameter set obtained during the control surface effectiveness step, outlined in Table 3.5, are listed in Table 4.11.

Table 4.11: Converged control surface effectiveness step calibration parameters for the Cessna 172 Skyhawk flight simulation model

Factor	Converged Value
$K_{\delta,e_{slope}}$	2.0747
$K_{\delta,e_{offset}}$	1.1145 m^2/s
$K_{\delta,a_{slope}}$	1.1865
$K_{\delta,a_{offset}}$	0.6710 m^2/s
$K_{\delta,r_{slope}}$	2.5196
$K_{\delta,r_{offset}}$	0.0460 m^2/s
K_{PF}	0.0709

For all three control surface slope and offset combinations, the offset terms are small relative to their allowable bounds, indicating that the dominant calibration effect arises from the slope terms. The elevator and rudder converged parameters indicate that the slope of the circulation prediction must be adjusted by more than double the baseline values to match flight test data control surface deflections. Alternatively, the aileron slope factor converges to indicate an error of approximately 20%. The disparity between the effectiveness errors in the tail mounted control surfaces and the wing-mounted ailerons suggests the baseline spanwise loading model under-predicts the lift increment due to control surface deflection much more significantly at the tail surfaces than at the wing. These under-predictions may be attributable to a combination of lack of propeller slipstream modeling, the lack of influence of wing downwash on tail control surfaces, and other un-modeled aerodynamic effects. Additionally, the large correction on the elevator likely arises from the substantial increase in pitching moment on the wing applied in the pitching moment calibration step. Similar to the results of the pitching moment calibration results, the various modeling deficiencies or inaccuracies are lumped into these control surface circulation modification parameters and

allow for matching control surface deflections at quasi-steady-state points. The converged P-factor correction term, K_{PF}, is small and allows for corrections to high-power, high-angle of attack climb situations to match flight test rudder deflections.

Validation of the converged parameters is assessed using the trimmed control surface positions compared to real-world flight test data control positions. Figures 4.7- 4.9 present parity plots for a subset of climb and cruise points, including both the optimizer target and additional points. All assessed points fall within a tight $\pm 1^\circ$ tolerance. Further validation of the converged parameter set is accomplished by examining the trimmed control surface positions reported as initial conditions for the time-domain objective tests presented in Appendix C, Full Cessna 172 Skyhawk Calibrated Model Time-Domain Results.

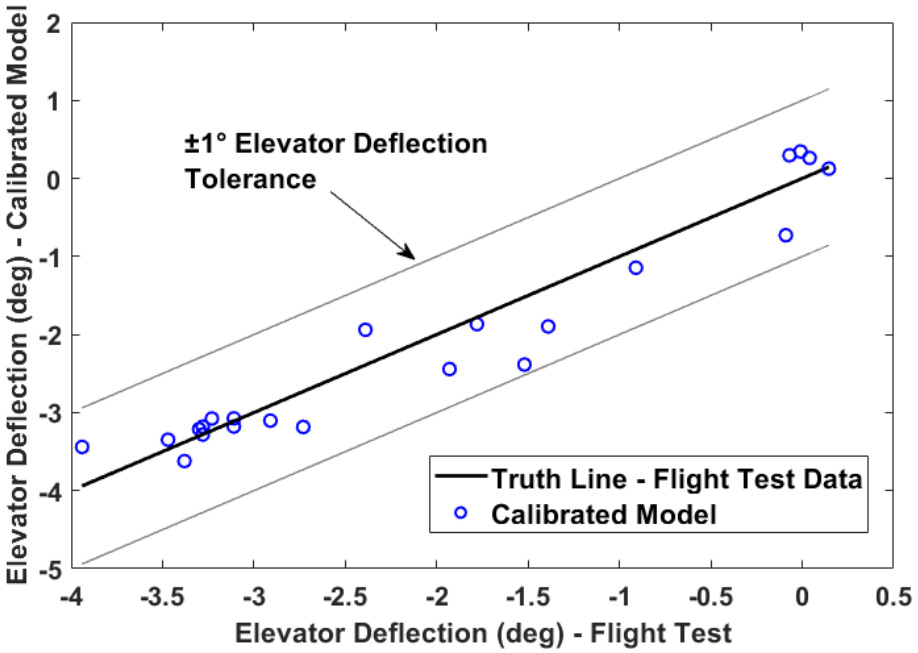

Figure 4.7: Parity plot of calibrated Cessna 172 Skyhawk elevator deflection versus flight test data for a subset of climb and cruise trim points following control surface effectiveness step

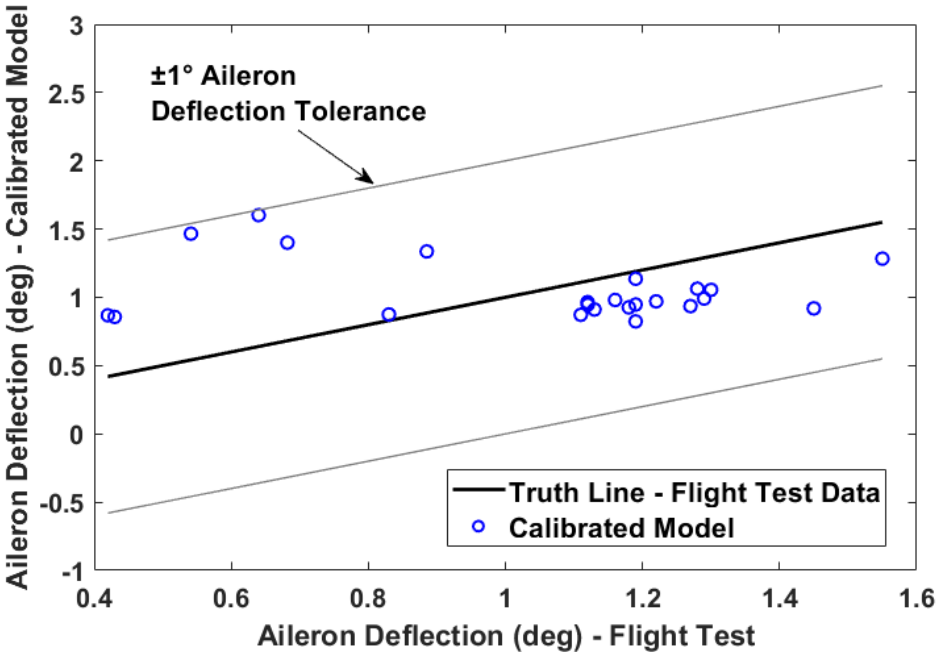

Figure 4.8: Parity plot of calibrated Cessna 172 Skyhawk aileron deflection versus flight test data for a subset of climb and cruise trim points following control surface effectiveness step

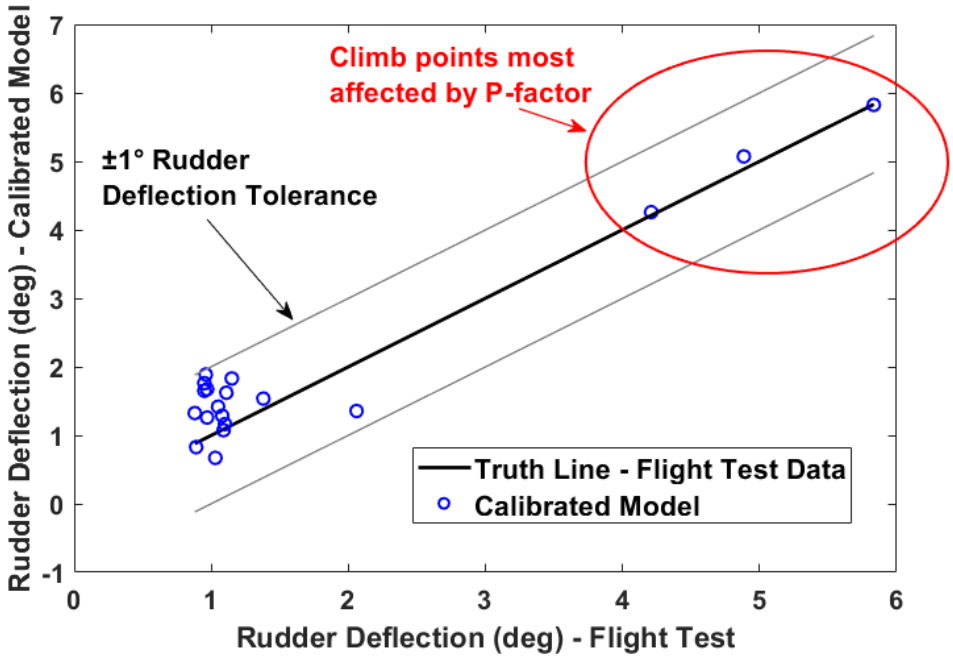

Figure 4.9: Parity plot of calibrated Cessna 172 Skyhawk rudder deflection versus flight test data for a subset of climb and cruise trim points following control surface effectiveness step

4.2.3 Flaps Aerodynamics Calibration Step

The converged parameter set obtained during the flaps aerodynamics calibration step, outlined in Table 3.6, are listed in Table 4.12. The positive converged value for the parasitic drag increment due to flap deflection, $K_{\Delta c_{d,0_{flaps}}}$, suggests the baseline and steady-state calibrated models required an increase in the applied drag to match flaps-down climb rates reported in flight test data. This is consistent with the expectation that three-dimensional installation and interference effects produce additional drag beyond what the baseline strip theory model is equipped to capture. The negative converged value for the pitching moment increment due to flap deflection, $K_{\Delta c_{m_{flaps}}}$, indicates that an additional nose-down pitching moment correction must be present to match flaps-down trimmed pitch attitudes in flight test data. The calibrated aerodynamic coefficient curves at each flap increment in the time-domain calibrated Cessna 172 Skyhawk model is included in Figure 4.10. The C_L curves represent the model's characteristics with the implemented spanwise loading prediction and is not modified during this flaps aerodynamic calibration step. All flaps-down climb rate corrections are lumped into the calibrated parasitic drag increment with effects shown in the C_D curves with drag coefficient increments increasing with flap deflection. The C_m curves show a progressive nose-up pitching moment shift with increasing flap deflection, as expected. The converged incremental pitching moment factor decreases this increase with flap deflection when compared to the uncalibrated version of the model.

Table 4.12: Converged flaps aerodynamics step calibration parameters for the Cessna 172 Skyhawk flight simulation model

Factor	**Converged Value**
$K_{\Delta c_{d,0_{flaps}}}$	0.8392
$K_{\Delta c_{m_{flaps}}}$	-1.8507

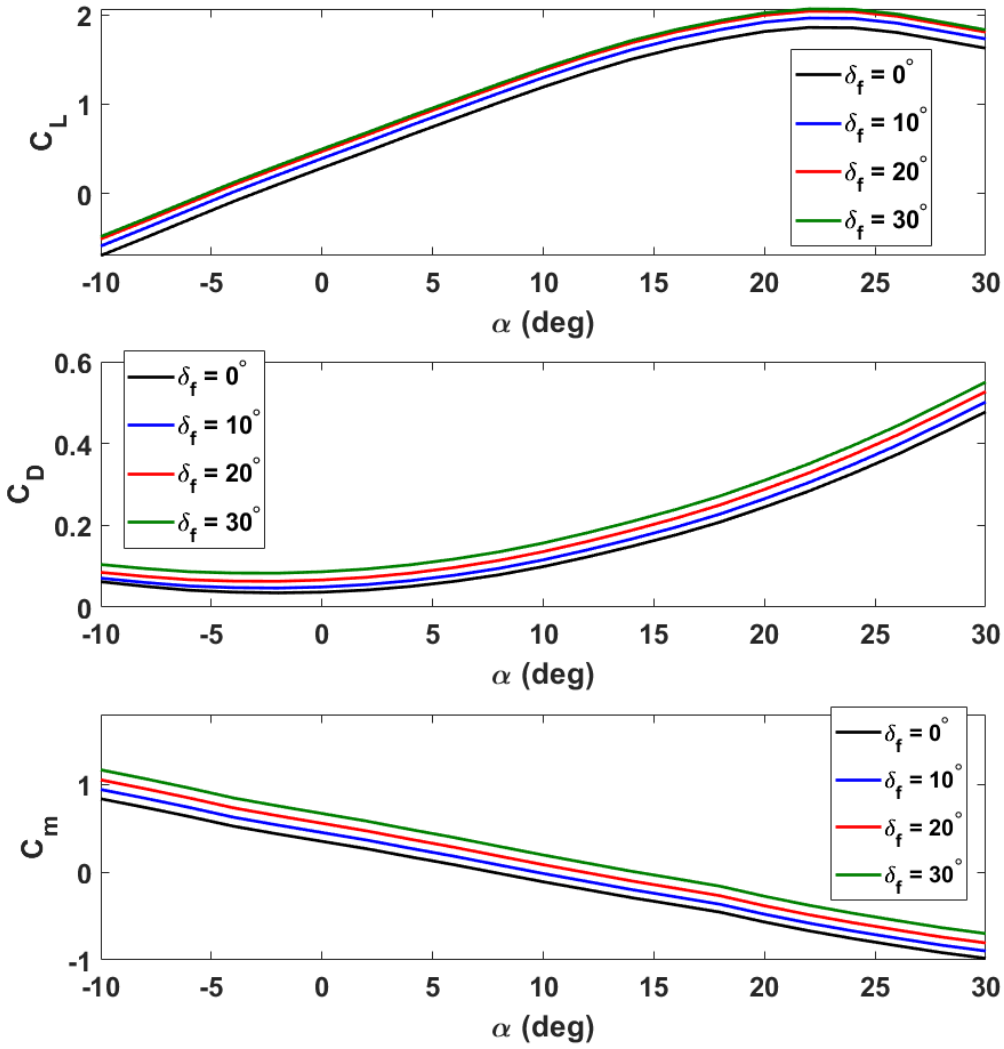

Figure 4.10: Flap deflection aerodynamic coefficient curves for the Cessna 172 Skyhawk flight simulation model after flap aerodynamic calibration step

Only one case of flaps-down climb, takeoff position (10°), is included in the provided Cessna 172 flight test package with three quasi-steady-state climb trim points extracted for validation. The comparison of these points after flaps aerodynamic step calibration are presented in Table 4.13 and assessed against the widely used ±100 FPM climb rate tolerance. All points fall within the tolerance and can be assessed further in the time-domain flaps down tests presented in Appendix C, Full Cessna 172 Skyhawk Calibrated Model Time-Domain Results.

Table 4.13: Flaps-down (10°) climb rate comparison between the calibrated Cessna 172 Skyhawk flight simulation model and flight test data following the flap aerodynamics calibration step

Weight (lb)	**Pressure Altitude (ft)**	**Climb Speed (KTAS)**	**Climb Rate (FPM)**			**Pass/Fail (±100 FPM)**
			Flight Test Data	**Model**	**Error**	
2442	3454	84	554	560	6	**PASS**
2442	3773	83	570	562	-8	**PASS**
2442	4719	86	539	495	-44	**PASS**

Validation of the converged parameter set is completed using the trimmed pitch attitudes in flaps-down climb and cruise compared to real-world flight test data. Limitations in the parameterization of this calibration step arise when examining the parity plot presents in Figure 4.11 where a significant number of the model's pitch attitude predictions fall slightly above the prescribed ±1° pitch tolerance. Three possible limiting sources have been identified: (1) The single scalar pitching moment correction factor is applied uniformly across all flap deflection angles and flight conditions, requiring the optimizer to find a compromise solution across the full data set. (2) Trimmed pitch attitude is coupled to the lift balance which is not modified in this optimizer step. Errors in the lift increment due to flap deflection may manifest in the trimmed pitching attitude. (3) The pitch attitude error parameter is coupled with the climb rate discrepancy within the step's cost function introducing coupling, as changes in the drag correction influence trim solutions and pitch attitudes. The validation cases available for flap-down climb includes only three trimmed points, making the dataset small and introducing a danger of overfitting the drag calibration factor for only one flap setting. Expanding the parameterization to include flap deflection dependent corrections, lift increment factors, and sequential calibration of the climb rate and pitch attitude parameters are possible avenues for future refinement of the methodology to improve trimmed

pitch attitude for flaps-down trimmed conditions. The sequential calibration approach mirrors the clean aerodynamics treatment, where the steady-state stage handles lift and drag calibration to meet climb rate requirements and the time-domain pitching moment step handles pitch attitude requirements. Despite the limitations, required pitch tolerances are met where required within the full results presented in Appendix C, Full Cessna 172 Skyhawk Calibrated Model Time-Domain Results and may be validated by comparing the trimmed pitch attitudes presented as initial conditions for flaps-down tests.

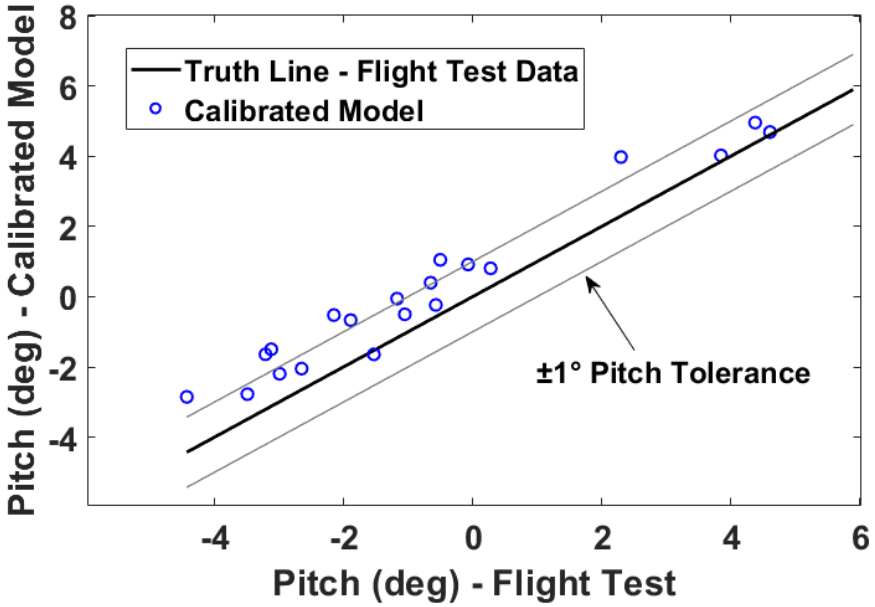

Figure 4.11: Parity plot of calibrated Cessna 172 Skyhawk pitch attitude versus flight test data for a subset of climb and cruise trim points following flaps aerodynamics step

4.2.4 Damping Step

The converged parameter set resulting from the damping calibration step, outlined in Table 3.7, are listed in Table 4.14. All three converged parameters are positive indicating, by their formulation explained in Section 3.2.4, that the corrections oppose their respective body rates. This suggests, as mentioned previously, that the baseline model was underpredicting aerodynamic damping on all axes. The roll and yaw damping terms introduced are significantly smaller than the correction applied on the pitch axes, consistent with the

reasoning presented previously that the reference lengths differ between the longitudinal axes and lateral/directional axes.

Table 4.14: Converged damping step calibration parameters for the Cessna 172 flight simulation model

Factor	Converged Value
$K_{C_{L,p}}$	0.0141
$K_{C_{M,q}}$	0.4876
$K_{C_{N,r}}$	0.0081

To validate the output of this step, dynamic control check test results for the pitch, roll, and yaw axes, which are targets of the calibration step, are presented in Figures 4.12, 4.13, and 4.14 respectively. In all three presented cases, the calibrated model's maximum body rate falls within the prescribed ±20% tolerance derived from Level 7 FTD objective tests, exceeding the methodology adopted Level 5 requirements. This demonstrates the calibrated model's dynamic response characteristics generalize beyond minimum regulatory standards.

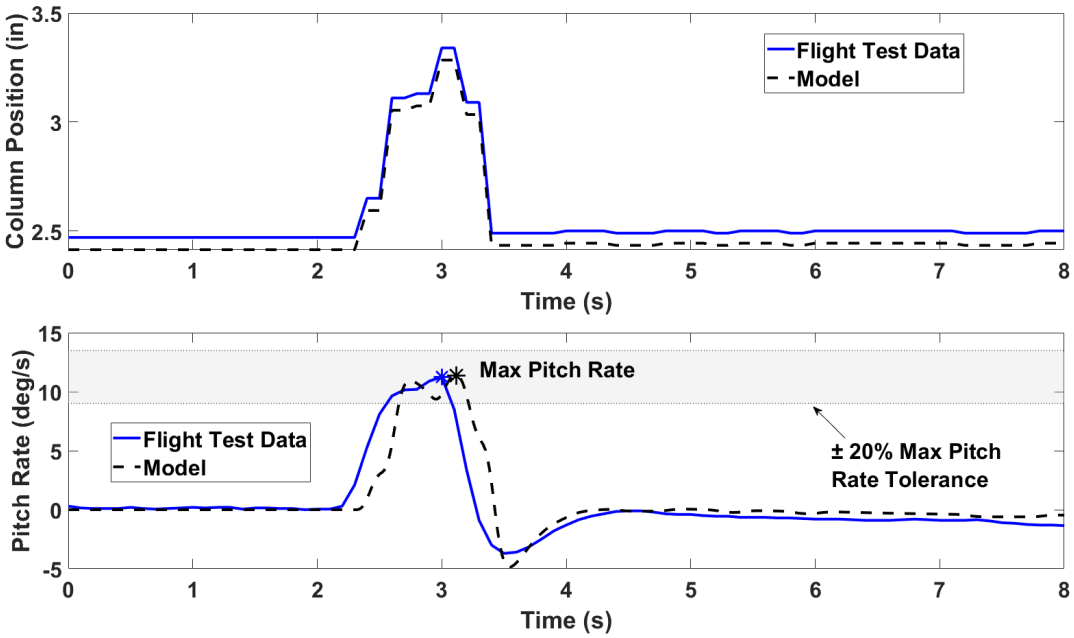

Figure 4.12: Dynamic control check pitch rate response comparison between the calibrated Cessna 172 Skyhawk flight simulation model and flight test data following the damping calibration step

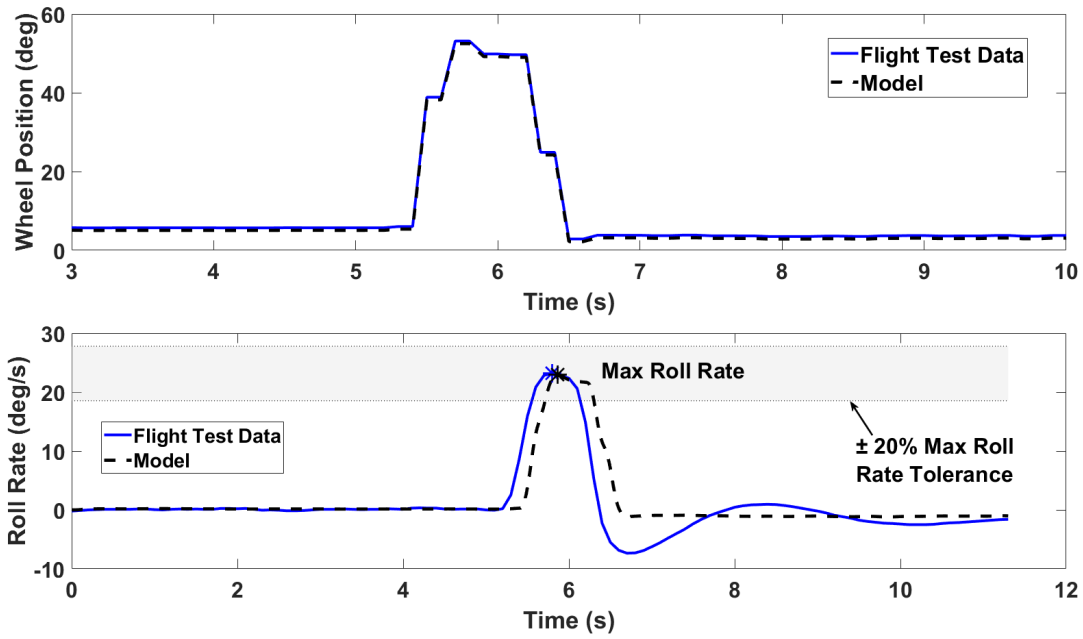

Figure 4.13: Dynamic control check roll rate response comparison between the calibrated Cessna 172 Skyhawk flight simulation model and flight test data following the damping calibration step

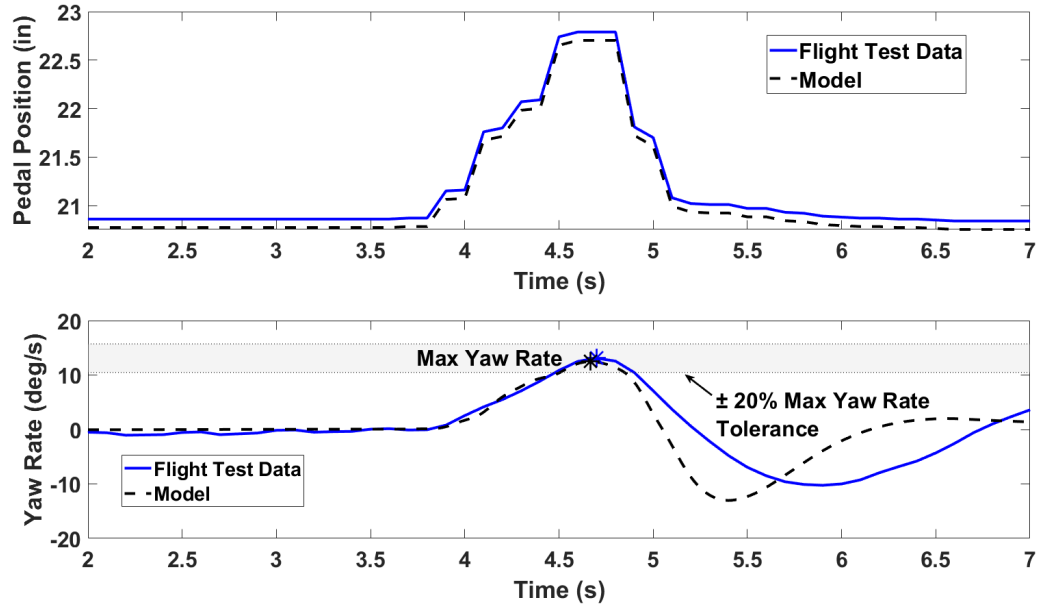

Figure 4.14: Dynamic control check yaw rate response comparison between the calibrated Cessna 172 Skyhawk flight simulation model and flight test data following the damping calibration step

Further validation of this step can be completed by assessing the model's match to validation data for the following tests included in Appendix C, Full Cessna 172 Skyhawk Calibrated Model Time-Domain Results: (1) roll axis - Roll Response tests, (2) pitch axis - Phugoid and Short Period tests, and (3) yaw axis - Dutch roll test. Additional dynamic control check cases for each axis are also included in Appendix C for further validation.

4.2.5 Time-Domain Validation Test Suite Summary

The final calibrated Cessna 172 Skyhawk model is evaluated against a comprehensive test suite of objective tests to meet FAA Part 60 Level 5 FTD requirements [8], with additional tests derived from Level 6 and 7 requirements to provide additional verification of model characteristics where flight test data is available. The full set of tests and results is presented in Appendix C, Full Cessna 172 Skyhawk Calibrated Model Time-Domain Results, where each test case includes the validation data, simulation data, and prescribed tolerance bands for direct comparison. Where standard test procedures or tolerances could not be directly applied due to limitations in the available flight test data package or the current simulation framework, adaptations are noted within the individual test results. A summary of all test cases included in the validation suite is provided in Table 4.15, organized by FAA Part 60 test category and qualification level.

Table 4.15: Summary of objective tests included in the validation suite for the calibrated Cessna 172 Skyhawk flight simulation model

Test ID	Test Name	Qualification Level	Flight Condition
1. Performance			
1.c Climb			
1.c.1	Normal climb, All Engines Operating	5	Clean configuration
N/A	Flaps-down climb	N/A	Flaps-down configuration
1.f Engines			
1.f.1	Acceleration	5	Approach or Landing
1.f.2	Deceleration	5	On ground
2. Handling Qualities			
2.a Static Control Tests			
2.a.1.a/b	Pitch controller position versus force and surface position calibration	5/6	On ground
2.a.2.a/b	Roll controller position versus force and surface position calibration	5/6	On ground
2.a.3.a/b	Rudder pedal position versus force and surface position calibration	5/6	On ground
2.b Dynamic Control Tests			
2.b.1/2.b.4	Pitch Control/Small Control Inputs - Pitch	7	As available
2.b.2/2.b.5	Roll Control/Small Control Inputs - Roll	7	As available
2.b.3/2.b.6	Yaw Control/Small Control Inputs - Yaw	7	As available
2.c Longitudinal Control Tests			
2.c.1.b	Power Change Force	5	Approach

Continued on next page

Table 4.15 – continued from previous page

Test ID	Test Name	Qualification Level	Flight Condition
2.c.2.a/b	Flap Change Dynamics/Force	5/6	Takeoff through initial flap retraction and approach to landing
2.c.5	Longitudinal Trim	5	Cruise, Approach, and Landing
2.c.6	Longitudinal Maneuvering Stability	6	Cruise, Approach, and Landing
2.c.7	Longitudinal Static Stability	5	Approach
2.c.9.b	Phugoid Dynamics	5	Cruise
2.c Lateral Directional Tests			
2.d.2	Roll Response (Rate)	5	Cruise, and Approach or Landing
2.d.4	Spiral Stability	5	Cruise
2.d.6	Rudder Response	5	Approach or Landing
2.d.7	Dutch Roll	6	Cruise, and Approach or Landing
2.d.8	Steady Heading Sideslip	5	Approach or Landing

4.3 Summary

The results presented within this chapter demonstrate the effectiveness of the proposed two-stage calibration methodology when applied to the Cessna 172 Skyhawk flight simulation model. The steady-state calibration routine modifies the baseline model to produce a version that meets prescribed performance tolerances across a full set of POH cruise and climb performance chart data. A supplementary case is presented with the steady-state

stage exercised on a Cirrus SR20 flight simulation model as an initial demonstration of the method's generality. The time-domain stage then modifies the steady-state calibrated model to match aircraft attitudes, control surface deflections, and dynamic response characteristics to match flight test data. The final model output is demonstrated in compliance with FAA Part 60 Level 5 FTD objective test requirements [8] with additional higher-level test cases presented where data is available. The complete objective test results for the time-domain calibrated model are presented in Appendix C, Full Cessna 172 Skyhawk Calibrated Model Time-Domain Results. The following chapter summarizes the presented methodology and results, drawing conclusions and identifying pathways for future work and improvements.

Chapter 5

Conclusions and Future Work

5.1 Conclusions

This work presents an automated two-stage methodology for calibrating general aviation flight simulation models to available manufacturer and flight test data, targeting a final goal of compliance with FAA Part 60 Level 5 FTD objective test requirements (subject to model function limitations). The methodology was demonstrated on a Cessna 172 Skyhawk flight simulation model with a PEACE-generated baseline model executed within the MADCASP framework. A supplementary steady-state stage validation case was presented using a Cirrus SR20 baseline model.

The steady-state calibration stage is presented as a seventeen factor parameterization of the baseline model's aerodynamic, propulsion, and propeller characteristics. The cost function of the stage targets steady-state climb and cruise performance points presented in the aircraft's POH. For the Cessna 172 Skyhawk model, the optimization converged in under eleven minutes, meeting prescribed performance tolerances across the full set of POH climb and cruise performance tables with the exception of a small subset of fuel flow validation points that lie in the extrema of the aircraft's recommended operating envelope. Additionally, a check against key climb airspeeds, such as best rate and angle of climb speeds, that were not directly targeted by the optimization routine revealed the calibrated model is capable of meeting a wide range of validation targets. An additional case of the steady-state calibration stage applied to a Cirrus SR20 flight simulation model demonstrated that the parameterization and optimization routine is applicable to aircraft with different propeller configurations, with discrepancies isolated to operating conditions not recommended by the

manufacturer. This stage alone offers a viable calibration approach for engineers seeking an efficient alternative to manual tuning when no flight test data is available.

The time-domain stage extends the calibration effort to flight test data matching through a sequential, multi-step process, targeting model characteristics that can not be addressed through manufacturer data alone. The steps target pitch attitudes, control surface deflections, and flap-down aerodynamics using quasi-steady-state points derived from flight test data along with dynamic damping characteristics which target matching full 6-DOF test runs to available data. Each step was designed to target a specific set of model deficiencies while treating prior results as fixed, limiting parameter coupling across the calibration steps. The complete time-domain calibration process required approximately 70 minutes of total optimization time, demonstrating the computational efficiency of the proposed staged approach. The final calibrated Cessna 172 Skyhawk model demonstrates compliance with FAA Part 60 Level 5 FTD objective test requirements, with full results presented in Appendix C. The appendix includes additional higher-level test cases where flight test data exists for further validation.

The proposed methodology addresses the gap identified in the literature for an automated, efficient calibration approach specifically targeting general aviation flight simulation models using objective performance tolerances as the means of validation, demonstrated here against regulatory qualification requirements. Existing methods address adjacent problems such as high-fidelity aerodynamic database updates for aircraft with extensive wind tunnel data [14, 15] and flight simulation model calibration with the goal of safety analysis on general aviation aircraft [21, 22], but neither directly targets calibration of flight simulation models to available data for FTD-like qualification. Manual tuning, while practiced widely in industry for lower-level FTD devices, relies heavily on individual engineer judgment and requires extensive time for iterative model corrections. The presented methodology fills the gap by offering a systematic, repeatable, and computationally efficient framework that produces a regulatory-compliant flight simulation model using only the data sources

commonly available to flight simulation engineers without the burden of full system identification campaigns or iterative manual tuning. Application of the methodology to the Cessna 172 Skyhawk flight simulation model demonstrates that the identified gap can be addressed within the PEACE/MADCASP framework, with the methodology structured to generalize to other general aviation aircraft. While the proposed methodology demonstrates strong agreement with available validation data and satisfies prescribed performance tolerances, several limitations and opportunities for extension remain, which are discussed in the following section.

While the methodology is demonstrated using Level 5 objective test data, the underlying structure is not limited to this application. The staged calibration approach is designed to adapt to the type and availability of validation data, allowing it to be applied more broadly to cases where only partial or non-regulatory datasets are available.

5.2 Limitations and Future Work

The methodology presented demonstrates the ability to produce a regulatory-complaint flight simulation model, with reasonable adaptations of tolerances and objective tests to align with the model's scope, but, in its current state, is subject to several limitations that should be considered when interpreting the results and evaluating the scope of the approach as it currently exists.

The most significant limitation of the current model structure, when comparing against Level 5 objective test requirements, is the absence of a control loading model. A large set of Level 5 objective testing tolerances are control force-based and cannot be complied with without a reversible control system model that simulates aerodynamic hinge moments and mechanical feel experienced by the pilot. Control forces are a critical component of a training device as a pilot's perception of aircraft handling is as much a function of how the controls feel as how the aircraft responds. As a result, several objective test tolerances were adapted to enable validation against response-based equivalent parameters during calibrated model

assessment. While this approach allows for a thorough evaluation of the flight forces and moments in the model, the lack of simulated control loading leaves a meaningful gap relative to the Level 5 FTD objective testing requirements.

The lack of a propeller slipstream model in the aerodynamic framework manifests throughout the time-domain calibration results. The absence of slipstream effects on the tail surfaces results in control surface effectiveness corrections that are larger than would be expected from aerodynamic modeling error alone, as these corrections absorb both modeling error and unrepresented slipstream contributions.

As noted in the results, the pitching moment calibration step applies corrections exclusively to the wing sectional strips, forcing absorption of all pitching error contributions that may be better attributed to other model components. Sources of error in horizontal tail coefficients, downwash model, and fuselage interference are lumped into a single source and corrected with the single-surface calibration target. While restricting the correction to a single surface produces a well-posed optimization problem and produces acceptable results in the case of the Cessna 172 Skyhawk model, it leads to wing pitching moment adjustments that may not accurately reflect the true distribution of pitching moment contributions across the aircraft's aerodynamic surfaces.

The flaps aerodynamics calibration step uses a simple scalar correction approach applied uniformly across all flap deflection angles and flight conditions. While convenient and simple, this limits the step's ability to capture deflection-dependent aerodynamic behavior and introduces coupling between the drag and pitching moment correction factors which are characterized within a shared cost function. A notable failure to meet all pitching moment attitude tolerances across a range of conditions is presented. However, the overall agreement remains within an acceptable range for the purposes of this study, and the approach provides a sufficient representation of flap-induced aerodynamic effects given the limited available data.

The sequential structure of the time-domain calibration stage does not include a mechanism to assess interactions and coupling between calibration steps. Each step treats the prior results as fixed, simplifying the optimization problem and contributing to the efficiency of the method, but may allow residual coupling effects between parameters to interact across steps. This limitation did not prevent the calibrated Cessna 172 model from meeting prescribed performance tolerances as demonstrated, but may manifest in more complex configurations or datasets. A possible path for mitigation is the incorporation of an outer iteration loop which would ensure prior steps' improvements are intact during sequential steps. This approach was considered during development, however, the current sequential structure was selected due to its ability to produce satisfactory agreement with flight test data in the presented validation case while preserving computational efficiency of the method.

The quality and completeness of the available validation data introduces a limitation specific to the Cessna 172 Skyhawk validation case. The propulsion system validation data available for this aircraft is limited. As a result, propulsion errors are likely lumped within aerodynamic corrections obtained during the four steps of the time-domain calibration stage. When higher-fidelity propulsion system is available, additional steps within the time-domain stage should be introduced to more directly isolate and calibrate propulsion performance and dynamics rather than relying on aerodynamic optimization only.

The method's current reliance on the PEACE/MADCASP modeling framework is a notable limitation. The parameterization and calibration structure are tightly integrated with the specific model architecture, including the strip-theory-based aerodynamic representation and the specific formulation of propeller and propulsion models. Because of this, direct application of this method to alternative simulation frameworks would require additional adaption of the parameterization and structure based on the model's capabilities, setup, and data accessibility. However, the overall staged calibration philosophy and optimization-based approach remain applicable and could be extended to other frameworks with a reasonable level of modifications.

The final limitation arises from the scope of validation presented in this work. The generality of the methodology has been demonstrated only for single-engine, fixed-pitch and constant-speed piston-propeller general aviation aircraft. Extension to other aircraft classes would require assessment of the parameterization's applicability to more complex configurations. The validation was limited to two aircraft due to the effort required to develop suitable baseline models for calibration. While the calibration process itself is computationally efficient, the upfront effort associated with assembling and verifying initial aircraft models remains a practical constraint on expanding the validation set.

The stated limitations open several avenues for future development of this methodology. The most practical addition to the simulation framework would be the incorporation of a simulated control loading system, suitable for modeling of aerodynamic hinge moments, control dynamics, and mechanical feel characteristics. This would allow for quantitative assessment against force-based tolerances across the full Level 5 objective test suite and represent a significant improvement toward a complete automated calibration methodology for FTD qualification.

Incorporation of an explicit propeller slipstream model within the aerodynamic modeling framework would be the second most significant improvement to the methodology, improving the physical accuracy of the model and limiting the lumped error absorption in time-domain calibration steps, particularly in the pitch moment and control surface effectiveness calibration steps.

To address the limitation arising from the scalar flap correction approach, the calibration stage could be extended to include deflection-dependent corrections and a separate lift calibration parameter, similar to the clean configuration calibration approach for which the steady-state stage adjusts the lift-to-drag ratio and the time-domain stage handles the pitching moment corrections. For aircraft with available flaps-down POH data, flap-related performance metrics, such as climb rate, could be incorporated into the steady-state calibration stage to better establish the aerodynamic baseline prior to time-domain refinement.

Finally, the most natural and important future goal of the methodology would be extension to a wider range of aircraft types. Twin-engine piston, turboprop, and high-performance single-engine general aviation aircraft would be valuable validation cases and present different parameterization challenges, particularly in the propulsion model parameterization where more sophisticated engine and governor modeling and parameterization may be required. Demonstrating the effectiveness of the methodology across these configurations would substantially strengthen the argument for its generality.

Despite the discussed limitations, the proposed methodology demonstrates a practical and efficient automated approach for calibrating general aviation flight simulation models to available manufacturer and flight test data. The results show that regulatory performance tolerances can be satisfied without the engineering efforts associated with system identification techniques or iterative manual tuning. The structure of the methodology, combined with its computational efficiency and validated output, provides a strong foundation for continued development and extension to more complex aircraft configurations and frameworks.

Bibliography

[1] Allerton, D., *Principles of Flight Simulation*, AIAA Institue of Aeronatuics and Astronautics, Inc. and John Wiley & Sons Ltd., 2009, DOI: https://doi.org/10.2514/4.867033.

[2] Stevens, B. L., Lewis, F. L., and Johnson, E. N., *Aircraft Control and Simulation: Dynamics, Controls Design, and Autonomous Systems*, John Wiley & Sons, Inc, 2015, DOI: 10.1002/9781119174882.

[3] Finick, R. D., "USAF (United States Air Force) Stability and Control DATCOM (Data Compendium)," Tech. Rep. AFWAL-TR-83-3048, McDonnell Douglas Corporation, 1978.

[4] Roskam, J., *Airplane Design, Part VI: Preliminary Calculation of Aerodynamic, Thrust and Power Characteristics*, DARcorporation, Lawrence, Kansas, 2004.

[5] Frederick, M. A., Smith, M. S., Yoo, S. Y., Wallace, R., Duensing, J. C., Housman, J. A., Deere, K. A., and Viken, J. K., "Development of the X-57 Aerodynamic Database," Tech. Rep. NASA/TM-20250001715, Armstrong Flight Research Center, 2025.

[6] Taylor, H. L., Talleur, D. A., Emanuel Jr., T. W., and Rantanen, E., "Effectiveness of Flight Training Devices Used for Instrument Training," Final Technical Report AHFD-05-9/FAA-05-4, University of Illinois at Urbana-Champaign, Aviation Human Factors Division, Institute of Aviation, Savoy, IL, May 23, 2005.

[7] Macchiarella, N. D., Arban, P. K., and Doherty, S. M., "Transfer of Training from Flight Training Devices to Flight for Ab-Initio Pilots," *International Journal of Applied Aviation Studies*, Vol. 6, No. 2, 2006, pp. 299–314.

[8] Federal Aviation Administration, "14 CFR Part 60 - Flight Simulation Training Device Initial and Continuing Qualification and Use," Online: https://www.ecfr.gov/current/title-14/chapter-I/subchapter-D/part-60.

[9] European Aviation Safety Agency, "Certification Specifications for Aeroplane Flight Simulation Training Devices 'CS-FSTD(A)'," Online: https://www.easa.europa.eu/en/document-library/certification-specifications/cs-fstda-issue-2, 3 May 2018, Issue 2.

[10] Transport Canada, "Aeroplane and Rotorcraft Simulator Manual - TP9685," Revision 3.

[11] Morelli, E. A. and Grauer, J. A., "Advances in Aircraft System Identification at NASA Langley Research Center," *Journal of Aircraft*, Vol. 60, No. 5, 2023, pp. 1354–1370, DOI: https://doi.org/10.2514/1.C037274.

[12] Jategaonkar, R. V., *Flight Vehicle System Identification: A Time-Domain Methodology, Second Edition*, American Institute of Aeronatuics and Astronautics, Inc., 2015, DOI: https://doi.org/10.2514/4.102790.

[13] Morelli, E. A. and Klein, V., *Aircraft System Indification: Theory and Practice, Second Edition*, Sunflyte Enterprises, 2016.

[14] Morelli, E. A., "Efficient Global Aerodynamic Modeling from Flight Data," *50th AIAA Aerospace Sciences Meeting and Exhibit*, 2012, DOI: https://doi.org/10.2514/6.2012-1050.

[15] Morelli, E. A. and Ward, D. G., "Automated Simulation Updates based on Flight Data," *AIAA Atmospheric Flight Mechanics Conference and Exhibit*, 2007, DOI: https://doi.org/10.2514/6.2007-6714.

[16] Simmons, B. M., Gresham, J. L., and Woolsey, C. A., "Flight-Test System Identification Techniques and Applications for Small, Low-Cost, Fixed-Wing Aircraft," *Journal of Aircraft*, Vol. 60, No. 5, 2023, pp. 1503–1521, DOI: https://doi.org/10.2514/1.C037260.

[17] Brian, G. and Morelli, E. A., "Rapid Automated Aircraft Simulation Model Updating From Flight Data," *14th Australian Internation Aerospace Congress*, 2011.

[18] Deiler, C., "Aerodynamic model adjustment for an accurate flight performance representation using a large operational flight data base," *CEAS Aeronautical Journal*, Vol. 14, 527–538, DOI: https://doi.org/10.1007/s13272-023-00659-w.

[19] Gray, J. S., Hwang, J. T., Martins, J. R. R. A., Moore, K. T., and Naylor, B. A., "OpenMDAO: An open-source framework for multidisciplinary design, analysis, and optimization," *Structural and Multidisciplinary Optimization*, Vol. 59, No. 4, April 2019, pp. 1075–1104.

[20] Thacker, R. P. and Blaesser, N., "Modeling of a Modern Aircraft Through Calibration Techniques," *AIAA Aviation 2019 Forum*, 2019, DOI: https://doi.org/10.2514/6.2019-2984.

[21] Puranik, T. G., Harrison, E. D., Min, S., Chakraborty, I., and Mavris, D. N., "A Framework for General Aviation Aircraft Performance Model Calibration and Validation," *Aviation Technology, Integration, and Operations Conference*, 2018, DOI: https://doi.org/10.2514/6.2018-3191.

[22] Puranik, T., Harrison, E., Chakraborty, I., and Mavris, D., "Aircraft Performance Model Calibration and validation for General Aviation Safety Analysis," *Journal of Aircraft*, Vol. 57, No. 4, 2020, pp. 678–688, DOI: https://doi.org/10.2514/1.C035458.

[23] Harper, M. E., Mishra, A. A., Kunwar, B., and Chakraborty, I., "Towards an Automated Methodology for Simulation Model Calibration to Manufacturer and Flight Test Performance Data," *AIAA SCITECH 2025 Forum*, 2025, DOI: https://doi.org/10.2514/6.2025-1567.

[24] Mishra, A. A., Harper, M. E., and Chakraborty, I., "Uncertainty Quantification in the Conceptual Design of Hybrid-Electric General Aviation Aircraft," *AIAA AVIATION FORUM AND ASCEND*, 2025, DOI: https://doi.org/10.2514/6.2025-3696.

[25] MATLAB, "fmincon," Online: https://www.mathworks.com/help/optim/ug/fmincon.html, 2025.

[26] Harper, M. E., Kunwar, B., and Chakraborty, I., "Extending an Automated Methodology for Simulation Model Calibration to Manufacturer and Flight Test Validation Data," *AIAA SCITECH 2026 Forum*, 2026, DOI: https://doi.org/10.2514/6.2026-2019.

[27] "Modular Generalized Framework for Assessing Aircraft Aero-Propulsive, Stability, and Control Characteristics," Transformational Tools and Technologies (TTT) Project, NASA Aeronautics Research Mission Directorate (ARMD), NASA Langley Research Center, 2018.

[28] Chakraborty, I. and Mishra, A. A., "Generalized Energy-Based Flight Vehicle Sizing and Performance Analysis Methodology," *Journal of Aircraft*, Vol. 58, No. 4, 2021, pp. 762–780, DOI: https://doi.org/10.2514/1.C036101.

[29] Chakraborty, I. and Mishra, A. A., "Sizing and Analysis of a Lift-Plus-Cruise Aircraft with Electrified Propulsion," *Journal of Aircraft*, Vol. 60, No. 3, 2023, pp. 747–765, DOI: https://doi.org/10.2514/1.C037044.

[30] Cessna Aircraft Company, *Information Manual, Skyhawk SP*, 1998, Revision 5.

[31] X-Plane, "X-Plane Flight Simulation Software," Online: https://www.x-plane.com/, (accessed March 2026).

[32] FlightGear, "Open-Source FlightGear Flight Simulator Software," Online: https://www.flightgear.org/, (accessed March 2026).

[33] Cessna by Textron Aviation, "Cessna Skyhawk, The Ultimate Training Aircraft," Online: https://cessna.txtav.com/-/media/cessna/files/brochures/piston/skyhawk_brochure.pdf, 2025, (accessed March 2026).

[34] Raymer, D. P., *Aircraft Design: A Conceptual Approach, Sixth Edition*, AIAA Education Series, 2018, DOI: https://doi.org/10.2514/4.104909.

[35] Kunwar, B., Mishra, A. A., Bhandari, R., and Chakraborty, I., "Sizing and Optimization of an Advanced Air Mobility Aircraft Using Parametric Aero-Propulsive Model," *AIAA AVIATION 2023 Forum*, 2023, p. 3662, DOI: https://doi.org/10.2514/6.2023-3662.

[36] Drela, M., "XFOIL: An Analysis and Design System for Low Reynolds Number Airfoils," *Low Reynolds Number Aerodynamics*, Springer, 1989, p. 1–12.

[37] Deyoung, J., "Theoretical Symmetric Span Loading Due to Flap Deflection for Wings of Arbitrary Plan Form at Subsonic Speeds," Tech. Rep. 1071, National Advisory Committee for Aeronautics, 1952.

[38] John D. Anderson, Jr., *Fundamentals of Aerodynamics, Fifth Edition*, McGraw-Hill, 2011, p. 424-428.

[39] Decker, J. L., *Prediction of downwash at various angles of attack for arbitrary tail locations*, Institute of the Aeronautical Sciences, 1956.

[40] Gudmundsson, S., *General Aviation Aircraft Design, Applied Methods and Procedures, Second Edition*, Butterworth-Heinemann, 2022, p. 945. DOI: 10.1016/C2018-0-03861-X.

[41] Deyoung, J., "Theoretical Antisymmetric Span Loading for Wings of Arbitrary Plan Form at Subsonic Speeds," Tech. Rep. 1056, National Advisory Committee for Aeronautics, 1951.

[42] Ahuja, V. and Hartfield, R., "Reduced-Order Aerodynamics with the Method of Integrated Circulation," *AIAA SCITECH 2022*, San Diego, CA, 2022.

[43] Drela, M., "QMIL User Guide," Online: `https://web.mit.edu/drela/Public/web/qprop/`, 2005.

[44] Drela, M., "QPROP Formulation," 2006, Massachusetts Inst. of Technology Aeronautics and Astronautics, Cambridge, MA.

[45] Systems, M. P., *MPC-26, Propeller Owner/Operator Information Manual*, 2009, Revision 1.

[46] Lycoming, *Operator's Manual, O-360, HO-360, IO-360, AIO-360, HIO-360 & TIO-360 Series*, 2005, 8th Edition.

[47] MATLAB, "lsqnonlin," Online: `https://www.mathworks.com/help/optim/ug/lsqnonlin.html`, 2025.

[48] Nicolosi, F., Vecchia, P. D., Ciliberti, D., and Cusati, V., "Fuselage aerodynamic prediction methods," *Aerospace Science and Technology*, Vol. 55, 2016, p.332-343. DOI: `https://doi.org/10.1016/j.ast.2016.06.012`.

[49] MATLAB, "Optimization Toolbox," Online: `https://www.mathworks.com/products/optimization.html` (accessed March 2026).

[50] Federal Aviation Administration, "Pilot's Handbook of Aeronautical Knowledge," Tech. Rep. FAA-H-8083-25C, U.S. Department of Transportation, Federal Aviation Administration, 2023, Online: `https://www.faa.gov/regulations_policies/handbooks_manuals/aviation/phak`.

[51] Royal Aeronautical Society, *Aeroplane Flight Simulator Evaluation Handbook*, 2005, Third Edition.

[52] Cirrus Aircraft, *Pilot's Operating Handbook and FAA Approved Airplane Flight Manual for the Cirrus Design SR20, Aircraft Serials 1268 and Subsequent with Analog or Avidyne Avionics System*, 2011, Revision A10.

[53] wunderground, "Savoy, IL Weather History," Online: `https://www.wunderground.com/history/daily/KCMI/date/2002-4-23` (accessed March 2026).

Appendices

Appendix A

Level 5 FTD Regulatory Objective Tests

A summary of the FAA Part 60 Level 5 objective tests and tolerances, along with basic maneuver descriptions [8, 51] and notes applicable to evaluation against the MADCASP 6-DOF flight simulation framework, is provided in Table A.1.

Table A.1: Overview of Level 5 FTD objective test requirements (adapted from [8, 51])

Test ID	Test Title	Tolerance	Flight Conditions	Description	Notes
1. Performance					
1.c – Climb					
1.c.1	Normal Climb, all engines operating	±3 kt airspeed; ±100 FPM or ±5% rate of climb	Clean configuration	Fly at nominal climb speed and mid-initial climb altitude over an interval of at least 1,000 ft	For Level 5 FTDs, snapshot test results are acceptable.
1.f – Engines					
1.f.1	Acceleration	±1 s from 10% (T_i) to 90% of engine response (T_t)	Approach or Landing	From a trimmed condition, rapidly advance throttle from idle to go-around power	FAA-provided alternative data source for FTD Level 5 – small, single engine (reciprocating) airplane authorizes a response time between 2-4 s (Table B2B [8]).
1.f.2	Deceleration	±1 s from 10% (T_i) to 90% of engine response (T_t)	On ground	While on ground with engines stabilized at maximum takeoff power, retard throttle to the idle power position	FAA-provided alternative data source for FTD Level 5 – small, single engine (reciprocating) airplane authorizes a response time between 2-4 s (Table B2B [8]).
2. Handling Qualities					
2.a – Static Control Tests					
2.a.1.a*/b*	Pitch controller position versus force *and surface position calibration*	±2 lb breakout force; ±5 lb or ±10% of force; *±2° elevator angle*	On ground	An uninterrupted control sweep to control end stops	*Italicized information represents Level 6/7 FTD requirements.* No control loading simulation is implemented; therefore, the Level 6/7 surface position calibration portion of this test is utilized in lieu of the force-based requirements.

Continued on next page

Table A.1 – continued from previous page

Test ID	Test Title	Tolerance	Flight Conditions	Description	Notes
2.a.2.a/*b*	Roll controller position versus force *and surface position calibration*	±2 lb breakout force; ±5 lb or ±10% of force; *±2° aileron angle; ±3° spoiler angle*	On ground	An uninterrupted control sweep to control end stops	See notes for 2.a.1.a/*b*. Most general aviation aircraft do not have spoilers; therefore, the spoiler angle tolerance is not applicable.
2.a.3.a/*b*	Rudder pedal position versus force *and surface position calibration*	±2 lb breakout force; ±5 lb or ±10% of force; *±2° rudder angle*	On ground	An uninterrupted control sweep to control end stops	See notes for 2.a.1.a/*b*.
2.c – Longitudinal Control Tests					
2.c.1.b	Power Change Force	±5 lb or ±20% pitch control force	Approach	Trim the aircraft at power required for level flight and increasing the throttle quickly to maximum power, recording the pitch controller force required to maintain the trimmed aircraft speed. Test is repeated with a rapid throttle movement to idle.	No control loading simulation is implemented. This test is therefore evaluated qualitatively, verifying that the elevator necessary to hold altitude after a rapid throttle input exhibits the correct trend and magnitude (CT&M) relative to flight test observations.
2.c.2.b	Flap/Slat Change Force	±5 lb or ±20% pitch control force	Takeoff through initial flap retraction, and approach to landing	Trim the aircraft at initial flap position then extend or retract flaps, recording the pitch controller force required to maintain the trimmed aircraft speed.	See note for 2.c.1.b. CT&M of pitch response to flap extension or retraction is compared. Slats are not generally present on general aviation aircraft; therefore, this acts as a purely flap change test.
2.c.4.b	Gear Change Force	±5 lb or ±20% pitch control force	Takeoff (retraction) and Approach (extension)	Trim the aircraft at the given initial conditions then extend or retract the gear, recording the pitch controller force required to maintain the trimmed aircraft speed.	See note for 2.c.1.b. CT&M of pitch response to gear extension or retraction is compared.

Continued on next page

Table A.1 – continued from previous page

Test ID	Test Title	Tolerance	Flight Conditions	Description	Notes
2.c.5	Longitudinal Trim	±1° elevator angle; ±0.5° stabilizer or trim surface angle; ±1° pitch angle; ±5% of net thrust or equivalent	Cruise, Approach, and Landing	Trim the aircraft for steady-state wings level trim with thrust for level flight.	N/A
2.c.7	Longitudinal Static Stability	±5 lb or ±10% of pitch controller force; Alternative method: ±1° or ±10% of the change of elevator angle	Approach	Trim the aircraft for level flight then apply a longitudinal control command to achieve at least two speeds above and two speeds below trim speed.	No control loading simulation is implemented. The alternative tolerance method is observed.
2.c.8.b	Stall Warning (actuation of stall warning device)	±3 kt airspeed; ±2° bank for speeds greater than actuation of stall warning device or initial buffet	Second Segment Climb, and Approach or Landing	Enter stall maneuver with thrust at or near idle power and wings level. Record the stall warning signal and/or initial buffet.	Systems are not modeled in the MADCASP-based flight simulation model; therefore, this test is not applicable.
2.c.9.b	Phugoid Dynamics	±10% period; Representative damping	Cruise	From the trimmed conditions, excite the phugoid mode by applying longitudinal control in one direction, changing the airspeed by approximately 10 kt then releasing. Include three full cycles or number of cycles sufficient to determine representative damping.	True “free-response” is not possible due to the lack of reversible controls model. Despite that, tolerances will apply as normal.
2.d – Lateral Directional Tests					
2.d.2	Roll Response (Rate)	±2°/s or ±10% of roll rate	Cruise, and Approach or Landing	From trimmed condition, roll the aircraft using a wheel step input of approximately one-third of maximum roll controller travel.	N/A

Continued on next page

Table A.1 – continued from previous page

Test ID	Test Title	Tolerance	Flight Conditions	Description	Notes
2.d.4	Spiral Stability	Correct trend; *Alternate test method: correct trend and ±2° aileron angle*	Cruise	Establish a 20-30° bank then release the roll controller. Alternate method: Show lateral control required to maintain a steady turn with a roll angle of approximately 30°.	*Italicized tolerance represents Level 7 FTD tolerances when using the alternate method.* The alternate method and higher-level tolerances are adopted for this test.
2.d.6.*a*/b	Rudder Response	*±2°/s or ±10% of yaw rate;* ±2°/s roll rate; ±3° bank angle	Approach or Landing	Trim the aircraft and apply a rapid rudder input of approximately 25% of the rudder pedal travel.	*Italicized information represents Level 6/7 FTD objective test information.* The higher level tolerances are adopted for validation.
2.d.8	Steady State Sideslip	For a given rudder position: ±2° roll angle; ±1° sideslip angle; ±2° or ±10% of aileron angle; ±5° or 10% of roll controller position or force	Approach or Landing	Trim the aircraft in a steady-state sideslip condition using constant rudder input. Input two rudder deflections while maintaining heading with roll controller (in both directions for propeller-driven aircraft)	May be a series of snapshot tests. Alternate method performed where a ±2° tolerance is applied to the rudder position while matching sideslip time histories.

Appendix B

Full Cessna 172 Skyhawk Steady-State Calibration Results

Appendix B includes the complete steady-state calibration results for the Cessna 172 Skyhawk flight simulation model. This appendix serves as a stand alone reference with all applicable validation results including the converged optimization parameter set and calibrated aerodynamic, propeller, and propulsion curves. The full set of POH climb and cruise performance validation data are included.

B.1 Converged optimization parameters

The final, converged optimization parameters for the steady-state stage of the Cessna 172 calibration routing are repeated in Table B.1 for reference. Figures B.1 - B.3 are included for an illustration of the effects of the converged optimization parameters on the model's aerodynamic and propeller coefficient curves and engine performance tables.

Table B.1: Reproduced from Table 3.1 for reference: Converged steady-state stage optimization parameters for the Cessna 172 Skyhawk flight simulation model

Factor	**Converged Value**
α_{shift}	0.3044°
$K_{c_{l_{slope}}}$	1.1002
$K_{c_{l,0_{offset}}}$	-0.0552
$K_{c_{d,0_{slope}}}$	0.9878
$K_{c_{d,0_{offset}}}$	0.0271
$K_{c_{d,i}}$	1.0632
J_{anchor}	0.5901
$K_{C_{T_{shift}}}$	0.0074
$K_{C_{T_{scale}}}$	1.0264
$K_{C_{T_{tilt}}}$	-0.0713
$K_{C_{T_{quad}}}$	-0.0204
$K_{C_{Q_{shift}}}$	-0.0660
$K_{C_{Q_{scale}}}$	1.0195
$K_{C_{Q_{tilt}}}$	0.0792
$K_{C_{Q_{quad}}}$	0.0500
K_{HP}	0.9829
K_{FF}	0.9000

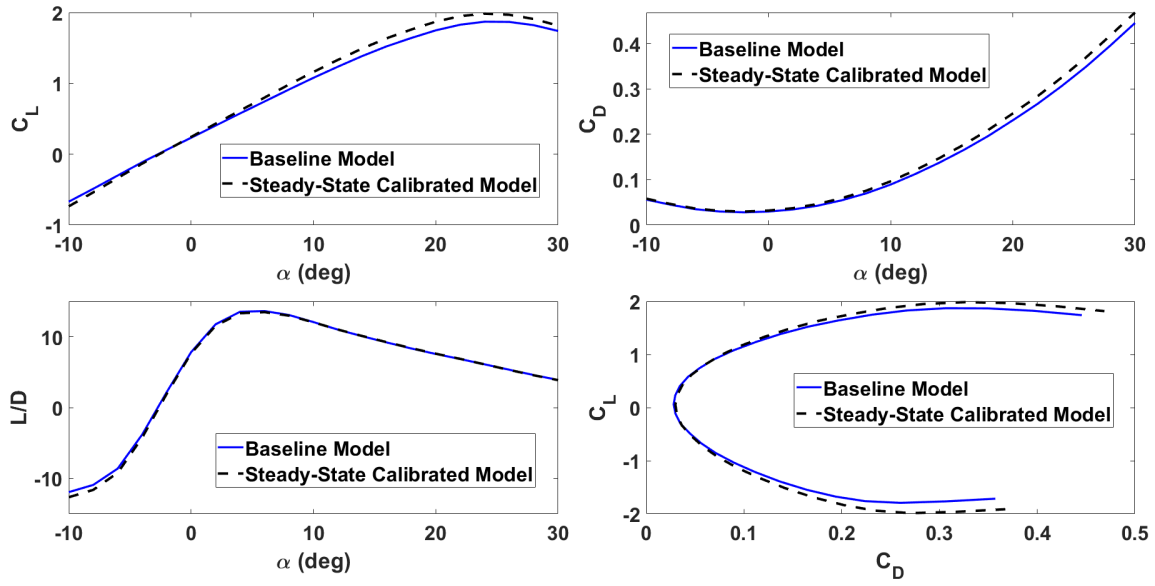

Figure B.1: Reproduced from Figure 4.1 for reference: Steady-state calibrated aerodynamic coefficient curves for the Cessna 172 Skyhawk model, compared to baseline model

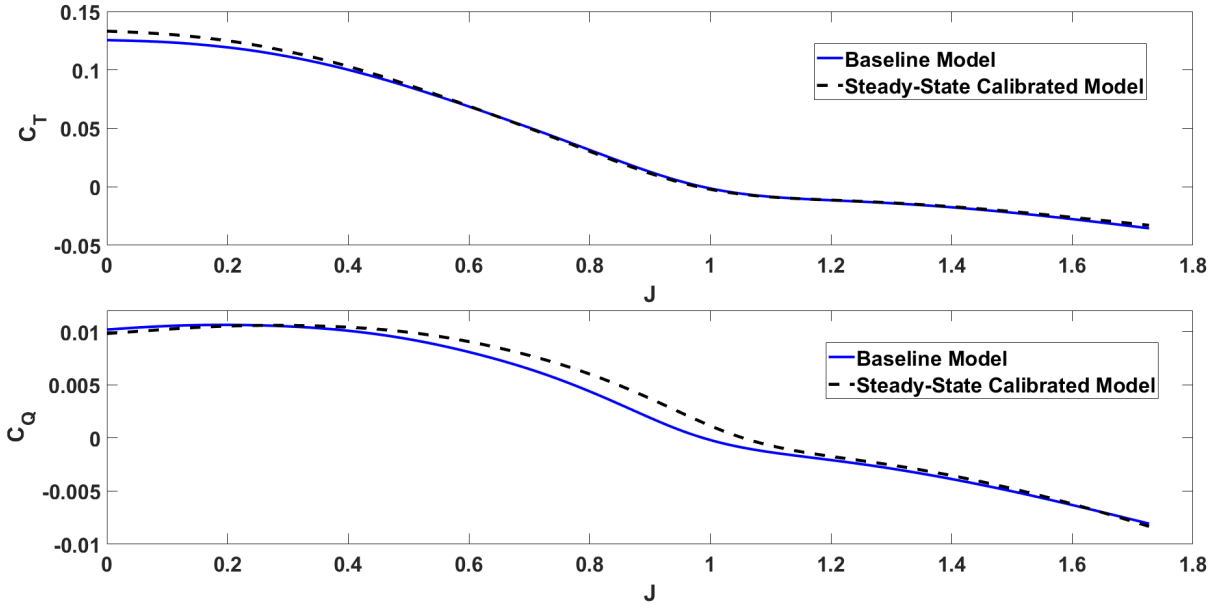

Figure B.2: Reproduced from Figure 4.2 for reference: Steady-state calibrated propeller coefficient curves for the Cessna 172 Skyhawk model, compared to baseline model

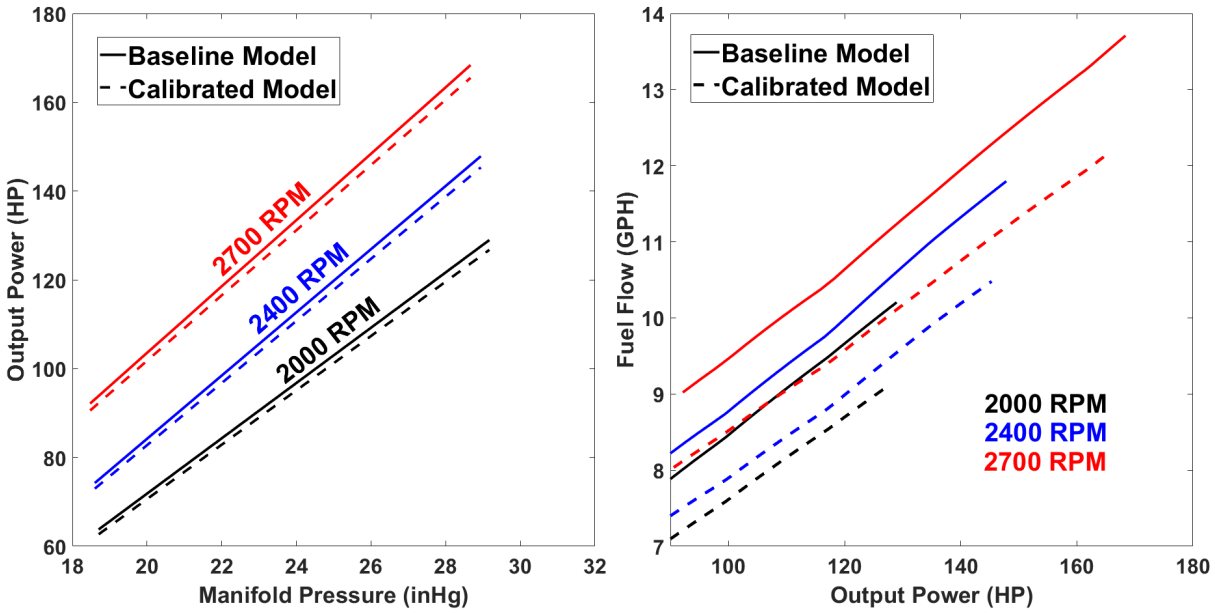

Figure B.3: Reproduced from Figure 4.3 for reference: Steady-state calibrated propulsion model sea level output power and fuel flow curves for the Cessna 172 Skyhawk model, compared to baseline model

B.2 Performance Charts

B.2.1 Maximum Rate of Climb Performance

Maximum rate of climb results at 2,550 lb gross weight, clean configuration, maximum throttle, and full rich mixture are presented across all available atmospheric conditions in Table B.2. All climb rate points are evaluated against the prescribed ±100 FPM tolerance and are marked as pass/fail within the table. All validation points are within tolerance.

B.2.2 Cruise Performance

Cruise performance results at 2,550 lb gross weight for standard, below standard, and above standard temperature atmospheric conditions are presented in Tables B.3 - B.5. All

Table B.2: Reproduced from Figure 4.3 for reference: Steady-state calibrated Cessna 172 Skyhawk model maximum rate of climb results at 2,550 lb, clean configuration, maximum throttle (POH data from [30])

Outside Air Temp (°C)	**Pressure Altitude (ft)**	**Climb Speed (KIAS)**	**Climb Rate (FPM)**			**Pass/Fail (±100 FPM)**
			POH	**Model**	**Error**	
-20	0	74	855	831	-24	**PASS**
	2000	73	760	704	-56	**PASS**
	4000	73	685	649	-36	**PASS**
	6000	73	575	548	-27	**PASS**
	8000	72	465	450	-15	**PASS**
	10000	72	360	346	-14	**PASS**
	12000	72	255	222	-33	**PASS**
0	0	74	785	784	-1	**PASS**
	2000	73	695	657	-38	**PASS**
	4000	73	620	602	-18	**PASS**
	6000	73	515	502	-13	**PASS**
	8000	72	405	405	0	**PASS**
	10000	72	300	301	1	**PASS**
	12000	72	195	178	-17	**PASS**
20	0	74	710	739	29	**PASS**
	2000	73	625	613	-12	**PASS**
	4000	73	555	558	3	**PASS**
	6000	73	450	459	9	**PASS**
	8000	72	345	363	18	**PASS**
	10000	72	240	262	22	**PASS**
	12000	72	135	138	3	**PASS**
40	0	74	645	697	52	**PASS**
	2000	73	560	571	11	**PASS**
	4000	73	495	521	26	**PASS**
	6000	73	390	433	43	**PASS**
	8000	72	285	343	58	**PASS**
	10000	72	180	242	62	**PASS**
	12000	72	–	–	–	–

points are validated against the ±5% output power, ±50 RPM, and ±5% fuel flow tolerances. Only two points fall outside of the prescribed tolerances, two fuel flow values at high-temperature, high-altitude conditions which represent extreme operating conditions.

Table B.3: Steady-state calibrated Cessna 172 Skyhawk model cruise performance at 2,550 lb and 20°C below standard temperature (POH data from [30])

Press Alt (ft)	KTAS	RPM			% Power			GPH		
		POH	Model	Error	POH	Model	Error	POH	Model	Error
2000	117	2550	2550	0	83	79	-4	11.1	10.6	-4.5%
	115	2500	2510	10	78	75	-3	10.6	10.1	-4.7%
	111	2400	2430	30	69	69	0	9.6	9.3	-3.1%
	105	2300	2320	20	61	61	0	8.6	8.3	-3.5%
	99	2200	2210	10	53	54	1	7.7	7.4	-3.9%
	92	2100	2090	-10	47	47	0	6.9	6.8	-1.4%
4000	120	2600	2610	10	83	80	-3	11.1	10.8	-2.7%
	118	2550	2570	20	79	77	-2	10.6	10.4	-1.9%
	115	2500	2510	10	74	72	-2	10.1	9.8	-3.0%
	110	2400	2420	20	65	65	0	9.1	8.8	-3.3%
	104	2300	2310	10	58	58	0	8.2	8.0	-2.4%
	98	2200	2210	10	51	51	0	7.4	7.2	-2.7%
	91	2100	2090	-10	45	45	0	6.6	6.6	0.0%
6000	122	2650	2660	10	83	80	-3	11.1	10.9	-1.8%
	120	2600	2620	20	78	76	-2	10.6	10.4	-1.9%
	115	2500	2520	20	70	69	-1	9.6	9.5	-1.0%
	109	2400	2410	10	62	61	-1	8.6	8.5	-1.2%
	103	2300	2310	10	54	55	1	7.8	7.7	-1.3%
	96	2200	2190	-10	48	48	0	7.1	6.9	-2.8%
8000	125	2700	2720	20	83	81	-2	11.1	11.1	0.0%
	122	2650	2670	20	78	76	-2	10.5	10.5	0.0%
	120	2600	2630	30	74	73	-1	10.0	10.1	1.0%
	114	2500	2520	20	65	65	0	9.1	9.1	0.0%
	108	2400	2410	10	58	58	0	8.2	8.2	0.0%
	101	2300	2290	-10	52	51	-1	7.5	7.4	-1.3%
	94	2200	2180	-20	46	46	0	6.8	6.7	-1.5%
10000	124	2700	2710	10	78	76	-2	10.5	10.6	1.0%
	122	2650	2680	30	73	73	0	10.0	10.2	2.0%
	119	2600	2620	20	69	69	0	9.5	9.7	2.1%
	113	2500	2520	20	62	62	0	8.7	8.8	1.1%
	106	2400	2390	-10	55	55	0	7.9	7.8	1.3%
	100	2300	2300	0	49	50	1	7.2	7.2	0.0%
12000	121	2650	2670	20	69	69	0	9.5	9.8	3.2%
	118	2600	2620	20	65	66	1	9.1	9.3	2.2%
	111	2500	2500	0	58	58	0	8.3	8.4	1.2%
	105	2400	2400	0	52	53	1	7.5	7.6	1.3%
	98	2300	2290	-10	47	47	0	6.9	7.0	1.4%

Table B.4: Reproduced from Table 4.4 for reference: Steady-state calibrated Cessna 172 Skyhawk model standard atmospheric conditions cruise performance at 2,550 lb (POH data from [30])

Press Alt (ft)	KTAS	RPM			% Power			GPH		
		POH	Model	Error	POH	Model	Error	POH	Model	Error
2000	118	2550	2570	20	77	76	1	10.5	10.3	-1.9%
	115	2500	2510	10	73	71	-2	9.9	9.7	-2.0%
	110	2400	2420	20	64	64	0	9.0	8.8	-2.2%
	104	2300	2310	10	57	57	0	8.1	7.9	-2.5%
	97	2200	2190	-10	50	50	0	7.3	7.1	-2.7%
	90	2100	2080	-20	44	44	0	6.6	6.4	-3.0%
4000	120	2600	2620	20	77	75	-2	10.4	10.4	0.0%
	117	2550	2560	10	73	71	-2	9.9	9.8	-1.0%
	115	2500	2530	30	69	68	-1	9.5	9.4	-1.1%
	109	2400	2420	20	61	61	0	8.5	8.5	0.0%
	102	2300	2300	0	54	53	-1	7.7	7.6	-1.3%
	96	2200	2200	0	48	48	0	7.0	6.9	-1.4%
	89	2100	2090	-10	42	43	1	6.4	6.3	-1.6%
6000	122	2650	2670	20	77	75	2	10.4	10.4	0.0%
	119	2600	2610	10	73	71	2	9.9	9.9	0.0%
	114	2500	2520	20	65	65	0	9.0	9.0	0.0%
	108	2400	2420	20	57	58	-1	8.2	8.2	0.0%
	101	2300	2300	0	51	51	0	7.4	7.4	0.0%
	94	2200	2190	-10	45	46	1	6.7	6.7	0.0%
8000	124	2700	2720	20	77	75	-2	10.4	10.5	1.0%
	122	2650	2680	30	72	72	0	9.9	10.2	3.0%
	119	2600	2630	30	68	69	1	9.4	9.6	2.1%
	112	2500	2500	0	61	60	-1	8.6	8.6	0.0%
	106	2400	2400	0	54	54	0	7.8	7.8	0.0%
	99	2300	2290	-10	48	49	1	7.1	7.1	0.0%
	92	2200	2190	-10	43	44	1	6.5	6.4	-1.5%
10000	123	2700	2710	10	72	71	-1	9.8	10.1	3.1%
	120	2650	2660	10	68	67	-1	9.4	9.6	2.1%
	117	2600	2610	10	64	64	0	9.0	9.1	1.1%
	111	2500	2500	0	57	58	1	8.2	8.3	1.2%
	104	2400	2390	-10	51	52	1	7.5	7.5	0.0%
	97	2300	2280	-20	46	47	1	6.8	6.9	1.5%
12000	119	2650	2660	10	64	64	0	8.9	9.2	3.4%
	116	2600	2610	10	61	61	0	8.5	8.9	4.7%
	109	2500	2490	-10	54	55	1	7.8	8.0	2.6%
	102	2400	2380	-20	49	49	0	7.1	7.3	2.8%
	95	2300	2290	-10	44	45	1	6.6	6.8	3.0%

Table B.5: Steady-state calibrated Cessna 172 Skyhawk model cruise performance at 2,550 lb and 20°C above standard temperature (POH data from [30])

Press Alt (ft)	KTAS	RPM			% Power			GPH		
		POH	Model	Error	POH	Model	Error	POH	Model	Error
2000	117	2550	2560	10	72	71	-1	9.9	9.8	-1.0%
	115	2500	2530	30	68	68	0	9.4	9.4	0.0%
	109	2400	2420	20	60	61	1	8.5	8.4	-1.2%
	102	2300	2300	0	53	53	0	7.7	7.5	-2.6%
	95	2200	2180	-20	47	47	0	6.9	6.8	-1.4%
	89	2100	2090	-10	42	43	1	6.3	6.3	0.0%
4000	119	2600	2610	10	72	71	-1	9.8	9.9	1.0%
	117	2550	2580	30	68	68	0	9.4	9.5	1.1%
	114	2500	2520	20	64	64	0	8.9	9	1.1%
	107	2400	2400	0	57	57	0	8.1	8	-1.2%
	101	2300	2300	0	51	51	0	7.3	7.3	0.0%
	94	2200	2190	-10	45	46	1	6.7	6.6	-1.5%
	87	2100	2100	0	40	41	1	6.1	6.1	0.0%
6000	121	2650	2660	10	72	71	-1	9.8	9.9	1.0%
	118	2600	2610	10	68	67	-1	9.4	9.4	0.0%
	112	2500	2500	0	60	60	0	8.5	8.6	1.2%
	106	2400	2400	0	54	54	0	7.7	7.8	1.3%
	99	2300	2290	-10	48	48	0	7.0	7.1	1.4%
	92	2200	2190	-10	43	44	1	6.4	6.4	0.0%
8000	123	2700	2720	20	71	71	0	9.7	10	3.1%
	120	2650	2660	10	67	67	0	9.3	9.5	2.2%
	117	2600	2610	10	64	64	0	8.9	9.1	2.2%
	111	2500	2510	10	57	57	0	8.1	8.3	2.5%
	104	2400	2390	-10	51	51	0	7.4	7.5	1.4%
	97	2300	2290	-10	46	47	1	6.8	6.9	1.5%
	90	2200	2200	0	41	43	2	6.2	6.3	1.6%
10000	122	2700	2710	10	67	67	0	9.3	9.6	3.2%
	119	2650	2660	10	63	64	1	8.9	9.2	3.4%
	115	2600	2590	-10	60	60	0	8.5	8.7	2.4%
	109	2500	2490	-10	54	54	0	7.8	8	2.6%
	102	2400	2390	-10	49	49	0	7.1	7.3	2.8%
	95	2300	2290	-10	44	45	1	6.5	6.8	4.6%
12000	117	2650	2650	0	60	60	0	8.5	8.8	3.5%
	114	2600	2600	0	57	57	0	8.1	8.5	4.9%
	107	2500	2490	-10	51	52	1	7.4	7.8	5.4%
	100	2400	2390	-10	46	48	2	6.8	7.2	5.9%
	92	2300	2300	0	41	44	3	6.3	6.6	4.8%

B.3 Key Climb Airspeeds

Key climb airspeeds, as presented in Table B.6, are evaluated as an independent check on the aerodynamic-propulsive balance of the calibrated model. A ±3 kt airspeed tolerance is applied to the POH speeds. The steady-state calibrated model's rate of climb, V_y, and best angle of climb, V_x, speeds at sea level and 10,000 ft altitudes fall within the prescribed tolerance.

Table B.6: Reproduced from Table 4.5 for reference: Steady-state calibrated Cessna 172 Skyhawk model key climb airspeed results (POH data from [30])

Key Airspeed	**Altitude (ft)**	**Airspeed (KIAS)**			**Pass/Fail (±3 KIAS)**
		POH	**Model**	**Error**	
V_x	0	62	64	2	**PASS**
V_x	10,000	67	68	1	**PASS**
V_y	0	74	76	2	**PASS**
V_y	10,000	72	71	-1	**PASS**

Appendix C

Full Cessna 172 Skyhawk Calibrated Model Time-Domain Results

Appendix C contains the complete set of test results, derived from Frasca International, Inc. provided flight test package and listed in Table 4.15, used to validate the Cessna 172 Skyhawk flight simulation model after application of both calibration stages, steady-state and time-domain. The results presented demonstrate compliance with FAA Level 5 FTD objective tests [8] with additional higher-level tests included as data availability allows. Test objectives and descriptions are derived from the Part 60 document and the Royal Aeronautical Society's *Aeroplane Flight Simulator Evaluation Handbook* [51]. Each test section includes initial conditions, representative time-history comparisons between simulation and flight test data, and summary metrics where applicable. Where test procedures or tolerances could not be directly applied due to limitations in the available flight test data or simulation framework, adaptations are noted within the individual test results. The following describes flight test data package and simulation model limitations that apply broadly across the validation suite, along with how each is addressed within the results.

- *Control forces* - The flight simulation model does not contain a simulated control loading framework making tolerances based on control forces inapplicable. Instead, responses to control behavior or required control movement to achieve a flight maneuver are compared. Each time this limitation is applicable to a test, an engineering judgment comment is included to describe the test objective adaption.

- *Propulsion system flight test data* - Useful propulsion system information is a gap identified in the provided flight test package and will not be used to compare against. For example, many tests report illogical throttle positions for the given maneuvers and output power and manifold pressure readings are not present in any test cases.

Appropriate adaptions are described on a per-test basis as necessary. Throttle position is included as an initial condition only for climb tests where full throttle is noted in the flight test data, and is not reported as a comparison metric for the trimmed model's throttle position in any other test cases.

- *Propeller speed data* - The flight test report states that propeller speed data was recorded by connecting to the magnetos on the engine and counting the pulses. The data is described as inaccurate due to noise in the system and post-processing functions attempted to recreate reasonable propeller speed traces using fitting functions that correlate the actual value displayed by the engine indicators to the lapboard reported data. Due to this information from the flight test package and excessive noise in the propeller speed signal, propeller speed validation data should be treated with skepticism and tolerances should not be applied directly. Where appropriate, propeller speeds may be obtained from POH performance charts as a rough estimate of the expected RPM at given conditions.

- *Atmospheric conditions* - Atmospheric conditions, such as outside air temperature, is not reported in flight test cases and must be assumed. Due to their effect on aerodynamic and propulsion modeling, additional research was conducted to obtain a reasonable estimate. The flight test was flown at Frasca Field (C16) in Urbana, Illinois, on April 23, 2002 at approximately 1:30 to 4:00 PM. Using past weather data recorded in Savoy, Illinois at airport KCMI (approximately 11 miles from C16), surface temperatures ranged from 56-61°F [53]. The elevation of KCMI is 735 ft at which the standard atmospheric temperature is approximately 56°F. Therefore, at terrain level, the flight test was conducted in temperatures ranging from approximately 0 - 5°F above standard atmospheric temperature. From this simplification, deviation from standard temperature is assumed to be 0°F for all test cases.

- *Pilot technique variability* - Dynamic flight test maneuvers are inherently dependent on pilot technique. Small variations in control input timing, magnitude, or release relative to the prescribed test procedure can introduce discrepancies between flight test data and simulation results that are not attributable to modeling error. These variations are expected and should be considered when interpreting time-domain response comparisons.

- *Data sampling rate mismatch* - Flight test data is recorded at a sampling rate of 10 Hz (0.1 second time steps) while the simulation integrates at a rate of 60 Hz (1/60 second time steps). Interpolation between flight test data points introduces minor discrepancies in time-domain comparisons, particularly during rapid transient maneuvers where the response changes significantly within a single 0.1 second interval.

- *Pitch trim control surface* - The pitch trim tab is not modeled in the flight simulation framework. This simplification is made on the basis that the trim tab functions primarily to alleviate hinge moments for pilot control force trimming and does not produce aerodynamic forces of sufficient magnitude to meaningfully affect the trimmed flight condition. The trim tab surface area is approximately 11 times smaller than the elevator, making its aerodynamic contribution negligible relative to the elevator's trimming authority.

- *Mixture setting* - Mixture lever position is not recorded in the flight test data. Full rich mixture is assumed for all climb cases and best power mixture is assumed for all other cases, consistent with standard operating procedures for the Cessna 172 Skyhawk at the recorded flight conditions.

C.1 1.c.1 Normal Climb, all engines operating

Test Objective

Demonstrate that the simulation accurately captures engine thrust and aerodynamic drag in a steady state normal climb condition.

Test Information

FAA Part 60 requires a normal climb to be performance at nominal climb speed and mid-initial climb altitude in a clean configuration. Performance is to be recorded over an interval of at least 1,000 ft. For Level 5 and 6 devices, snapshot data is acceptable.

Tolerances

±3 kt airspeed

±100 FPM or ±5% climb rate

Flight Conditions

Clean configuration

Engineering Judgment/Comments

Snapshot Data Approach When attempting to trim available flight test data to a 1,000 ft or greater interval, it was clear that the pilot was not flying a well trimmed out position in many segments of the flight with fluctuations present in airspeed and vertical speed, especially at higher altitudes. Due to this, three smaller time samples are trimmed from the climb data and compared against as *snapshot data*, as allowed for Level 5 FTDs.

Use of Averaged Values Tolerance bands are plotted against the raw data traces for airspeed and vertical speed. Additionally, root-mean-square error (RMSE) is reported for airspeed and vertical speed across the tested range. It is recommended to use the RMSE

values when evaluating whether results are acceptable as it provides a holistic view of performance over the interval instead of focusing on individual data points which may differ because of pilot technique or changing atmospheric conditions.

Results

Snapshot 1

Table C.1: Initial conditions for 1.c.1 Normal Climb (Snapshot 1)

Parameter	**Units**	**Validation**	**Model**
Aircraft Configuration			
Weight	lbs	2433	2433
Station Center of Gravity	in	42.1	42.1
Flaps Position	deg	0	0
Flight Conditions			
Pressure Altitude	ft	3374	3374
Airspeed	KTAS	83	83
Vertical Speed	FPM	708	689
Aircraft Attitude			
Pitch	deg	7.4	7.5
Roll	deg	0.5	0.5
Heading	deg	107.1	107.1
Control Surfaces			
Elevator Position	deg	-0.1	0.4
Aileron Position	deg	0.5	1.5
Rudder Position	deg	5.8	5.7
Cockpit Controls			
Column Position	in	2.7	2.7
Wheel Position	deg	2.1	6.4
Pedal Position	deg	21.6	21.5
Propulsion			
Throttle Position	norm	1	1

Table C.2: Averaged results for 1.c.1 Normal Climb (Snapshot 1)

Metric	Tolerance	Validation (Mean ± SD)	Model (Mean ± SD)	Error (RMSE)	Pass/ Fail
Airspeed (KTAS)	±3 kt	83.0 ± 0.0	83.3 ± 0.2	0.3	**PASS**
Vertical Speed (FPM)	±100 FPM	650 ± 32	660 ± 32	33	**PASS**

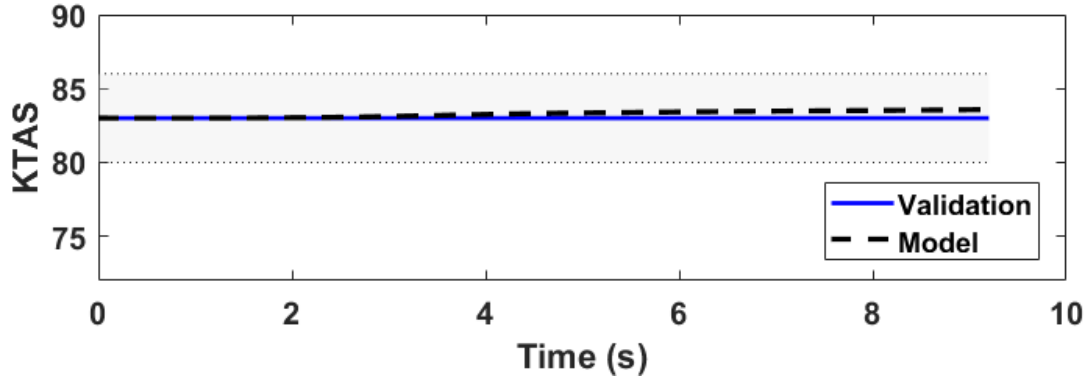

Figure C.1: Airspeed trace for 1.c.1 Normal Climb (Snapshot 1)

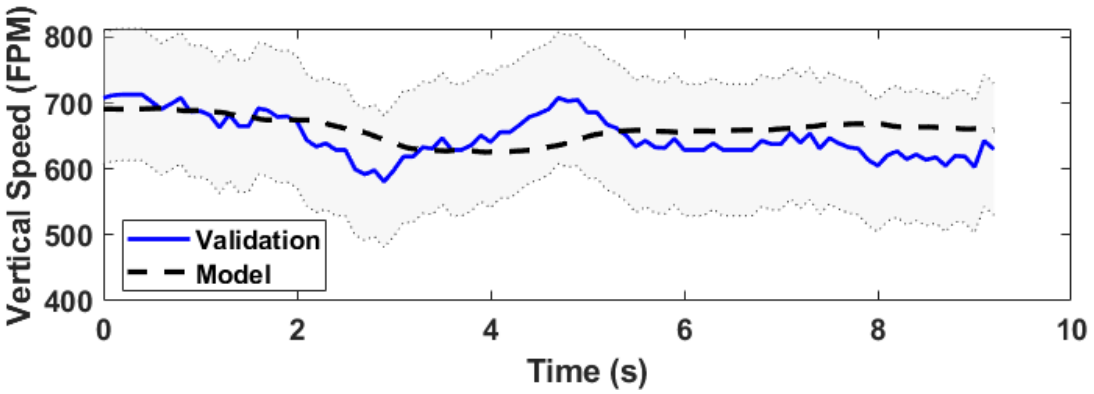

Figure C.2: Vertical speed trace for 1.c.1 Normal Climb (Snapshot 1)

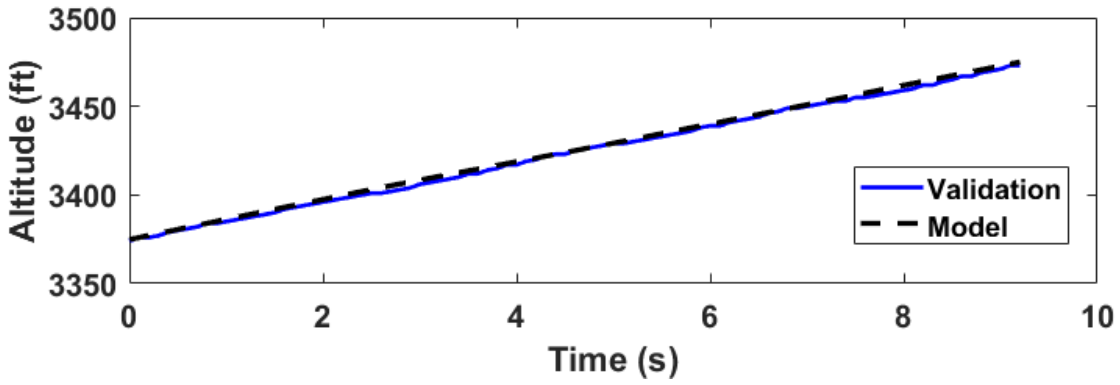

Figure C.3: Altitude trace for 1.c.1 Normal Climb (Snapshot 1)

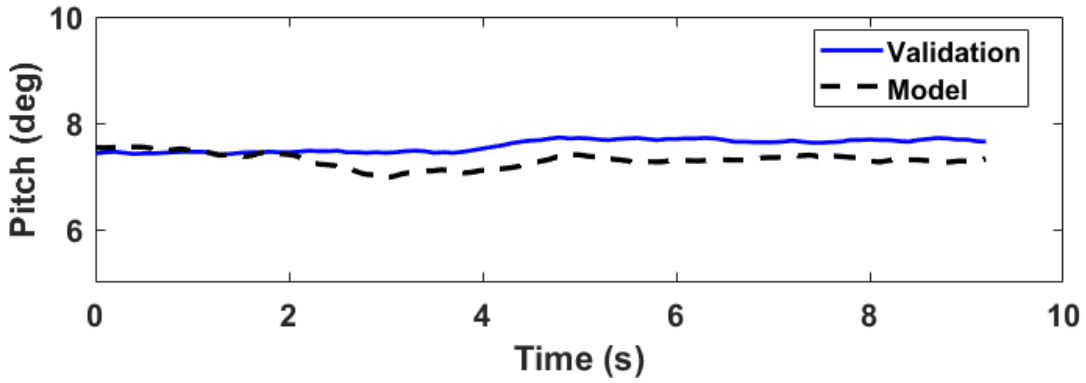

Figure C.4: Pitch trace for 1.c.1 Normal Climb (Snapshot 1)

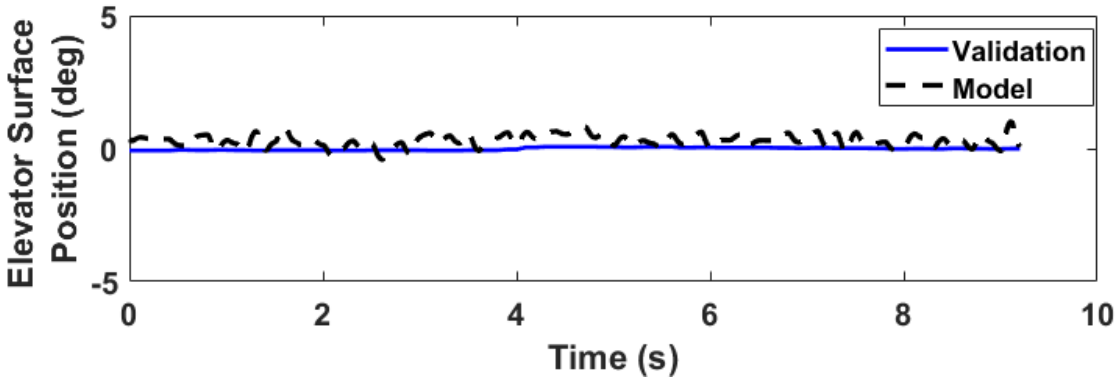

Figure C.5: Elevator surface position trace for 1.c.1 Normal Climb (Snapshot 1)

Snapshot 2

Table C.3: Initial conditions for 1.c.1 Normal Climb (Snapshot 2)

Parameter	Units	Validation	Model
Aircraft Configuration			
Weight	lbs	2433	2433
Station Center of Gravity	in	42.1	42.1
Flaps Position	deg	0	0
Flight Conditions			
Pressure Altitude	ft	5490	5490
Airspeed	KTAS	86	86
Vertical Speed	FPM	610	589
Aircraft Attitude			
Pitch	deg	6.5	6.6
Roll	deg	1.4	1.4
Heading	deg	92.5	92.5
Control Surfaces			
Elevator Position	deg	-0.1	0.3
Aileron Position	deg	0.8	1.4
Rudder Position	deg	4.9	5.0
Cockpit Controls			
Column Position	in	2.7	2.6
Wheel Position	deg	3.5	6.2
Pedal Position	deg	21.4	21.4
Propulsion			
Throttle Position	norm	1	1

Table C.4: Averaged results for 1.c.1 Normal Climb (Snapshot 1)

Metric	Tolerance	Validation (Mean ± SD)	Model (Mean ± SD)	Error (RMSE)	Pass/ Fail
Airspeed (KTAS)	±3 kt	86.0 ± 0.0	85.9 ± 0.1	0.1	**PASS**
Vertical Speed (FPM)	±100 FPM	597 ± 49	582 ± 34	32	**PASS**

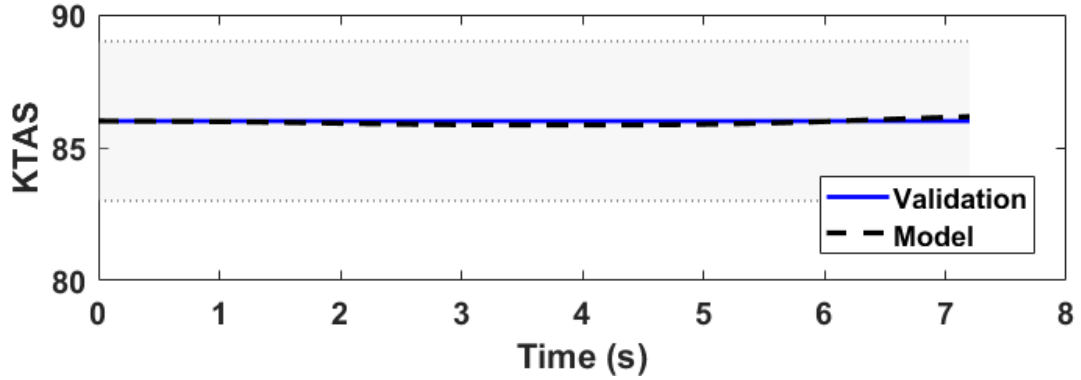

Figure C.6: Airspeed trace for 1.c.1 Normal Climb (Snapshot 2)

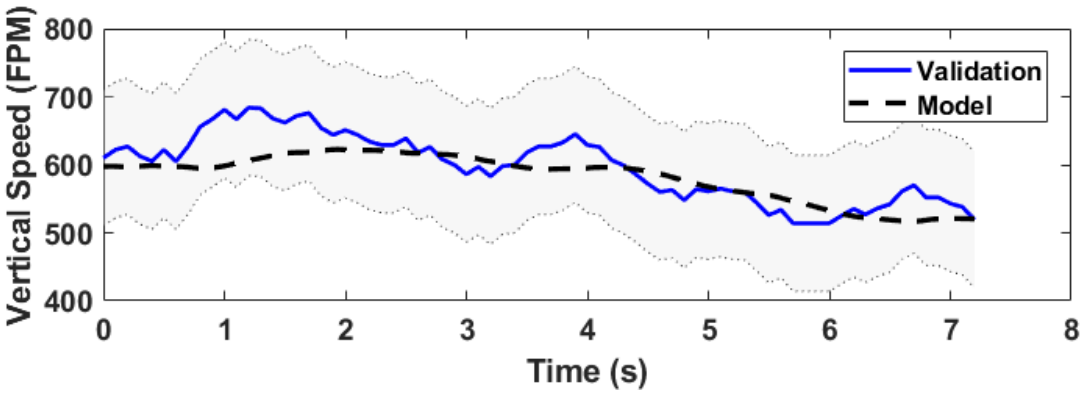

Figure C.7: Vertical speed trace for 1.c.1 Normal Climb (Snapshot 2)

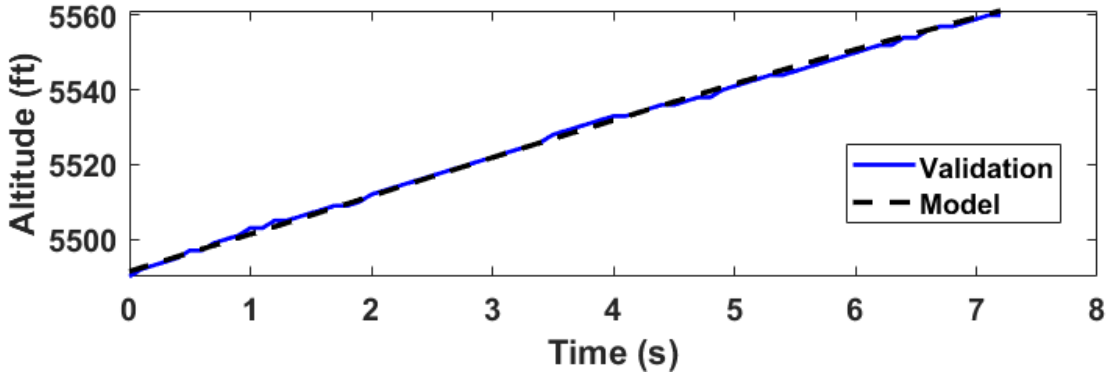

Figure C.8: Altitude trace for 1.c.1 Normal Climb (Snapshot 2)

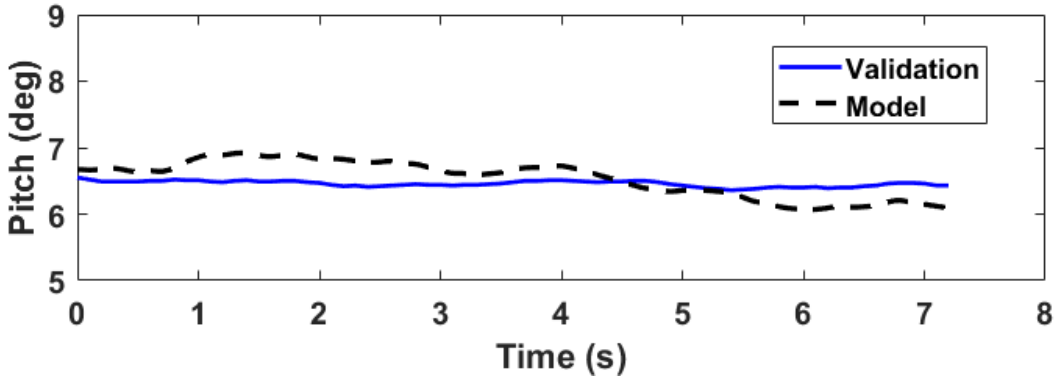

Figure C.9: Pitch trace for 1.c.1 Normal Climb (Snapshot 2)

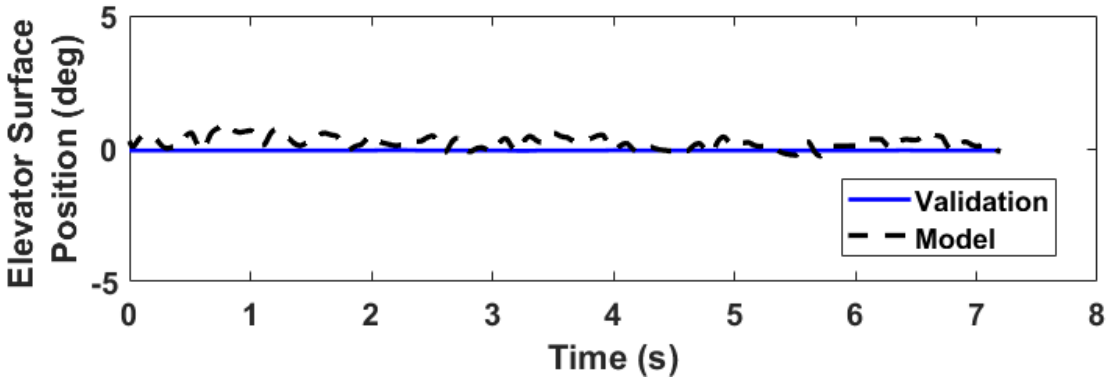

Figure C.10: Elevator surface position trace for 1.c.1 Normal Climb (Snapshot 2)

Snapshot 3

Table C.5: Initial conditions for 1.c.1 Normal Climb (Snapshot 3)

Parameter	**Units**	**Validation**	**Model**
Aircraft Configuration			
Weight	lbs	2433	2433
Station Center of Gravity	in	42.1	42.1
Flaps Position	deg	0	0
Flight Conditions			
Pressure Altitude	ft	7798	7798
Airspeed	KTAS	90	90
Vertical Speed	FPM	486	499
Aircraft Attitude			
Pitch	deg	5.6	5.7
Roll	deg	1.3	1.3
Heading	deg	108.5	108.5
Control Surfaces			
Elevator Position	deg	0.1	0.1
Aileron Position	deg	1.2	1.4
Rudder Position	deg	4.2	3.7
Cockpit Controls			
Column Position	in	2.7	2.6
Wheel Position	deg	5.0	6.1
Pedal Position	deg	21.3	21.2
Propulsion			
Throttle Position	norm	1	1

Table C.6: Averaged results for 1.c.1 Normal Climb (Snapshot 3)

Metric	Tolerance	Validation (Mean ± SD)	Model (Mean ± SD)	Error (RMSE)	Pass/ Fail
Airspeed (KTAS)	±3 kt	90.0 ± 0.0	90.5 ± 0.4	0.7	**PASS**
Vertical Speed (FPM)	±100 FPM	389 ± 37	424 ± 42	44	**PASS**

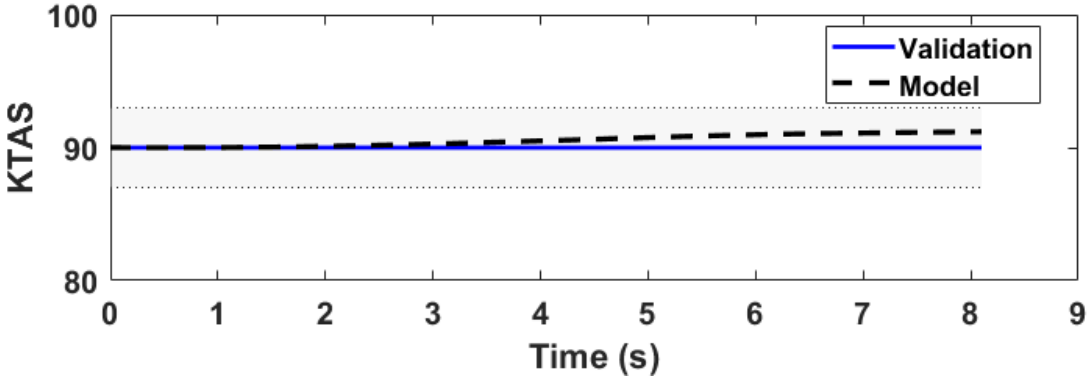

Figure C.11: Airspeed trace for 1.c.1 Normal Climb (Snapshot 3)

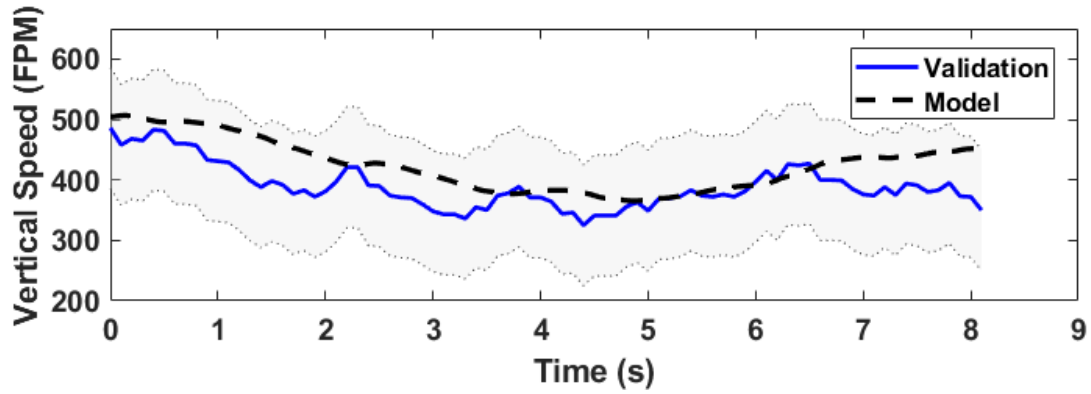

Figure C.12: Vertical speed trace for 1.c.1 Normal Climb (Snapshot 3)

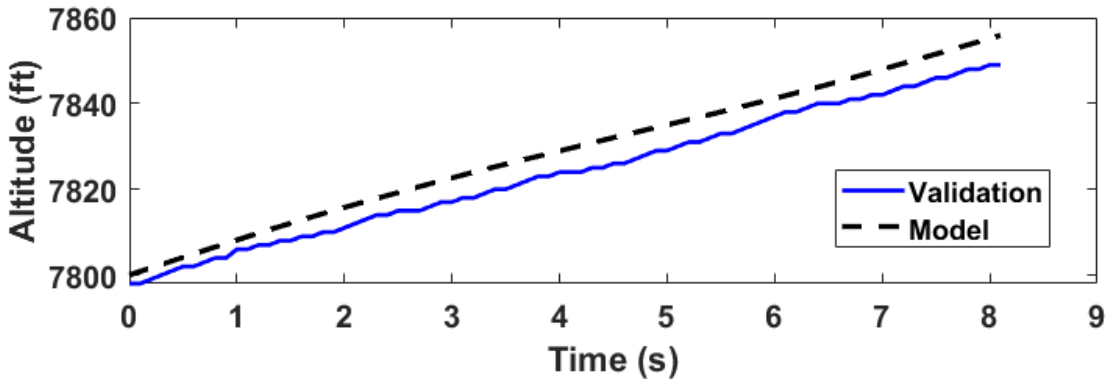

Figure C.13: Altitude trace for 1.c.1 Normal Climb (Snapshot 3)

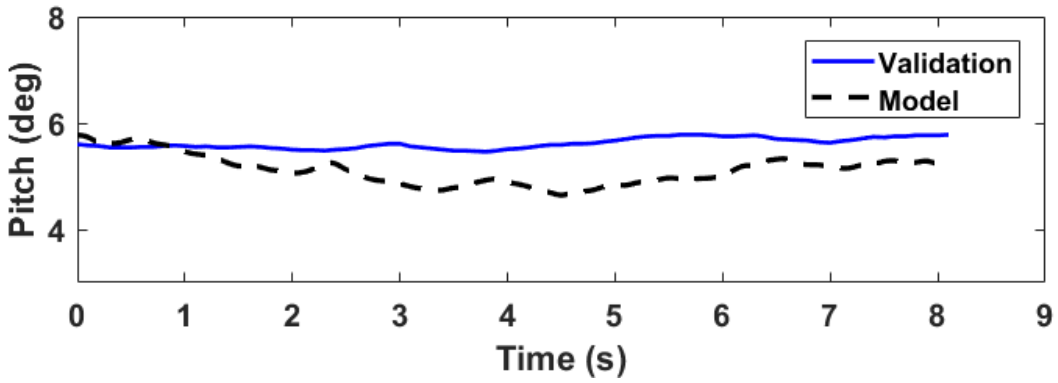

Figure C.14: Pitch trace for 1.c.1 Normal Climb (Snapshot 3)

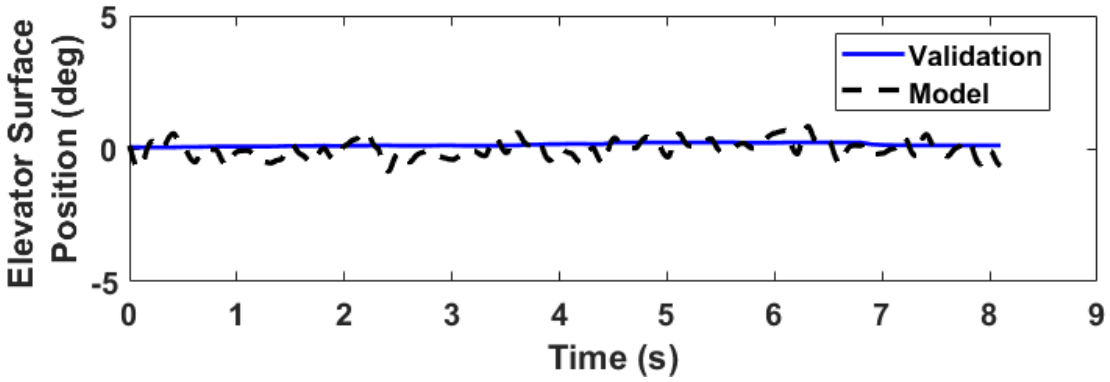

Figure C.15: Elevator surface position trace for 1.c.1 Normal Climb (Snapshot 3)

C.2 Flaps Down Climb – Supplemental

Test Objective

Demonstrate that the simulation accurately captures engine thrust and aerodynamic drag in a steady state climb condition with flaps deployed.

Test Information

FAA Part 60 requires a normal climb to be performance at nominal climb speed. Performance is to be recorded over an interval of at least 1,000 ft. For Level 5 and 6 devices, snapshot data is acceptable.

Tolerances

±3 kt airspeed
±100 FPM or ±5% climb rate

Flight Conditions

Takeoff configuration

Engineering Judgment/Comments

Supplemental Test This test is not required for any level of FTD but has been included to provide validation for flaps-down climb performance cases.

Snapshot Data Approach When attempting to trim available flight test data to a 1,000 ft or greater interval, it was clear that the pilot was not flying a well trimmed out position in many segments of the flight with fluctuations present in airspeed and vertical speed, especially at higher altitudes. Due to this, three smaller time samples are trimmed from the climb data and compared against as *snapshot data*, as allowed for Level 5 FTDs.

Use of Averaged Values Tolerance bands are plotted against the raw data traces for airspeed and vertical speed. Additionally, root-mean-square error (RMSE) is reported for airspeed and vertical speed across the tested range. It is recommended to use the RMSE values when evaluating whether results are acceptable as it provides a holistic view of performance over the interval instead of focusing on individual data points which may differ because of pilot technique or changing atmospheric conditions.

Results

Snapshot 1

Table C.7: Initial conditions for Flaps Down Climb, supplemental (Snapshot 1)

Parameter	**Units**	**Validation**	**Model**
Aircraft Configuration			
Weight	lbs	2442	2442
Station Center of Gravity	in	42.1	42.1
Flaps Position	deg	10	10
Flight Conditions			
Pressure Altitude	ft	3773	3773
Airspeed	KTAS	83	83
Vertical Speed	FPM	570	592
Aircraft Attitude			
Pitch	deg	4.4	5.2
Roll	deg	0.1	0.1
Heading	deg	46.8	46.8
Control Surfaces			
Elevator Position	deg	-5.3	-3.6
Aileron Position	deg	1.4	1.5
Rudder Position	deg	4.3	3.6
Cockpit Controls			
Column Position	in	2.1	2.3
Wheel Position	deg	5.8	6.5
Pedal Position	deg	21.3	21.2
Propulsion			
Throttle Position	norm	1	1

Table C.8: Averaged results for Flaps Down Climb, supplemental (Snapshot 1)

Metric	Tolerance	Validation (Mean ± SD)	Model (Mean ± SD)	Error (RMSE)	Pass/ Fail
Airspeed (KTAS)	±3 kt	83.0 ± 0.0	83.0 ± 0.0	0.01	**PASS**
Vertical Speed (FPM)	±100 FPM	574 ± 17	594 ± 5	26	**PASS**

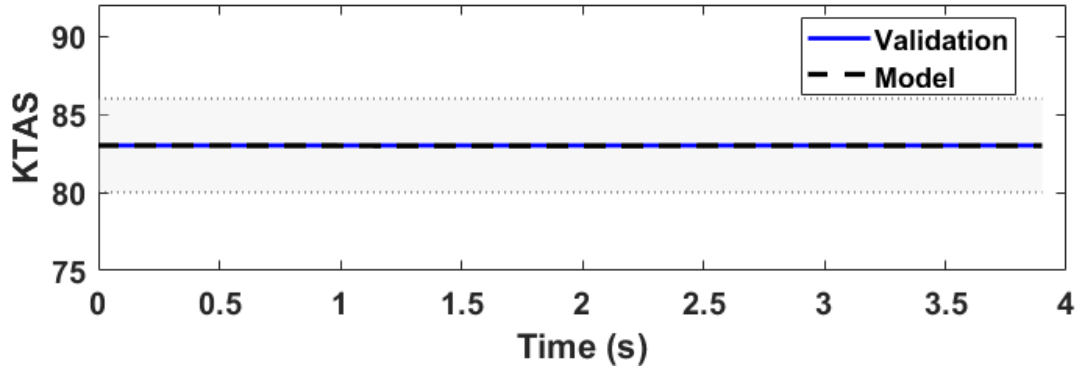

Figure C.16: Airspeed trace for Flaps Down Climb, supplemental (Snapshot 1)

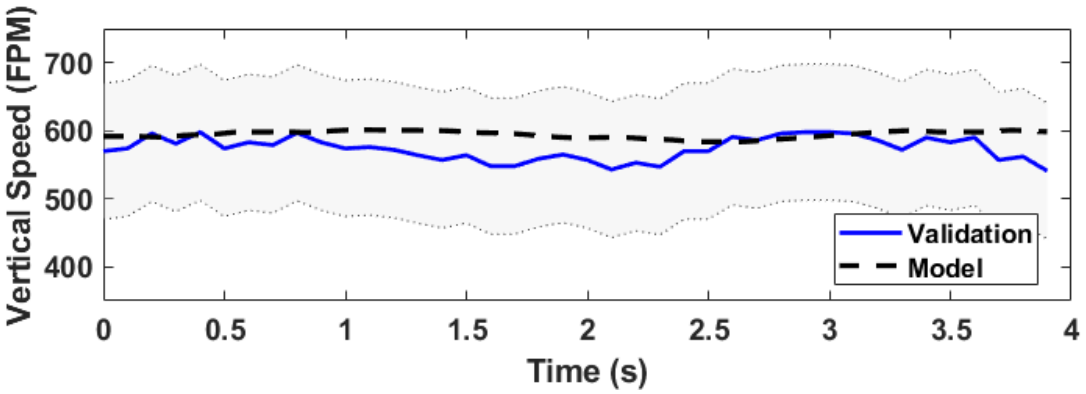

Figure C.17: Vertical speed trace for Flaps Down Climb, supplemental (Snapshot 1)

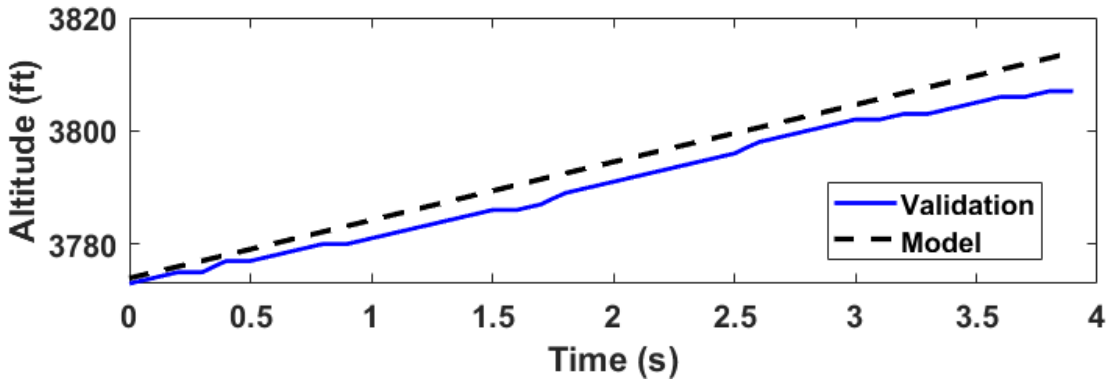

Figure C.18: Altitude trace for Flaps Down Climb, supplemental (Snapshot 1)

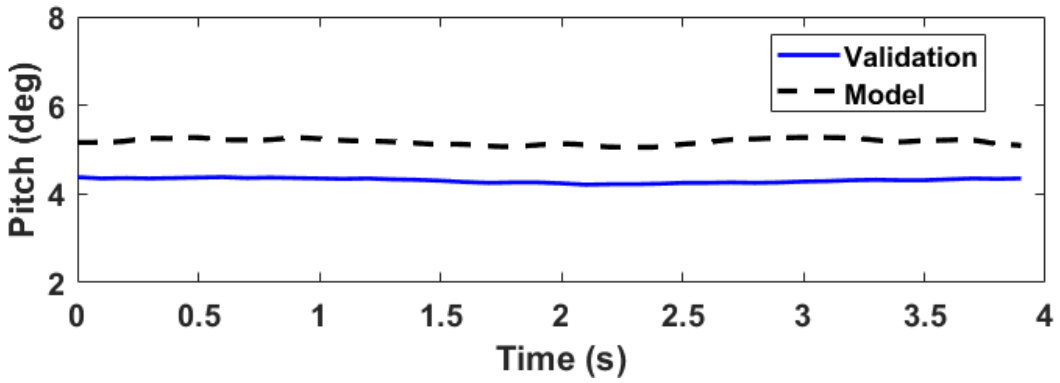

Figure C.19: Pitch trace for Flaps Down Climb, supplemental (Snapshot 1)

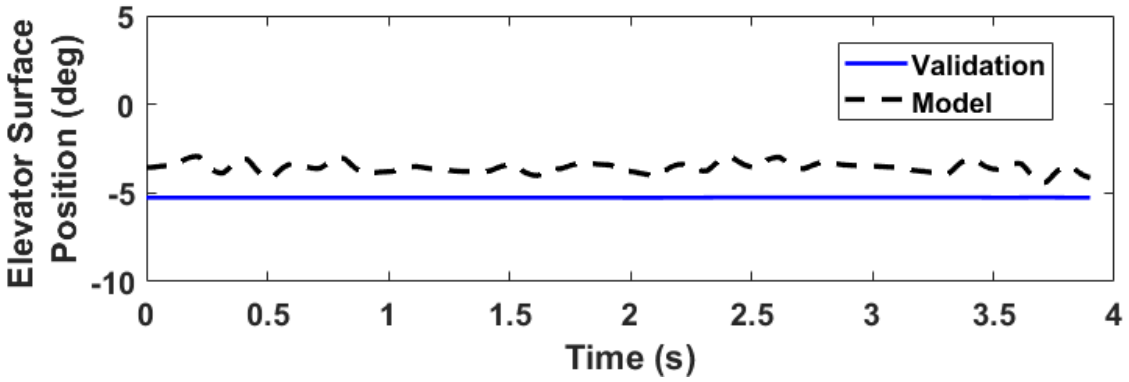

Figure C.20: Elevator surface position trace for Flaps Down Climb, supplemental (Snapshot 1)

Snapshot 2

Table C.9: Initial conditions for Flaps Down Climb, supplemental (Snapshot 2)

Parameter	Units	Validation	Model
Aircraft Configuration			
Weight	lbs	2442	2442
Station Center of Gravity	in	42.1	42.1
Flaps Position	deg	10	10
Flight Conditions			
Pressure Altitude	ft	4719	4719
Airspeed	KTAS	86	86
Vertical Speed	FPM	539	525
Aircraft Attitude			
Pitch	deg	3.9	4.2
Roll	deg	0.7	0.7
Heading	deg	47.9	47.9
Control Surfaces			
Elevator Position	deg	-5.3	-3.9
Aileron Position	deg	1.2	1.4
Rudder Position	deg	3.8	3.6
Cockpit Controls			
Column Position	in	2.1	2.1
Wheel Position	deg	5.2	6.0
Pedal Position	deg	21.3	21.2
Propulsion			
Throttle Position	norm	1	1

Table C.10: Averaged results for Flaps Down Climb, supplemental (Snapshot 2)

Metric	Tolerance	Validation (Mean ± SD)	Model (Mean ± SD)	Error (RMSE)	Pass/ Fail
Airspeed (KTAS)	±3 kt	86.0 ± 0.0	86.1 ± 0.1	0.1	**PASS**
Vertical Speed (FPM)	±100 FPM	525 ± 20	513 ± 14	20	**PASS**

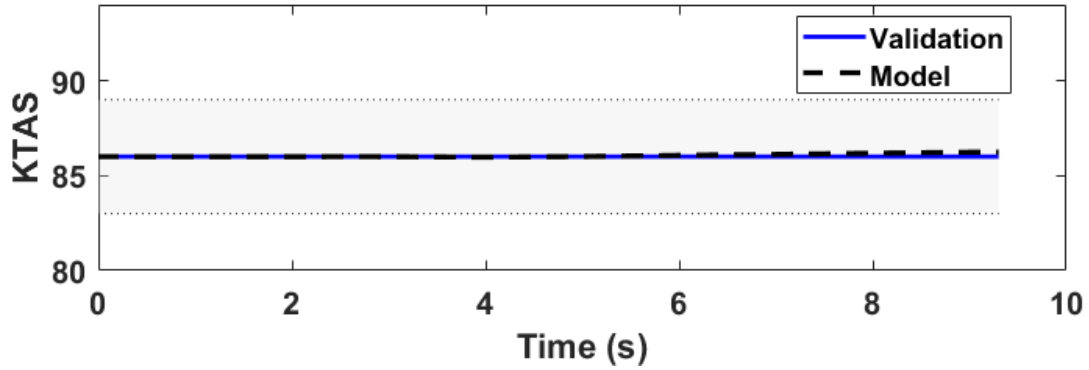

Figure C.21: Airspeed trace for Flaps Down Climb, supplemental (Snapshot 2)

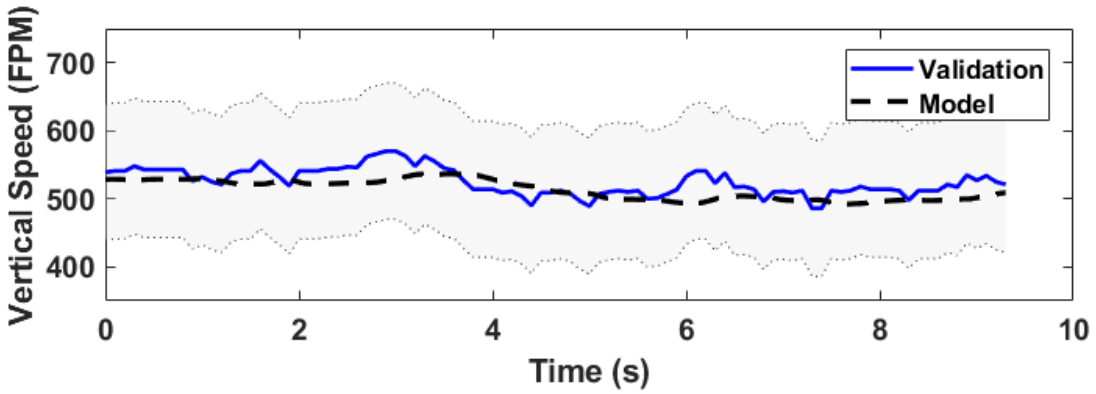

Figure C.22: Vertical speed trace for Flaps Down Climb, supplemental (Snapshot 2)

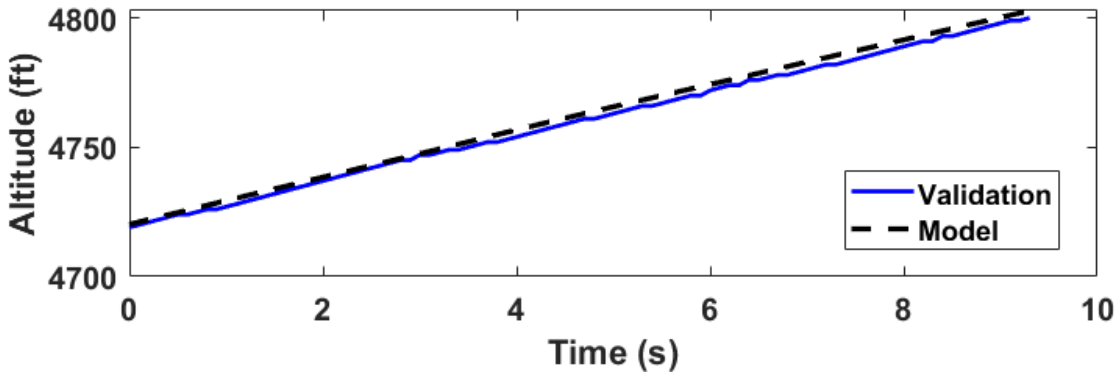

Figure C.23: Altitude trace for Flaps Down Climb, supplemental (Snapshot 2)

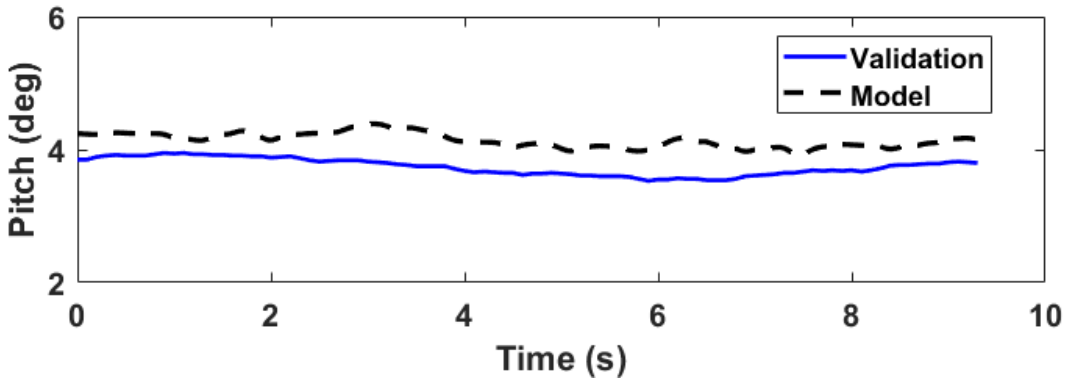

Figure C.24: Pitch trace for Flaps Down Climb, supplemental (Snapshot 2)

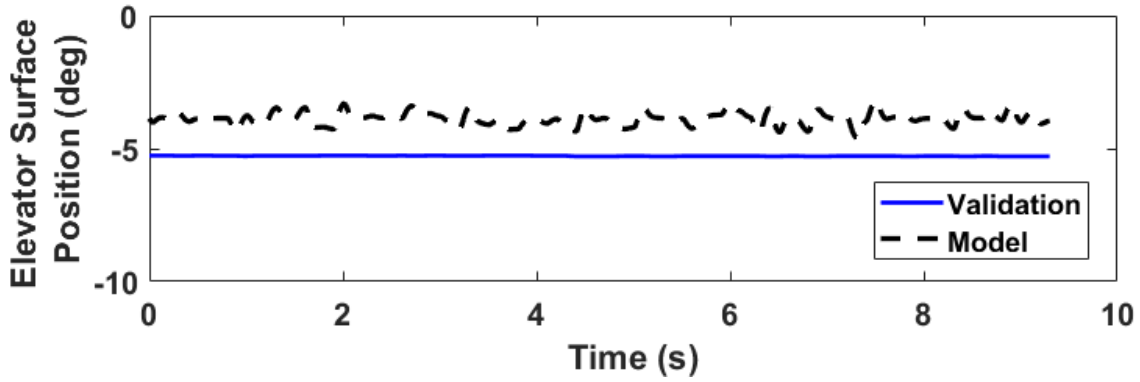

Figure C.25: Elevator surface position trace for Flaps Down Climb, supplemental (Snapshot 2)

C.3 1.f.1 Engine Acceleration

Test Objective

Demonstrate that engine acceleration characteristics match the aircraft.

Test Information

Trim the aircraft in an approach or landing condition then rapidly advance throttles from idle power to go-around thrust setting.

Tolerances

± 1 sec of the time from 10% (T_i) to 90% (T_t) of engine parameter response

Flight Conditions

Approach or Landing

Engineering Judgment/Comments

Propulsion system flight test data As previously mentioned, the propulsion system data sets from the flight test package are treated with skepticism and should not be directly compared.

Use of Alternative Data Source FAA Part 60 Table B2B provides a set of alternative data sources for Level 5 FTDs (Small, Single Engine (Reciprocating) Airplanes) [8] to be used for objective test result comparison in the absence of reliable flight test data. This test makes use of those provided performance figures. For 1.f.1 Engine Acceleration, the alternative data source authorizes an **engine parameter (RPM) response time of 2 - 4 seconds** for advancement of throttle from idle to takeoff power.

Results

Table C.11: Initial conditions for 1.f.1 Engine Acceleration

Parameter	**Units**	**Validation**	**Model**
Aircraft Configuration			
Weight	lbs	N/A	2355
Station Center of Gravity	in	N/A	42.1
Flaps Position	deg	N/A	20
Flight Conditions			
Pressure Altitude	ft	N/A	2000
Airspeed	KTAS	N/A	80
Vertical Speed	FPM	N/A	-1208
Aircraft Attitude			
Pitch	deg	N/A	-9.2
Roll	deg	N/A	0
Heading	deg	N/A	200
Propulsion			
Throttle Position	norm	N/A	0

Table C.12: Results summary for 1.f.1 Engine Acceleration

Metric	**Tolerance**	**Validation**	**Model**	**Error**	**Pass/ Fail**
T_i	N/A	N/A	2.3	N/A	N/A
T_t	N/A	N/A	4.3	N/A	N/A
ΔT	$\pm$ 1 sec	2 - 4	2.0	0	**PASS**

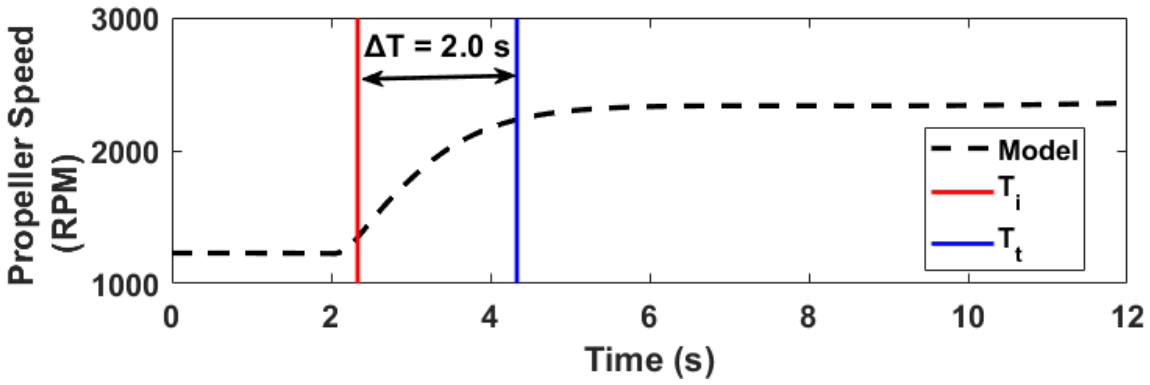

Figure C.26: Propeller speed trace for 1.f.1 Engine Acceleration

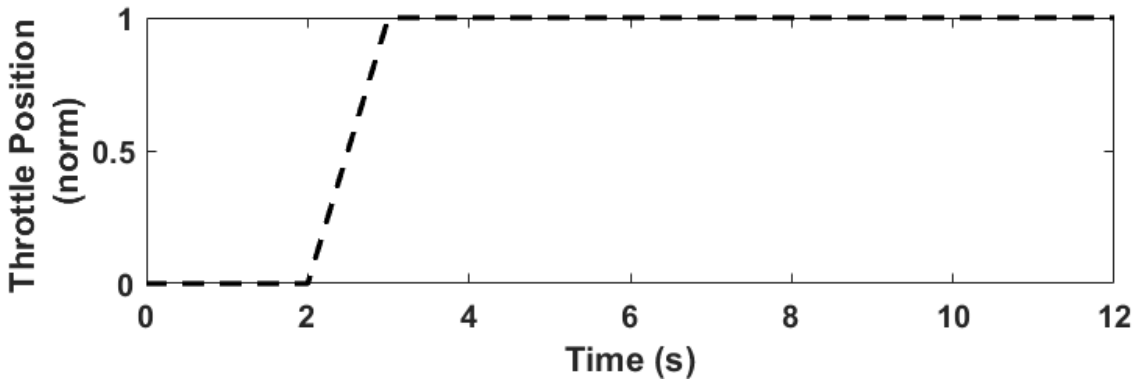

Figure C.27: Throttle trace for 1.f.1 Engine Acceleration

C.4 1.f.2 Engine Deceleration

Test Objective

Demonstrate that engine deceleration characteristics match the aircraft.

Test Information

With the aircraft placed on the ground with throttles at maximum takeoff power, rapidly decrease the throttle to idle power position.

Tolerances

± 1 sec of the time from 10% (T_i) to 90% (T_t) of engine parameter response

Flight Conditions

On ground

Engineering Judgment/Comments

Propulsion system flight test data As previously mentioned, the propulsion system data sets from the flight test package are treated with skepticism and should not be directly compared.

Use of Alternative Data Source FAA Part 60 Table B2B provides a set of alternative data sources for Level 5 FTDs (Small, Single Engine (Reciprocating) Airplanes) [8] to be used for objective test result comparison in the absence of reliable flight test data. This test makes use of those provided performance figures. For 1.f.2 Engine Deceleration, the alternative data source authorizes an **engine parameter (RPM) response time of 2 - 4 seconds** for a rapid decrease of throttle from takeoff to idle power.

Results

Table C.13: Initial conditions for 1.f.2 Engine Deceleration – On ground

Parameter	Units	Validation	Model
Aircraft Configuration			
Weight	lbs	N/A	2444
Station Center of Gravity	in	N/A	42.1
Flaps Position	deg	N/A	0
Flight Conditions			
Pressure Altitude	ft	N/A	735
Airspeed	KTAS	N/A	0
Vertical Speed	FPM	N/A	0
Propulsion			
Throttle Position	norm	N/A	1

Table C.14: Results summary for 1.f.2 Engine Deceleration

Metric	Tolerance	Validation	Model	Error	Pass/ Fail
T_i	N/A	N/A	2.5	N/A	N/A
T_t	N/A	N/A	6.3	N/A	N/A
ΔT	$\pm$ 1 sec	2 - 4	3.7	0	**PASS**

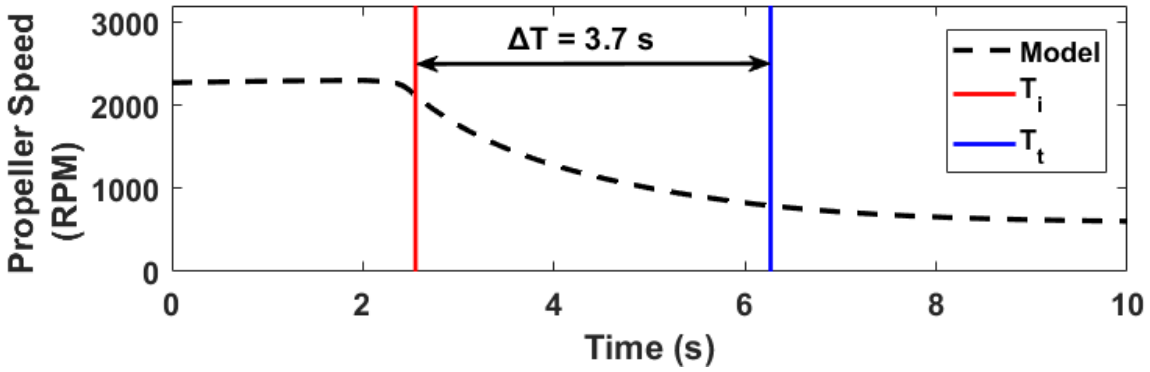

Figure C.28: Propeller speed trace for 1.f.2 Engine Deceleration

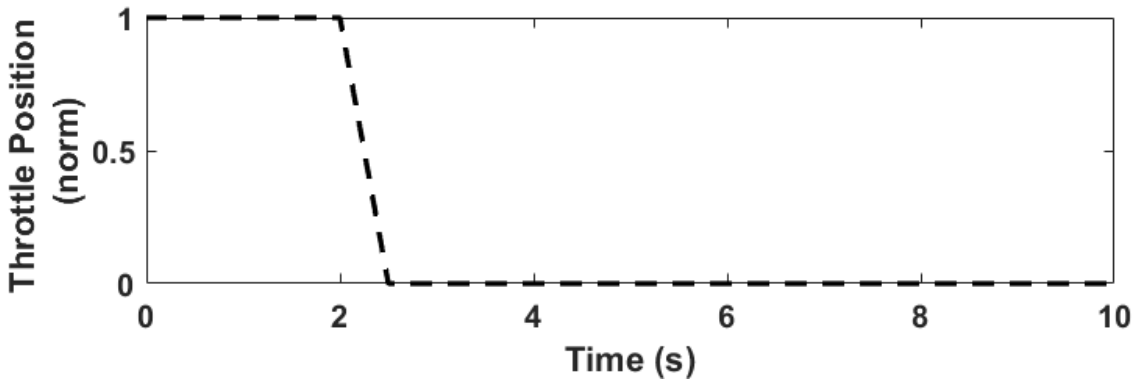

Figure C.29: Throttle trace for 1.f.2 Engine Deceleration

C.5 2.a.1.a/b Pitch controller position versus force and surface position calibration

Test Objective

Demonstrate that the model's pitch controller (column) to elevator position mapping accurately represents the aircraft.

Test Information

Move the pitch controller at a slow rate over its full range.

Tolerances

±2 lb breakout force *(N/A, see engineering judgment)*
±5 lb or ±10% of force *(N/A, see engineering judgment)*
±2° elevator angle - *Level 6 tolerance*

Flight Conditions

On ground

Engineering Judgment/Comments

Control force modeling The flight simulation model does not contain a simulated control loading framework making the force-based tolerances on 2.a.1.a non-applicable.

Higher-Level Tolerance Adoption The Level 5 version of this test only applies tolerances on the forces during the column sweep. Level 6 and 7 extend this test to serve as a column position to elevator mapping validation test (2.a.1.b). The higher-level elevator position tolerances are adopted as validation for this test, demonstrating the mapping between the pilot's cockpit control and the resulting control surface deflection. Validating this relationship is essential as later dynamic maneuver tests rely on accurate control surface

response to pilot inputs. If the mapping is incorrect, errors in dynamic test results cannot be attributed solely to the flight dynamics model.

Results

Table C.15: Initial conditions for 2.a.1.a/b Pitch controller position versus force and surface position calibration – On ground

Parameter	Units	Validation	Model
Aircraft Configuration			
Weight	lbs	N/A	2452
Station Center of Gravity	in	N/A	42.1
Flaps Position	deg	N/A	0
Flight Conditions			
Pressure Altitude	ft	N/A	735
Airspeed	KTAS	N/A	0
Vertical Speed	FPM	N/A	0
Propulsion			
Throttle Position	norm	N/A	0.1

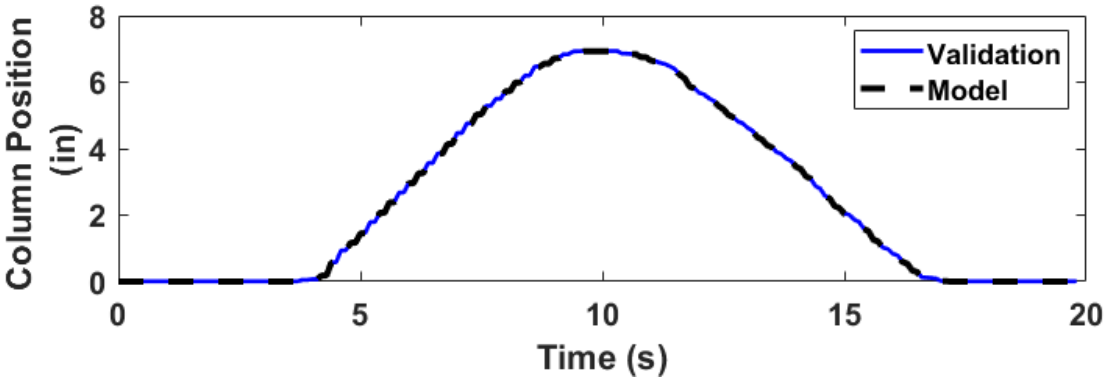

Figure C.30: Column position trace for 2.a.1.a/b Pitch controller position versus force and surface position calibration

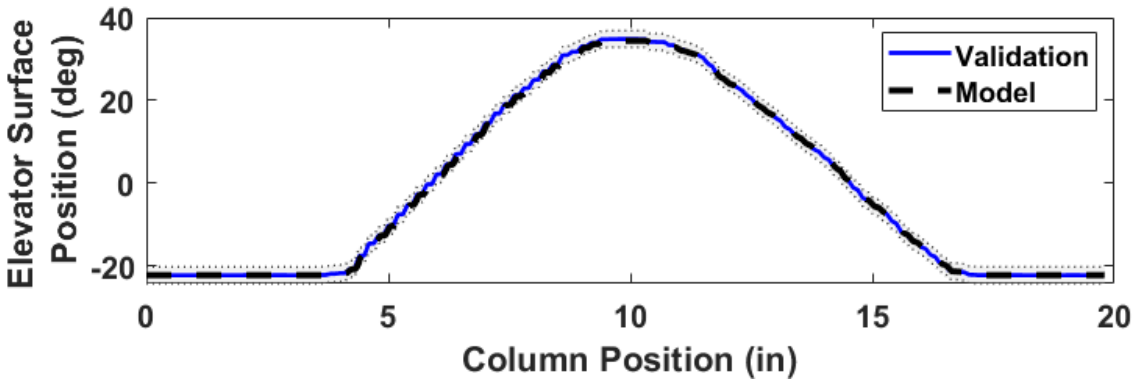

Figure C.31: Elevator surface position trace for 2.a.1.a/b Pitch controller position versus force and surface position calibration

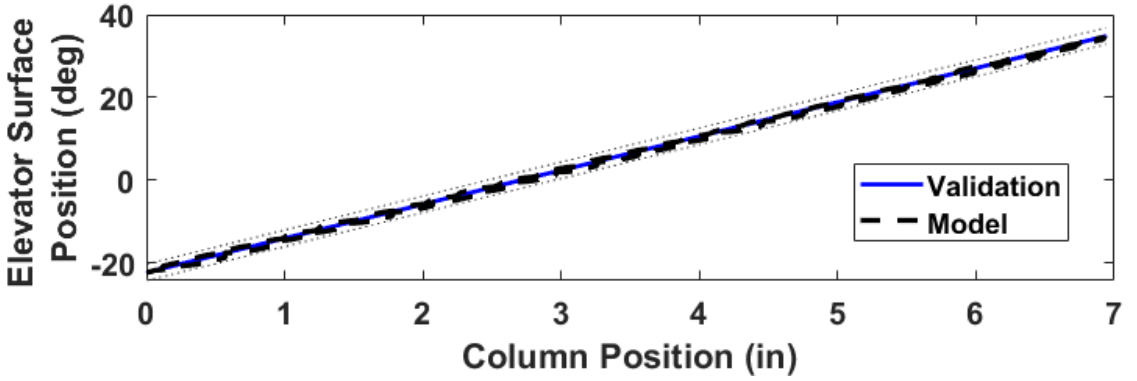

Figure C.32: Elevator surface position vs. column position mapping trace for 2.a.1.a/b Pitch controller position versus force and surface position calibration

C.6 2.a.2.a/b Roll controller position versus force and surface position calibration

Test Objective

Demonstrate that the model's roll controller (wheel) to aileron position mapping accurately represents the aircraft.

Test Information

Move the roll controller at a slow rate over its full range.

Tolerances

±2 lb breakout force *(N/A, see engineering judgment)*
±5 lb or ±10% of force *(N/A, see engineering judgment)*
±2° aileron angle - *Level 6 tolerance*

Flight Conditions

On ground

Engineering Judgment/Comments

Control force modeling The flight simulation model does not contain a simulated control loading framework making the force-based tolerances on 2.a.2.a non-applicable.

Higher-Level Tolerance Adoption The Level 5 version of this test only applies tolerances on the forces during the wheel sweep. Level 6 and 7 extend this test to serve as a wheel position to aileron mapping validation test (2.a.2.b). The higher-level aileron position tolerances are adopted as validation for this test, demonstrating the mapping between the pilot's cockpit control and the resulting control surface deflection. Validating this relationship is essential as later dynamic maneuver tests rely on accurate control surface response to

pilot inputs. If the mapping is incorrect, errors in dynamic test results cannot be attributed solely to the flight dynamics model.

Results

Table C.16: Initial conditions for 2.a.2.a/b Roll controller position versus force and surface position calibration – On ground

Parameter	Units	Validation	Model
Aircraft Configuration			
Weight	lbs	N/A	2452
Station Center of Gravity	in	N/A	42.1
Flaps Position	deg	N/A	0
Flight Conditions			
Pressure Altitude	ft	N/A	735
Airspeed	KTAS	N/A	0
Vertical Speed	FPM	N/A	0
Propulsion			
Throttle Position	norm	N/A	0.1

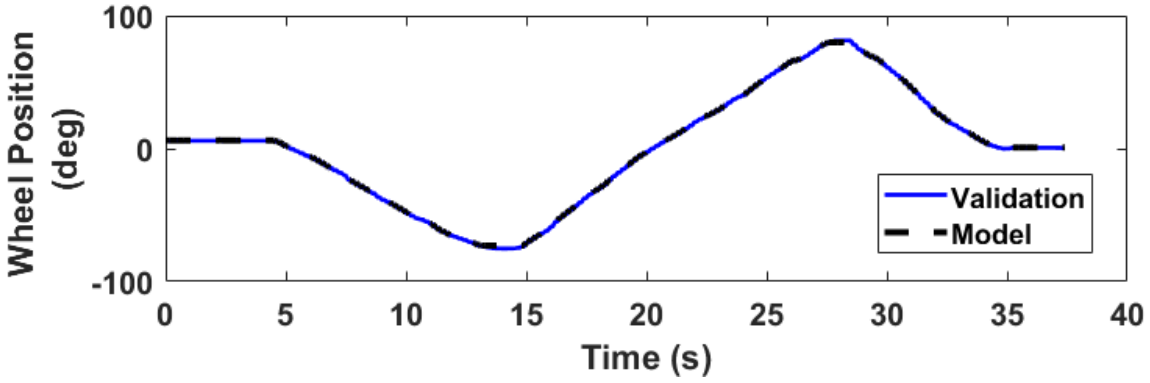

Figure C.33: Wheel position trace for 2.a.2.a/b Roll controller position versus force and surface position calibration

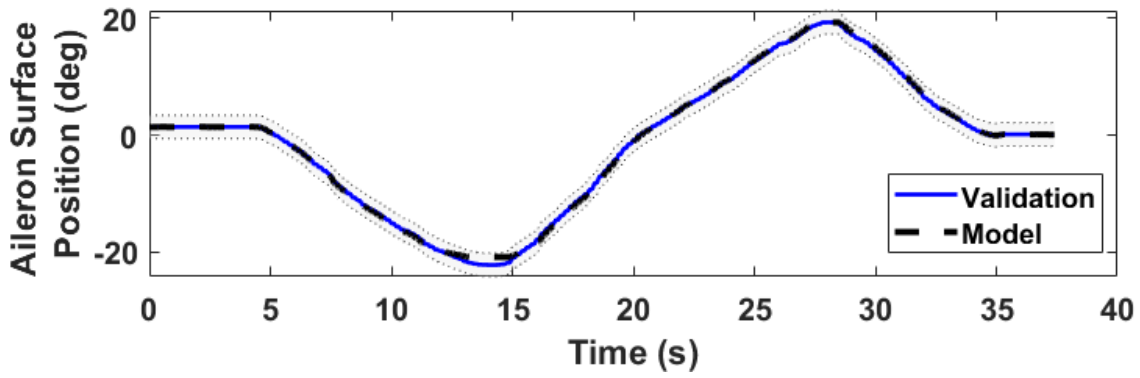

Figure C.34: Aileron surface position trace for 2.a.2.a/b Roll controller position versus force and surface position calibration

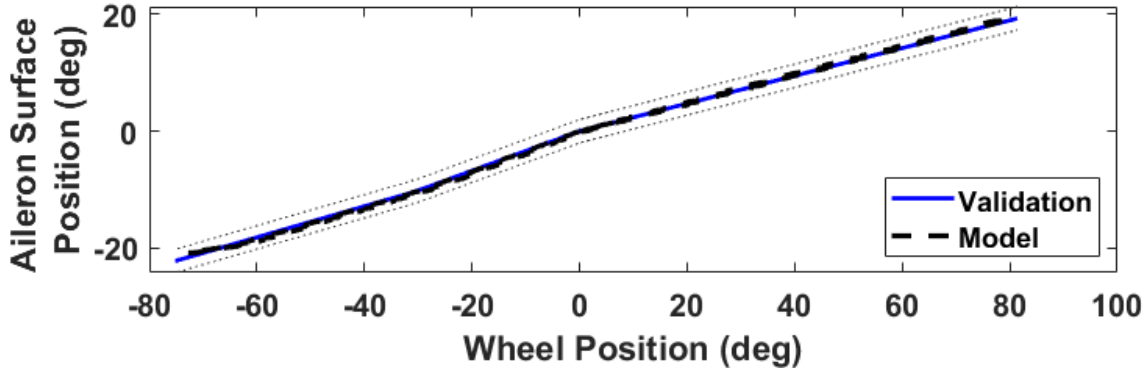

Figure C.35: Aileron surface position vs. wheel position mapping trace for 2.a.2.a/b Roll controller position versus force and surface position calibration

C.7 2.a.2.a/b Rudder pedal position versus force and surface position calibration

Test Objective

Demonstrate that the model's pedal to rudder position mapping accurately represents the aircraft.

Test Information

Move the pedals at a slow rate over its full range.

Tolerances

±2 lb breakout force *(N/A, see engineering judgment)*
±5 lb or ±10% of force *(N/A, see engineering judgment)*
±2° rudder angle - *Level 6 tolerance*

Flight Conditions

On ground

Engineering Judgment/Comments

Control force modeling The flight simulation model does not contain a simulated control loading framework making the force-based tolerances on 2.a.3.a non-applicable.

Higher-Level Tolerance Adoption The Level 5 version of this test only applies tolerances on the forces during the pedal sweep. Level 6 and 7 extend this test to serve as a pedal position to rudder mapping validation test (2.a.3.b). The higher-level rudder position tolerances are adopted as validation for this test, demonstrating the mapping between the pilot's cockpit control and the resulting control surface deflection. Validating this relationship is essential as later dynamic maneuver tests rely on accurate control surface response to

pilot inputs. If the mapping is incorrect, errors in dynamic test results cannot be attributed solely to the flight dynamics model.

Results

Table C.17: Initial conditions for 2.a.3.a/b Pedal position versus force and surface position calibration – On ground

Parameter	Units	Validation	Model
Aircraft Configuration			
Weight	lbs	N/A	2452
Station Center of Gravity	in	N/A	42.1
Flaps Position	deg	N/A	0
Flight Conditions			
Pressure Altitude	ft	N/A	735
Airspeed	KTAS	N/A	0
Vertical Speed	FPM	N/A	0
Propulsion			
Throttle Position	norm	N/A	0.1

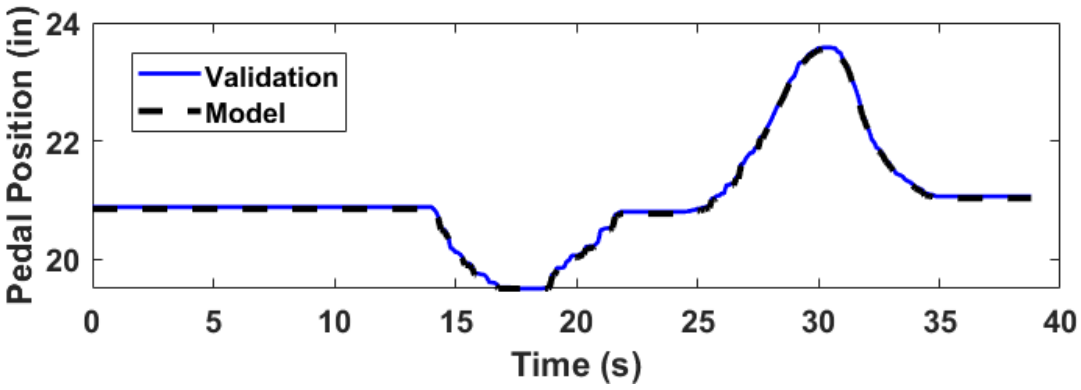

Figure C.36: Pedal position trace for 2.a.3.a/b Pedal position versus force and surface position calibration

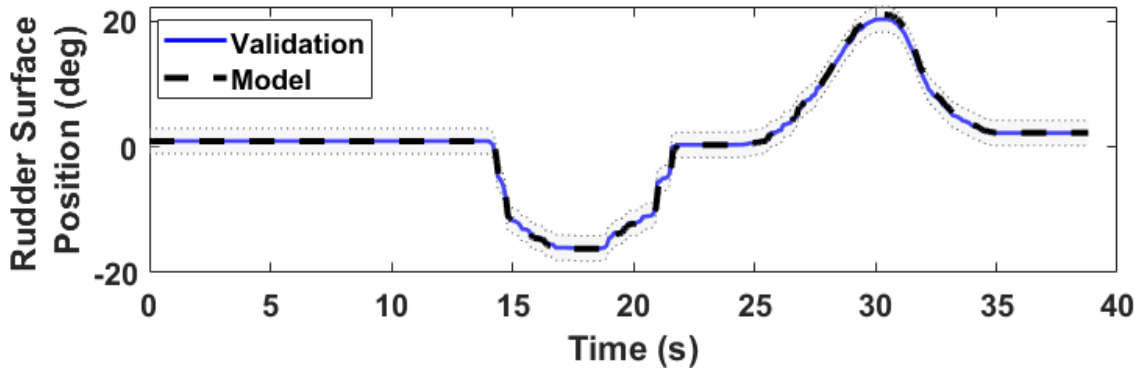

Figure C.37: Rudder surface position trace for 2.a.3.a/b Pedal position versus force and surface position calibration

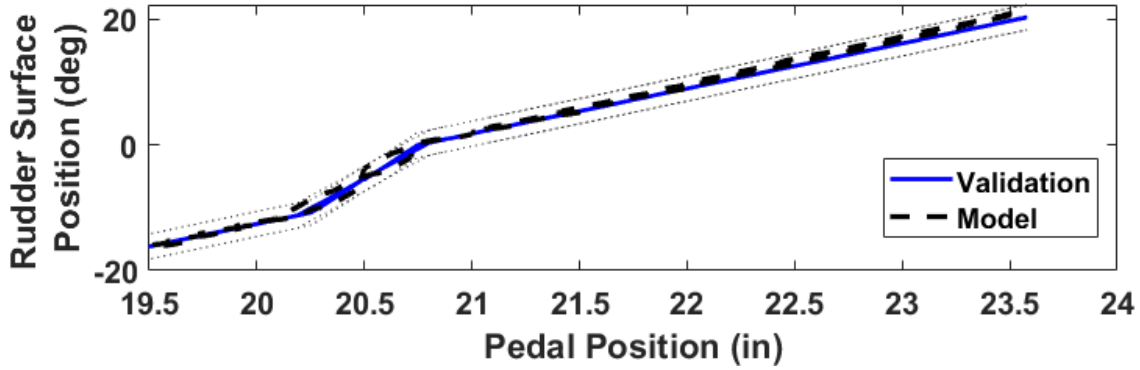

Figure C.38: Rudder surface position vs. pedal position mapping trace for 2.a.3.a/b Pedal position versus force and surface position calibration

C.8 2.b.1/2.b.4 Pitch Control / Small Control Inputs - Pitch

Test Objective

Demonstrate that the model's dynamic pitch response to column input accurately represents the aircraft.

Test Information

The longitudinal controller is displaced with an approximately one second pulse input and released. The maximum body pitch rate response is compared against flight test data.

Tolerances

$\pm 0.15°$/s body pitch rate or $\pm 20\%$ of peak body pitch rate - *Level 7 tolerance (2.b.4)*

Flight Conditions

As available - Cruise and Takeoff Configurations

Engineering Judgment/Comments

Control force modeling The flight simulation model does not contain a simulated control loading framework making true free response behavior, as required by the pitch control response test (2.b.1), not achievable. The test is instead executed as a prescribed pulse input to the column.

Hybrid Test Approach and Adoption of Level 7 Tolerance The available flight test data does not fall cleanly within the test procedures for any single FAA Part 60 objective test. The maneuver resembles a combination of the pitch control response test (2.b.1) and the small control inputs test (2.b.4). The test is executed closely to the pitch control response procedure, but the $\pm 20\%$ of peak body pitch rate tolerance is adopted from the small control inputs test as it provides a physically meaningful metric for comparing peak

dynamic response between the model and flight test data. These tests are not required for Level 5 qualification but provide valuable characterization of the model's pitch axis dynamic response.

Results

Cruise Case 1

Table C.18: Initial conditions for 2.b.1/2.b.4 Pitch Control / Small Control Inputs - Pitch (Cruise Case 1)

Parameter	**Units**	**Validation**	**Model**
Aircraft Configuration			
Weight	lbs	2402	2402
Station Center of Gravity	in	42.0	42.0
Flaps Position	deg	0	0
Flight Conditions			
Pressure Altitude	ft	5457	5457
Airspeed	KTAS	110	110
Vertical Speed	FPM	-231	-231
Aircraft Attitude			
Pitch	deg	-1.0	-1.7
Roll	deg	1.2	1.2
Heading	deg	266.2	266.2
Control Surfaces			
Elevator Position	deg	-1.9	-2.4
Aileron Position	deg	1.2	0.9
Rudder Position	deg	1.0	1.9
Cockpit Controls			
Column Position	in	2.5	2.4
Wheel Position	deg	5.0	4.3
Pedal Position	deg	20.9	21.0
Propulsion			
Throttle Position	norm	N/A	0.28

Table C.19: Results summary for 2.b.1/2.b.4 Pitch Control / Small Control Inputs - Pitch (Cruise Case 1)

Metric	Tolerance	Validation	Model	Error	Pass/ Fail
Maximum Pitch Rate	±20% (2.2°/s)	11.2	11.4	0.2	**PASS**

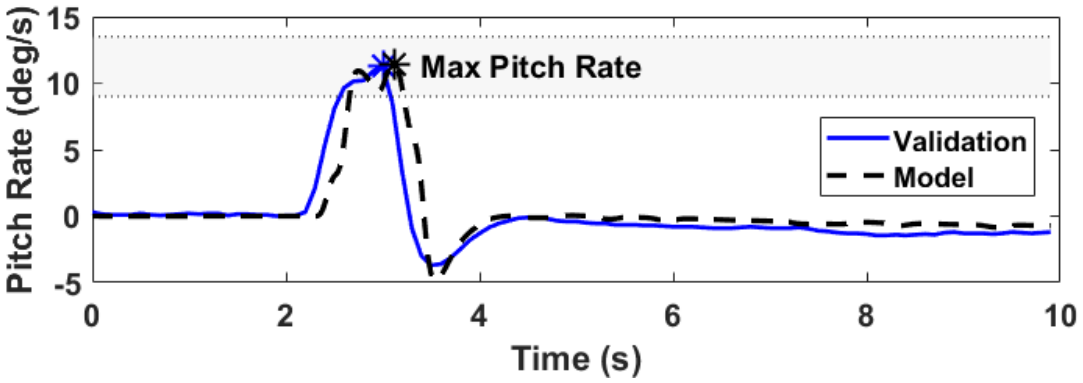

Figure C.39: Pitch rate trace for 2.b.1/2.b.4 Pitch Control / Small Control Inputs - Pitch (Cruise Case 1)

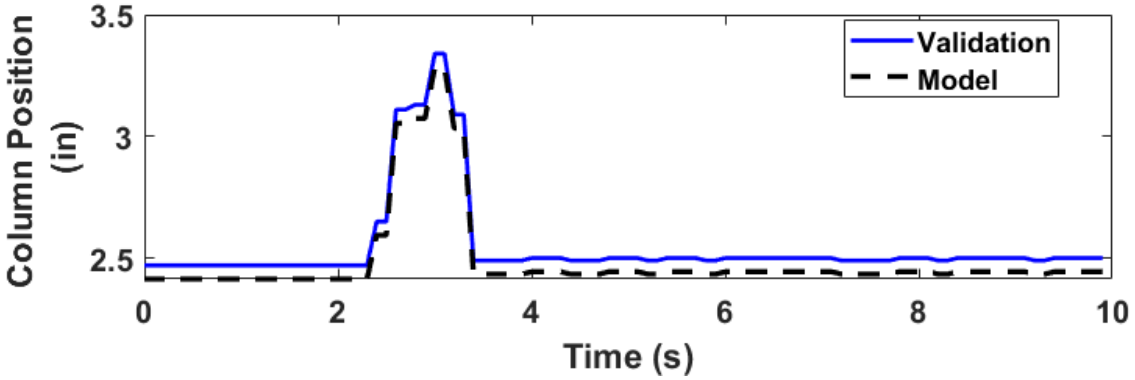

Figure C.40: Column position trace for 2.b.1/2.b.4 Pitch Control / Small Control Inputs - Pitch (Cruise Case 1)

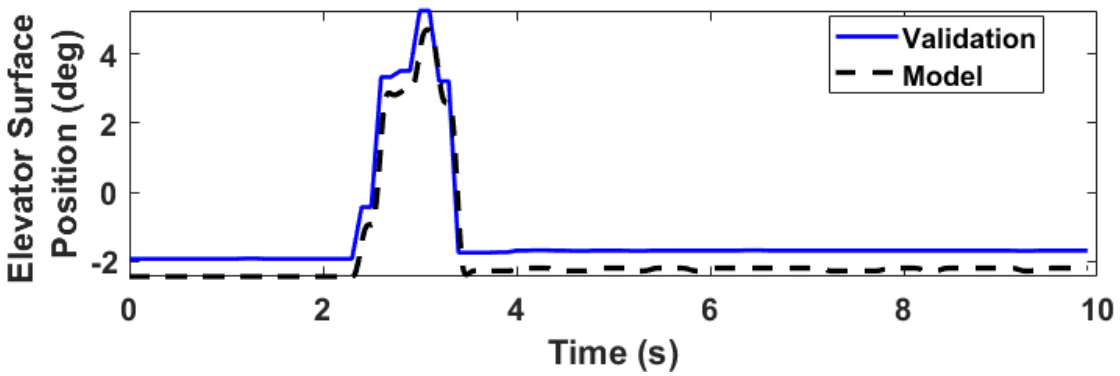

Figure C.41: Elevator surface position trace for 2.b.1/2.b.4 Pitch Control / Small Control Inputs - Pitch (Cruise Case 1)

Cruise Case 2

Table C.20: Initial conditions for 2.b.1/2.b.4 Pitch Control / Small Control Inputs - Pitch (Cruise Case 2)

Parameter	Units	Validation	Model
Aircraft Configuration			
Weight	lbs	2401	2401
Station Center of Gravity	in	42.0	42.0
Flaps Position	deg	0	0
Flight Conditions			
Pressure Altitude	ft	5305	5305
Airspeed	KTAS	107	107
Vertical Speed	FPM	-203	-203
Aircraft Attitude			
Pitch	deg	-0.6	-1.3
Roll	deg	1.0	1.0
Heading	deg	274.1	274.1
Control Surfaces			
Elevator Position	deg	-1.5	-2.2
Aileron Position	deg	1.2	1.0
Rudder Position	deg	0.9	1.8
Cockpit Controls			
Column Position	in	-1.5	-2.2
Wheel Position	deg	5.2	4.5
Pedal Position	deg	20.9	21.0
Propulsion			
Throttle Position	norm	N/A	0.27

Table C.21: Results summary for 2.b.1/2.b.4 Pitch Control / Small Control Inputs - Pitch (Cruise Case 2)

Metric	Tolerance	Validation	Model	Error	Pass/ Fail
Maximum Pitch Rate	±20% (4.2°/s)	21.0	22.9	2.9	**PASS**

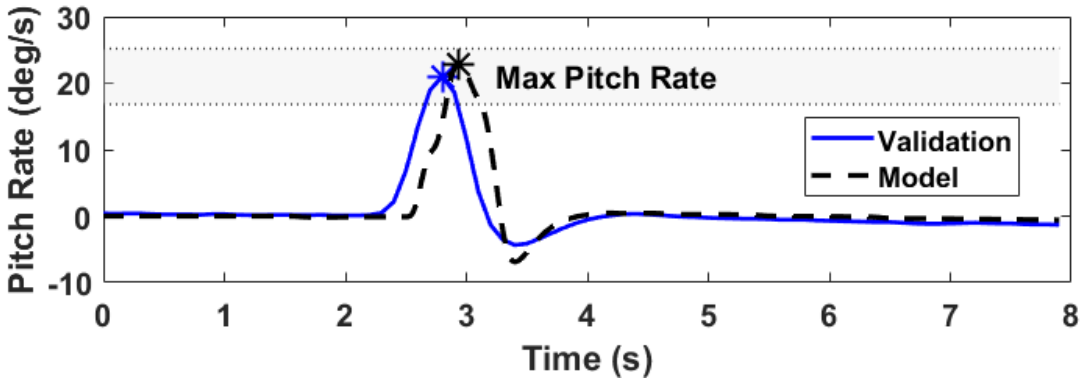

Figure C.42: Pitch rate trace for 2.b.1/2.b.4 Pitch Control / Small Control Inputs - Pitch (Cruise Case 2)

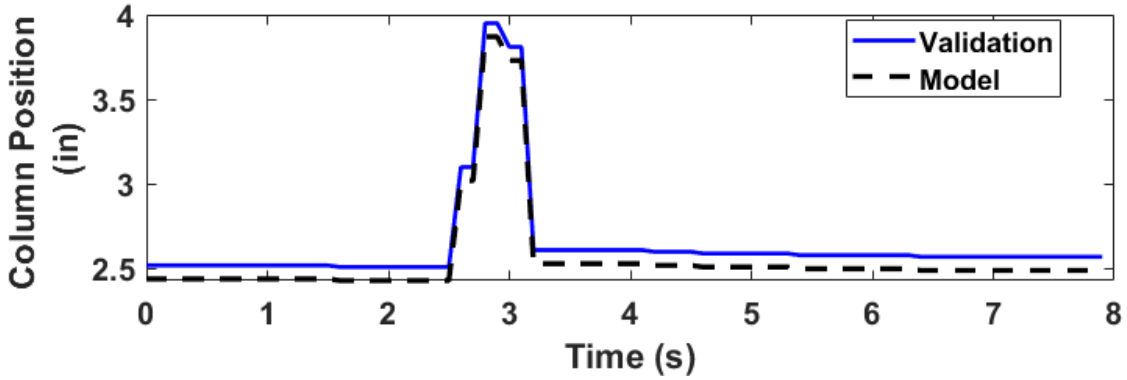

Figure C.43: Column position trace for 2.b.1/2.b.4 Pitch Control / Small Control Inputs - Pitch (Cruise Case 2)

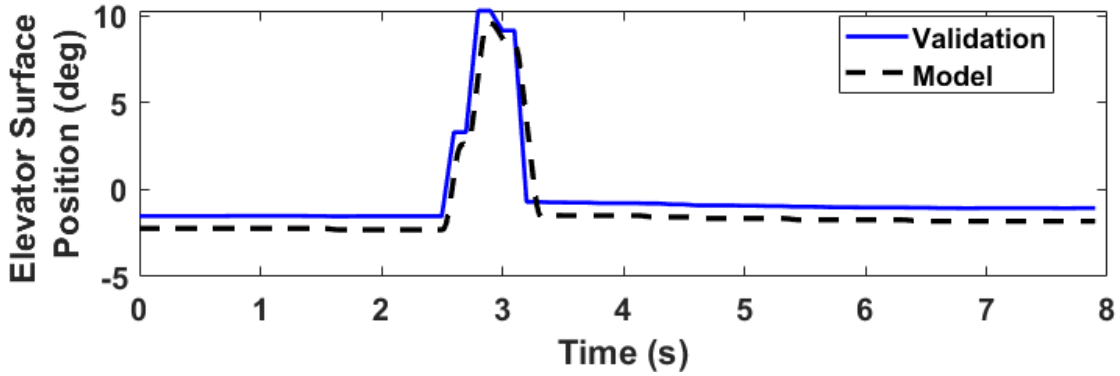

Figure C.44: Elevator surface position trace for 2.b.1/2.b.4 Pitch Control / Small Control Inputs - Pitch (Cruise Case 2)

Takeoff Case

Table C.22: Initial conditions for 2.b.1/2.b.4 Pitch Control / Small Control Inputs - Pitch (Takeoff Case)

Parameter	Units	Validation	Model
Aircraft Configuration			
Weight	lbs	2395	2395
Station Center of Gravity	in	42.0	42.0
Flaps Position	deg	10	10
Flight Conditions			
Pressure Altitude	ft	5630	5630
Airspeed	KTAS	96	96
Vertical Speed	FPM	89	89
Aircraft Attitude			
Pitch	deg	-0.6	-0.2
Roll	deg	1.4	1.4
Heading	deg	128.5	128.5
Control Surfaces			
Elevator Position	deg	-5.7	-5.1
Aileron Position	deg	1.4	1.3
Rudder Position	deg	1.0	0.6
Cockpit Controls			
Column Position	in	2.0	2.1
Wheel Position	deg	6.0	5.6
Pedal Position	deg	20.9	20.8
Propulsion			
Throttle Position	norm	N/A	0.4

Table C.23: Results summary for 2.b.1/2.b.4 Pitch Control / Small Control Inputs - Pitch (Takeoff Case)

Metric	Tolerance	Validation	Model	Error	Pass/ Fail
Maximum Pitch Rate	±20% (3.0°/s)	14.9	16.3	1.4	**PASS**

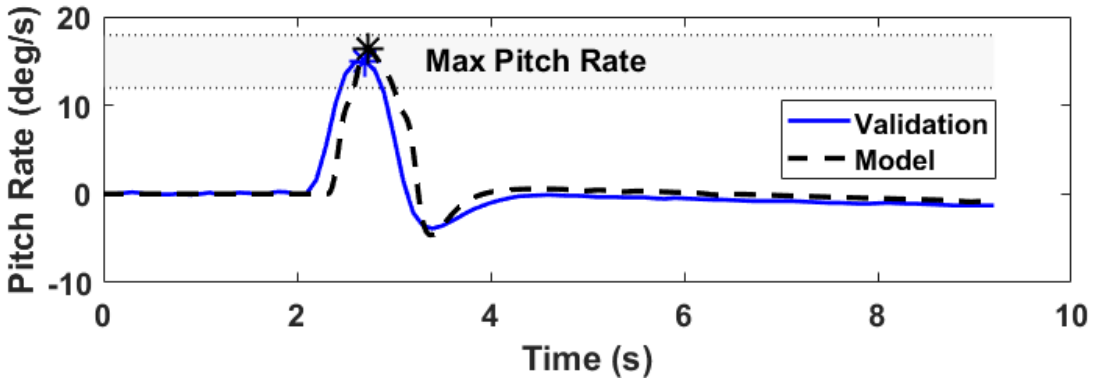

Figure C.45: Pitch rate trace for 2.b.1/2.b.4 Pitch Control / Small Control Inputs - Pitch (Takeoff Case)

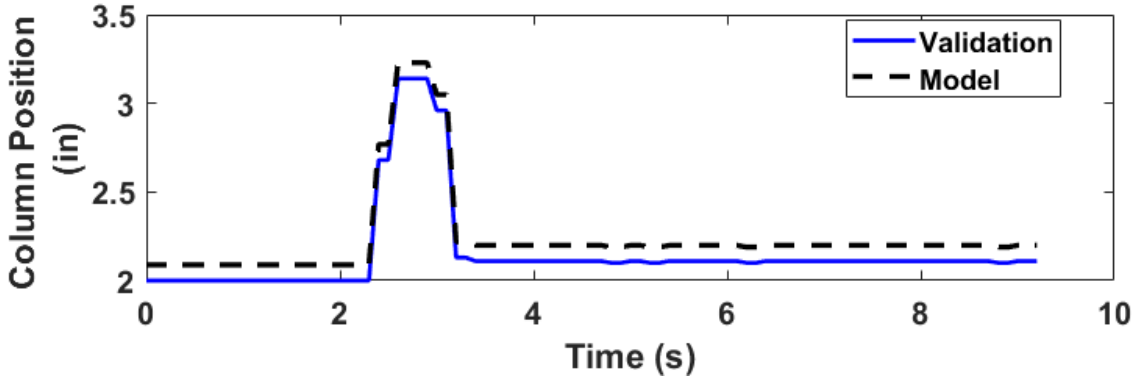

Figure C.46: Column position trace for 2.b.1/2.b.4 Pitch Control / Small Control Inputs - Pitch (Takeoff Case)

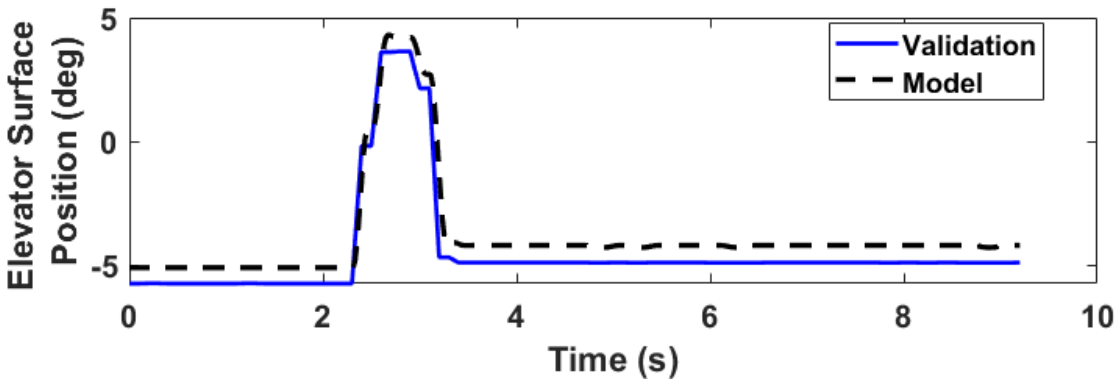

Figure C.47: Elevator surface position trace for 2.b.1/2.b.4 Pitch Control / Small Control Inputs - Pitch (Takeoff Case)

C.9 2.b.2/2.b.5 Roll Control / Small Control Inputs - Roll

Test Objective

Demonstrate that the model's dynamic roll response to wheel input accurately represents the aircraft.

Test Information

The lateral controller is displaced with an approximately one second pulse input and released. The maximum body roll rate response is compared against flight test data.

Tolerances

$\pm 0.15°$/s body roll rate or $\pm 20\%$ of peak body roll rate - *Level 7 tolerance (2.b.5)*

Flight Conditions

As available - Cruise, Takeoff, and Approach/Landing Configurations

Engineering Judgment/Comments

Control force modeling The flight simulation model does not contain a simulated control loading framework making true free response behavior, as required by the pitch control response test (2.b.2), not achievable. The test is instead executed as a prescribed pulse input to the wheel.

Hybrid Test Approach and Adoption of Level 7 Tolerance The available flight test data does not fall cleanly within the test procedures for any single FAA Part 60 objective test. The maneuver resembles a combination of the roll control response test (2.b.2) and the small control inputs test (2.b.5). The test is executed closely to the roll control response procedure, but the $\pm 20\%$ of peak body roll rate tolerance is adopted from the small control inputs test as it provides a physically meaningful metric for comparing peak dynamic response between

the model and flight test data. These tests are not required for Level 5 qualification but provide valuable characterization of the model's roll dynamic response.

Results

Cruise Case

Table C.24: Initial conditions for 2.b.2/2.b.5 Roll Control / Small Control Inputs - Roll (Cruise Case)

Parameter	**Units**	**Validation**	**Model**
Aircraft Configuration			
Weight	lbs	2400	2400
Station Center of Gravity	in	42.0	42.0
Flaps Position	deg	0	0
Flight Conditions			
Pressure Altitude	ft	5251	5251
Airspeed	KTAS	103	103
Vertical Speed	FPM	-118	-118
Aircraft Attitude			
Pitch	deg	-1.2	-0.5
Roll	deg	0.7	0.7
Heading	deg	275.6	275.6
Control Surfaces			
Elevator Position	deg	-1.4	-1.9
Aileron Position	deg	1.3	1.1
Rudder Position	deg	1.0	1.7
Cockpit Controls			
Column Position	in	2.5	2.4
Wheel Position	deg	5.4	4.8
Pedal Position	deg	20.9	20.9
Propulsion			
Throttle Position	norm	N/A	0.27

Table C.25: Results summary for 2.b.2/2.b.5 Roll Control / Small Control Inputs - Roll (Cruise Case)

Metric	Tolerance	Validation	Model	Error	Pass/ Fail
Maximum Roll Rate	±20% (4.6°/s)	23.1	23.0	-0.1	**PASS**

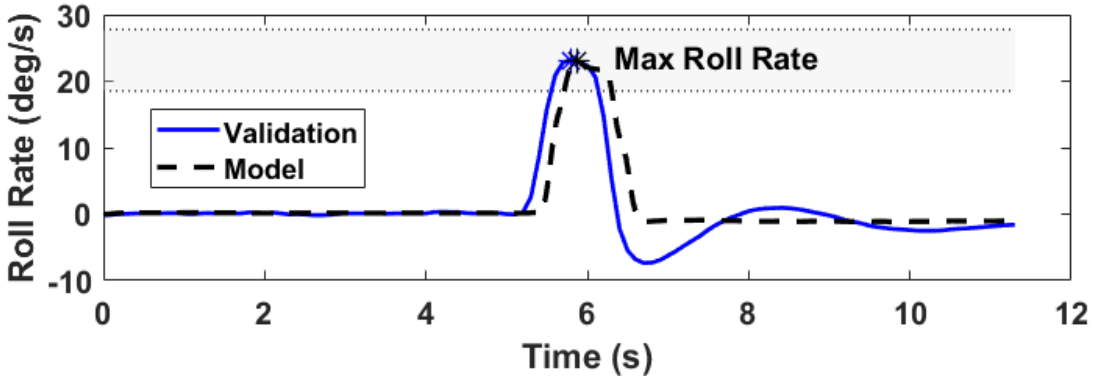

Figure C.48: Roll rate trace for 2.b.2/2.b.5 Roll Control / Small Control Inputs - Roll (Cruise Case)

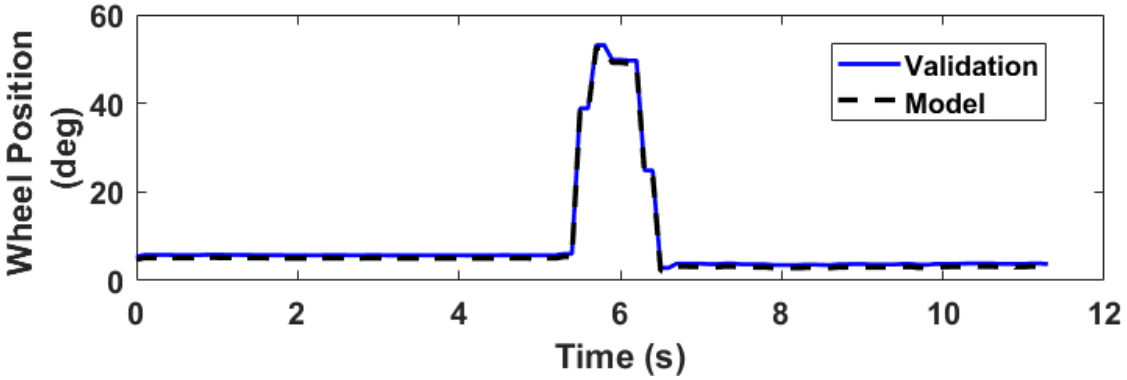

Figure C.49: Wheel position trace for 2.b.2/2.b.5 Roll Control / Small Control Inputs - Roll (Cruise Case)

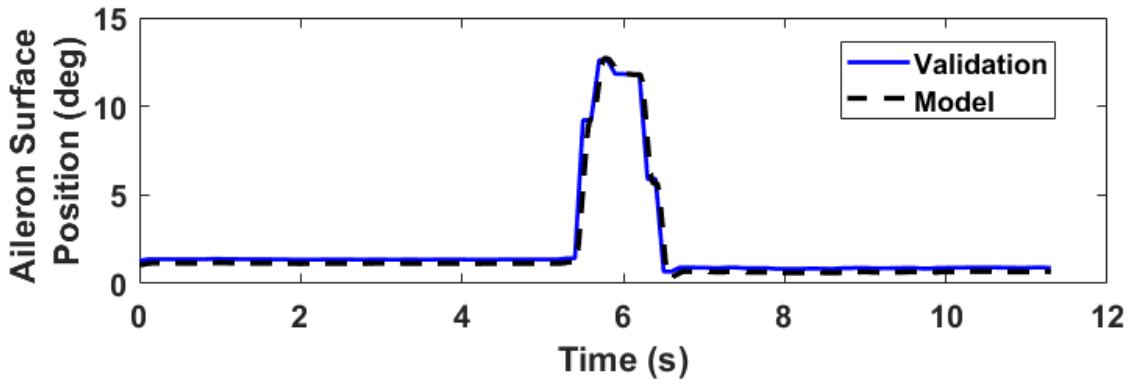

Figure C.50: Aileron surface position trace for 2.b.2/2.b.5 Roll Control / Small Control Inputs - Roll (Cruise Case)

Takeoff Case

Table C.26: Initial conditions for 2.b.2/2.b.5 Roll Control / Small Control Inputs - Roll (Takeoff Case)

Parameter	Units	Validation	Model
Aircraft Configuration			
Weight	lbs	2392	2392
Station Center of Gravity	in	42.0	42.0
Flaps Position	deg	10	10
Flight Conditions			
Pressure Altitude	ft	5745	5745
Airspeed	KTAS	102	102
Vertical Speed	FPM	-29	-29
Aircraft Attitude			
Pitch	deg	-1.5	-1.6
Roll	deg	1.0	1.0
Heading	deg	115.4	115.4
Control Surfaces			
Elevator Position	deg	-5.6	-5.7
Aileron Position	deg	1.4	1.1
Rudder Position	deg	0.9	0.9
Cockpit Controls			
Column Position	in	2.0	2.0
Wheel Position	deg	5.7	5.1
Pedal Position	deg	20.9	20.8
Propulsion			
Throttle Position	norm	N/A	0.41

Table C.27: Results summary for 2.b.2/2.b.5 Roll Control / Small Control Inputs - Roll (Takeoff Case)

Metric	Tolerance	Validation	Model	Error	Pass/ Fail
Maximum Roll Rate	±20% (4.5°/s)	22.3	21.0	-1.3	**PASS**

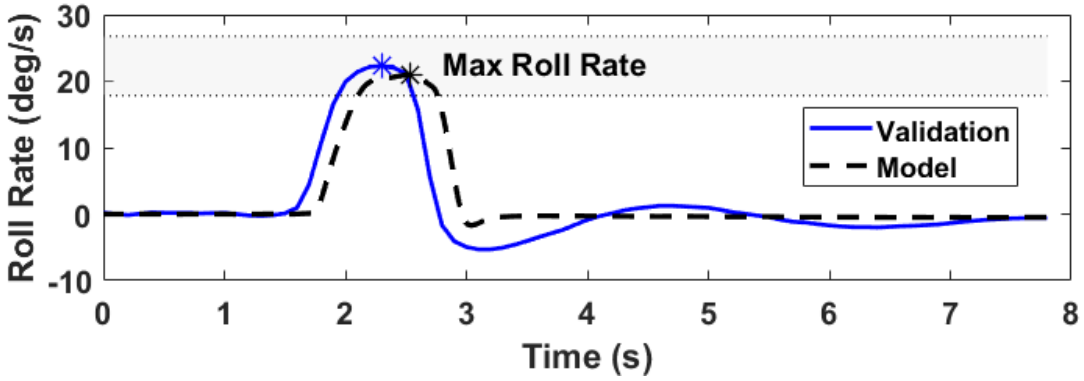

Figure C.51: Roll rate trace for 2.b.2/2.b.5 Roll Control / Small Control Inputs - Roll (Takeoff Case)

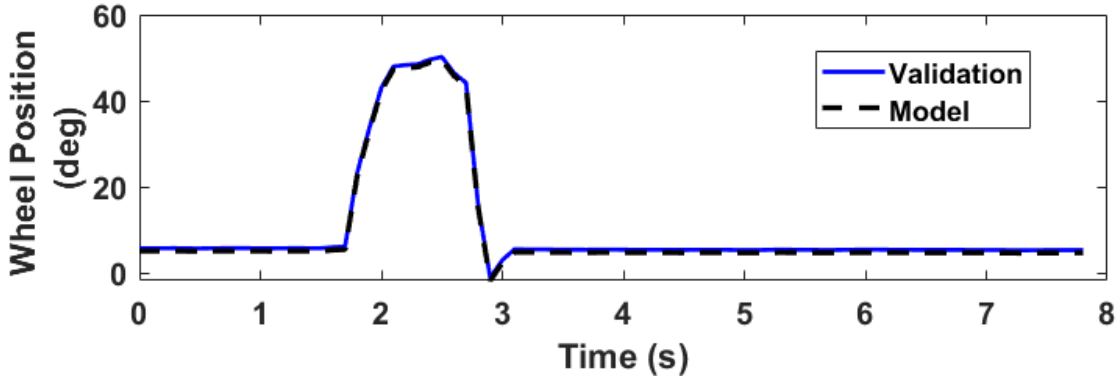

Figure C.52: Wheel position trace for 2.b.2/2.b.5 Roll Control / Small Control Inputs - Roll (Takeoff Case)

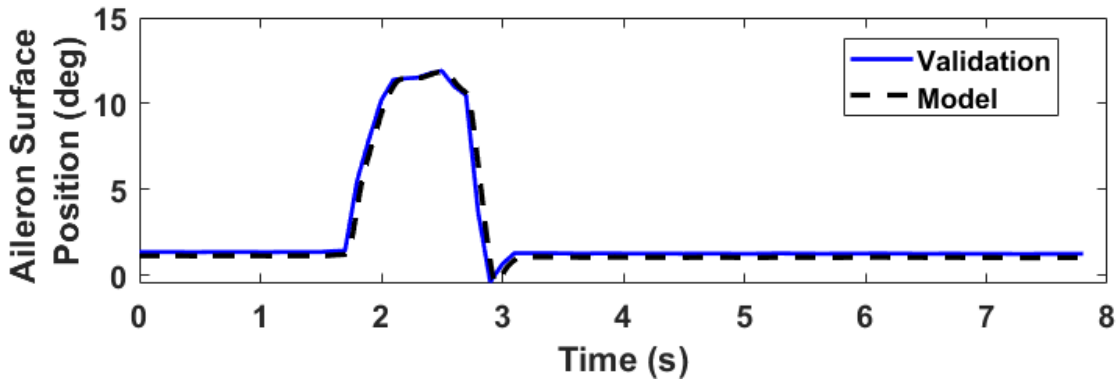

Figure C.53: Aileron surface position trace for 2.b.2/2.b.5 Roll Control / Small Control Inputs - Roll (Takeoff Case)

Approach/Landing Case

Table C.28: Initial conditions for 2.b.2/2.b.5 Roll Control / Small Control Inputs - Roll (Landing Case)

Parameter	Units	Validation	Model
Aircraft Configuration			
Weight	lbs	2389	2389
Station Center of Gravity	in	42.0	42.0
Flaps Position	deg	30	30
Flight Conditions			
Pressure Altitude	ft	5843	5843
Airspeed	KTAS	86	86
Vertical Speed	FPM	0	0
Aircraft Attitude			
Pitch	deg	-3.1	-1.5
Roll	deg	-0.1	-0.1
Heading	deg	128.0	128.0
Control Surfaces			
Elevator Position	deg	-9.9	-10.9
Aileron Position	deg	1.6	1.5
Rudder Position	deg	0.8	-0.2
Cockpit Controls			
Column Position	in	1.5	1.4
Wheel Position	deg	6.9	6.6
Pedal Position	deg	20.9	20.7
Propulsion			
Throttle Position	norm	N/A	0.76

Table C.29: Results summary for 2.b.2/2.b.5 Roll Control / Small Control Inputs - Roll (Landing Case)

Metric	Tolerance	Validation	Model	Error	Pass/ Fail
Maximum Roll Rate	±20% (5.5°/s)	27.3	23.6	-3.7	**PASS**

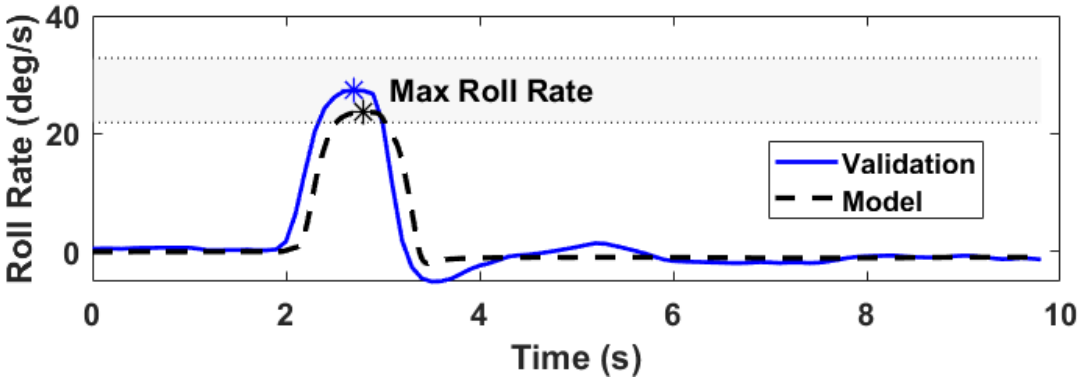

Figure C.54: Roll rate trace for 2.b.2/2.b.5 Roll Control / Small Control Inputs - Roll (Landing Case)

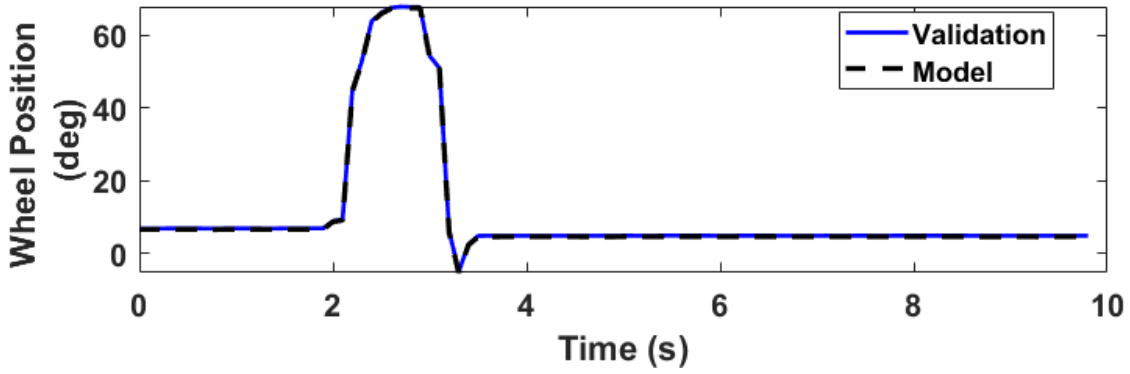

Figure C.55: Wheel position trace for 2.b.2/2.b.5 Roll Control / Small Control Inputs - Roll (Landing Case)

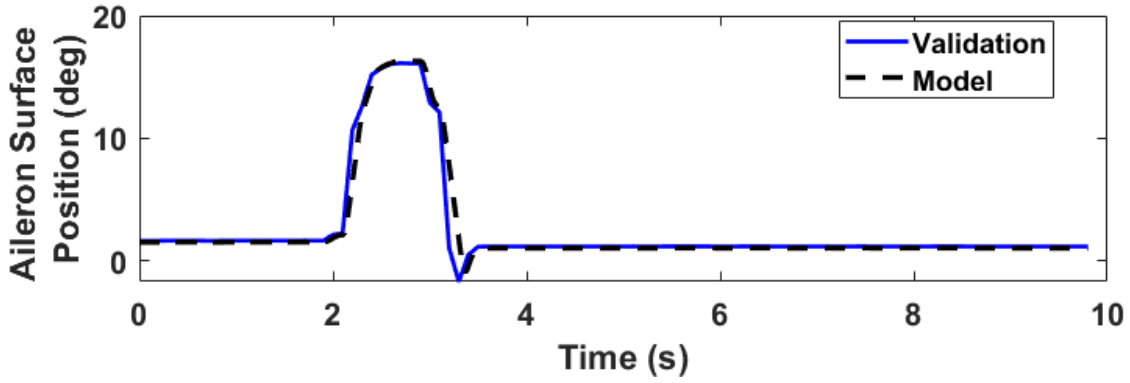

Figure C.56: Aileron surface position trace for 2.b.2/2.b.5 Roll Control / Small Control Inputs - Roll (Landing Case)

C.10 2.b.3/2.b.6 Yaw Control / Small Control Inputs - Yaw

Test Objective

Demonstrate that the model's dynamic yaw response to pedal input accurately represents the aircraft.

Test Information

The pedals are displaced with an approximately one second pulse input and released. The maximum body yaw rate response is compared against flight test data.

Tolerances

$\pm 0.15°/s$ body yaw rate or $\pm 20\%$ of peak body yaw rate - *Level 7 tolerance (2.b.6)*

Flight Conditions

As available - Cruise, Takeoff, and Approach/Landing Configurations

Engineering Judgment/Comments

Control force modeling The flight simulation model does not contain a simulated control loading framework making true free response behavior, as required by the pitch control response test (2.b.3), not achievable. The test is instead executed as a prescribed pulse input to the pedals.

Hybrid Test Approach and Adoption of Level 7 Tolerance The available flight test data does not fall cleanly within the test procedures for any single FAA Part 60 objective test. The maneuver resembles a combination of the yaw control response test (2.b.3) and the small control inputs test (2.b.6). The test is executed closely to the yaw control response procedure, but the $\pm 20\%$ of peak yaw roll rate tolerance is adopted from the small control inputs test as it provides a physically meaningful metric for comparing peak dynamic response between

the model and flight test data. These tests are not required for Level 5 qualification but provide valuable characterization of the model's yaw dynamic response.

Results

Cruise Case

Table C.30: Initial conditions for 2.b.3/2.b.6 Yaw Control / Small Control Inputs - Yaw (Cruise Case)

Parameter	**Units**	**Validation**	**Model**
Aircraft Configuration			
Weight	lbs	2397	2397
Station Center of Gravity	in	42.0	42.0
Flaps Position	deg	0	0
Flight Conditions			
Pressure Altitude	ft	5451	5451
Airspeed	KTAS	99	99
Vertical Speed	FPM	55	55
Aircraft Attitude			
Pitch	deg	1.0	1.0
Roll	deg	2.1	2.1
Heading	deg	77.2	77.2
Control Surfaces			
Elevator Position	deg	-1.0	-1.5
Aileron Position	deg	1.5	1.2
Rudder Position	deg	0.9	1.0
Cockpit Controls			
Column Position	in	2.6	2.5
Wheel Position	deg	6.2	5.4
Pedal Position	deg	20.9	20.9
Propulsion			
Throttle Position	norm	N/A	0.3

Table C.31: Results summary for 2.b.3/2.b.6 Yaw Control / Small Control Inputs - Yaw (Cruise Case)

Metric	Tolerance	Validation	Model	Error	Pass/ Fail
Maximum Yaw Rate	±20% (2.7°/s)	13.3	12.5	-0.8	**PASS**

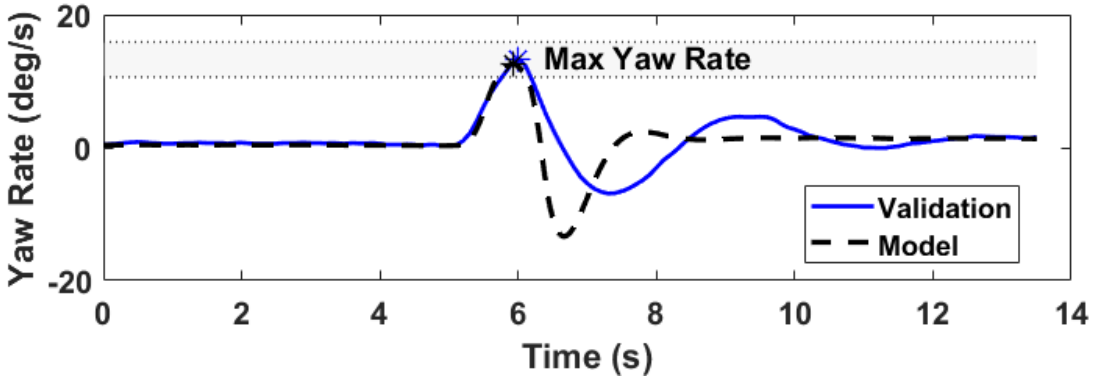

Figure C.57: Yaw rate trace for 2.b.3/2.b.6 Yaw Control / Small Control Inputs - Yaw (Cruise Case)

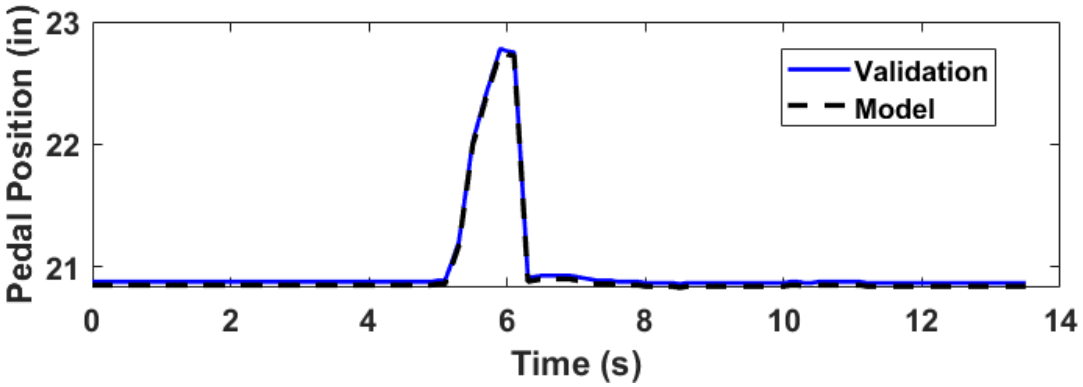

Figure C.58: Pedal position trace for 2.b.3/2.b.6 Yaw Control / Small Control Inputs - Yaw (Cruise Case)

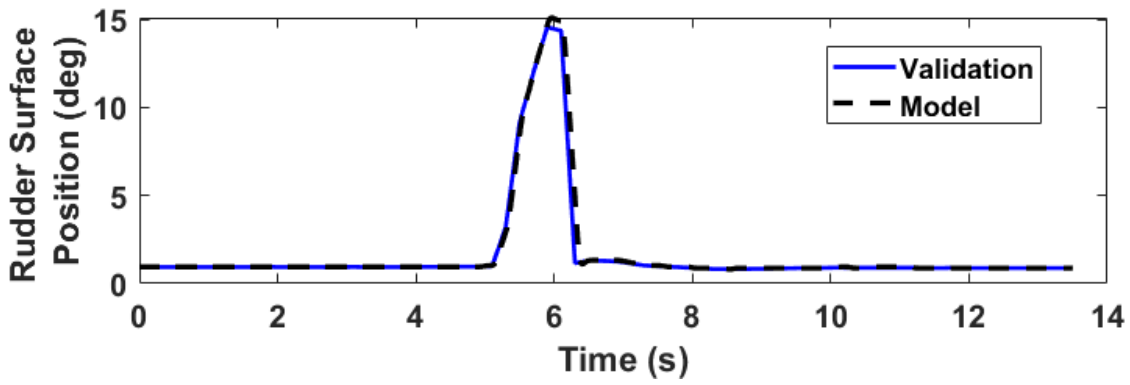

Figure C.59: Rudder surface position trace for 2.b.3/2.b.6 Yaw Control / Small Control Inputs - Yaw (Cruise Case)

Takeoff Case

Table C.32: Initial conditions for 2.b.3/2.b.6 Yaw Control / Small Control Inputs - Yaw (Takeoff Case)

Parameter	Units	Validation	Model
Aircraft Configuration			
Weight	lbs	2391	2391
Station Center of Gravity	in	42.0	42.0
Flaps Position	deg	10	10
Flight Conditions			
Pressure Altitude	ft	5782	5782
Airspeed	KTAS	102	102
Vertical Speed	FPM	169	169
Aircraft Attitude			
Pitch	deg	-2.1	-0.5
Roll	deg	-0.6	-0.6
Heading	deg	159.9	159.9
Control Surfaces			
Elevator Position	deg	-5.8	-5.7
Aileron Position	deg	1.5	1.2
Rudder Position	deg	0.8	0.4
Cockpit Controls			
Column Position	in	2.0	2.0
Wheel Position	deg	6.2	5.3
Pedal Position	deg	20.9	20.8
Propulsion			
Throttle Position	norm	N/A	0.71

Table C.33: Results summary for 2.b.3/2.b.6 Yaw Control / Small Control Inputs - Yaw (Takeoff Case)

Metric	Tolerance	Validation	Model	Error	Pass/ Fail
Maximum Yaw Rate	±20% (2.6°/s)	13.1	12.5	-0.6	**PASS**

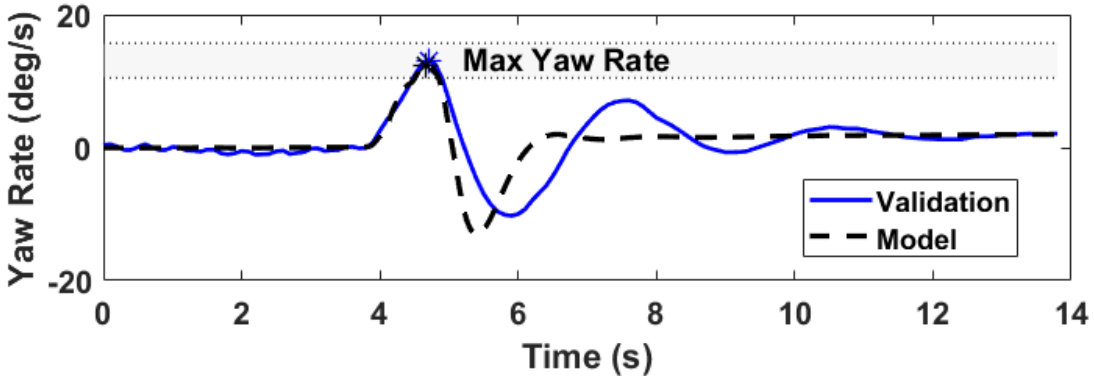

Figure C.60: Yaw rate trace for 2.b.3/2.b.6 Yaw Control / Small Control Inputs - Yaw (Takeoff Case)

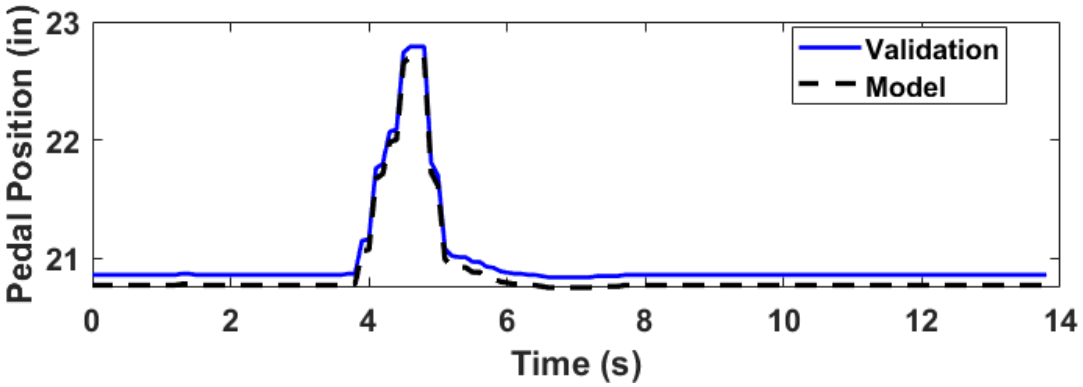

Figure C.61: Pedal position trace for 2.b.3/2.b.6 Yaw Control / Small Control Inputs - Yaw (Takeoff Case)

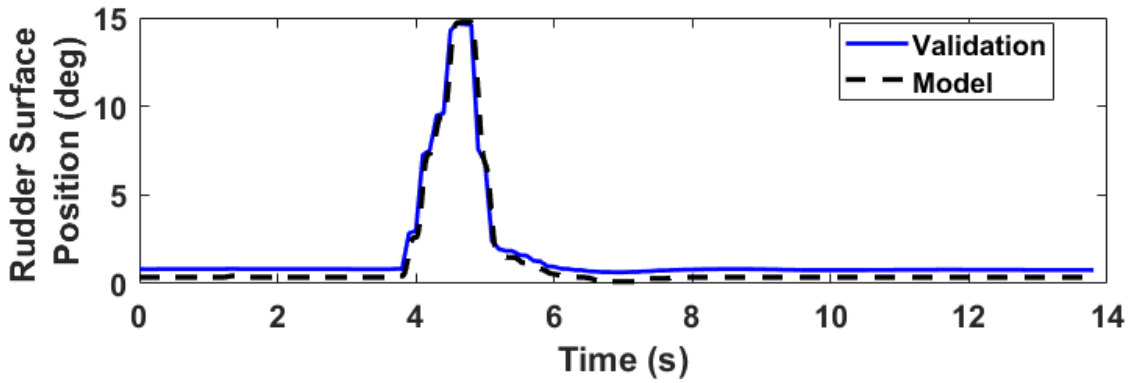

Figure C.62: Rudder surface position trace for 2.b.3/2.b.6 Yaw Control / Small Control Inputs - Yaw (Takeoff Case)

Approach/Landing Case

Table C.34: Initial conditions for 2.b.3/2.b.6 Yaw Control / Small Control Inputs - Yaw (Landing Case)

Parameter	Units	Validation	Model
Aircraft Configuration			
Weight	lbs	2390	2390
Station Center of Gravity	in	42.0	42.0
Flaps Position	deg	30	30
Flight Conditions			
Pressure Altitude	ft	5855	5855
Airspeed	KTAS	81	81
Vertical Speed	FPM	-29	-29
Aircraft Attitude			
Pitch	deg	-1.9	-0.7
Roll	deg	0.0	0.0
Heading	deg	134.9	134.9
Control Surfaces			
Elevator Position	deg	-9.8	-10.0
Aileron Position	deg	1.5	1.6
Rudder Position	deg	2.0	1.2
Cockpit Controls			
Column Position	in	1.5	1.5
Wheel Position	deg	6.3	6.8
Pedal Position	deg	21.0	20.9
Propulsion			
Throttle Position	norm	N/A	0.41

Table C.35: Results summary for 2.b.3/2.b.6 Yaw Control / Small Control Inputs - Yaw (Landing Case)

Metric	Tolerance	Validation	Model	Error	Pass/ Fail
Maximum Yaw Rate	±20% (2.4°/s)	12.0	12.8	0.8	**PASS**

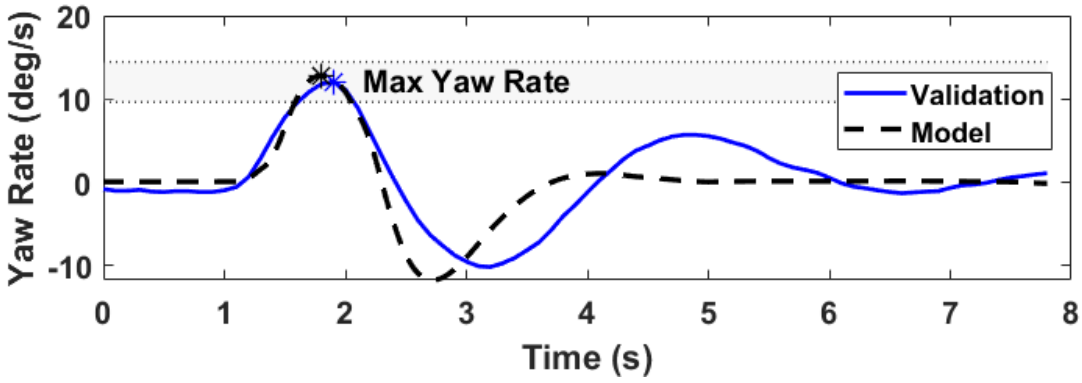

Figure C.63: Yaw rate trace for 2.b.3/2.b.6 Yaw Control / Small Control Inputs - Yaw (Landing Case)

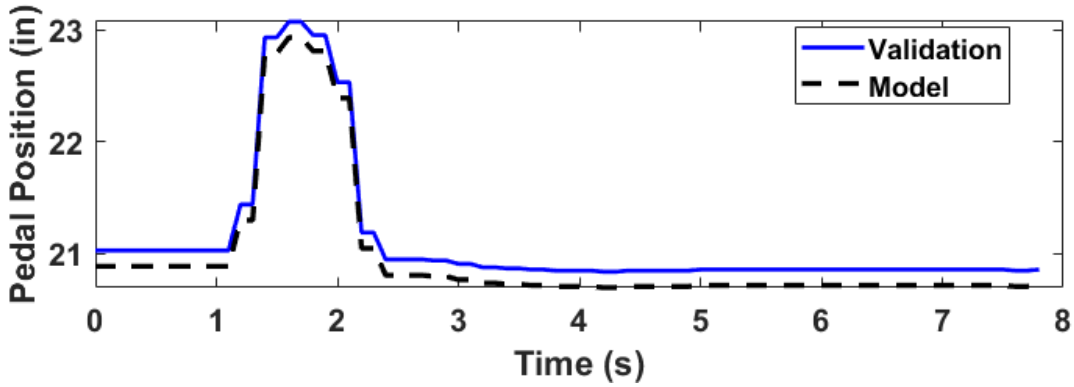

Figure C.64: Pedal position trace for 2.b.3/2.b.6 Yaw Control / Small Control Inputs - Yaw (Landing Case)

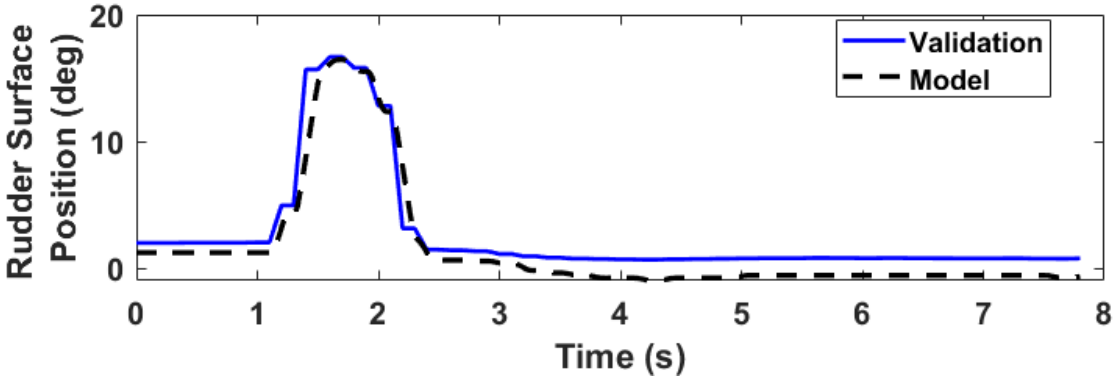

Figure C.65: Rudder surface position trace for 2.b.3/2.b.6 Yaw Control / Small Control Inputs - Yaw (Landing Case)

C.11 2.c.1.b Power Change Force

Test Objective

Demonstrate that the model's requires the same pitch controller input to maintain attitude after a rapid change of throttle.

Test Information

After trimming aircraft with a power setting close to idle, rapidly advance throttles while applying column input necessary to maintain original flight conditions (airspeed or altitude).

Tolerances

±5 lb or ±20% pitch control force *(N/A, see engineering judgment)*
Adopted tolerance: Correct trend and magnitude

Flight Conditions

Approach *(No usable approach cases are available therefore a cruise configuration case is presented.)*

Engineering Judgment/Comments

Control force modeling The flight simulation model does not contain a simulated control loading framework making force-based tolerances on 2.c.1.b non-applicable. The pitch control force required to maintain trimmed airspeed following a power change cannot be assessed.

Throttle Position Throttle position is recorded in the flight test data but as noted in the general limitations, propulsion system data reliability is a known gap in the available flight test package. The throttle trace presented in the validation data reflects the pilot's physical throttle lever position during the maneuver and is included for reference only. The

simulation throttle is driven to reflect the correct magnitude of change — advancing from approach power to full throttle — consistent with the intent of the test, but exact throttle position values are not expected to match the recorded flight test data due to its documented unreliability. The resulting RPM and altitude traces provide a more reliable indication of the propulsive state of the aircraft during the maneuver.

Elevator Response Magnitude The calibrated model correctly reproduces the direction of elevator response to a power increase — deflecting nose-down to oppose the pitch-up tendency, consistent with expected aircraft behavior. However, the magnitude of the elevator deflection is underpredicted relative to flight test data. *This discrepancy is most likely attributable to a combination of: (1) the lack of slipstream modeling, (2) lack of calibration effort on engine forces and moments during the time-domain stage (due to data constraints) and/or (3) a manifestation of the lumped wing pitching moment step correction.* **This is a known limitation of the current modeling framework.**

Adopted Tolerances The prescribed ±5 lb or ±20% pitch control force can not be assessed in the absence of a control loading model and instead the comparison to this test is assessed by the elevator deflection required to hold trimmed altitude after throttle advancement. The elevator deflection tolerance is applied as a correct trend and magnitude check instead of a numerical tolerance per Level 5 FTD requirements.

Propeller Speed As noted in the general limitations, propeller speed data should be treated with skepticism due to noise in the recording system. Despite this, the general trend and averaged values of the validation RPM trace are consistent with the simulated propeller speed response, providing a reasonable indication that the power setting achieved during the maneuver is broadly representative of the intended full throttle condition. Exact point-to-point comparison of RPM values is not appropriate given the data quality.

Results

Table C.36: Initial conditions for 2.c.1.b Power Change Force

Parameter	**Units**	**Validation**	**Model**
Aircraft Configuration			
Weight	lbs	2431	2431
Station Center of Gravity	in	42.1	42.1
Flaps Position	deg	0	0
Flight Conditions			
Pressure Altitude	ft	4968	4968
Airspeed	KTAS	92	92
Vertical Speed	FPM	-127	-127
Aircraft Attitude			
Pitch	deg	1.1	0.9
Roll	deg	0.8	0.8
Heading	deg	98.1	98.1
Control Surfaces			
Elevator Position	deg	-0.1	-0.7
Aileron Position	deg	1.3	1.1
Rudder Position	deg	2.3	3.7
Cockpit Controls			
Column Position	in	2.7	2.6
Wheel Position	deg	5.5	4.6
Pedal Position	deg	21.1	21.2
Propulsion			
Throttle Position	norm	N/A	0.22

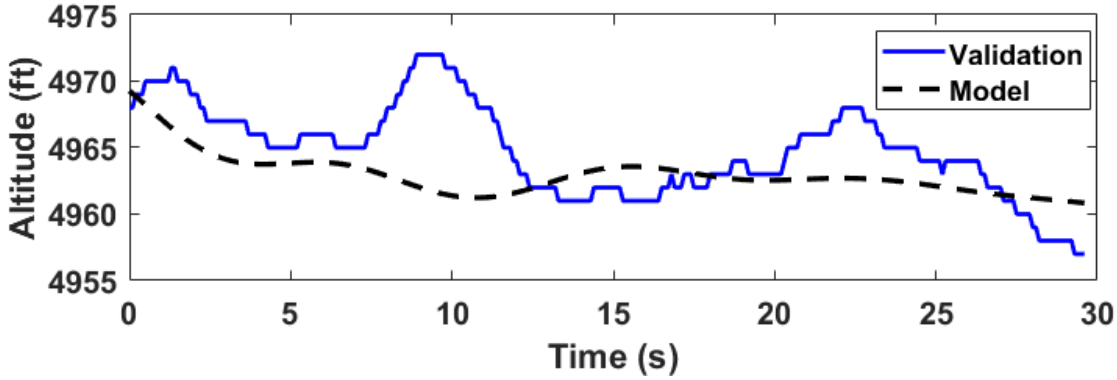

Figure C.66: Altitude trace for 2.c.1.b Power Change Force

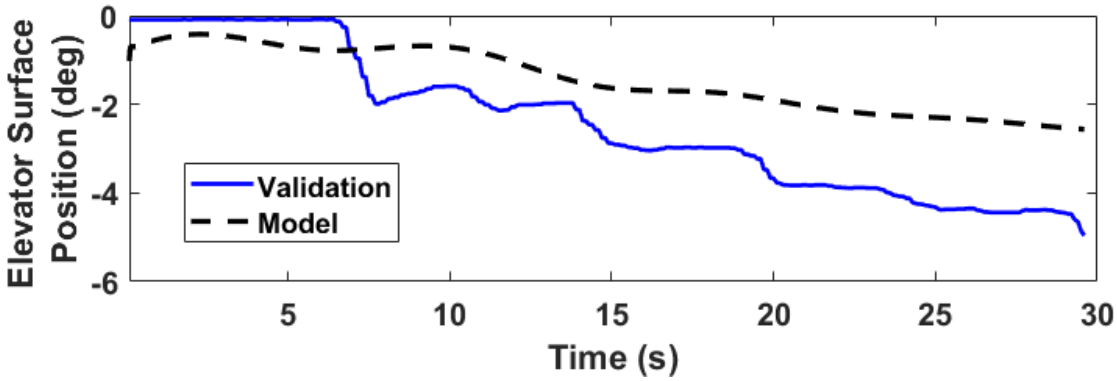

Figure C.67: Elevator surface position trace for 2.c.1.b Power Change Force

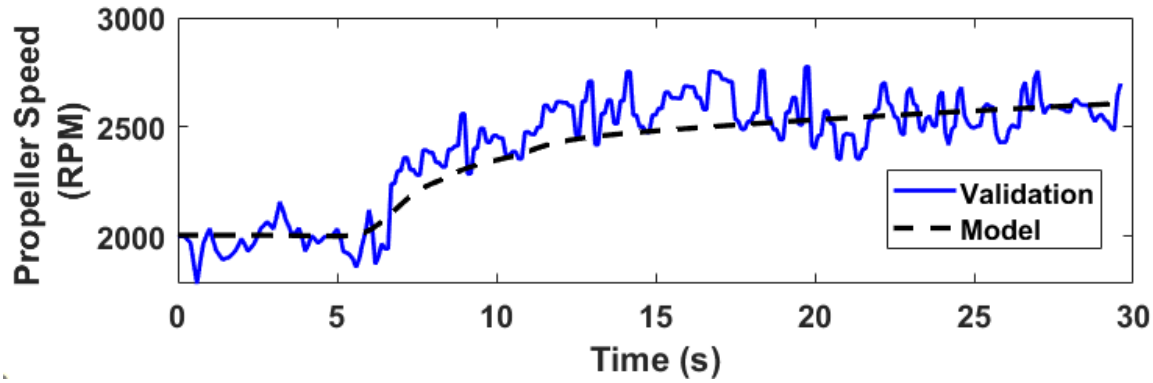

Figure C.68: Propeller speed trace for 2.c.1.b Power Change Force

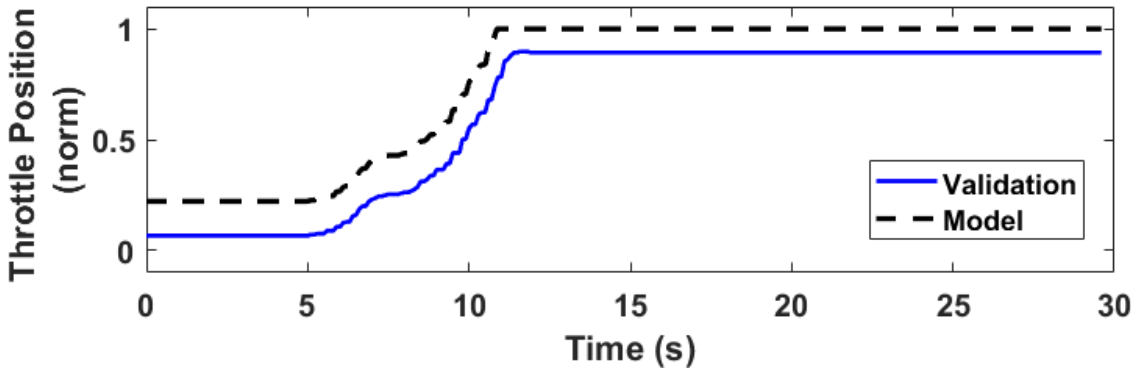

Figure C.69: Throttle position trace for 2.c.1.b Power Change Force

C.12 2.c.1.a/b Flap Change Dynamics/Force

Test Objective

Demonstrate that the model exhibits the same response to flap extension or retraction as the aircraft.

Test Information

After trimming the aircraft at a specified flap position extend or retract the flaps. Record the initial pitch response to the flap change.

Tolerances

±5 lb or ±20% pitch control force *(N/A, see engineering judgment)*
Adopted tolerance: Correct trend and magnitude *(see engineering judgment)*

Flight Conditions

Takeoff through initial flap retraction and approach to landing

Engineering Judgment/Comments

Control force modeling The flight simulation model does not contain a simulated control loading framework making force-based tolerances on 2.c.1.b non-applicable. The pitch control force required to maintain trimmed airspeed following a flap change change cannot be assessed.

Flight test data availability No usable flight test data is available for this test as no flap position data is recorded over the time-domain and is only reported at initial conditions of the test. The extension and retraction profile is not able to be reproduced due to this limitation.

CT&M adopted tolerances

Trend-Only Evaluation The flight simulation model does not contain a simulated control loading framework making true free response behavior not achievable, and no reliable flight test data is available for this maneuver. Representative test cases have been set up to demonstrate that the model exhibits the correct pitch response trend to both flap extension and retraction. A nose-up pitch response to flap retraction and a nose-down response to flap extension are the expected trends consistent with the aerodynamic effect of flap deployment on the pitching moment balance. The test is set up in accordance with the FTD Level 6 2.c.2.a - Flap Change Dynamics procedure.

Results

Flap Extension Case - Approach to Landing

Expected response: initial nose-up pitch tendency following flap extension.

Table C.37: Initial conditions for 2.c.2.a/b Flap Change Dynamics/Force (Extension)

Parameter	**Units**	**Validation**	**Model**
Aircraft Configuration			
Weight	lbs	N/A	2550
Station Center of Gravity	in	N/A	42.0
Flaps Position	deg	N/A	0
Flight Conditions			
Pressure Altitude	ft	N/A	3000
Airspeed	KTAS	N/A	75
Vertical Speed	FPM	N/A	0

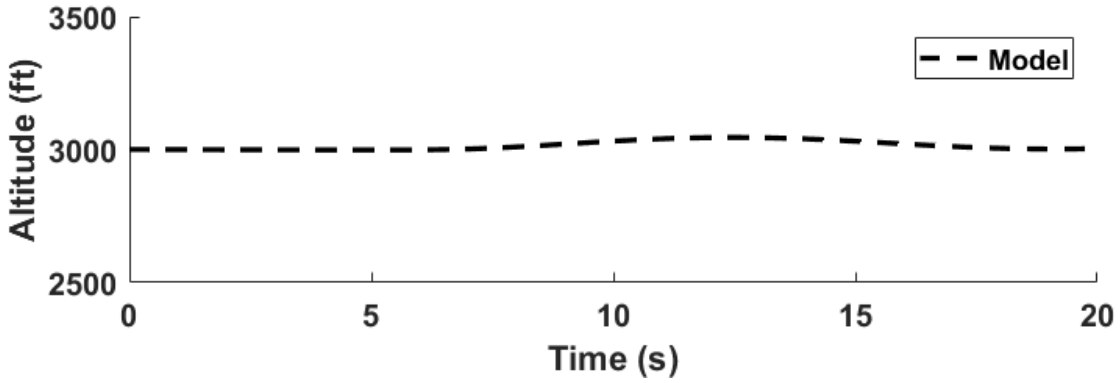

Figure C.70: Altitude trace for 2.c.2.a/b Flap Change Dynamics/Force (Extension)

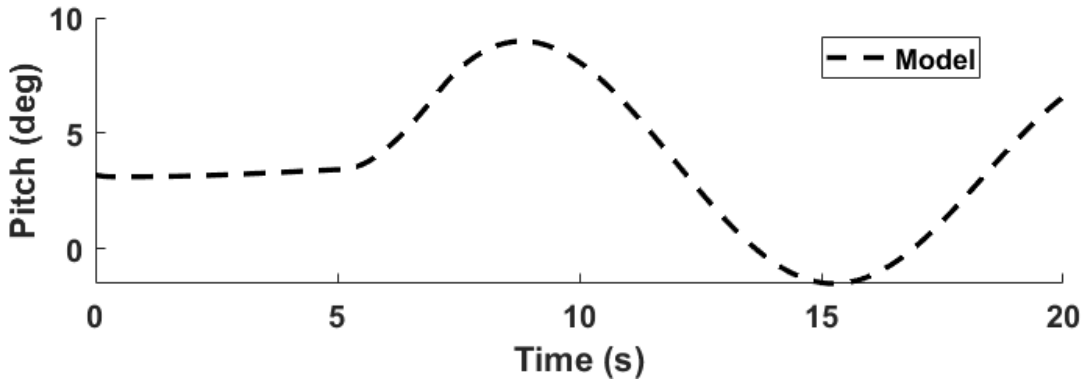

Figure C.71: Pitch trace for 2.c.2.a/b Flap Change Dynamics/Force (Extension)

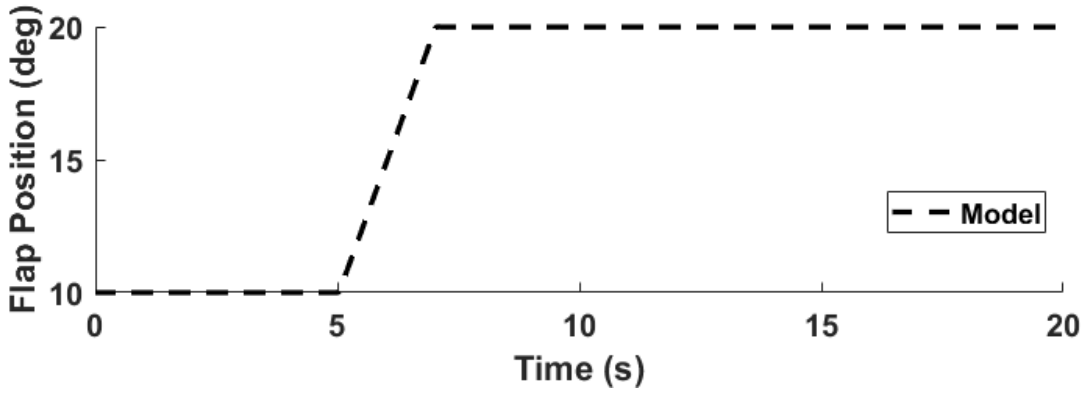

Figure C.72: Flaps position trace for 2.c.2.a/b Flap Change Dynamics/Force (Extension)

Summary: PASS – The model shows a pitch up moment following flap extension.

Flap Extension Case - Takeoff through initial flap retraction

Expected response: initial nose-down pitch tendency following flap retraction.

Table C.38: Initial conditions for 2.c.2.a/b Flap Change Dynamics/Force (Retraction)

Parameter	**Units**	**Validation**	**Model**
Aircraft Configuration			
Weight	lbs	N/A	2550
Station Center of Gravity	in	N/A	42.0
Flaps Position	deg	N/A	10
Flight Conditions			
Pressure Altitude	ft	N/A	3000
Airspeed	KTAS	N/A	75
Vertical Speed	FPM	N/A	0

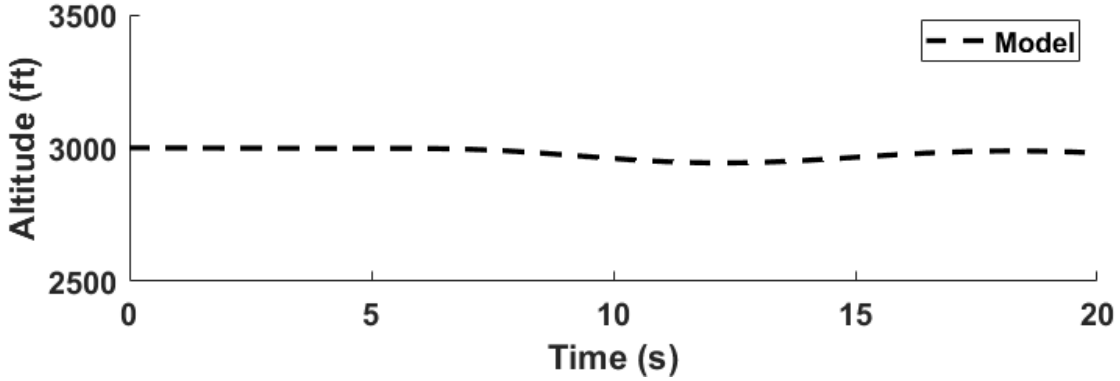

Figure C.73: Altitude trace for 2.c.2.a/b Flap Change Dynamics/Force (Retraction)

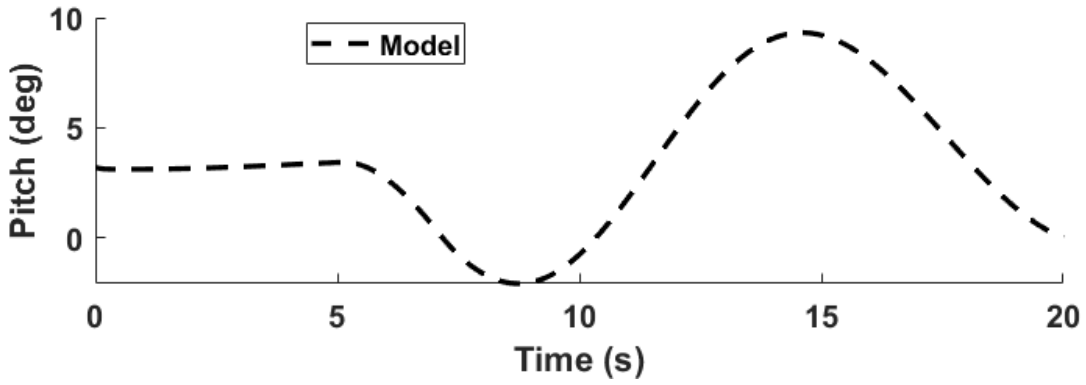

Figure C.74: Pitch trace for 2.c.2.a/b Flap Change Dynamics/Force (Retraction)

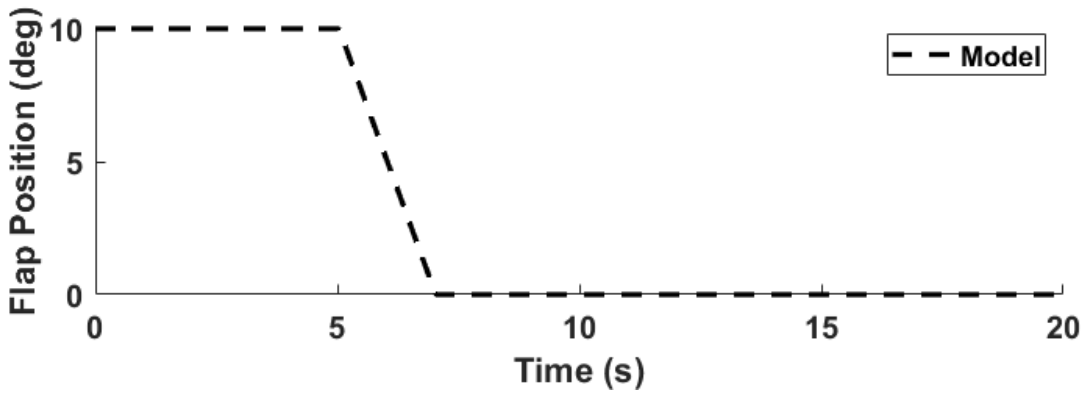

Figure C.75: Flaps position trace for 2.c.2.a/b Flap Change Dynamics/Force (Retraction)

Summary: PASS – The model shows a pitch down moment following flap retraction.

C.13 2.c.1.b Gear Change Force

The Cessna 172 Skyhawk does not have retractable gear, therefore this Level 5 FTD test is not applicable.

C.14 2.c.5 Longitudinal Trim

Test Objective

Demonstrate that the model's lift, drag, and thrust relationships and longitudinal trim characteristics accurately represents the aircraft.

Test Information

Establish steady-state trim with thrust for target airspeed. A series of snapshots may be presented.

Tolerances

$\pm 1^\circ$ elevator angle

$\pm 0.5^\circ$ trim surface angle *(N/A, refer to engineering judgment)*

$\pm 1^\circ$ pitch angle

$\pm 5\%$ of net thrust or equivalent *(see engineering judgment comments)*

Flight Conditions

Cruise, Approach, and Landing

Engineering Judgment/Comments

Pitch trim control surface The pitch trim tab is not modeled in the flight simulation framework. This simplification is made on the basis that the trim tab functions primarily to alleviate hinge moments for pilot control force trimming and does not produce aerodynamic forces of sufficient magnitude to meaningfully affect the trimmed flight condition. The trim tab surface area is approximately 11 times smaller than the elevator, making its aerodynamic contribution negligible relative to the elevator's trimming authority. The trim surface angle tolerance is therefore not applicable.

Propulsion Tolerance The ±5% net thrust tolerance cannot be directly assessed as thrust is not recorded in the flight test data. For the clean configuration trim case, percent power has been interpolated from the POH cruise performance tables at the corresponding flight conditions and is presented alongside the model predictions with the ±5% power tolerance applied. Propeller speed is also included from table interpolation for additional context. For flaps-down trim cases, no equivalent performance chart data is available and this tolerance is not applied.

Results

Clean Configuration Case

Table C.39: Initial conditions for 2.c.5 Longitudinal Trim (Clean Configuration Case)

Parameter	**Units**	**Validation**	**Model**
Aircraft Configuration			
Weight	lbs	2391	2391
Station Center of Gravity	in	42.0	42.0
Flaps Position	deg	0	0
Flight Conditions			
Pressure Altitude	ft	2998	2998
Airspeed	KTAS	123	123
Vertical Speed	FPM	-2	-2
Aircraft Attitude			
Pitch	deg	-2.2	-1.8
Roll	deg	1.6	1.6
Heading	deg	99.0	99.0
Control Surfaces			
Elevator Position	deg	-3.9	-3.4
Aileron Position	deg	1.3	0.9
Rudder Position	deg	1.0	0.7
Cockpit Controls			
Column Position	in	2.2	2.3
Wheel Position	deg	5.3	4.2
Pedal Position	deg	20.9	20.8
Propulsion			
Throttle Position	norm	N/A	0.63
Propeller Speed	RPM	N/A	2668

Table C.40: Averaged results for 2.c.5 Longitudinal Trim (Clean Configuration Case)

Metric	Tolerance	Validation (Average)	Model (Average)	Error	Pass/ Fail
Elevator Angle	±1°	-3.9	-3.4	0.5	**PASS**
Pitch	±1°	-2.2	-1.7	0.5	**PASS**
Percent Power	±5% Power	82%	81%	-1%	**PASS**
RPM	N/A	2650	2668	18	N/A

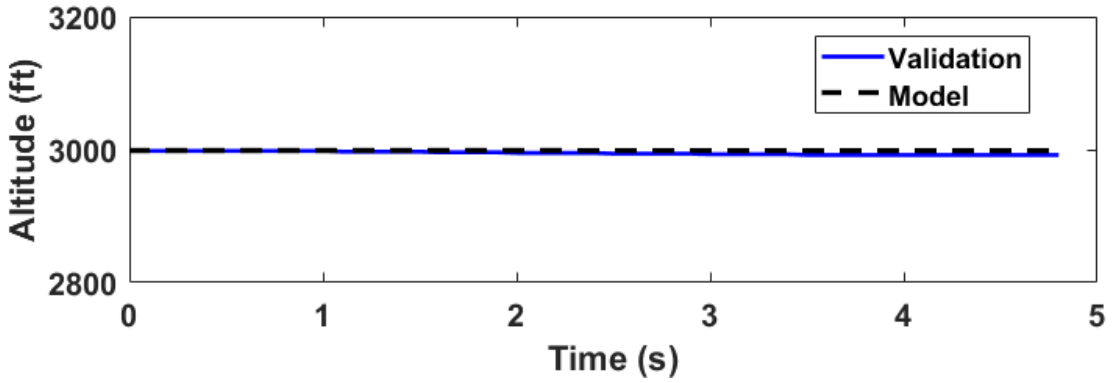

Figure C.76: Altitude trace for 2.c.5 Longitudinal Trim (Clean Configuration Case)

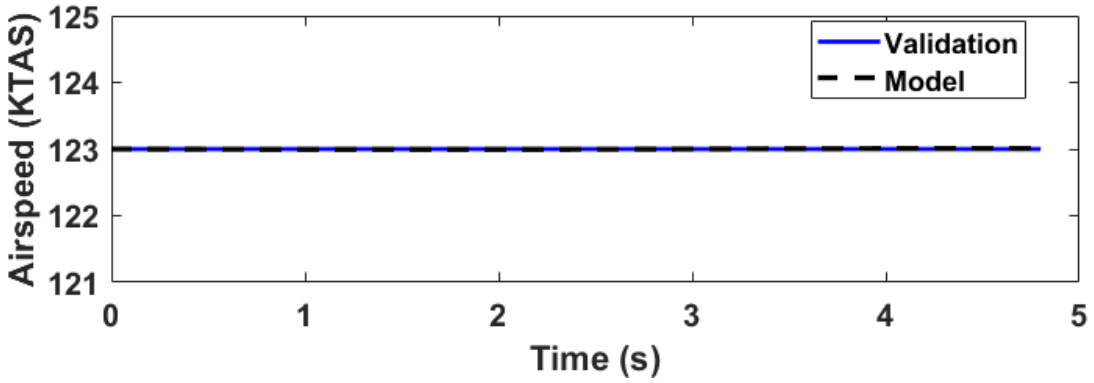

Figure C.77: Airspeed trace for 2.c.5 Longitudinal Trim (Clean Configuration Case)

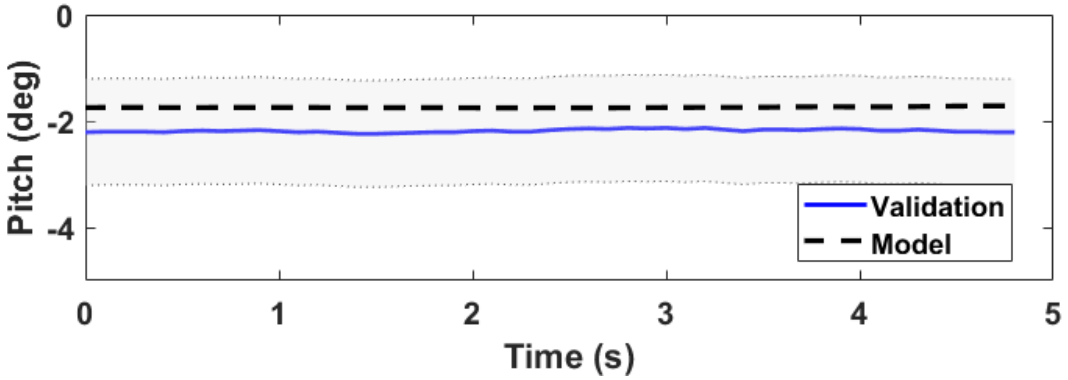

Figure C.78: Pitch trace for 2.c.5 Longitudinal Trim (Clean Configuration Case)

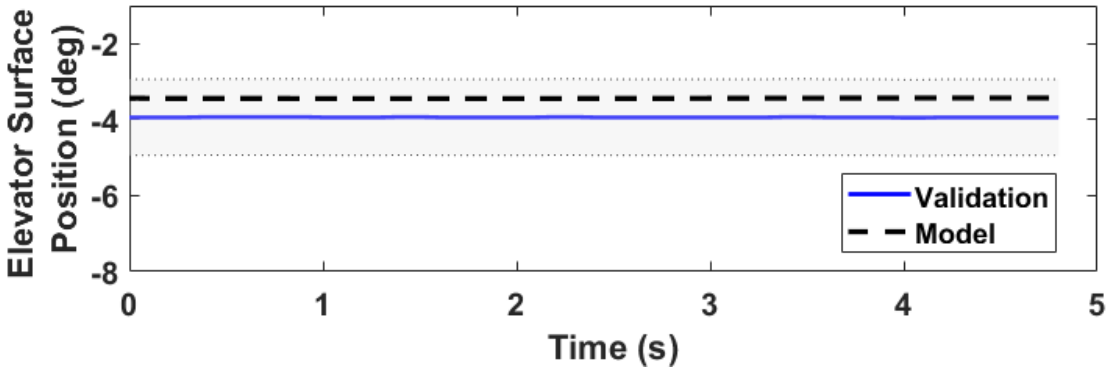

Figure C.79: Elevator surface position trace for 2.c.5 Longitudinal Trim (Clean Configuration Case)

Takeoff Configuration Case

Table C.41: Initial conditions for 2.c.5 Longitudinal Trim (Takeoff Configuration Case)

Parameter	Units	Validation	Model
Aircraft Configuration			
Weight	lbs	2375	2375
Station Center of Gravity	in	42.0	42.0
Flaps Position	deg	10	10
Flight Conditions			
Pressure Altitude	ft	3007	3007
Airspeed	KTAS	111	111
Vertical Speed	FPM	0	0
Aircraft Attitude			
Pitch	deg	-3.5	-2.8
Roll	deg	1.1	1.1
Heading	deg	324.6	324.6
Control Surfaces			
Elevator Position	deg	-6.6	-6.7
Aileron Position	deg	1.5	1.1
Rudder Position	deg	1.1	0.4
Cockpit Controls			
Column Position	in	1.9	1.9
Wheel Position	deg	6.2	4.7
Pedal Position	deg	20.9	20.8
Propulsion			
Throttle Position	norm	N/A	0.77
Propeller Speed	RPM	N/A	2553

Table C.42: Averaged results for 2.c.5 Longitudinal Trim (Takeoff Configuration Case)

Metric	Tolerance	Validation (Average)	Model (Average)	Error	Pass/ Fail
Elevator Angle	±1°	-6.6	-6.7	-0.1	**PASS**
Pitch	±1°	-3.3	-2.7	0.6	**PASS**

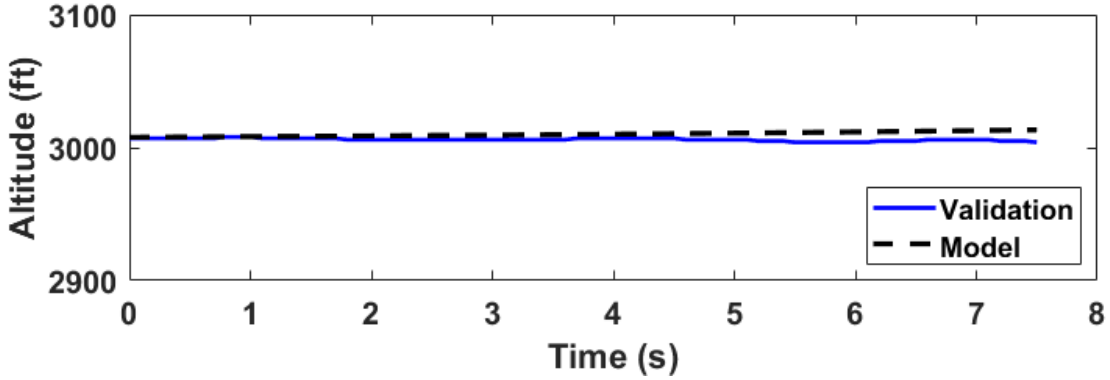

Figure C.80: Altitude trace for 2.c.5 Longitudinal Trim (Takeoff Configuration Case)

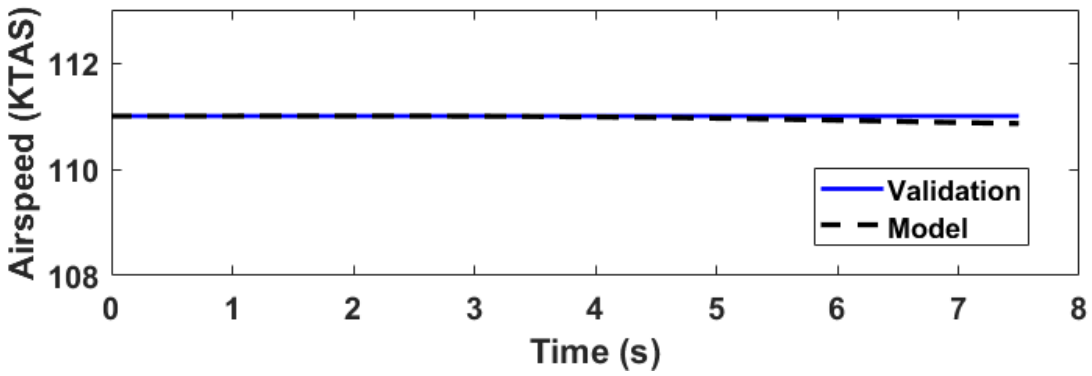

Figure C.81: Airspeed trace for 2.c.5 Longitudinal Trim (Takeoff Configuration Case)

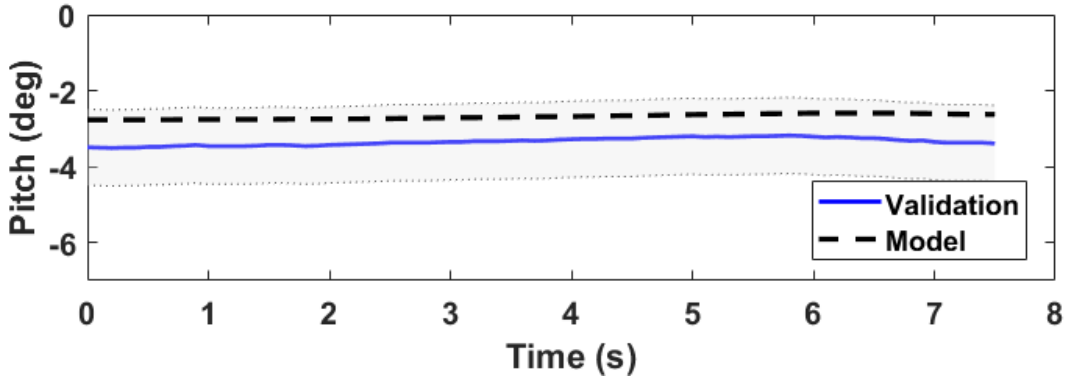

Figure C.82: Pitch trace for 2.c.5 Longitudinal Trim (Takeoff Configuration Case)

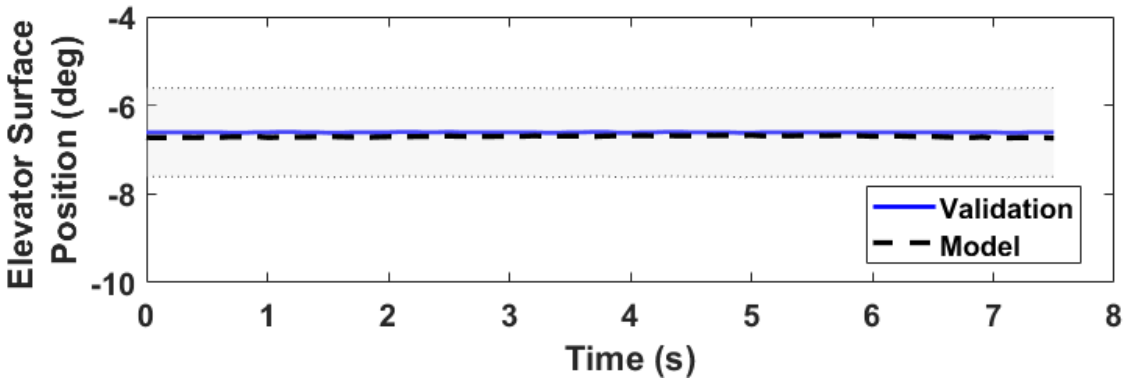

Figure C.83: Elevator surface position trace for 2.c.5 Longitudinal Trim (Takeoff Configuration Case)

Approach/Landing Configuration Case 1

Table C.43: Initial conditions for 2.c.5 Longitudinal Trim (Approach/Landing Configuration Case 1)

Parameter	**Units**	**Validation**	**Model**
Aircraft Configuration			
Weight	lbs	2356	2356
Station Center of Gravity	in	41.9	41.9
Flaps Position	deg	20	20
Flight Conditions			
Pressure Altitude	ft	2900	2900
Airspeed	KTAS	96	96
Vertical Speed	FPM	-118	-118
Aircraft Attitude			
Pitch	deg	-3.9	-3.5
Roll	deg	0.1	0.1
Heading	deg	242.4	242.4
Control Surfaces			
Elevator Position	deg	-8.6	-9.3
Aileron Position	deg	1.4	1.2
Rudder Position	deg	1.1	0.5
Cockpit Controls			
Column Position	in	1.6	1.6
Wheel Position	deg	6.1	5.4
Pedal Position	deg	20.9	20.8
Propulsion			
Throttle Position	norm	N/A	0.43
Propeller Speed	RPM	N/A	2323

Table C.44: Averaged results for 2.c.5 Longitudinal Trim (Approach/Landing Configuration Case 1)

Metric	Tolerance	Validation (Average)	Model (Average)	Error	Pass/ Fail
Elevator Angle	±1°	-8.7	-9.3	-0.6	**PASS**
Pitch	±1°	-4.1	-3.5	0.6	**PASS**

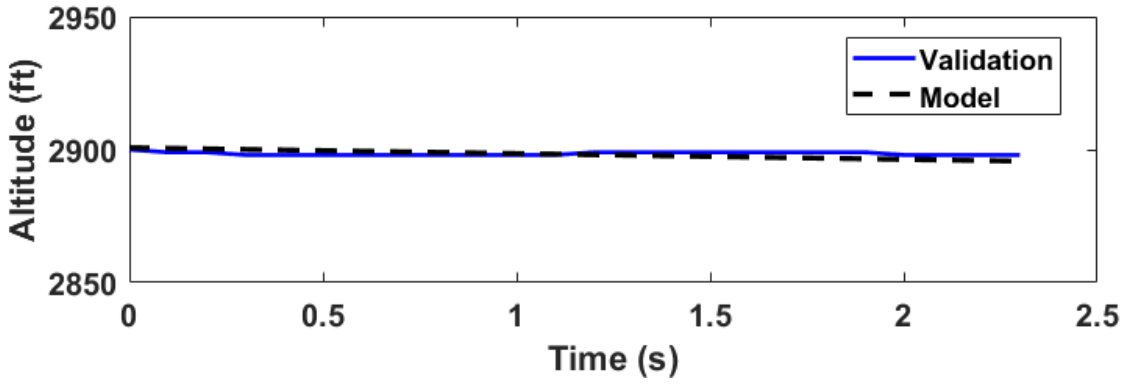

Figure C.84: Altitude trace for 2.c.5 Longitudinal Trim (Approach/Landing Configuration Case 1)

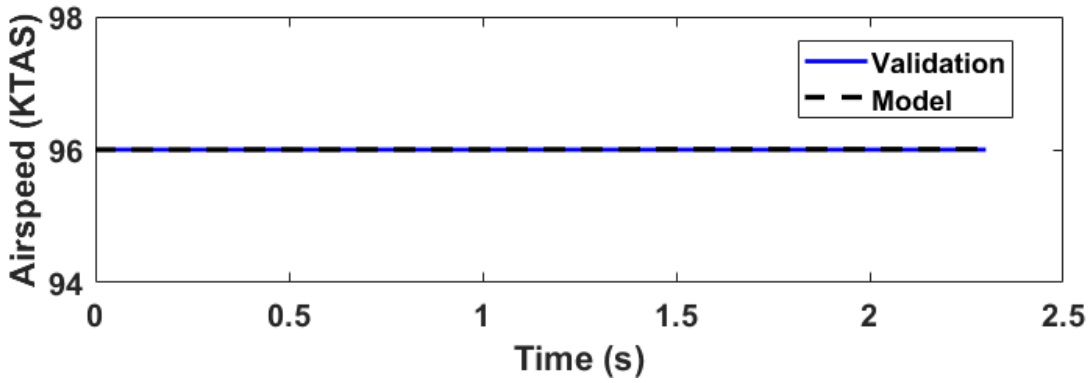

Figure C.85: Airspeed trace for 2.c.5 Longitudinal Trim (Approach/Landing Configuration Case 1)

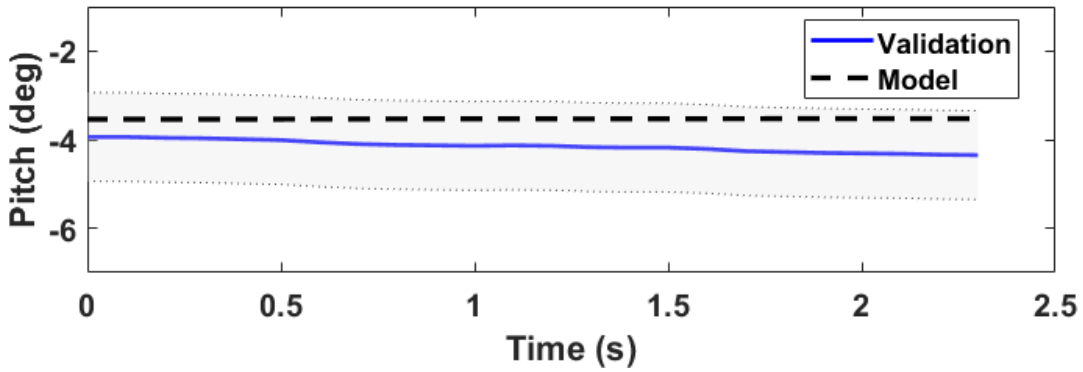

Figure C.86: Pitch trace for 2.c.5 Longitudinal Trim (Approach/Landing Configuration Case 1)

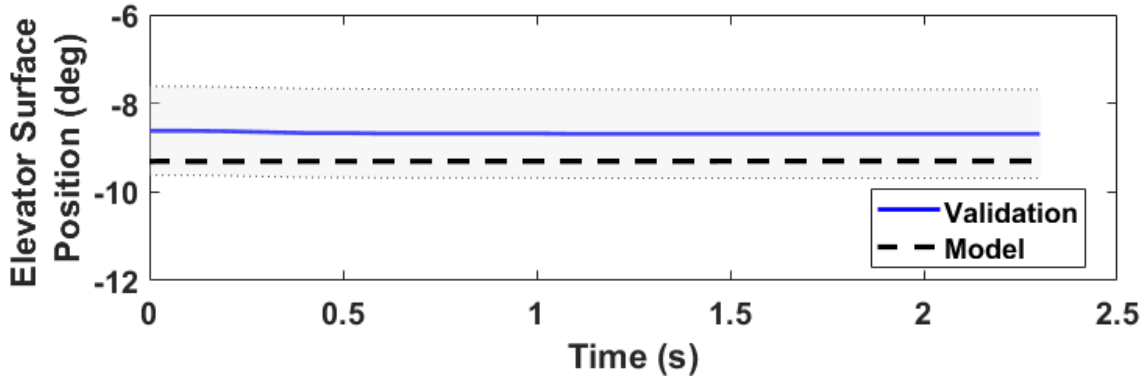

Figure C.87: Elevator surface position trace for 2.c.5 Longitudinal Trim (Approach/Landing Configuration Case 1)

Approach/Landing Configuration Case 2

Table C.45: Initial conditions for 2.c.5 Longitudinal Trim (Approach/Landing Configuration Case 2)

Parameter	Units	Validation	Model
Aircraft Configuration			
Weight	lbs	2352	2352
Station Center of Gravity	in	41.9	41.9
Flaps Position	deg	30	30
Flight Conditions			
Pressure Altitude	ft	2998	2998
Airspeed	KTAS	74	74
Vertical Speed	FPM	-115	-115
Aircraft Attitude			
Pitch	deg	-1.2	-0.6
Roll	deg	2.2	2.2
Heading	deg	138.7	138.9
Control Surfaces			
Elevator Position	deg	-9.0	-9.3
Aileron Position	deg	1.5	1.8
Rudder Position	deg	1.6	1.2
Cockpit Controls			
Column Position	in	1.6	1.6
Wheel Position	deg	6.3	7.6
Pedal Position	deg	21.0	20.9
Propulsion			
Throttle Position	norm	N/A	0.27
Propeller Speed	RPM	N/A	1963

Table C.46: Averaged results for 2.c.5 Longitudinal Trim (Approach/Landing Configuration Case 2)

Metric	Tolerance	Validation (Average)	Model (Average)	Error	Pass/ Fail
Elevator Angle	±1°	-9.0	-9.3	-0.3	**PASS**
Pitch	±1°	-1.0	-0.6	0.4	**PASS**

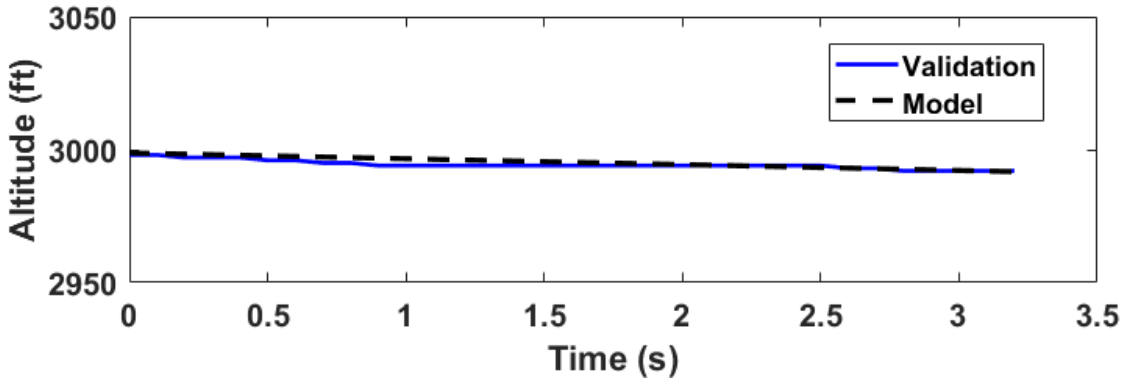

Figure C.88: Altitude trace for 2.c.5 Longitudinal Trim (Approach/Landing Configuration Case 2)

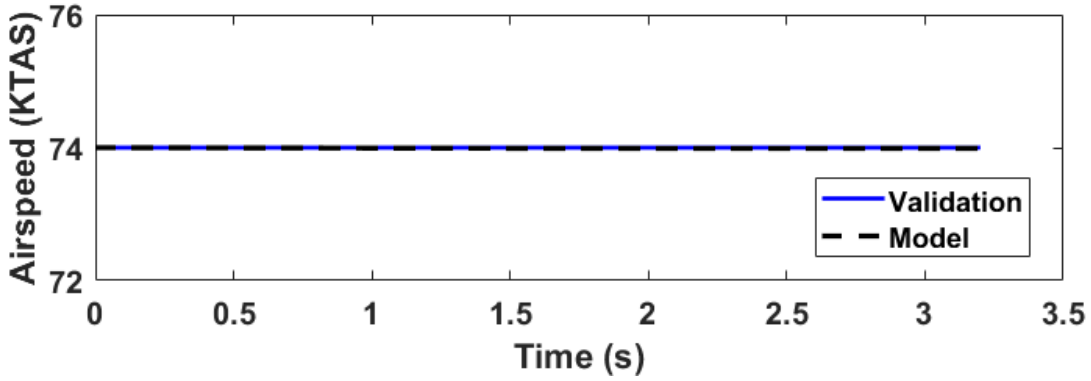

Figure C.89: Airspeed trace for 2.c.5 Longitudinal Trim (Approach/Landing Configuration Case 2)

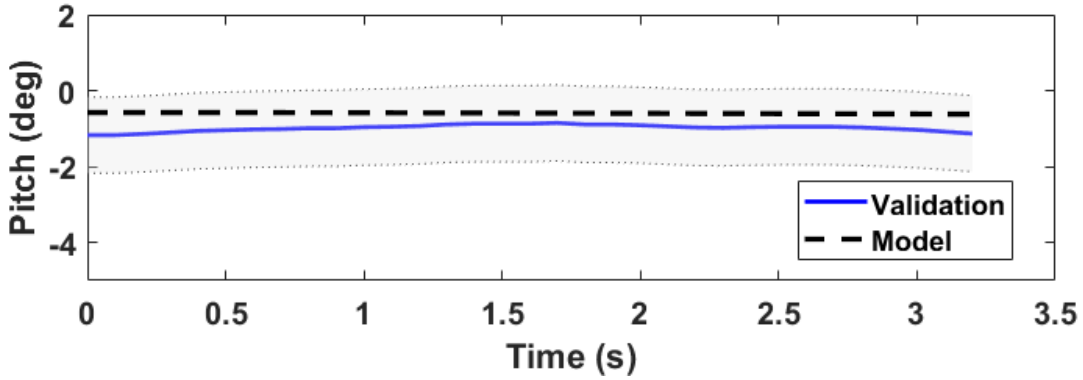

Figure C.90: Pitch trace for 2.c.5 Longitudinal Trim (Approach/Landing Configuration Case 2)

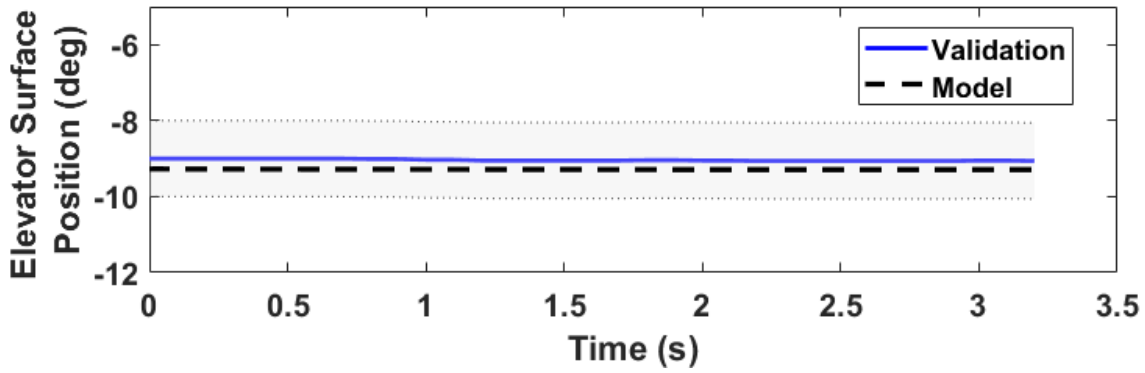

Figure C.91: Elevator surface position trace for 2.c.5 Longitudinal Trim (Approach/Landing Configuration Case 2)

C.15 2.c.6 Longitudinal Maneuvering Stability

Test Objective

Demonstrate that the model's maneuvering stability matches the aircraft.

Test Information

Trim with wings level then establish steady-state conditions at several intermediate bank angles, using the longitudinal controller to maintain trim speed.

Tolerances

Level 6/7 Tolerances:

±5 lb or ±10% of pitch controller force

Alternative method: ±1° or ±10% of the change in elevator position

Flight Conditions

Cruise, Approach, and Landing

Engineering Judgment/Comments

Control force modeling The flight simulation model does not contain a simulated control loading framework making force-based tolerances on 2.c.6 non-applicable. The pitch control force required to maintain trimmed airspeed at established bank angles cannot be assessed.

Use of alternative method Due to the lack of simulated control loading, the alternative tolerance on the change in elevator angle (given in Part 60 regulations) is adopted.

Higher-level test inclusion This test is only required for Level 6 and 7 FTDs, but is included due to data availability and to provide additional confidence in the model's

longitudinal stability characteristics, complementing the alternate data approach adopted for the following test, 2.c.7 Longitudinal Static Stability.

Change in elevator position tolerance The change in elevator position, $\Delta\delta_e$, is defined as the difference between the elevator surface deflection at initial trimmed conditions and the current time step's elevator deflection angle.

Results

Cruise Case

Table C.47: Initial conditions for 2.c.6 Longitudinal Maneuvering Stability (Cruise Case)

Parameter	Units	Validation	Model
Aircraft Configuration			
Weight	lbs	2344	2344
Station Center of Gravity	in	41.9	41.9
Flaps Position	deg	0	0
Flight Conditions			
Pressure Altitude	ft	3038	3038
Airspeed	KTAS	117	117
Vertical Speed	FPM	-90	-90
Aircraft Attitude			
Pitch	deg	-2.3	-1.9
Roll	deg	0.6	0.6
Heading	deg	197.5	197.5
Control Surfaces			
Elevator Position	deg	-3.3	-3.2
Aileron Position	deg	5.0	4.2
Rudder Position	deg	10.9	20.9
Cockpit Controls			
Column Position	in	2.3	2.2
Wheel Position	deg	5.0	4.2
Pedal Position	deg	20.9	20.9
Propulsion			
Throttle Position	norm	N/A	0.41

Table C.48: Snapshot results for 2.c.6 Longitudinal Maneuvering Stability (Cruise Case)

Trim Point	t_{start} **(s)**	t_{end} **(s)**	**Bank (deg)**		**KTAS**		$\Delta\delta_e$ **(deg)**			**Pass/ Fail**
			FT	**Sim**	**FT**	**Sim**	**FT**	**Sim**	**Error**	**($\pm 1^\circ$ or $\pm 10\%$ $\Delta\delta_e$)**
1	0	0	0.6	0.6	117	117	0	0	0	**PASS**
2	22.5	32.5	20.3	19.7	117	117	0.8	0.8	0	**PASS**
3	52	60	30.3	29.3	116	116	0.9	1	0.1	**PASS**
4	67.5	71	45.3	41.4	120	121	2.5	2.6	0.1	**PASS**

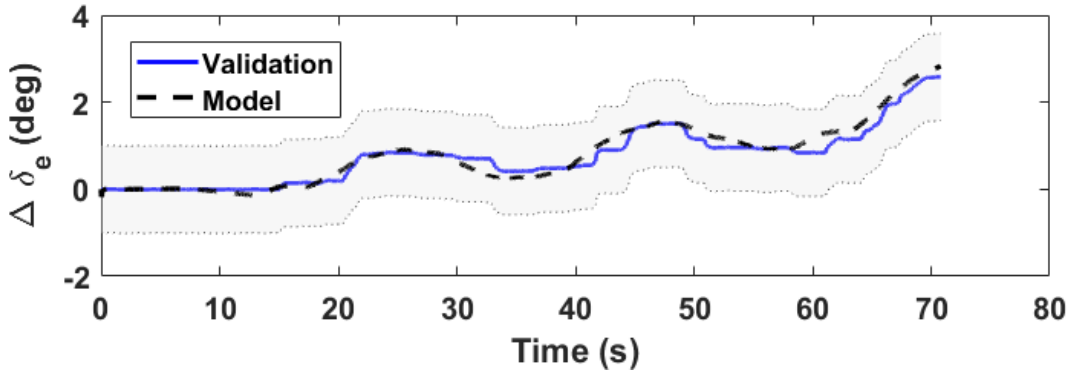

Figure C.92: Change in elevator position ($\Delta\delta_e$) trace for 2.c.6 Longitudinal Maneuvering Stability (Cruise Case)

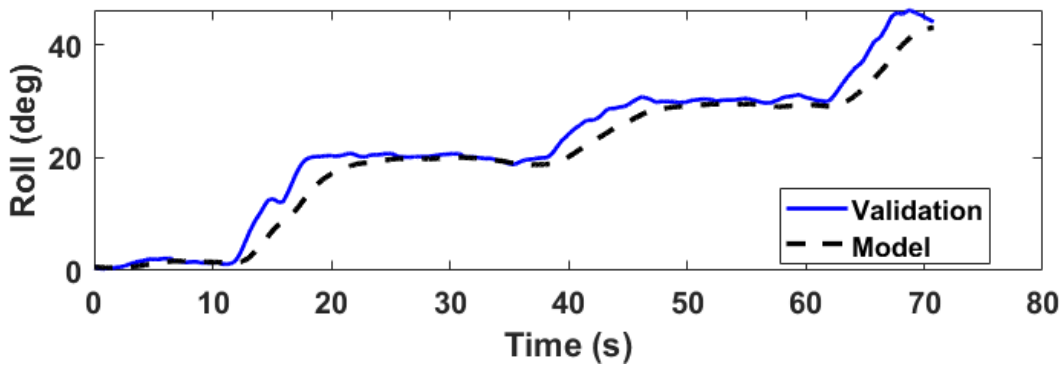

Figure C.93: Roll trace for 2.c.6 Longitudinal Maneuvering Stability (Cruise Case)

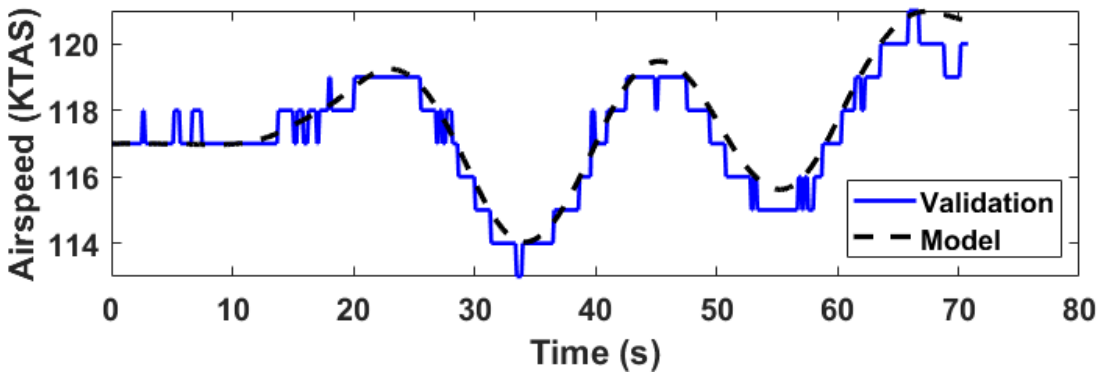

Figure C.94: Airspeed trace for 2.c.6 Longitudinal Maneuvering Stability (Cruise Case)

Approach Case

Table C.49: Initial conditions for 2.c.6 Longitudinal Maneuvering Stability (Approach Case)

Parameter	Units	Validation	Model
Aircraft Configuration			
Weight	lbs	2340	2340
Station Center of Gravity	in	41.9	41.9
Flaps Position	deg	10	10
Flight Conditions			
Pressure Altitude	ft	3064	3064
Airspeed	KTAS	107	107
Vertical Speed	FPM	57	57
Aircraft Attitude			
Pitch	deg	-3.0	-2.2
Roll	deg	0.6	0.6
Heading	deg	244.5	244.5
Control Surfaces			
Elevator Position	deg	-6.8	-6.5
Aileron Position	deg	1.6	1.1
Rudder Position	deg	1.1	0.7
Cockpit Controls			
Column Position	in	1.9	1.8
Wheel Position	deg	6.5	4.9
Pedal Position	deg	20.9	20.8
Propulsion			
Throttle Position	norm	N/A	0.55

Table C.50: Snapshot results for 2.c.6 Longitudinal Maneuvering Stability (Approach Case)

Trim Point	t_{start} **(s)**	t_{end} **(s)**	**Bank (deg)**		**KTAS**		$\Delta\delta_e$ **(deg)**			**Pass/ Fail**
			FT	**Sim**	**FT**	**Sim**	**FT**	**Sim**	**Error**	**($\pm$1° or $\pm$10% $\Delta\delta_e$)**
1	0	0	0.6	0.6	107	107	0	0	0	**PASS**
2	11	20	19.2	19	106	106	0.6	0.8	0.2	**PASS**
3	30	42	29.3	29.1	107	107	1.3	1.6	0.3	**PASS**
4	61	66	-19.7	-19.7	104	104	0.5	0.6	0.1	**PASS**
5	82	88	-31.5	-31.5	105	106	1	1.4	0.4	**PASS**

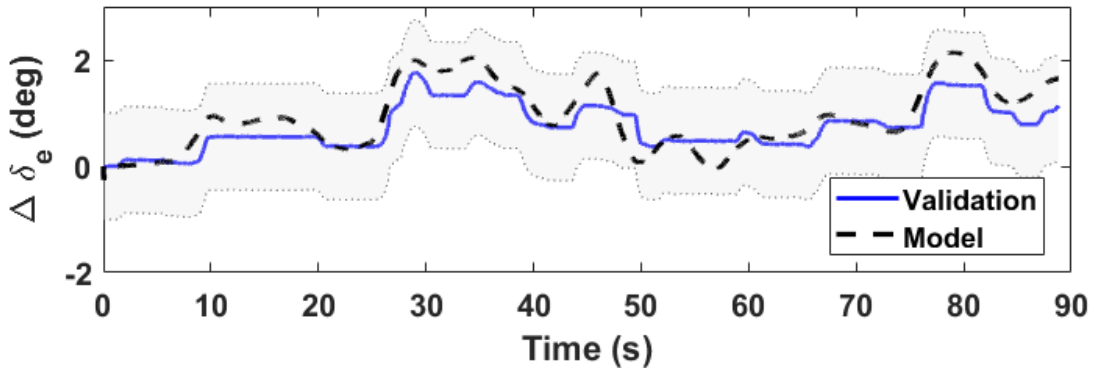

Figure C.95: Change in elevator position ($\Delta\delta_e$) trace for 2.c.6 Longitudinal Maneuvering Stability (Approach Case)

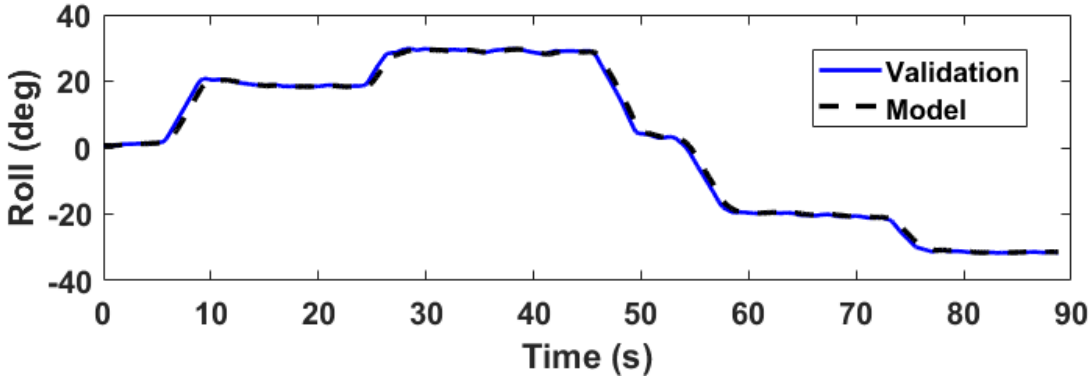

Figure C.96: Roll trace for 2.c.6 Longitudinal Maneuvering Stability (Approach Case)

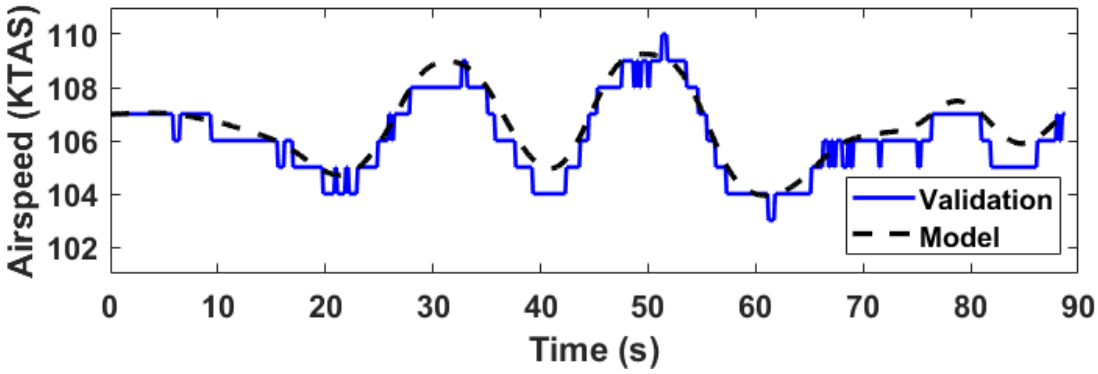

Figure C.97: Airspeed trace for 2.c.6 Longitudinal Maneuvering Stability (Approach Case)

Landing Case

Table C.51: Initial conditions for 2.c.6 Longitudinal Maneuvering Stability (Landing Case)

Parameter	Units	Validation	Model
Aircraft Configuration			
Weight	lbs	2338	2338
Station Center of Gravity	in	41.9	41.9
Flaps Position	deg	20	20
Flight Conditions			
Pressure Altitude	ft	3212	3212
Airspeed	KTAS	90	90
Vertical Speed	FPM	-2	-2
Aircraft Attitude			
Pitch	deg	-2.6	-2.0
Roll	deg	0.5	0.5
Heading	deg	254.8	254.8
Control Surfaces			
Elevator Position	deg	-8.9	-8.6
Aileron Position	deg	1.6	1.4
Rudder Position	deg	1.0	0.5
Cockpit Controls			
Column Position	in	1.6	1.9
Wheel Position	deg	6.9	6.0
Pedal Position	deg	20.9	20.8
Propulsion			
Throttle Position	norm	N/A	0.38

Table C.52: Snapshot results for 2.c.6 Longitudinal Maneuvering Stability (Landing Case)

Trim Point	t_{start} **(s)**	t_{end} **(s)**	**Bank (deg)**		**KTAS**		$\Delta\delta_e$ **(deg)**			**Pass/ Fail**
			FT	**Sim**	**FT**	**Sim**	**FT**	**Sim**	**Error**	**($\pm1^\circ$ or $\pm10\%$ $\Delta\delta_e$)**
1	0	0	0.5	0.5	90	90	0	0	0	**PASS**
2	15	25	19.5	19.4	89	90	0.8	0.8	0	**PASS**
3	38	45	29.5	29.4	90	91	1.9	2.6	0.7	**PASS**
4	58	67	-20.9	-20.8	90	90	0.6	1.3	0.7	**PASS**

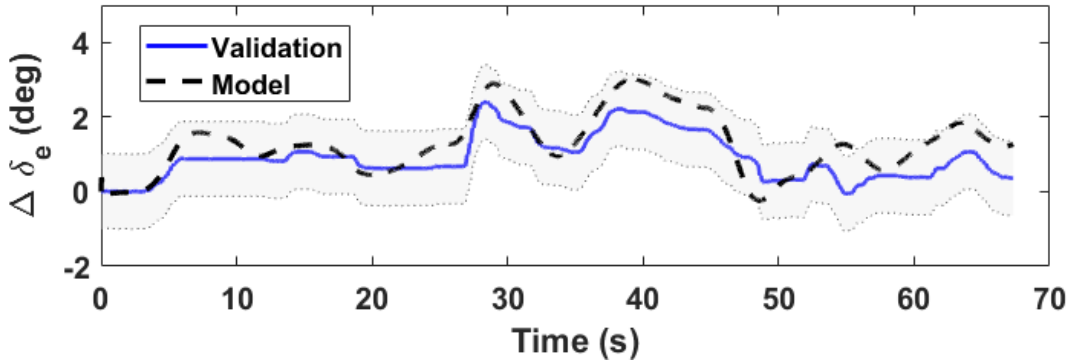

Figure C.98: Change in elevator position ($\Delta\delta_e$) trace for 2.c.6 Longitudinal Maneuvering Stability (Landing Case)

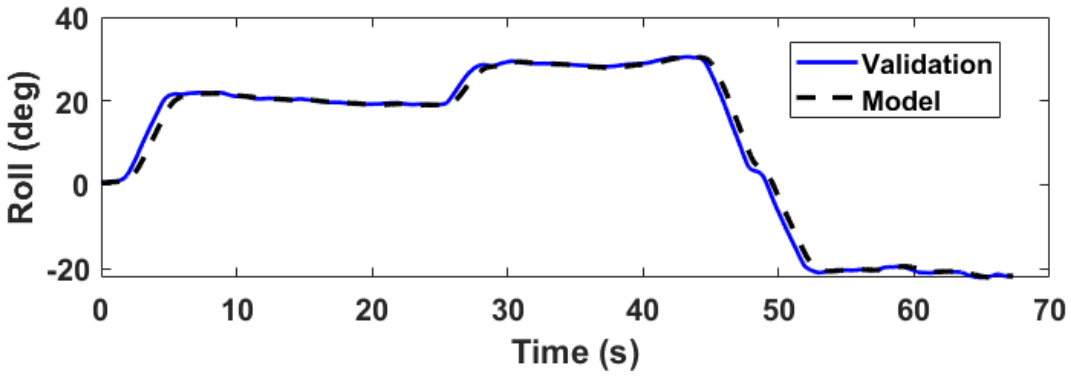

Figure C.99: Roll trace for 2.c.6 Longitudinal Maneuvering Stability (Landing Case)

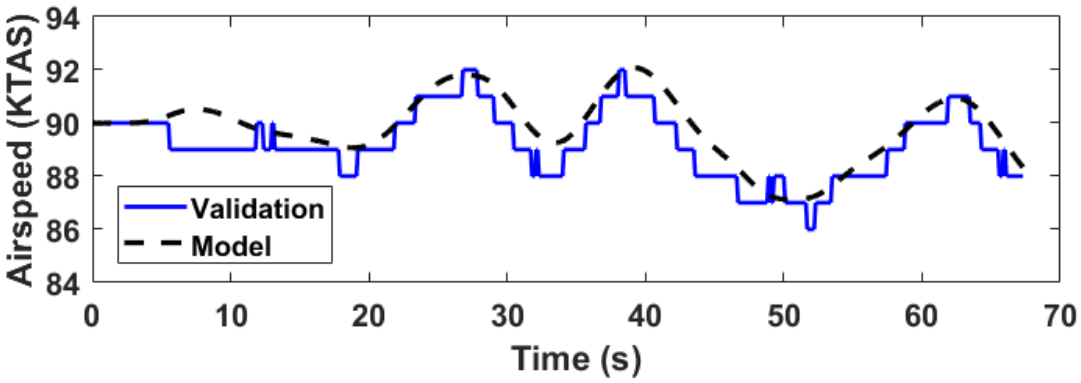

Figure C.100: Airspeed trace for 2.c.6 Longitudinal Maneuvering Stability (Landing Case)

C.16 2.c.7 Longitudinal Static Stability

Test Objective

Demonstrate that the model's static stability matches the aircraft.

Test Information

Trim wings level then, using longitudinal control, apply a deviation from the trimmed airspeed while maintaining wings level attitude.

Tolerances

Level 5 must exhibit positive static stability, but need not comply with numerical tolerances.

Flight Conditions

Approach

Engineering Judgment/Comments

Use of Alternative Data Source FAA Part 60 Table B2B provides a set of alternative data sources for Level 5 FTDs (Small, Single Engine (Reciprocating) Airplanes) [8] to be used in the absence of reliable flight test data. The available flight test data did not produce sufficiently stable trim points across the required airspeed range to support a quantitative comparison. The alternative Level 5 criterion is therefore adopted, requiring only that the model exhibit positive longitudinal static stability with no numerical tolerance applied.

Interpreting Results Positive longitudinal static stability is indicated by a positive (pull) elevator input required to maintain an airspeed below trim and a negative (push) input required to maintain an airspeed above trim, producing a negative slope of elevator position versus airspeed trend.

Results

Table C.53: Initial conditions for 2.c.7 Longitudinal Static Stability

Parameter	**Units**	**Validation**	**Model**
Aircraft Configuration			
Weight	lbs	N/A	2332
Station Center of Gravity	in	N/A	41.8
Flaps Position	deg	N/A	20
Flight Conditions			
Pressure Altitude	ft	N/A	3000
Airspeed	KTAS	N/A	70
Vertical Speed	FPM	N/A	0
Aircraft Attitude			
Pitch	deg	N/A	2.3
Roll	deg	N/A	0.0
Heading	deg	N/A	202.4
Control Surfaces			
Elevator Position	deg	N/A	-5.0
Aileron Position	deg	N/A	2.0
Rudder Position	deg	N/A	0.8
Cockpit Controls			
Column Position	in	N/A	2.1
Wheel Position	deg	N/A	8.8
Pedal Position	deg	N/A	20.8
Propulsion			
Throttle Position	norm	N/A	0.24

Table C.54: Snapshot results for 2.c.7 Longitudinal Static Stability

Test Point	t_{start} **(s)**	t_{end} **(s)**	**KTAS**	δ_e **(deg)**
1	0	0	70	0
2	35	45	66	1.4
3	65	75	61	3.1
4	140	155	75	-1.1
5	180	195	79	-2.1

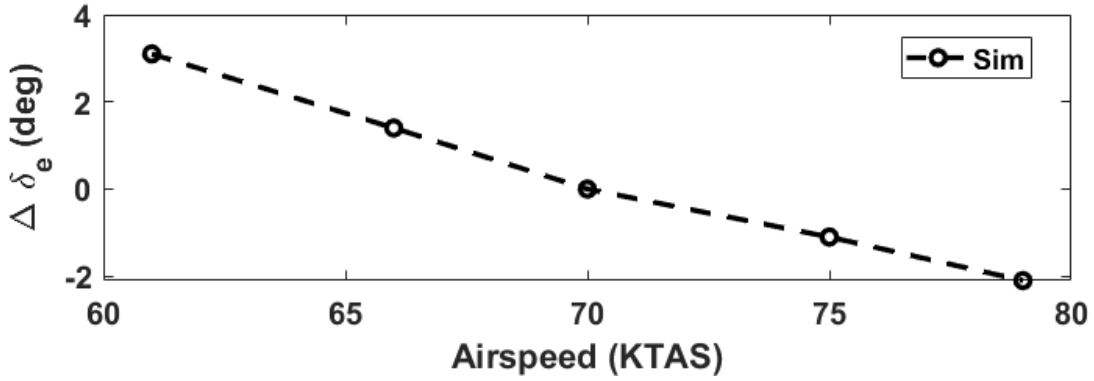

Figure C.101: Change in elevator position ($\Delta\delta_e$) averaged points as a function of Airspeed for 2.c.7 Longitudinal Static Stability

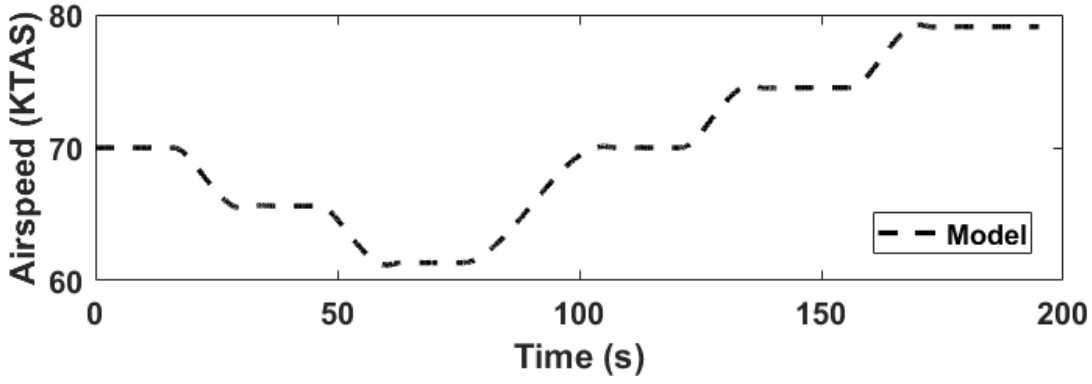

Figure C.102: Airspeed trace for 2.c.7 Longitudinal Static Stability

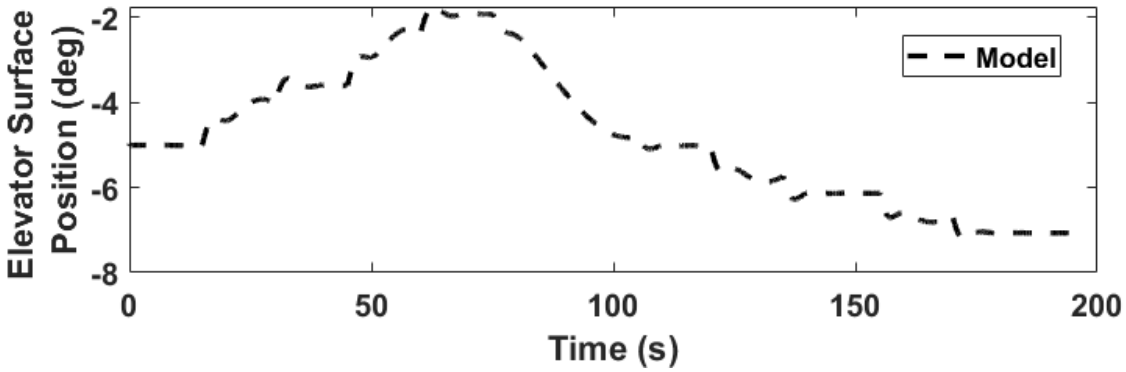

Figure C.103: Elevator surface position trace for 2.c.7 Longitudinal Static Stability

Summary: PASS – The model exhibits positive longitudinal static stability.

C.17 2.c.8.b Stall Warning (actuation of stall warning device)

The stall warning actuation system is not modeled within the current flight simulation framework. As no stall warning device is implemented, this test is not applicable and no results are presented.

C.18 2.c.9.b Phugoid Dynamics

Test Objective

Demonstrate that the model's phugoid dynamics characteristics match the aircraft.

Test Information

From the trimmed cruise point, apply longitudinal control in one direction and record dynamic characteristics of the response.

Tolerances

±10% Period

Representative damping

Flight Conditions

Cruise

Results

Table C.55: Initial conditions for 2.c.9.b - Phugoid Dynamics

Parameter	**Units**	**Validation**	**Model**
Aircraft Configuration			
Weight	lbs	2329	2329
Station Center of Gravity	in	41.8	41.8
Flaps Position	deg	0	0
Flight Conditions			
Pressure Altitude	ft	3087	3087
Airspeed	KTAS	115	115
Vertical Speed	FPM	-27	-27
Aircraft Attitude			
Pitch	deg	-1.7	-1.5
Roll	deg	0.3	0.3
Heading	deg	200.4	200.4
Control Surfaces			
Elevator Position	deg	-3.2	-3.1
Aileron Position	deg	1.1	1.0
Rudder Position	deg	1.4	1.5
Cockpit Controls			
Column Position	in	2.3	2.3
Wheel Position	deg	4.7	4.3
Pedal Position	deg	20.9	20.9
Propulsion			
Throttle Position	norm	N/A	0.41

Table C.56: Results summary for 2.c.9.b - Phugoid Dynamics

Metric	Tolerance	Validation	Model	Error	Pass/ Fail
Period	±10% (±3.5 sec)	35.0	37.7	2.7	**PASS**
Damping Ratio	N/A	0.048	0.040	0.008	N/A

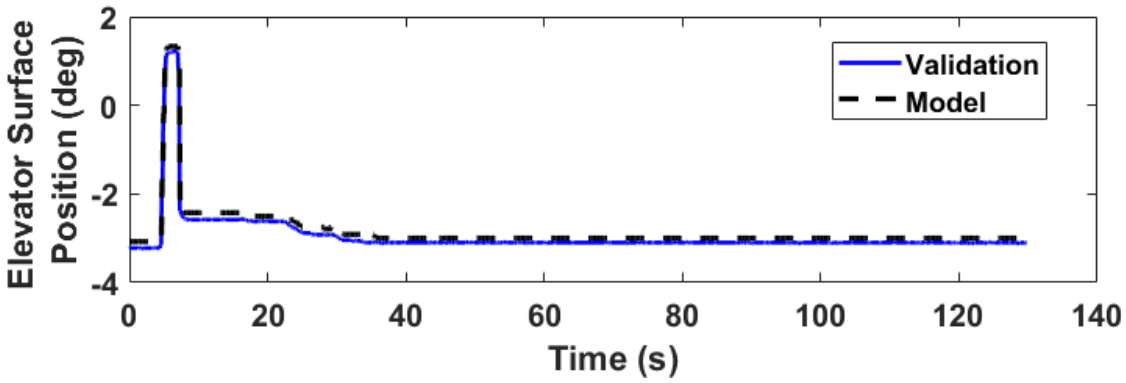

Figure C.104: Elevator surface position trace for 2.c.9.b Phugoid Dynamics

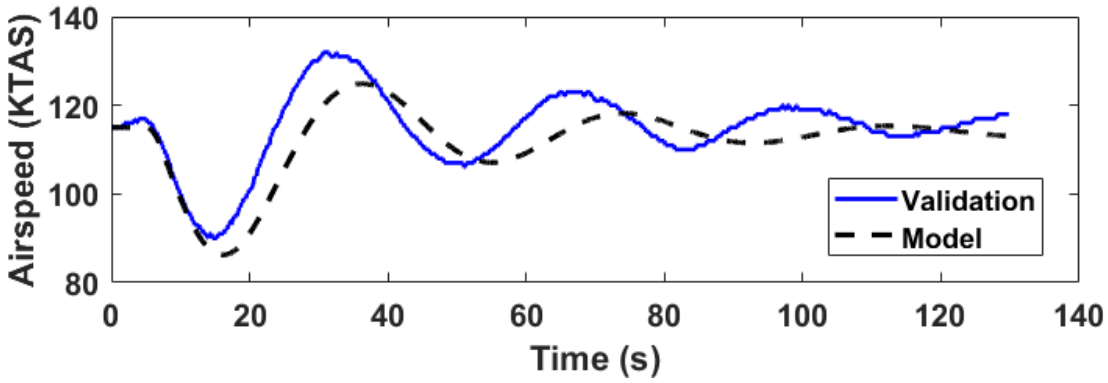

Figure C.105: Airspeed trace for 2.c.9.b Phugoid Dynamics

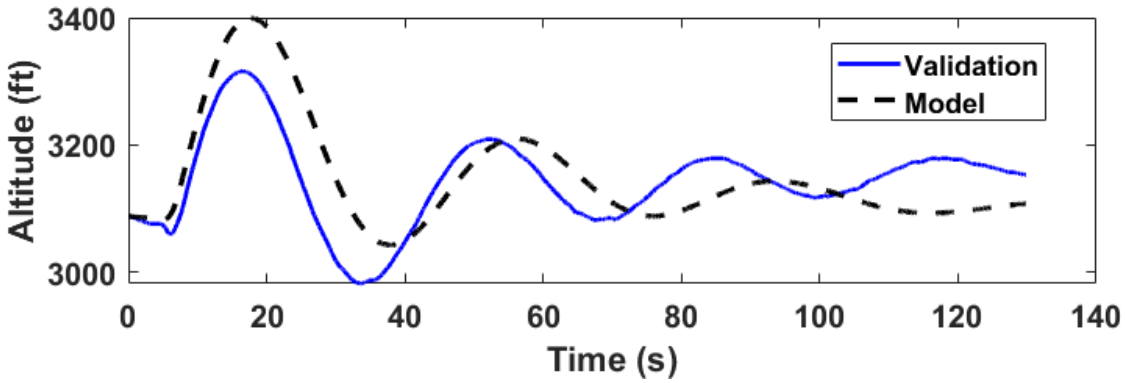

Figure C.106: Altitude trace for 2.c.9.b Phugoid Dynamics

C.19 2.d.2 Roll Response (Rate)

Test Objective

Demonstrate that the model's roll-rate response to wheel input matches the aircraft.

Test Information

Establish a trimmed condition with wings-level then quickly displace the roll controller by approximately 1/3 of maximum controller travel and evaluate the resulting roll rate.

Tolerances

$\pm 2^\circ$/s or $\pm 10\%$ of roll rate

Flight Conditions

Cruise, and Approach or Landing

Engineering Judgment/Comments

Evaluation of Results The roll response test is evaluated by comparing the average steady-state roll rate over the period of held wheel deflection rather than applying the tolerance band across the full time history, as the noisy nature of the flight test data during transient response makes point-by-point comparison unrepresentative of model performance. The tolerance is applied to the averaged steady-state values.

Longitudinal Trim at Extreme Bank Angles Discrepancies in pitch attitude and elevator position are observed in cases where initial conditions are trimmed at more extreme bank angles. These are noted as an observation and do not affect the primary roll rate evaluation metric.

Results

Cruise Case

Table C.57: Initial conditions for 2.d.2 Roll Response (Cruise Case)

Parameter	**Units**	**Validation**	**Model**
Aircraft Configuration			
Weight	lbs	2435	2435
Station Center of Gravity	in	42.1	42.1
Flaps Position	deg	0	0
Flight Conditions			
Pressure Altitude	ft	2914	2914
Airspeed	KTAS	114	114
Vertical Speed	FPM	-376	-375
Aircraft Attitude			
Pitch	deg	0.1	-1.3
Roll	deg	40.6	40.6
Heading	deg	288.3	288.3
Control Surfaces			
Elevator Position	deg	0.1	0.2
Aileron Position	deg	0.3	0.9
Rudder Position	deg	2.8	6.7
Cockpit Controls			
Column Position	in	2.7	2.7
Wheel Position	deg	1.2	3.9
Pedal Position	deg	28.0	28.0
Propulsion			
Throttle Position	norm	N/A	0.30

Table C.58: Results summary for 2.d.2 Roll Response (Cruise Case)

Metric	Tolerance	Validation	Model	Error	Pass/ Fail
Steady-state Roll Rate	±2°/s	-18.3	-19.2	-0.9	**PASS**

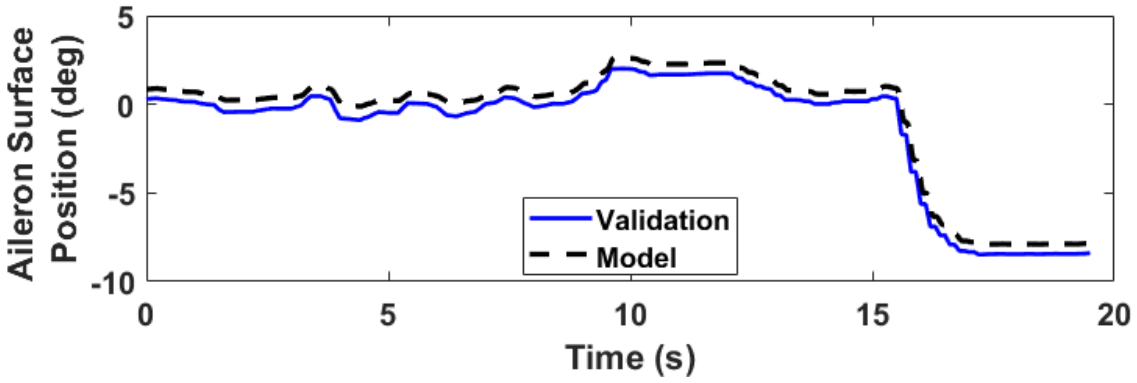

Figure C.107: Aileron surface position trace for 2.d.2 Roll Response (Cruise Case)

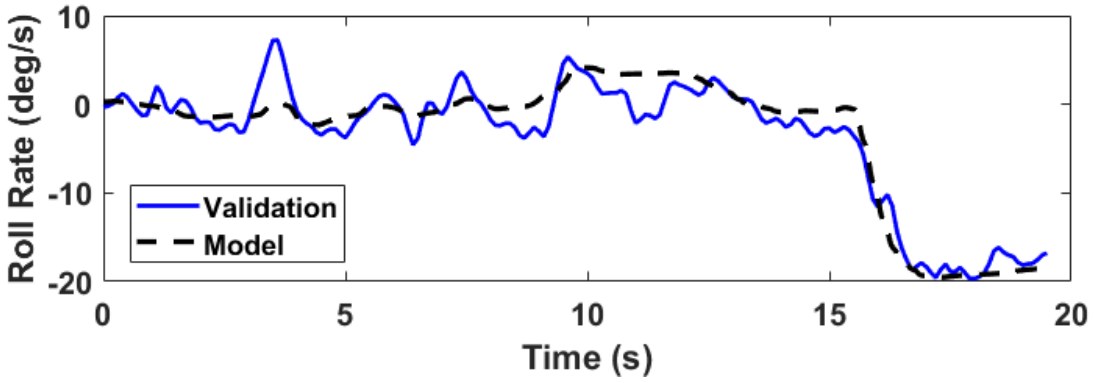

Figure C.108: Roll rate trace for 2.d.2 Roll Response (Cruise Case)

Approach Case

Table C.59: Initial conditions for 2.d.2 Roll Response (Approach Case)

Parameter	Units	Validation	Model
Aircraft Configuration			
Weight	lbs	2432	2432
Station Center of Gravity	in	42.1	42.1
Flaps Position	deg	20	20
Flight Conditions			
Pressure Altitude	ft	3241	3241
Airspeed	KTAS	94	94
Vertical Speed	FPM	-217	-216
Aircraft Attitude			
Pitch	deg	1.4	-0.5
Roll	deg	45.4	45.4
Heading	deg	186.9	186.9
Control Surfaces			
Elevator Position	deg	-4.8	-3.0
Aileron Position	deg	1.1	1.0
Rudder Position	deg	3.1	7.9
Cockpit Controls			
Column Position	in	2.1	2.3
Wheel Position	deg	4.5	4.6
Pedal Position	deg	21.2	21.8
Propulsion			
Throttle Position	norm	N/A	0.42

Table C.60: Results summary for 2.d.2 Roll Response (Approach Case)

Metric	Tolerance	Validation	Model	Error	Pass/ Fail
Steady-state Roll Rate	±2°/s	-20.8	-19.1	1.7	**PASS**

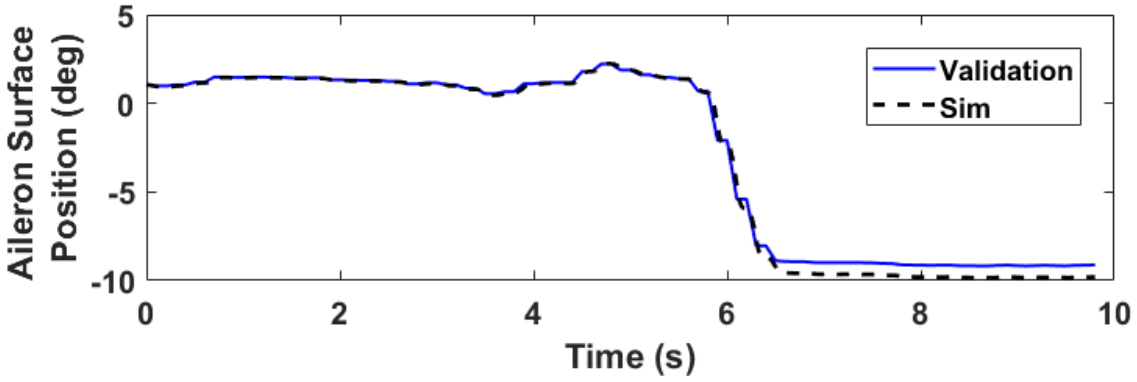

Figure C.109: Aileron surface position trace for 2.d.2 Roll Response (Approach Case)

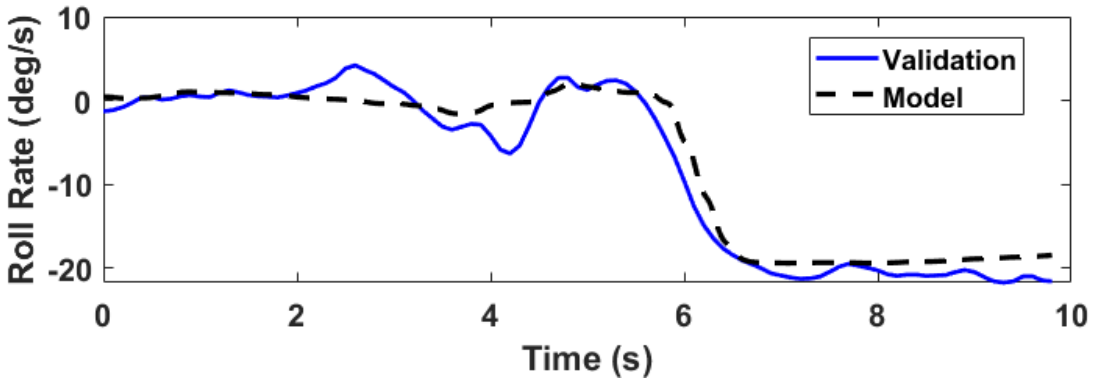

Figure C.110: Roll rate trace for 2.d.2 Roll Response (Approach Case)

C.20 2.d.4.a/c Spiral Stability

Test Objective

Demonstrate that the model's dynamic lateral/directional spiral mode characteristics match the aircraft.

Test Information

Establish a steady bank angle of approximately 30°, applying lateral control required to maintain the bank angle.

Tolerances

Level 5 Tolerance: Correct trend

Level 7 Tolerance: Correct trend and ±2° aileron angle

Flight Conditions

Cruise

Engineering Judgment/Comments

Higher-level test tolerance adoption Level 7 tolerances for the spiral stability demonstration tests are adopted for a quantitative assessment of the aircraft's characteristics.

Results

Left

Table C.61: Initial conditions for 2.d.4.a/c Spiral Stability (Left)

Parameter	**Units**	**Validation**	**Model**
Aircraft Configuration			
Weight	lbs	2420	2420
Station Center of Gravity	in	42.1	42.1
Flaps Position	deg	0	0
Flight Conditions			
Pressure Altitude	ft	3088	3088
Airspeed	KTAS	118	118
Vertical Speed	FPM	-31	-31
Aircraft Attitude			
Pitch	deg	-1.9	-1.5
Roll	deg	1.5	1.5
Heading	deg	226.6	226.6
Control Surfaces			
Elevator Position	deg	-2.9	-3.2
Aileron Position	deg	1.5	0.9
Rudder Position	deg	1.0	1.0
Cockpit Controls			
Column Position	in	2.4	2.3
Wheel Position	deg	6.4	4.2
Pedal Position	deg	20.9	20.9
Propulsion			
Throttle Position	norm	N/A	0.44

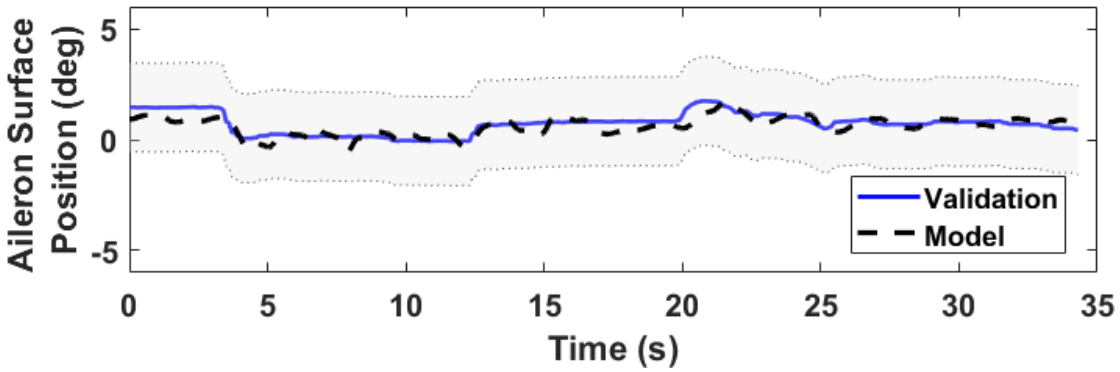

Figure C.111: Aileron surface position trace for 2.d.4.a/c Spiral Stability (Left)

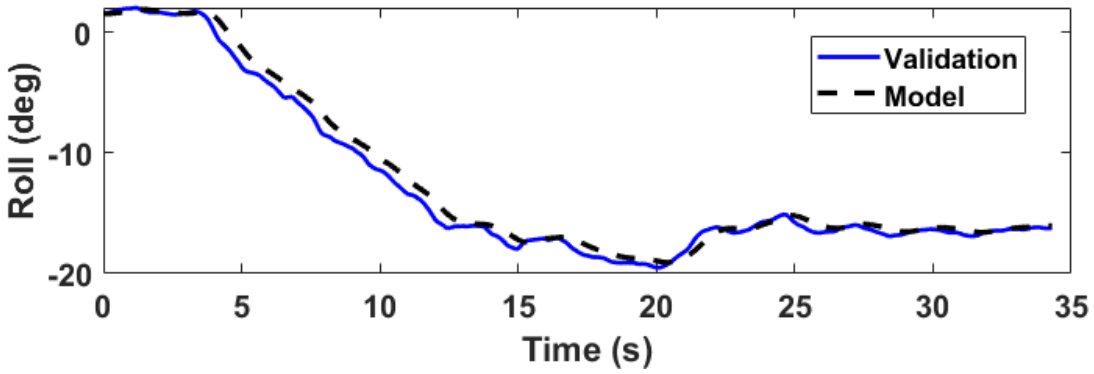

Figure C.112: Roll trace for 2.d.4.a/c Spiral Stability (Left)

Right

Table C.62: Initial conditions for 2.d.4.a/c Spiral Stability (Right)

Parameter	Units	Validation	Model
Aircraft Configuration			
Weight	lbs	2422	2422
Station Center of Gravity	in	42.1	42.1
Flaps Position	deg	0	0
Flight Conditions			
Pressure Altitude	ft	3349	3349
Airspeed	KTAS	121	121
Vertical Speed	FPM	123	123
Aircraft Attitude			
Pitch	deg	-2.4	-1.0
Roll	deg	2.8	2.7
Heading	deg	283.5	283.5
Control Surfaces			
Elevator Position	deg	-3.3	-3.3
Aileron Position	deg	0.8	0.9
Rudder Position	deg	0.9	1.7
Cockpit Controls			
Column Position	in	2.3	2.3
Wheel Position	deg	3.5	4.0
Pedal Position	deg	20.9	20.9
Propulsion			
Throttle Position	norm	N/A	0.98

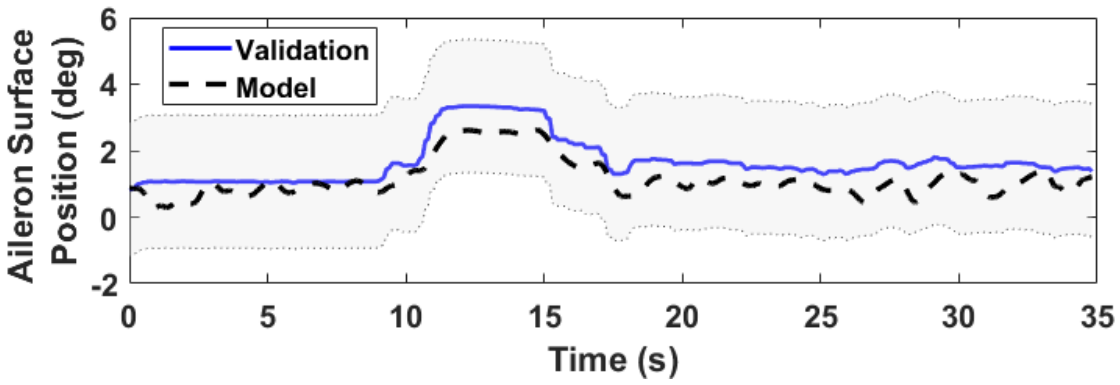

Figure C.113: Aileron surface position trace for 2.d.4.a/c Spiral Stability (Right)

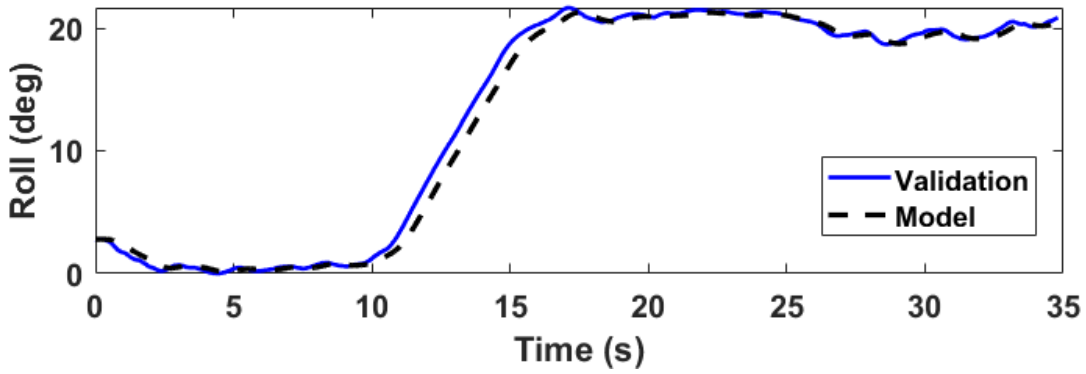

Figure C.114: Roll trace for 2.d.4.a/c Spiral Stability (Right)

C.21 2.d.6.a/b Rudder Response

Test Objective

Demonstrate that the model's directional response to rudder input matches the aircraft.

Test Information

Establish a trimmed condition with wings-level then quickly displace the pedals by approximately 1/3 of maximum controller travel and evaluate the resulting yaw rate.

Tolerances

$\pm 2^\circ$/s or $\pm 10\%$ of yaw rate

Flight Conditions

Approach or Landing

Engineering Judgment/Comments

Tolerances The Level 5 rudder response test assesses roll rate and bank angle. Level 6 and 7 replace this with a yaw rate response tolerance. As roll response is addressed elsewhere in the validation suite, the Level 6/7 yaw rate tolerance is adopted here to characterize the model's directional response to a rudder input, permitted within the test details in FAA Part 60 [8].

Results

Table C.63: Initial conditions for 2.d.6.a/b Rudder Response

Parameter	**Units**	**Validation**	**Model**
Aircraft Configuration			
Weight	lbs	2412	2412
Station Center of Gravity	in	42.0	42.0
Flaps Position	deg	30	30
Flight Conditions			
Pressure Altitude	ft	3631	3631
Airspeed	KTAS	73	73
Vertical Speed	FPM	28	28
Aircraft Attitude			
Pitch	deg	-0.1	1.2
Roll	deg	1.2	1.2
Heading	deg	181.8	181.8
Control Surfaces			
Elevator Position	deg	-9.4	-9.7
Aileron Position	deg	1.5	1.7
Rudder Position	deg	2.0	2.3
Cockpit Controls			
Column Position	in	1.6	1.7
Wheel Position	deg	6.2	7.5
Pedal Position	deg	2.0	2.3
Propulsion			
Throttle Position	norm	N/A	0.33

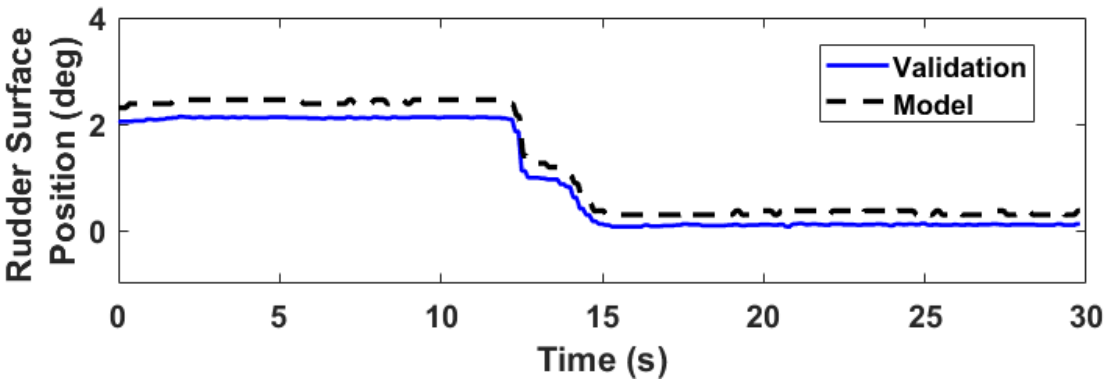

Figure C.115: Rudder surface position trace for 2.d.6.a/b Rudder Response

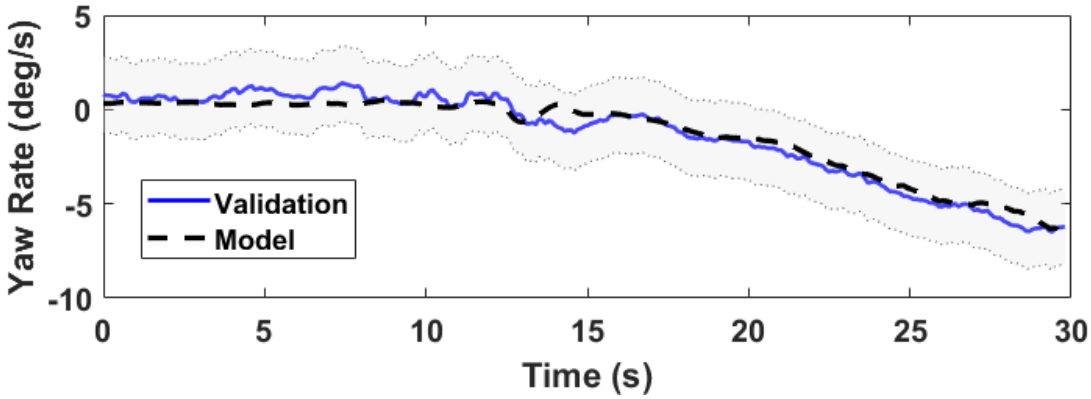

Figure C.116: Yaw rate trace for 2.d.6.a/b Rudder Response

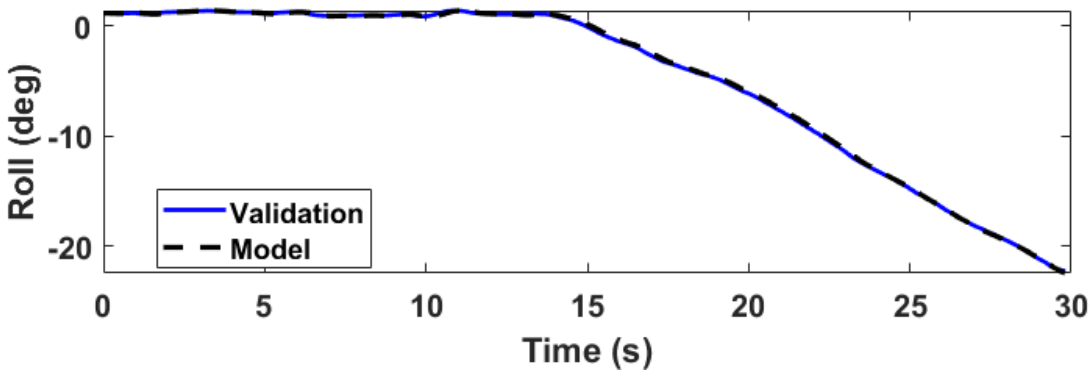

Figure C.117: Roll trace for 2.d.6.a/b Rudder Response

C.22 2.c.7 Dutch Roll

Test Objective

Demonstrate that the model's dutch roll characteristics match the aircraft.

Test Information

Trim with wings level then initiate a dutch roll oscillation using a rapid pedal doublet.

Tolerances

±0.5 s or ±10% of period

±10% of time to one half or double amplitude or ±0.2 of damping ratio

Flight Conditions

Cruise, and Approach or Landing

Engineering Judgment/Comments

Dutch Roll Response The Cessna 172 Skyhawk's Dutch roll mode is heavily damped and does produce enough of a response to compute oscillation parameters. As a result, standard period and damping ratio tolerances are not applied. The results are presented as a trend comparison, demonstrating the model exhibits the same damped response as the aircraft. Exact agreement during the excitation phase is not expected given the sensitivity of the response to pilot input timing and magnitude.

Results

Cruise Case

Table C.64: Initial conditions for 2.c.7 Approach Roll (Cruise Case)

Parameter	**Units**	**Validation**	**Model**
Aircraft Configuration			
Weight	lbs	2406	2406
Station Center of Gravity	in	42.0	42.0
Flaps Position	deg	0	0
Flight Conditions			
Pressure Altitude	ft	3551	3551
Airspeed	KTAS	122	122
Vertical Speed	FPM	0	0
Aircraft Attitude			
Pitch	deg	-2.6	-1.6
Roll	deg	0.1	0.1
Heading	deg	85.7	85.7
Control Surfaces			
Elevator Position	deg	-3.5	-3.3
Aileron Position	deg	1.1	0.9
Rudder Position	deg	0.9	1.3
Cockpit Controls			
Column Position	in	2.3	2.3
Wheel Position	deg	4.7	4.0
Pedal Position	deg	20.9	20.9
Propulsion			
Throttle Position	norm	N/A	0.58

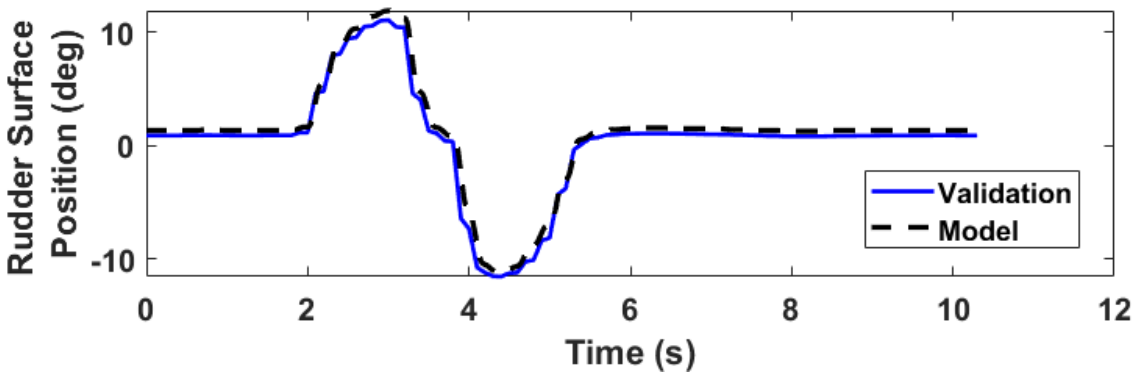

Figure C.118: Rudder surface position trace for 2.c.7 Dutch Roll (Cruise Case)

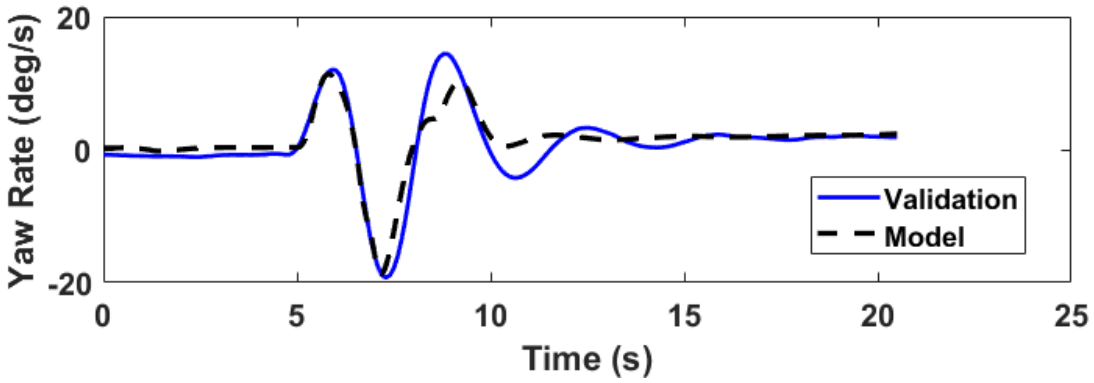

Figure C.119: Yaw rate trace for 2.c.7 Dutch Roll (Cruise Case)

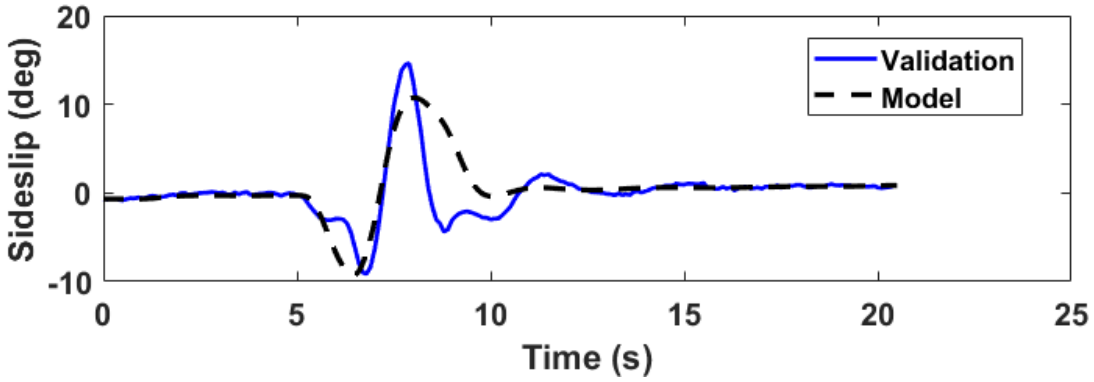

Figure C.120: Sideslip trace for 2.c.7 Dutch Roll (Cruise Case)

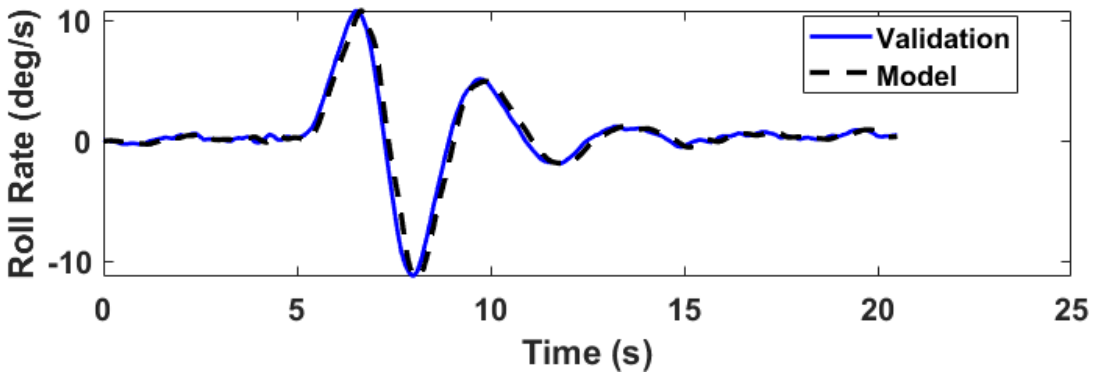

Figure C.121: Roll rate trace for 2.c.7 Dutch Roll (Cruise Case)

Approach Case

Table C.65: Initial conditions for 2.c.7 Approach Roll (Approach Case)

Parameter	Units	Validation	Model
Aircraft Configuration			
Weight	lbs	2408	2108
Station Center of Gravity	in	42.0	42.0
Flaps Position	deg	20	20
Flight Conditions			
Pressure Altitude	ft	3663	3663
Airspeed	KTAS	82	82
Vertical Speed	FPM	106	106
Aircraft Attitude			
Pitch	deg	-0.7	0.4
Roll	deg	0.9	0.9
Heading	deg	354.1	354.1
Control Surfaces			
Elevator Position	deg	-8.3	-7.3
Aileron Position	deg	1.3	1.5
Rudder Position	deg	1.4	1.0
Cockpit Controls			
Column Position	in	1.7	1.8
Wheel Position	deg	5.7	6.5
Pedal Position	deg	20.9	20.9
Propulsion			
Throttle Position	norm	N/A	0.35

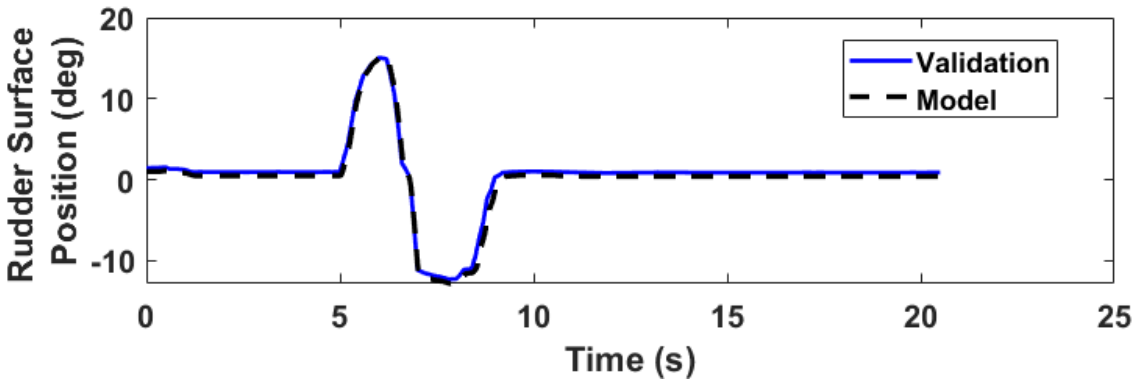

Figure C.122: Rudder surface position trace for 2.c.7 Dutch Roll (Approach Case)

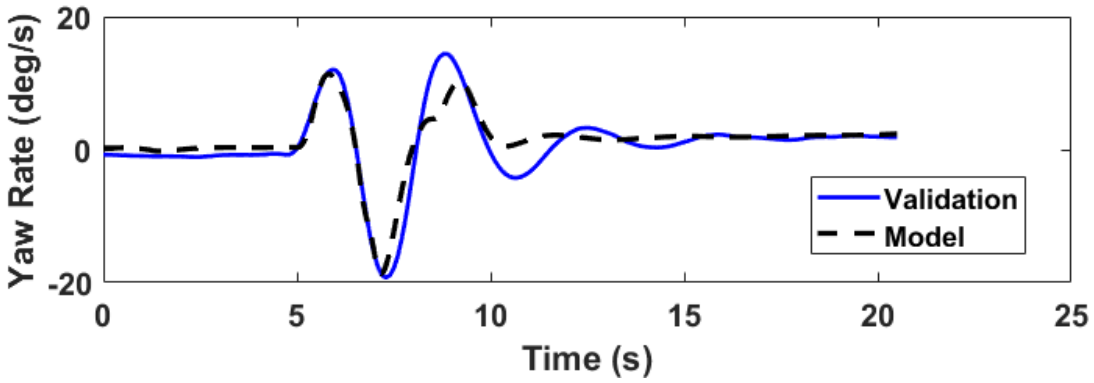

Figure C.123: Yaw rate trace for 2.c.7 Dutch Roll (Approach Case)

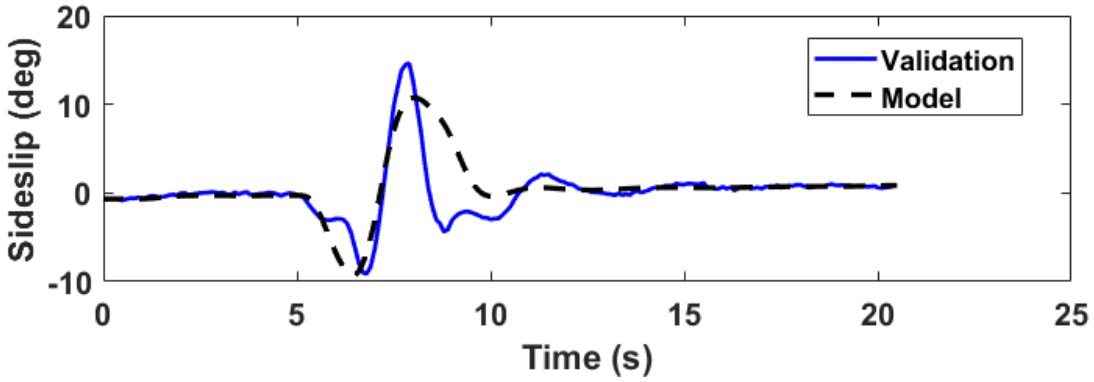

Figure C.124: Sideslip trace for 2.c.7 Dutch Roll (Approach Case)

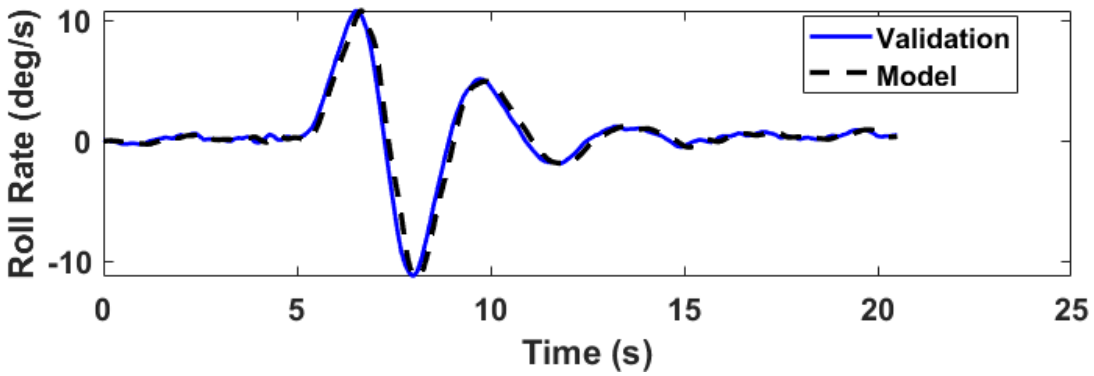

Figure C.125: Roll rate trace for 2.c.7 Dutch Roll (Approach Case)

C.23 2.d.8 Steady State Sideslip

Test Objective

Demonstrate that the model's lateral/directional flight characteristics match the aircraft's.

Test Information

Establish a steady-state sideslip condition using a constant rudder pedal position and required lateral control input to maintain a constant heading.

Tolerances

For a given rudder position:

$\pm 2^\circ$ roll angle

$\pm 1^\circ$ sideslip angle

$\pm 2^\circ$ or $\pm 10\%$ aileron angle

Adopted tolerance: $\pm 2^\circ$ or $\pm 10\%$ rudder angle

Flight Conditions

Approach or Landing

Engineering Judgment/Comments

Adopted Tolerance and Evaluation Approach The standard tolerances for this test include roll angle, sideslip angle, aileron angle, and rudder position. As the trim routine sets the bank and sideslip angles as target conditions, these are enforced as inputs rather than evaluated as outputs. The resulting aileron and rudder deflections required to achieve the prescribed bank and sideslip conditions are therefore the meaningful comparison metrics. The $\pm 2^\circ$ aileron tolerance is applied directly, and an equivalent $\pm 2^\circ$ tolerance is adopted for rudder angle.

Snapshot Data Approach Results are presented as steady-state trim snapshots at prescribed sideslip conditions. No time-domain data is available for this test and a tabular comparison of trimmed control surface deflections against flight test data is used for evaluation.

Table C.66: Snapshot results for 2.d.8 Steady State Sideslip

Bank (deg)	**Sideslip (deg)**	**Aileron (deg)**		**Pass/Fail ($\pm$2°)**	**Rudder (deg)**		**Pass/Fail ($\pm$2°)**
		FT	**Sim**		**FT**	**Sim**	
0.65	-1.25	1.3	1.8	**PASS**	3.1	2.7	**PASS**
-3.1	-6.1	0.2	1.4	**PASS**	9.4	9.7	**PASS**
10.1	10.7	4.1	2.9	**PASS**	-14.5	-14.9	**PASS**